Investigating DNA-Mediated Charge Transport by Time-Resolved Spectroscopy

Thesis by

Eric Daniel Olmon

In Partial Fulfillment of the Requirements

for the Degree of

Doctor of Philosophy

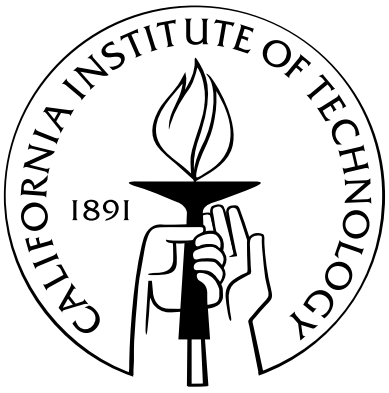

California Institute of Technology

Pasadena, California

2012

(Defended Sept 30, 2011)

Acknowledgements

As is true for any graduate student, most of this work could not have been completed without assistance from a large number of people. First and foremost, I want to thank my advisor, Jackie Barton, not only for her scientific guidance and her unwavering enthusiasm, but also for the subtle instruction she provides in the many duties of academia. Not every graduate student is given the opportunity to communicate their research, participate in grant writing, or critically review manuscripts, but proficiency in these areas is necessary to succeed in the academic world. Jackie has also been a strong role model. In my future endeavors, I will seek to emulate the tenacity with which she pursues answers to scientific questions, the boldness with which she follows her intuition, and the graciousness she shows even at the highest levels of professional success.

I also want to express my sincere gratitude to my thesis committee and to my collaborators. Although I didn't have as much interaction with them as I would have liked, I appreciate the input and encouragement of my committee: Harry Gray, Doug Rees, Tom Miller, and formerly Pat Collier. My collaborator Tony Vlček introduced the Barton Group to a new experimental method for the time-resolved observation of DNA-mediated CT. Besides providing access to a sensitive TRIR instrument in the UK and facilitating the measurement of our samples, Tony was a fantastic resource when the time came to work up and interpret the data. He was unfailingly cheerful and he always treated me as a scientific equal. Without his interest, generosity, and guidance, much of the work that is presented here would simply not have been possible. Similarly, I am indebted to Mike Hill for his assistance in conducting electrochemical and spectroelectrochemical measurements at Occidental College. Mike was always convivial, enthusiastic, and generous with his time. He made me feel at home each time I visited his laboratory, introducing me to his colleagues

and showing me what life is like as a chemistry professor at a liberal arts college.

Closer to home, I received a great deal of support and guidance from Eric Stemp and Jay Winkler. Eric, a perennial visitor and collaborator with the Barton Group, was always happy to discuss photophysics, group lore, and baseball. In addition, my work owes much to fundamental aspects of DNA-mediated CT that he established years ago. I am grateful to Jay partly for sharing his expertise in instrumentation and data analysis, but mostly for providing a strong example of scientific integrity. As difficult as it is to be held to the high standards that Jay demands, such attention to detail and logic is necessary to rigorously test complex scientific theories. I will continue to pursue that ideal.

I must thank the tireless administrators and adjuncts of Caltech who keep the Institute running. Thanks to Steve, Joe, and Ron for making sure that the materials I order find their way to me. Thanks to Agnes and her predecessors Laura and Dian for always knowing where I should go and what I should do next. Thanks to Mona, Dave, Scott, and Angelo for keeping the instruments running. Thanks to Tom, Rick, and Mike for fixing everything I broke. Thanks to Ernie for the food. Finally, thank you Mo, Administrative Assistant to Prof. Barton, and Mo, Administrative Assistant to the Chair, for being the glue that holds the whole place together.

While at Caltech, I have had the distinction of experiencing almost every facet of Chem 1, from grader to recitation TA to head TA. I have also observed the increase in clarity and organization that took place when Mike Vicic began his tenure as course coordinator. I want to thank Mike for showing me how to properly design and run a course. I also want to thank Sarah Reisman for taking me on as head TA during her first term teaching Chem 1b. These experiences have largely directed my ambition to establish a career in academia.

Music has served as a counterpoint to my scientific life at Caltech. My gratitude goes to Bill Bing, who encouraged me to join the concert band and later the jazz band. It has been a weekly pleasure to play percussion with Scott, Jeff, Dan, Joe, Wesley, Gregory, Heather, Chris, Mike, and Kris. I also want to thank Rob Usiskin, Brett Babin, and James McKone, who have given me the opportunity to explore jazz in a less structured setting.

Life is comprised of a series of interactions with other people, and the enjoyment

of life depends mainly on the quality of those interactions. I am fortunate to have been part of a supportive, creative, and at times eccentric lab group throughout my time in grad school. Of course I appreciate the help and advice they have given me in the lab, but I am more thankful for the personal memories. I will never forget Eddie's enthusiasm during summer softball and how he convinced every single person in the lab to play that first year; Brian's ability to make Pumpkinpalooza and Lablympics come to life and his even more impressive ability to convince us all that we wanted to participate; Paul's cat suit, paper cutouts, clay sculptures, skull stickers, suicide bunnies, and secret messages; physics discussions with Joey; 4th of July at the Rose Bowl; spending ages in the laser lab with Ben; the vacation cottage at ACS; Yosemite and King's Canyon, talent shows, long car rides, Whiskey Rock, fire breathing, and Christine's camp cooking; the cake-baking committee; the lunch train; late night trips to Pinkberry and Papa George's; karaoke and balls; Curtis's brews; crossword puzzles; flag football; beer and cheese pairings; and so much more. Thanks everyone.

I also want to thank my friends outside of lab for giving me some much needed perspective. Thanks to Arthur, Puneet, Andrew, Kathleen, Erik, Mary, Diana, Yvonne, Havala, and Claire for trips to the beach, hikes, and cookouts. Thanks Morgan, Andy, Rob, John, Val, and Sam for an amazing time in Korea. Thanks to the rest of the 2005 entering class, especially Gretchen, Alex, Jillian, and Matt for inviting me to your parties and poker games. Thanks Chithra and Keith for operas, plays, dinners out, and dinners in.

Thanks to my family. I am impressed by my mom, who has continued earning professional degrees while working full-time and raising three boys. I respect my dad for his thoughtfulness and broad knowledge of the world. I am proud of Matt for following his dreams to L.A. and for maintaining his ambition and integrity. I appreciate Rob's constant friendship and appropriate balance of support and criticism. I love you all.

Finally, I want to thank my fianceé, complement, and best friend Chethana Kulkarni for her constant understanding and love. Throughout the time I have been with her, she has reminded me to focus on what is important in life, and she has shown me so much of the world and of life that I would not have experienced on my own. Thank you.

Abstract

In all organisms, oxidation threatens the integrity of the genome. Numerous studies have suggested that DNA-mediated charge transport (CT) may play an important role in the sequestration, detection, and repair of oxidative damage. To fully understand the mechanism of DNA-mediated CT, it is necessary to characterize transient intermediates that arise during the reaction and to determine the lifetimes of these intermediates. Time-resolved spectroscopy is the most appropriate experimental method for such observations. Each intermediate has a characteristic spectrum. By observing time-dependent changes in the absorption spectrum of the sample, it is therefore possible to determine what species are present at a particular time and how long it exists in solution. Experiments presented here involve the use of time-resolved spectroscopy to better understand the process of DNA-mediated CT.

The study of DNA-mediated CT requires a robust and consistent method for triggering the CT reaction. The metal complexes that have traditionally been used for this purpose provide several advantages over organic phototriggers: they are synthetically versatile, they are stable in solution, they exhibit rich photophysics, and many are strong photooxidants. However, the spectroscopic features used to follow the photochemical processes triggered by these probes are generally broad optical bands. These can be difficult to resolve in samples that contain several absorbing species. For this reason, we have developed a Re photooxidant bearing a set of vibrationally active carbonyl ligands that can be covalently tethered to DNA. Unlike many absorption bands in the visible range, the vibrational absorption bands of these ligands are narrow, well-resolved, and specific. Such probes can be used to follow the complex photophysical pathways observed in biochemical systems with good precision, making them useful for the study of DNA-mediated CT.

Specifically, the complex $[Re(CO)_3(dppz)(py\text{-}OR)]^+$ (dppz = dipyrido[3,2-*a*:2′,3′-*c*]-phenazine; py′-OR = 4-functionalized pyridine) offers IR sensitivity and can oxidize DNA directly from the excited state. The behavior of several covalent and noncovalent Re-DNA constructs was monitored by time-resolved IR (TRIR) and UV/visible spectroscopies, as well as biochemical methods, confirming the ability of the complex to trigger long-range oxidation of DNA. Optical excitation of the complex leads to population of metal-to-ligand charge transfer excited states and at least two distinct intraligand charge transfer excited states. Several experimental observations are consistent with charge injection by excited Re*. These include similarity between TRIR spectra and the spectrum of reduced Re observed by spectroelectrochemistry, the appearance of a guanine radical signal in TRIR spectra, and the eventual formation of permanent guanine oxidation products. The majority of reactivity occurs on the ultrafast time scale, although processes dependent on slower conformational motions of DNA, such as the accumulation of oxidative damage at guanine, are also observed.

The photooxidation activity of this Re complex was compared directly to that of other metallointercalators that have been used previously in our laboratory to oxidize DNA. The complexes $[Rh(phi)_2(bpy')]^{3+}$ (phi = 9,10-phenanthrenequinone diimine; bpy′ = 4-methyl-4′-(butyric acid)-2,2′-bipyridine), $[Ir(ppy)_2(dppz')]^+$ (ppy = 2-phenylpyridine; dppz′ = 6-(dipyrido[3,2-*a*:2′,3′-*c*]phenazin-11-yl)hex-5-ynoic acid), and $[Re(CO)_3(dppz)(py'\text{-}OH)]^+$ (py′-OH = 3-(pyridin-4-yl)-propanoic acid) were each covalently tethered to DNA. Biochemical studies show that upon irradiation, the three complexes oxidize guanine by long-range DNA-mediated CT with the efficiency: Rh > Re > Ir. Comparison of spectra obtained by spectroelectrochemistry after bulk reduction of the free metal complexes with those obtained by transient absorption (TA) spectroscopy of the conjugates suggests that excitation of the conjugates at 355 nm results in the formation of the reduced metal states. Electrochemical experiments and kinetic analysis of the TA decays verify that the primary factors responsible for the trend observed in the guanine oxidation yield of the three complexes are the thermodynamic driving force for CT, variations in the efficiency of back electron transfer, and coupling to DNA.

The ability of redox-active DNA-binding proteins to act as hole sinks in DNA-mediated CT systems was also studied by time-resolved spectroscopy. Such experiments are designed to provide support for the utilization of DNA-mediated CT in biological systems. In studies involving the cell cycle regulator p53, photoexcitation results in the formation of a weak transient band at 405 nm. This band, which is not observed in samples lacking the protein, resembles the primary spectral feature of the tyrosine cation radical. Although the signal is weak and reproducibility is inconsistent, these results suggest that photolysis of the sample leads to DNA-mediated oxidation of tyrosine in p53. Similar experiments were conducted on the transcriptional activator SoxR. Here, the presence of dithionite, required in solution to keep the protein reduced, complicates the photochemistry of the system considerably. Regardless, a weak absorbance at 418 nm that develops following photolysis at 355 nm provides evidence for the DNA-mediated oxidation of the protein. The behavior of the base excision repair protein endonuclease III was also observed in the presence of DNA and metal complex oxidants. In flash-quench studies, addition of the protein results in the formation of a strong negative signal at 410 nm in TA traces. In studies involving direct photooxidation by Rh, Ir, and Re complexes, no new transients are detected upon the addition of protein, but changes in the intensities of the resultant TA spectra and in the steady-state absorbance spectra following photolysis indicate that DNA-mediated oxidation of the protein may be taking place.

The experiments described here comprise several new developments in the story of DNA-mediated CT. First, proof of concept has been given for a valuable new vibrationally-active Re probe. Further modifications on the characteristics of this complex and further study by time-resolved vibrational spectroscopy will allow us to observe DNA-mediated CT with high spectral resolution. Second, comparison between this Re probe and established photooxidants shows that the Re complex is a strong photooxidant in its own right and that this complex can be added to our growing toolbox of CT phototriggers. Third, time-resolved studies involving redox-active proteins have provided preliminary direct evidence for the ability of these proteins to serve as CT probes themselves. Further refinement of the experimental methods used in these experiments will allow us to observe such processes

with greater sensitivity, increasing our knowledge of the mechanism and applications of DNA-mediated CT.

Contents

List of Figures

List of Tables

List of Schemes

Chapter 1

DNA-Mediated Charge Transport*

*Adapted from J. K. Barton, E. D. Olmon, and P. A. Sontz, *Coord. Chem. Rev.* **255**, 619–634 (2011).

1.1 Introduction

Oxidative DNA damage has been implicated in a host of adverse medical conditions including aging, heart disease, and various forms of cancer.[1,2] Reactive oxygen species (ROS) such as singlet oxygen ($^1O_2$), superoxide anion ($O_2^{\bullet -}$), hydrogen peroxide (H_2O_2), and hydroxyl radical ($^{\bullet}OH$) are a constant threat. Exogenous sources of ROS, such as cigarette smoke, air pollution, and ultraviolet radiation, have been linked to the formation of DNA strand breaks and lesions, which can lead to mutagenesis and carcinogenesis.[3,4] The danger of endogenous sources of ROS is also considerable: ROS are byproducts of oxidative respiration in mitochondria; they are produced by macrophages during immune response; and they are generated during P450 metabolism.[5,6] In order to develop diagnostics and therapeutics for the prevention of medical conditions associated with DNA damage, it is necessary to understand the chemical mechanisms which result in oxidative DNA lesions, as well as the biological pathways that exist to prevent and repair them.

Before discussing factors that affect the oxidation of DNA, it is prudent to review the chemical characteristics of the macromolecule itself. DNA consists of long polymeric strands of nucleic acid bases, specifically the planar, aromatic heterocycles adenine (A), guanine (G), thymine (T), and cytosine (C). Pairs of strands are held together by specific hydrogen bonds formed between the nucleobases: A pairs with T, and G pairs with C. Within the strands, the bases are joined by anionic deoxyribophosphate units, which, upon formation of the duplex, wrap the stack of nucleobases in a negatively charged double helix. Consecutive base pairs are stacked closely together, allowing the aromatic π system of one to interact with that of its neighbors. In this way, the stacked aromatic bases resemble stacked sheets of graphite, as illustrated in Figure 1.1 on page 5. In much the same way that electricity can be conducted perpendicular to stacked graphite sheets,[7] DNA can mediate the transmission of charge along its length.

In our laboratory, we have utilized the rich redox chemistry of transition metal complexes in conjunction with the ability of DNA to mediate charge transport (CT) reactions to generate and study oxidative damage in DNA. In the first chapter, we examine the properties of metal complexes that make them ideal probes for initiating and monitoring DNA

CT events. We also discuss the ability of DNA to mediate charge transfer reactions between a charge donor and a charge acceptor, as well as the ability of DNA bases themselves to participate in DNA-mediated redox chemistry. Several biological implications of DNA-mediated CT are also described, including the accumulation of oxidative damage at sites of high guanine content, and the mechanism by which DNA may mediate cellular signaling and transcriptional regulation. In the second chapter, the design, synthesis, and characterization of a new Re photooxidant is described. The properties that make this a useful probe for the study of DNA-mediated CT are discussed. In the third chapter, the use of this new probe in time-resolved infrared spectroscopy experiments is detailed. In these experiments, it was shown that the Re photosensitizer is capable of oxidizing guanine from a distance. The mechanism of this reaction and the factors affecting the yield of guanine oxidation are discussed. In the fourth chapter, the oxidation strength of three DNA-binding metal complex photooxidants is compared directly in biochemical and spectroscopic experiments. Differences in the oxidatizing ability of the three complexes are discussed in terms of their DNA binding strength and redox properties. The fifth chapter outlines the results of time-resolved spectroscopic experiments that have been conducted on a number of redox-active DNA-binding proteins. Successes, failures, and opportunities for future work are discussed.

1.2 Metal Complexes as Probes for DNA-Mediated CT

Metal complexes are powerful initiators and probes of DNA-mediated CT. By varying photophysical properties, redox potentials, and DNA-binding abilities of many metal complexes, as well as the DNA sequences through which charge transport occurs, we have been able to characterize the parameters that govern long range DNA-mediated oxidation and reduction.

1.2.1 Advantages of Metal Complexes in Studies of DNA-Mediated CT

Any study of DNA CT must involve some means of injecting charge onto the DNA bridge and some means of reporting the CT event. Although there is a wide array of molecular probes that can carry out these tasks, the most effective ones share many chemical and physical characteristics. First, in order to utilize the electronic system of the bases as a

conduit for charge, the probe should interact strongly with the DNA base stack. Such an interaction can be difficult to achieve, considering the geometry of DNA. In general, the only access a diffusing molecule has to the base stack is either at the ends of the DNA strand or within the relatively narrow major and minor grooves which run lengthwise along the sides of the DNA molecule. Probes which are too large, or which are strongly negatively charged and therefore are repelled by the phosphate backbone of DNA, do not easily interface with the DNA π-stack. Second, depending on the function of the probe, it must provide a straightforward means of either initiating or reporting on DNA CT, or both. Often, the photophysical or electrochemical properties of a molecule are utilized for these purposes. Some probes may also report CT events through chemical pathways such as degradation. Third, the probe should not degrade or interact chemically with the DNA strand or with other components of the sample unless this is by design. Not only must the probe be stable enough to persist in solution, but the excited state of the molecule must also be stable if photochemical means are used to initiate or report CT, and the various redox states of the molecule must be able to withstand the charge transfer process. Finally, the ideal probe would be synthetically versatile and easy to build or modify in order to control sensitively the parameters of the experiment. Metallointercalators, transition metal complexes which bind DNA primarily by intercalation, are one class of molecules that fulfill all of these requirements.

Intercalation, first reported by Lerman in 1961,[8] is a binding mode in which the ligand, usually a planar, aromatic moiety, slips between two adjacent bases in the DNA base stack. Structural changes in the DNA associated with intercalation include a slight unwinding of the helix at the intercalation site, an extension in length equal to the height of one base pair, and an increase in DNA stability, as indicated by a higher duplex melting temperature. The overall structure of the DNA is unperturbed: no bending or kinking of the helix is observed,[9] and the C2′-endo sugar pucker found at non-intercalation sites is retained.[10] The effect of intercalation on the structure of DNA is shown in Figure 1.2. Intercalators, often large, heterocyclic structures, physically and electronically resemble the DNA bases themselves, so intimate associations may form between the DNA base stack

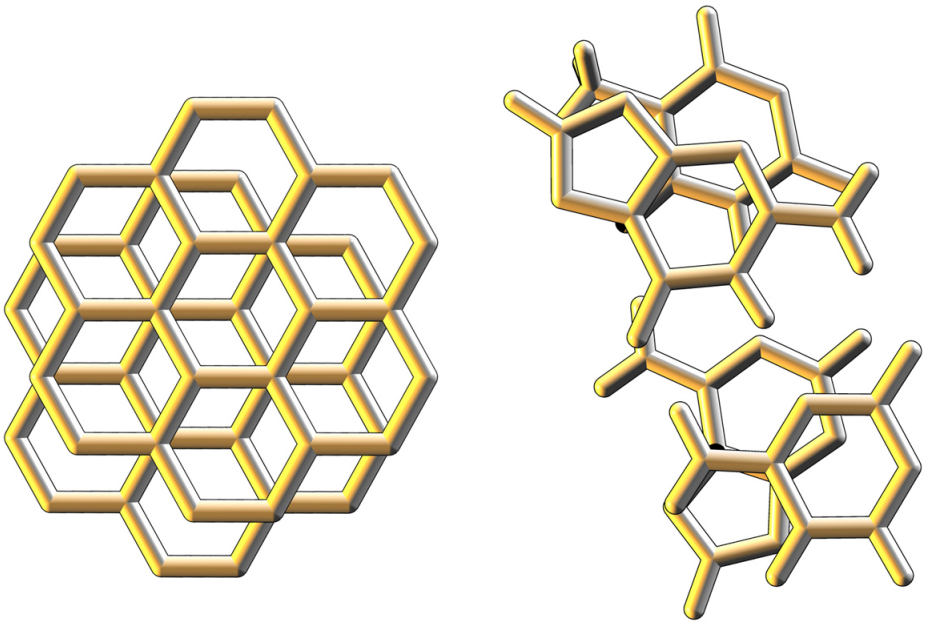

Figure 1.1: The structure and geometry of stacked graphene sheets (left) is similar to that of stacked DNA base pairs (right).

and the binding ligand. In a sense, the intercalating molecule acts as an additional base, enabling strong interactions with the electronic structures of the flanking bases.[10] Many molecules are known to bind DNA through this mode, including the organic intercalating drugs 9-aminoacridine, ethidium, and daunomycin,[9] among others. Many metal complexes, also, may bind DNA through intercalation if they bear one or more planar, aromatic ligands such as phen (1,10-phenanthroline), phi (9,10-phenanthrenequinone diimine), or dppz (dipyrido[3,2-a:2′,3′-c]phenazine). Interestingly, by incorporating a ligand that is slightly wider than DNA, it is possible to selectively target binding at thermodynamically destabilized mismatch sites through the insertion binding mode, where the bulky ligand enters the helix from the minor groove, pushing the mismatched base pair out into the major groove.[11–13] Because insertion involves substitution in the base stack of the inserting ligand for the mismatched base pair, insertion, like intercalation, should facilitate strong electronic interactions between the inserting metal complex and the DNA base stack. Although other DNA binding modes such as electrostatic binding and groove binding have been observed,[14,15] these do not offer the strong electronic coupling to the base stack that is characteristic of intercalation and insertion.

Not only do metallointercalators bind strongly to DNA, but they also possess rich and well understood photochemistry and photophysics, which make them advantageous for use as probes for DNA interactions, as injectors of charge onto the DNA bridge, and as reporters of DNA CT events. Particularly interesting and effective examples are the dppz complexes of ruthenium, which display the "light switch effect".[16] $[Ru(bpy)_2dppz]^{2+}$ and $[Ru(phen)_2dppz]^{2+}$ are not luminescent in aqueous solution due to deactivation of the luminescent state via hydrogen bonding of the dppz ligand with water. However, in solutions containing duplex DNA, the complexes intercalate, the dppz ligand is protected from solution, and luminescence is restored.[16–20] Although most metal complexes do not display this remarkable discrimination, many do luminesce. In addition, many complexes absorb strongly in the visible region due to their intense metal-to-ligand charge transfer (MLCT) and intraligand (IL) charge transfer transitions. These properties allow for manipulation and monitoring of the electronic and redox states of the metal complexes spectroscopically.

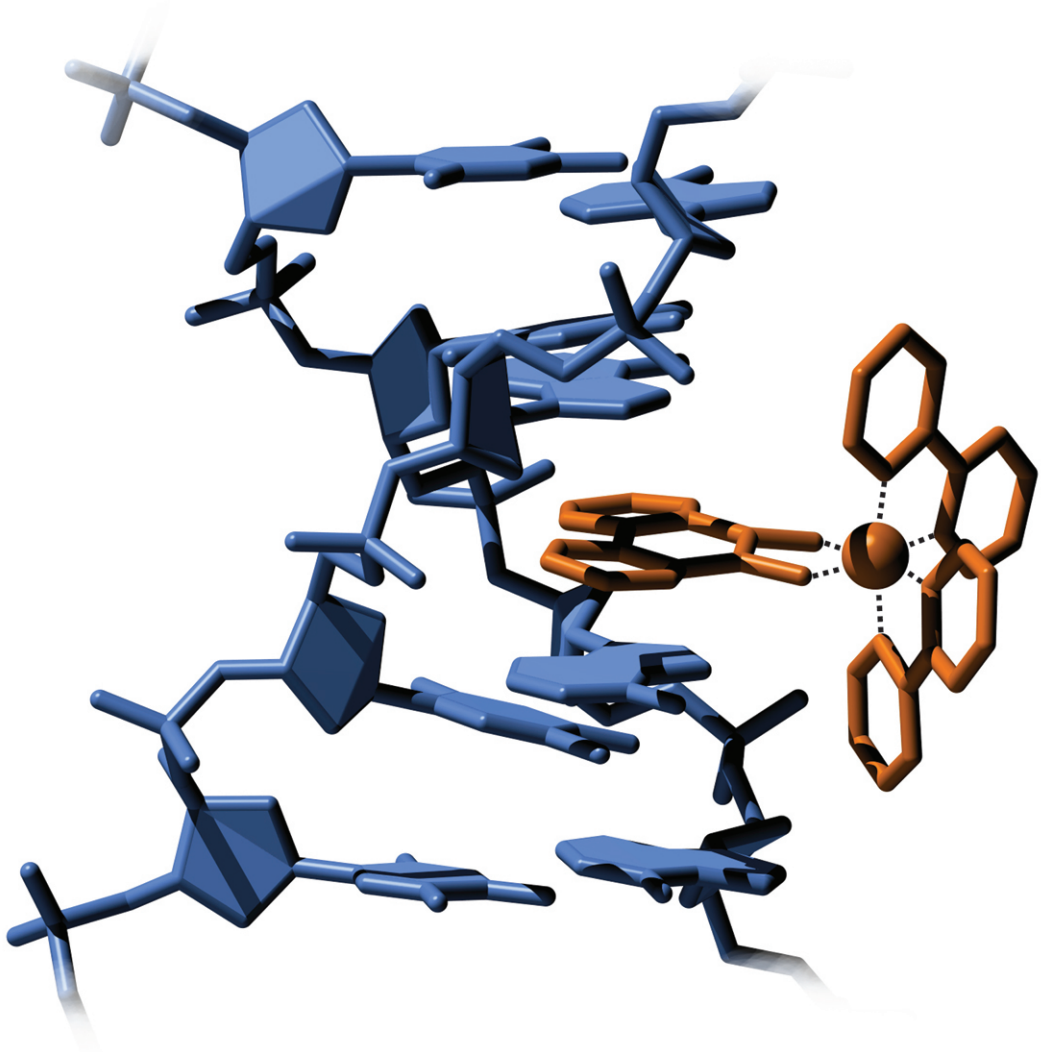

Figure 1.2: Intercalative binding to DNA results in an increase of the rise at the site of binding, as well as a slight unwinding of the helix. Shown is a model of $[Rh(phi)(bpy)_2]^{3+}$ (orange) bound to DNA (blue), adapted from the crystal structure of a similar construct.[11]

The MLCT transitions may also be exploited to initiate CT processes, since many metal complexes become strong oxidizing or reducing agents upon optical excitation. In circumstances under which the excited state of a metal complex cannot carry out the desired chemistry, it may be necessary to utilize the "flash-quench" technique.[21] This method involves the use of a diffusing molecule which is competent to oxidize or reduce the excited metal complex, thus creating a strong ground state oxidant or reductant.

Several other characteristics of metallointercalators make them suitable for studies of DNA-mediated CT. They are coordinatively saturated, substitutionally inert, and rigid, making them extremely stable in solution, and preventing coordination between the metal complexes and DNA. Metallointercalators are also modular. Unlike organic intercalators, the properties of metal complexes can be altered subtly and systematically by adding electron donating or withdrawing group to the constituent ligands, or by using different sets of ligands. In addition, the three-dimensional structure of metallointercalators enables them to interact with DNA in a stereospecific, and sometimes sequence-specific, manner, while organic intercalators, which are often planar, cannot. For example, many studies have shown that Δ complexes tend to bind more tightly to right-handed B-DNA, while Λ complexes have been useful in probing left-handed Z-DNA.[22–30] This result has mainly to do with the steric agreement between the intercalated metal complex and the DNA: the ancillary ligands of Δ complexes tend to lie along the major groove of the DNA helix, whereas those of Λ complexes collide with the phosphate backbone.

The versatility of metallointercalators also facilitates the sensitive tuning of their electronic and electrochemical properties. Complexes have been synthesized that absorb and emit across the visible spectrum and that sample a wide variety of redox potentials. The addition or elimination of a single functional group on either the intercalating ligand or the ancillary ligands can serve to alter the photophysical, electrochemical, or DNA binding properties of the complex. For example, addition of a carboxylic acid or benzyl group to the end of dppz, or introduction of an additional heterocyclic nitrogen, eliminates the light-switch effect and alters the absorption and emission maxima and luminescence lifetime of the complex.[17]

The modularity of metal complexes also makes it possible to extend their functionality by modifying their ancillary ligands. For example, it is possible to create a covalent linkage between a metal complex and DNA through the use of a carboxyalkyl chain.[31,32] Such linkages serve to ensure a binding ratio of unity between the metal complex and the DNA while precisely defining the binding site of the metal, without disrupting the mode of binding or DNA structure. Alkyl chains have also been used to append organic fluorophores to metallointercalators in an effort to develop luminescent reporters of mismatches.[33] Additionally, modification of a ruthenium complexes with octaarginine allows for the facile uptake of these complexes into the nuclei of cancer cells.[34,35] Functionalization of the ancillary ligands may also lead to sequence-selective recognition and cleavage by metallointercalators via hydrogen bonding or van der Waals interactions with modified ethylenediamine ligands,[36–40] peptide sequences,[41–43] or modified phen ligands.[44–47] Functionalization may also confer nuclease activity.[48]

Although many classes of molecules may serve as effective intercalators for the study of DNA-mediated CT, metallointercalators provide several advantages. The array of metal complexes described in this chapter is shown in Scheme 1.1 on page 11. In addition to their inherent stability in solution, they display strong coupling to the DNA base stack. Unlike organic intercalators, the photophysical, electrochemical, and DNA-binding properties of metallointercalators may be tuned in an efficient and systematic manner to modify their properties in sensitive and subtle ways. Finally, the modularity of metal complexes allows for external functionalities to be applied, expanding the utility of these probes.

1.2.2 Metal Complexes as Charge Donors and Acceptors in DNA CT

The first experiment that suggested the possibility of charge transport through the DNA base stack was an investigation of photoinduced electron transfer from $[Ru(phen)_3]^{2+}$ to either $[Co(bpy)_3]^{3+}$, $[Co(phen)_3]^{3+}$, or $[Co(dip)_3]^{3+}$ (dip = 4,7-diphenyl-1,10-phenanthroline).[30] It was found that quenching scaled with the DNA binding affinity of the quencher, and that Δ−$[Ru(phen)_3]^{2+}$ was quenched more efficiently than Λ−$[Ru(phen)_3]^{2+}$. Further, the estimated electron transfer rate was two orders of magnitude faster than the rate ob-

served in the absence of DNA. Although the increase in rate was primarily ascribed to the reduced dimensionality of diffusion at the DNA surface, it was suggested that electron transfer through the π-framework of DNA may play a role.

Evidence for DNA mediation of CT mounted in a study involving electron transfer from excited $[Ru(phen)_3]^{2+*}$ to either $[Co(phen)_3]^{3+}$, $[Rh(phen)_3]^{3+}$, $[Cr(phen)_3]^{3+}$, or $[Co(bpy)_3]^{3+}$.[49] These complexes are known to bind intercalatively in the major groove as well as electrostatically in the minor groove. Upon addition of DNA, luminescence quenching rates for each of these pairs increased. Interestingly, in 90% glycerol solutions at 253 K, where diffusion of all species is restricted, quenching rates were lower than in buffered aqueous solutions at ambient temperature, but they were still higher than the observed quenching rates in the absence of DNA. This result suggests that for these phen complexes, DNA-mediated electron transfer is a major quenching pathway. Nonetheless, with the use of freely diffusing charge donors and acceptors, it was difficult to discern the nature of DNA mediation due to rapid equilibration between binding modes and uncertainty in the distance between donor-acceptor pairs. Further experiments were necessary to establish DNA-mediated CT as an appreciable quenching mechanism.

Due to the larger hydrophobic surface area and further extension from the metal center, the incorporation of dppz allows for stronger DNA binding by intercalation than is allowed by phen. The use of $[Ru(phen)_2dppz]^{2+}$ in electron transfer experiments rather than $[Ru(phen)_3]^{3+}$ made it possible to probe ET events in which the donor was primarily bound by intercalation. Further, because non-intercalated $[Ru(phen)_2dppz]^{2+*}$ is quenched by water on an ultrafast timescale, any luminescence observed originates from the intercalated species. Steady-state and time-resolved emission quenching of $[Ru(phen)_2dppz]^{2+*}$ by either the strongly intercalating $[Rh(phi)_2phen]^{3+}$ or the groove binding $[Ru(NH_3)_6]^{3+}$ were examined.[50] In experiments involving the intercalated quencher, no change in emission rate was observed with increasing amounts of quencher; however, the initial luminescence intensity decreased. This result meant that quenching between the two intercalated species was occurring at rates faster than the instrument could detect. When $[Ru(NH_3)_6]^{3+}$ was used instead as quencher, increasing its concentration yielded an increase in the rate of

DNA Bases

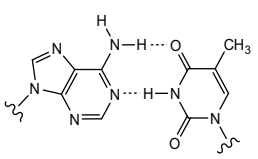

Adenine Thymine

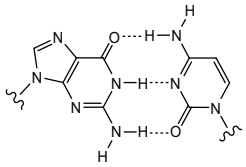

Guanine Cytosine

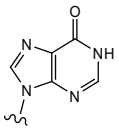

inosine

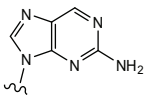

2-aminopurine

Metal Complexes

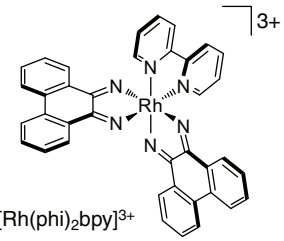

$[Rh(phi)_2bpy]^{3+}$

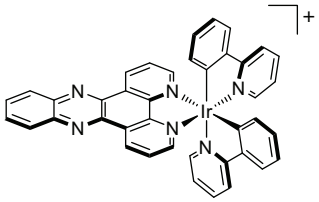

$[Ir(ppy)_2(dppz)]^{+}$

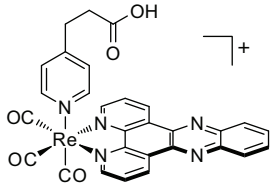

$[Re(CO)_3(dppz)(py')]^{+}$

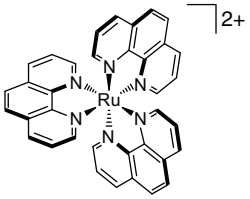

Δ-$[Ru(phen)_3]^{2+}$

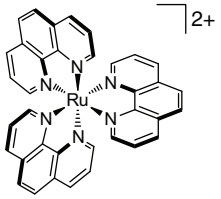

Λ-$[Ru(phen)_3]^{2+}$

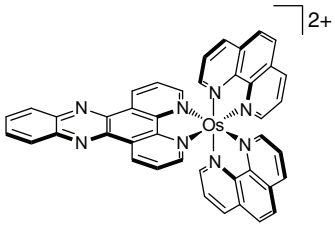

$[Os(phen)_2dppz]^{2+}$

Ligands

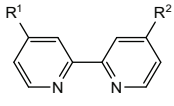

bpy: $R^1 = R^2 = H$

bpy′: $R^1 = CH_3$; R^2 =

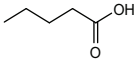

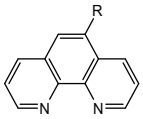

phen: R = H

phen′: R =

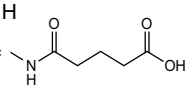

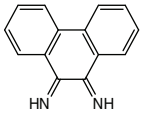

phi

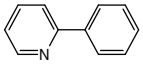

ppy

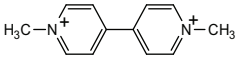

Methyl Viologen

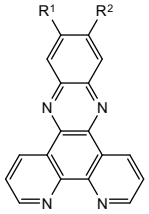

dppz: $R^1 = R^2 = H$

dmp: $R^1 = R^2 = CH_3$

DIP: $R^1 = R^2$ = phenyl

dppz′: $R^1 = H$; R^2 =

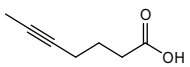

Scheme 1.1: Structures of DNA bases and representative metal complexes used in DNA-CT experiments

luminescence decay but did not alter the initial luminescence yield. These results, in addition to comparisons with results of steady-state emission quenching experiments, showed that quenching by $[Ru(NH_3)_6]^{3+}$ is a dynamic process, while quenching by the intercalated $[Rh(phi)_2phen]^{3+}$ is a static process.

Further mechanistic insight was gained by covalently tethering $[Ru(phen')_2dppz]^{2+}$ as an electron donor and $[Rh(phi)_2(phen')]^{3+}$ as an acceptor (phen′ = 5-amido-glutaric acid-1,10-phenanthroline) to complementary strands of a DNA oligomer,[51] as shown in Figure 1.3 on page 14 (top). The covalent tether was long enough to allow intercalation of the complexes, but short enough to prevent direct contact between them. By covalently attaching the donor and acceptor to opposite ends of the DNA duplex, the possibility for quenching through a diffusive mechanism was abolished, and the donor-acceptor distance was well defined. Excitation of assemblies in which the Ru-tethered strand was hybridized to its unmetallated complement resulted in strong luminescence. Addition of the covalently-tethered Rh complex to the complementary strand, however, resulted in complete quenching. Appropriate controls ensured that the quenching was intraduplex, and the imposed separation between the donor and acceptor precluded quenching by diffusion. These results meant that quenching of $[Ru(phen)_2dppz]^{2+}$ luminescence was occurring from over 35 Å away.

That the mechanism of quenching was in fact electron transfer and not energy transfer was irrefutably established by experiments involving charge donors other than $[Ru(phen)_2dppz]^{2+}$. In one study, the transient absorption of systems containing varying amounts of non-covalent $[Ru(dmp)_2dppz]^{2+}$ (dmp = 4,7-dimetheyl-1,10-phenanthroline) and $[Rh(phi)_2bpy]^{3+}$ with DNA were investigated and compared with the transient spectrum obtained upon oxidative $[Ru(dmp)_2dppz]^{2+*}$ quenching by $[Ru(NH_3)_6]^{3+}$.[52] With increasing amounts of Rh, the luminescence decay lifetimes did not change, but the initial luminescence yield did, again signifying that the quenching in this system involves a static mechanism. The transient spectrum obtained by using the Rh complex as the quencher matched that obtained using $[Ru(NH_3)_6]^{3+}$ as the quencher, positively identifying the transient intermediate in the Rh experiment as the oxidation product, $[Ru(dmp)_2dppz]^{3+}$, and the mechanism of luminescence quenching as electron transfer. In another study,

$[Os(phen)_2dppz]^{2+}$, rather than $[Ru(phen)_2dppz]^{2+}$, was used as the electron donor.[53] The Os complex emits at a higher wavelength, and its emission lifetime (< 10 ns) is several orders of magnitude shorter than that of $[Ru(phen)_2dppz]^{2+}$.[54] Despite these photophysical differences, $[Os(phen)_2dppz]^{2+}$ behaves similarly: it is also a light switch, it binds DNA primarily through intercalation, and quenching by $[Rh(phi)_2bpy]^{3+}$ in the presence of DNA takes place through a static mechanism. Interestingly, the dependence of the quenching yield on the concentration of $[Rh(phi)_2bpy]^{3+}$ is the same between $[Os(phen)_2dppz]^{2+}$ and $[Ru(phen)_2dppz]^{2+}$, so the quenching mechanism is the same despite photophysical and electronic differences. Also, transient spectra obtained upon photoexcitation of $[Os(phen)_2dppz]^{2+}$ in the presence of DNA and $[Rh(phi)_2bpy]^{3+}$ match spectra obtained through oxidative quenching of DNA-bound $[Os(phen)_2dppz]^{2+*}$ by $[Ru(NH_3)_6]^{3+}$ and through direct ground state oxidation of $[Os(phen)_2dppz]^{2+}$ by $[Ce(NO_3)_6]^{2-}$. The agreement between these three spectra indicates that the same oxidized Os species is being formed in each case. In addition, because the emission band of $[Os(phen)_2dppz]^{2+}$ does not overlap with the absorption band of the Rh complex, energy transfer is not a viable quenching pathway. These results together mean that $[Os(phen)_2dppz]^{2+*}$ and $[Ru(phen)_2dppz]^{2+*}$ are both quenched almost exclusively by $[Rh(phi)_2bpy]^{3+}$ through DNA-mediated electron transfer.

Incidentally, $[Ru(phen)_2dppz]^{2+}$ was not the complex used to identify the intermediate involved in DNA-mediated electron transfer because no long-lived transient that could be ascribed to Ru(III) was ever observed spectroscopically in mixed-sequence DNA. As was speculated and later confirmed, this was because the Ru(III) intermediate was a strong enough oxidant to oxidize the guanine bases within the DNA strand and was depleted as soon as it formed. This property was later utilized to great effect to gain a better understanding of the DNA CT process by oxidizing the bases of DNA directly.

1.2.3 Long-Range Oxidation of DNA

1.2.3.1 Characteristics of bases and base analogues

For metallointercalators of sufficiently high redox potential, the DNA bases themselves may serve as partners in charge transfer reactions. The redox potentials of the base nucleosides

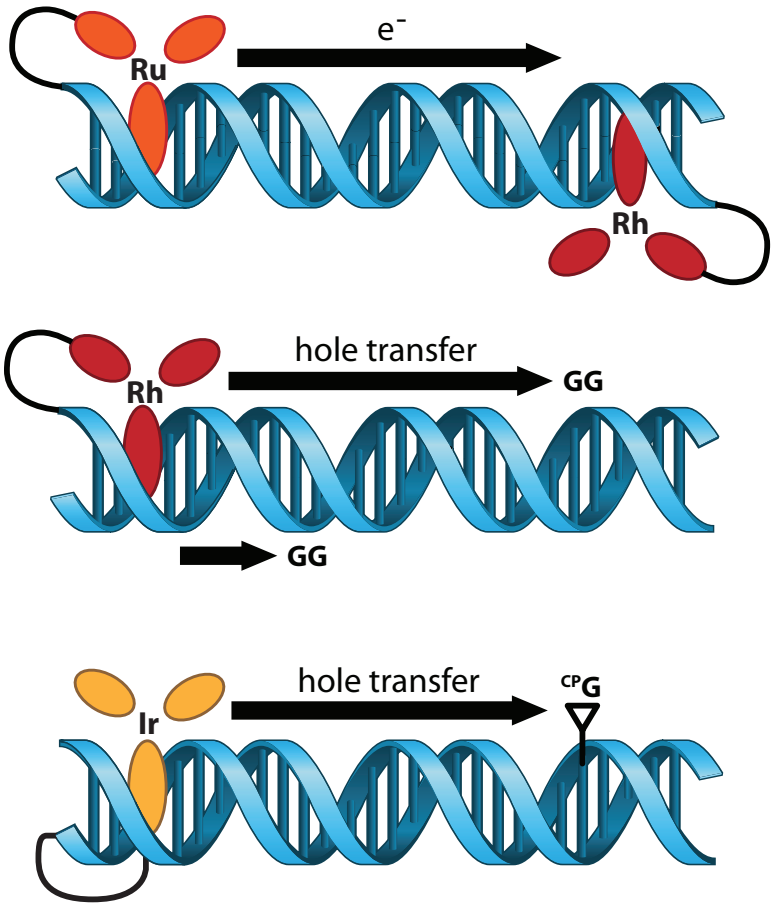

Figure 1.3: Metal complex-DNA conjugates used to study DNA-mediated CT. Top: covalent tethering of $[Ru(phen')_2(dppz)]^{2+}$ and $[Rh(phi)_2(phen')]^{3+}$ to complementary DNA strands enables the study of DNA-mediated CT over large distances. Middle: DNA-bound $[Rh(phi)_2(bpy')]^{3+}$ is competent to oxidize 5′-GG-3′ sites from the excited state. Bottom: cyclopropylamine traps enable the fast capture of a charge as it travels along the DNA bridge following excitation of tethered $[Ir(ppy)_2(dppz')]^{+}$.

increase in the order: G (1.29 V vs. NHE) < A (1.42 V) < T (1.6 V) < C (1.7 V).[55] Therefore, a metal complex such as $[Ru(phen)_2dppz]^{3+}$ [$E^{\circ}(3+/2+) = 1.63$ V vs. NHE] or excited $[Rh(phi)_2bpy]^{3+*}$ [$E^{\circ}(3+^*/2+) \approx 2.0$ V vs. NHE][50] should be competent to oxidize some or all of the bases. Interestingly, within the DNA base stack, the propensity for electron transfer to occur from a particular base is influenced by electronic interactions with its neighbors. For example, *ab initio* molecular orbital calculations have predicted that the electron donating ability of guanine should increase as: 5′-GT-3′, 5′-GC-3′ ≪ 5′-GA-3′ < 5′-GG-3′ < 5′-GGG-3′.[56] Further, the HOMO of the 5′-GG-3′ doublet is calculated to lie primarily on the 5′-G, indicating that the 5′-G site should be preferentially oxidized at guanine doublets, as has been observed experimentally. The relative ease with which guanine, guanine doublets, and guanine triplets are oxidized leads to biological implications: given a random sequence of bases, regions of high guanine content are the most likely places to find large amounts of oxidative damage.

The use of non-natural base analogues further extends the ability to exploit the intimate interactions between bases in the study of DNA CT. Many base analogues only slightly perturb the geometry and energetic structure of the base stack and interact in a natural way with the other bases, becoming part of the base stack and sometimes forming hydrogen bonds with natural bases. Base analogues provide advantageous functions for the study of DNA CT. For example, 2-aminopurine is fluorescent and pairs with thymine; and inosine, which shares a strong resemblance with guanine, nevertheless has a significantly higher oxidation potential (1.5 V vs. NHE).[57] Bases that are modified by a cyclopropylamino group in the major groove serve as sensitive indicators of charge occupation. The properties of natural bases, non-natural base analogues, and cyclopropylamine-modified bases, can be exploited for the study of DNA CT.

1.2.3.2 Oxidation of Guanine by a Metallointercalator

Direct proof of guanine oxidation by a ruthenium intercalator was obtained in a study involving $[Ru(phen)_2dppz]^{2+}$, DNA, and a variety of oxidative luminescence quenchers.[58] The quenchers used in the study, $[Ru(NH_3)_6]^{3+}$, methyl viologen (MV^{2+}), and $[Co(NH_3)_5Cl]^{2+}$,

associate with DNA through groove binding and quench $[Ru(phen)_2dppz]^{2+*}$ dynamically on the nanosecond timescale.[50] The study was an application of the flash-quench technique,[21] shown in Scheme 1.2 on page 17: following photoexcitation of the intercalated complex, oxidative quenching by a diffusible molecule creates the strong ground-state oxidant $[Ru(phen)_2dppz]^{3+}$ *in situ*, which then proceeds to oxidize guanine. The reaction may be interrupted by any of several processes, including depopulation of the $[Ru(phen)_2dppz]^{2+*}$ excited state through luminescence, reduction of the Ru(III) oxidized species by back electron transfer (BET) from the reduced quencher, or guanine cation radical neutralization by the reduced quencher. In the absence of these deactivation pathways, the guanine radical may react with O_2 or H_2O, forming permanent oxidation products.

In transient absorption experiments, the microsecond decay of a long-lived transient indicated formation of the oxidized ruthenium species in the presence of poly(dA-dT). In poly(dG-dC), no long-lived intermediate attributable to Ru(III) was observed; instead, a new transient species appeared on the timescale of Ru(II)* emission decay. This new transient was assigned to the neutral guanine radical, and its spectrum matched that previously observed by pulse radiolysis.[59]

The yield of oxidized guanine product formation was then studied by gel electrophoresis. $[Ru(phen)_2dppz]^{2+}$ was irradiated at 436 nm in the presence of 18 base pair DNA duplexes containing guanine doublets or triplets and a quencher. Following radiolabeling and treatment with aqueous piperidine, which cleaves DNA at sites of guanine damage, the cleaved strands were separated by polyacrylamide gel electrophoresis and imaged by phosphorimagery. Damage occurred primarily at the 5′-G in duplexes containing 5′-GG-3′ doublets, although small amounts of damage also occurred at single G sites, while strands incorporating both a 5′-GG-3′ and a 5′-GGG-3′ triplet exhibited damage mainly at the 5′-G of the triplet. Damage products were analyzed by enzymatic digestion followed by HPLC. Comparison with an authentic sample identified the major product as 7,8-dihydro-8-oxo-2′-deoxyguanosine (8-oxo-dG), the primary oxidative base lesion found within the cell.[60]

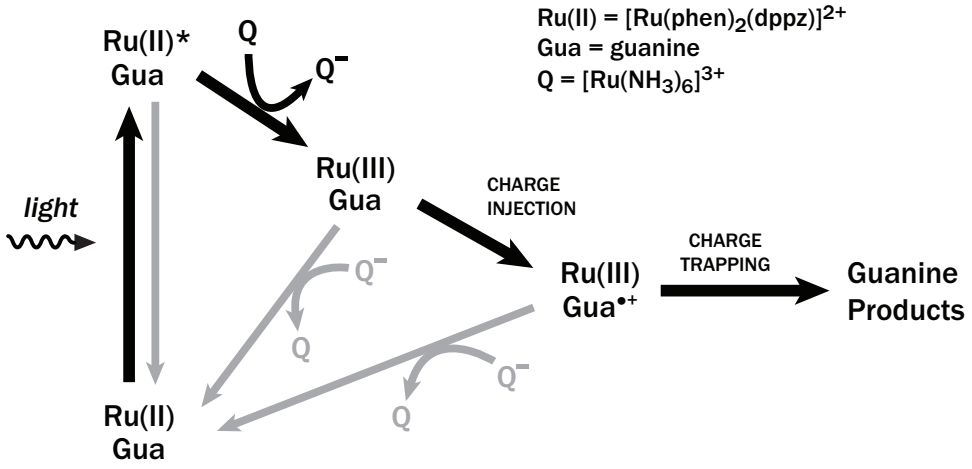

Scheme 1.2: The flash-quench technique. Following photoexcitation, Ru(II)* is oxidized by a diffusing quencher to form the powerful ground state oxidant Ru(III). Charge injection results on charge localization at guanine (Gua). Trapping by reaction of this radical with H_2O or O_2 results in charge trapping and the formation of permanent products. Several BET pathways ($Q^- \rightarrow Q$) lower the efficiency of formation of guanine damage products.

1.2.3.3 Guanine Oxidation Over Long Distances

Studies of guanine oxidation were also carried out in systems containing metal-DNA conjugates. In one notable experiment, $[Rh(phi)_2(bpy')]^{3+}$ [bpy′ = 4-methyl-4′-(butyric acid)-2,2′-bipyridine] was tethered to the end of a DNA 15-mer containing two 5′-GG-3′ doublets: one 17 Å away from the Rh binding site (proximal), and one 34 Å away from the binding site (distal).[61] Such a construct is shown in Figure 1.3 on page 14 (center). Rhodium complexes such as these serve as potent photooxidants when irradiated by 365 nm light, but promote direct strand cleavage at the site of intercalation when irradiated at 313 nm. When the conjugates were irradiated with 313 nm light, damage was only observed at the expected Rh binding site, three bases in from the end of the duplex. Upon excitation of the tethered complex with 365 nm light, guanine oxidation was observed primarily at the 5′-G of both 5′-GG-3′ doublets. While the irradiation experiment at 313 nm supported an intraduplex reaction, confirmation that the reaction was intraduplex was obtained in a mixed labeling experiment (Figure 1.4). Rhodium-DNA conjugates that were not radioactively tagged were mixed with DNA oligomers of the same sequence that were labeled but did not contain tethered Rh. Irradiation at 360 nm and subsequent piperidine treatment showed no damage to the DNA. Thus, in the Rh-tethered and labeled samples, oxidative damage was seen at distances of 17 Å and 34 Å from the bound Rh. This long-range damage was mediated by DNA.

Interestingly, very little difference was observed in the damage yields between distal and proximal 5′-GG-3′ sites in these experiments, meaning that radical delocalization and equilibration occurs more quickly than radical trapping and formation of permanent oxidation products. This suggests that the distance dependence of DNA CT is quite low. In addition, guanine oxidation yields in conjugates containing the Δ isomer were higher than in those containing the Λ isomer, indicating that the efficiency of guanine damage is dependent on the interaction of the photooxidant with the base stack. Incorporation of a 5′-GGG-3′ far from the binding site led to oxidation primarily of the 5′-G of the triplet, 37 Å away from the intercalated Rh complex. Similar damage patterns were observed with the use of $[Ru(phen)(bpy')(Me_2dppz)]^{2+}$ (Me_2dppz = 9,10-dimethyl-dipyrido[3,2-a:2′,3′-c]phenazine)

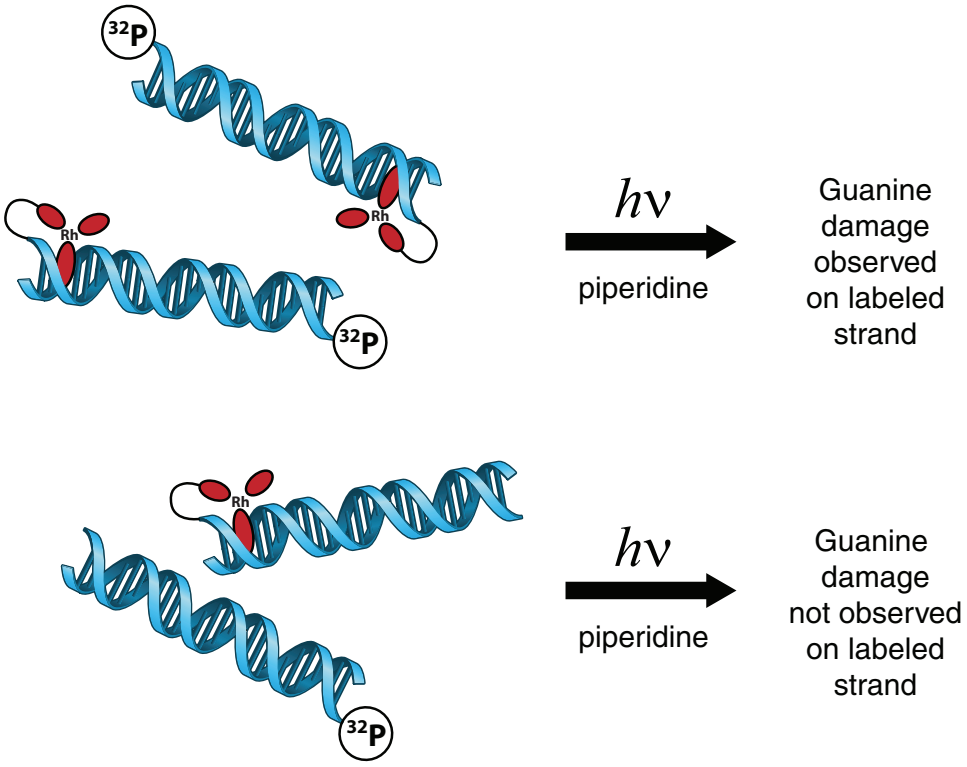

Figure 1.4: DNA-mediated oxidation is an intraduplex process. Top: guanine damage is observed by PAGE following irradiation and piperidine treatment of photooxidant-DNA conjugates that contain a ^{32}P label. Bottom: no guanine damage is observed following the irradiation and piperidine treatment of mixtures which contain unlabeled photooxidant-DNA conjugates and labeled DNA that has no photooxidant bound.

and the flash-quench reaction.[62] Interestingly, when only guanine singlets (no 5′-GG-3′ doublets) are incorporated into the base sequence, equal damage is observed at each guanine site, again suggesting that in the absence of a unique low energy site, charge migration and equilibration to sites of low oxidation potential occur at a faster rate than hole trapping.

Because oxidation yields at 5′-GG-3′ sites showed little variation with charge transfer distance over 11 base pairs, it was necessary to extend the length of the DNA to gain a better understanding of the distance dependence. To this end, a series of 28 base-pair duplexes were prepared with tethered $[Rh(phi)_2(bpy')]^{3+}$.[63] Each duplex in the series contained two 5′-GG-3′ sites that were separated from one another by increments of two base pairs, so that the distance between 5′-GG-3′ sites spanned a range from 41 to 75 Å. Upon irradiation, damage occurred at both sites, but the distal site consistently showed more damage than the proximal site. The ratio of damage between the distal and proximal sites decreased only slightly and fairly linearly over the distances measured. Because the 5′-GG-3′ sites were separated by increments of only two base pairs (6.8 Å, or one-fifth of a turn in the helix), any helical phasing effects on the relative damage yields could be ruled out. In order to test the effects of CT over even greater distances, 63 base-pair DNA duplexes containing six well-separated 5′-GG-3′ sites along their length and a tethered photooxidant (either $[Ru(phen)(bpy')dppz]^{2+}$ or $[Rh(phi)_2(bpy')]^{3+}$) were constructed by ligating smaller strands together. Irradiation of the ruthenated duplex by 436 nm light in the presence of MV^{2+} resulted in damage at the 5′ guanine of each doublet with a small diminution in oxidation with distance, showing that facile DNA-mediated oxidation can occur over 197 Å. The same experiment, carried out using the Rh-tethered duplex, yielded similar results. In these longer duplexes, damage yields decreased somewhat at longer distances, and this effect was more severe for ruthenium than for rhodium. The differences in damage yield at long distances were attributed to the ability of the flash-quench system to promote BET, differences in the extent of electronic coupling between the donor and the base stack in the two systems, and differences in the redox potentials of the donors. Interestingly, the damage yield ratio between distal and proximal sites increased dramatically with temperature, suggesting that higher temperatures facilitate charge equilibration along the length of the duplex.

In the 28 base-pair duplexes, replacement of a G·C base pair by a T·A base pair in the base sequence intervening between the two guanine doublets decreased the ratio of distal to proximal guanine damage by 38%.[63] This effect was more rigorously examined in subsequent work. Duplexes were constructed in which two guanine doublets were separated by increasing lengths of A- and T-containing sequences.[64] Photoexcitation of a tethered $[Rh(phi)_2(bpy')]^{3+}$ complex resulted in large differences in the ratio of distal to proximal oxidative damage. Sequences that showed the lowest ratio contained 5′-TATA-3′ sequences intervening between the guanine doublets, while those showing the highest ratio contained only adenine. Interestingly, when the number of thymine bases intervening between guanine doublets was increased from two to ten by increments of two, damage ratios were 0.9, 1.2, 2.2, and 0.4, respectively. These results illustrate that factors such as DNA conformation, energetics, and base dynamics, in addition to distance, affect the efficiency of CT.

Mismatches intervening between two guanine doublets also affect the distal-to-proximal damage ratio, although in a manner that is not intuitive. When each of the sixteen possible combinations of matched and mismatched base pairs were incorporated between two guanine doublets, the highest distal/proximal damage ratio was observed for the C·G matched pair (2.05), while the A·T matched pair showed the third lowest ratio (0.23), after the T·C (0.15) and T·T (0.19) mismatches.[65] The observed differences in damage ratios did not correlate with the duplex stability, the thermodynamic stability of the mismatches, or the redox potential of the mismatched base. While there was a reasonable correlation with the free energies of helix destabilization of the mismatches, the best qualitative agreement was with base pair lifetimes based on imino proton exchange rates between mismatched bases, as measured by ^{1}H NMR.

From these studies, it is apparent that many factors affect the yield of oxidative damage in DNA. Although shorter strands show little dependence on distance, damage yields are lower at longer distances in longer strands. Changes in the sequence intervening between two guanine doublets have a strong effect on the relative damage observed at the two sites, indicating that small changes in local conformation may disrupt the base stack locally, and that dynamic destacking at mismatch sites is sufficient to decrease severely

the amount of damage further down the strand. The observed temperature dependence in long strands is also an indication of the major role that dynamic motions in DNA play in facilitating CT, since higher temperatures allow the DNA to sample more conformational states within the lifetime of the radical. Finally, differences in damage yields depending on the oxidant used indicate that the ability of the oxidant to couple electronically to the base stack and the propensity for BET strongly affect the efficiency of long-range DNA CT. These experiments involving metal complexes, as well as experiments involving organic oxidants such as ethidium,[66–69] anthraquinone,[70] or thionine[71] and base analogues such as 1,N^6-ethenoadenine[57] and 2-aminopurine[72–74] have shown that long-range DNA oxidation is a general phenomenon.

1.2.4 Fast Charge Trapping to Monitor Charge Occupancy on the DNA Bridge

Traditionally, models for DNA CT (see Genereux and Barton[75] for a recent review) have fallen into two basic categories. The first is superexchange, in which the charge moves from the donor to the acceptor in a single coherent step, tunneling through an intermediating bridge. The second is localized hopping, in which the charge moves from base to base along the bridge, briefly occupying each site. These two models were refined as more sophisticated measurements of DNA-mediate CT were conceived and conducted. For example, during hole transport, simple hopping models predict hopping to occur between guanine sites, since they are lowest in energy. The observed charge occupation on bridging adenine led to the development of thermally assisted hopping models that resolve this inconsistency. Similarly, the influences of other bases and the solvation environment were included in even more complex polaron hopping models.

The guanine base, however, is a poor radical trap. The lifetime of a neutral guanine radical in DNA is greater than one millisecond,[58] and on that timescale, the electron can migrate extensively and equilibrate throughout the DNA duplex. In order to gain mechanistic insight into the process of DNA-mediated CT, cyclopropylamine-modified bases, which report on short-lived charge occupancy at specific sites in DNA, were incor-

porated into various sequence contexts. As illustrated in Scheme 1.3 on page 28, these modified bases, N^2-cyclopropylguanine (^{CP}G),[76] N^6-cyclopropylcytosine (^{CP}C),[77] and N^6-cyclopropyladenine (^{CP}A),[78] contain cyclopropyl groups that undergo a rapid ring-opening reaction upon oxidation. The rates of ring-opening are on the order of 10^{11} s^{-1}, as suggested by comparison with similar molecules,[79,80] making this reaction competitive with BET in most contexts. Further, the oxidation potentials, base pairing characteristics, and stacking properties of cyclopropyl-substituted bases are expected to be similar to those of the unmodified bases.[76,77,81]

Our first studies of DNA CT to ^{CP}G involved the use of photoexcited 2-aminopurine (Ap*) as the oxidant.[82] This analogue base-pairs with thymine and is well stacked in the DNA duplex. In addition, the CT process can be followed by monitoring quenching of Ap* fluorescence by guanine. In duplexes containing ^{CP}G, increasing temperatures caused an increase in the yield of ring-opened product until the melting temperature of the duplex was reached, at which point duplex stacking was lost and almost no product was formed. The same experiment, using free Ap* rather than Ap incorporated into the base stack, showed no temperature dependence, indicating that temperature only affects the CT process, not the trapping process. This increase in ring-opening yield with increasing temperature suggests that DNA CT is a dynamic process that is facilitated by the motion of the bases. In order to study the distance dependence of ^{CP}G ring-opening yield, several strands were synthesized in which adenine bridges of increasing length were incorporated between Ap and ^{CP}G. Surprisingly, the quenching data showed a reproducible nonmonotonic periodicity in the distance dependence. In addition, little damage was observed for sequences in which the Ap and ^{CP}G were neighbors, or were separated by one intervening base pair.[81] These observations suggest that charge delocalization among small, transient, well-stacked groups of bases facilitates charge transfer, and that at short distances, BET is kinetically favored over ring-opening. To accommodate these observations, a new model for DNA CT was proposed that involves conformationally gated hopping between well-stacked domains of delocalized charge.

This model was verified in further studies involving ^{CP}C oxidized by $[Rh(phi)_2(bpy')]^{3+}$.

When ^{CP}C was incorporated into strands 4–7 base pairs away from the tethered Rh complex, efficient ring-opening was observed upon photoexcitation, signifying that there must be some hole occupancy on cytosine during DNA CT, despite its high oxidation potential.[77] Interestingly, when ^{CP}G was incorporated at the site neighboring ^{CP}C, damage yields between the two traps were comparable, but when the distance between the ^{CP}C and the ^{CP}G traps was increased, the decomposition yield of the distal ^{CP}G decreased by a factor of two.[83] By examining ^{CP}C damage yields in various sequence contexts, the effects of neighboring bases were investigated further. In these studies, ^{CP}C decomposition depended not only on the sequence of bases intervening between the photooxidant and the hole trap, but also on the sequence distal to the hole trap. These results suggest that dynamic hole distribution on the DNA bridge is not just a function of the energies of the individual bases, and that some charge delocalization among the orbitals of neighboring bases must occur. Interestingly, while non-covalent $[Rh(phi)_2bpy]^{3+}$ is competent to oxidize both traps, non-covalent $[Ru(phen)(dppz)(bpy')]^{2+}$ in the presence of $[Ru(NH_3)_6]^{3+}$ does not show appreciable oxidation of ^{CP}C. This difference is consistent with the redox potentials of the two metal complexes.

The distance dependence of DNA CT was further studied by analyzing the decomposition yields of ^{CP}A and ^{CP}G within A tracts. Interestingly, when ^{CP}A was incorporated serially at each position along a 14 base pair A tract, very little change in decomposition was observed with distance following irradiation of the tethered $[Rh(phi)_2(bpy')]^{3+}$ photooxidant.[84] When ^{CP}G was incorporated at each position, however, the distance-dependent periodicity previously observed in 2-aminopurine studies was reproduced with the same apparent period, regardless of whether a $[Rh(phi)_2(bpy')]^{3+}$, anthraquinone, or Ap photooxidant was used.[85] Although this periodicity was similar to that observed earlier using an Ap* fluorescence quenching assay, the plots of damage yield versus distance obtained from the fluorescence quenching assay and the ^{CP}G assay were slightly different. These differences were explained recently: due to the nature of the assay, fluorescence quenching informs on the yield of single-step CT, while the ring-opening assay informs on total CT; therefore, any difference between the two is the yield of multistep CT.[86] At a distance of

8–9 bp, the yields obtained by Ap* fluorescence quenching and ^{CP}G ring-opening are equal, signifying that at this distance (27–30 Å), coherent transport takes place.

The ability of cyclopropyl traps to report on charge occupancy at various positions on the DNA bridge has allowed us to determine the relative influence of the various factors affecting the efficiency of DNA CT. Consistently and within a range of experiments, the ring-opening yield of the traps was observed to vary with distance, temperature, sequence context, and the redox potential of the donor. These observations support a model for DNA CT that consists of conformationally gated hopping of delocalized charge.

1.2.5 Comparing Long-Range DNA-Mediated Hole and Electron Transport with a Single Probe

Although the body of literature concerning DNA-mediated hole transport (HT) is quite extensive, complementary studies of DNA-mediated electron transport (ET) are relatively sparse. Our laboratory has extensively studied DNA-mediated ET using DNA-modified electrodes on gold.[87–93] While these experiments are interesting for many reasons, perhaps the most important question regarding DNA-mediated ET is whether the mechanism of this process differs in any way from that of DNA-mediated HT. Unfortunately, ET rates in these electrochemical constructs are limited by slow transfer through the thiol linker that connects the DNA to the gold surface.[94] Complexes such as $[(mes)_2Pt(dppz)]^{2+}$, which have been used both to oxidize ^{CP}G and to reduce ^{CP}C, are promising probes for solution state studies of DNA HT and ET, but these complexes are difficult to tether to DNA, making comparative studies of the distance dependence of HT and ET untenable.[95]

To this end, our laboratory has developed an iridium complex that is amenable to functionalization and acts as both a photooxidant and a photoreductant in the presence of DNA.[96] The complex, $[Ir(ppy)_2(dppz')]^+$ (ppy = 2-phenylpyridine), contains a dppz ligand modified with a carboxylic acid functionality that enables covalent tethering of the complex to the 5′ end of a DNA single strand via a C_6 alkyl chain. We envisage the intercalation of this complex as though the dppz ligand were threaded through the DNA, with the tether on one side of the duplex and the metal center and ancillary ligands on the other. Such

a binding mode could easily be achieved during annealing of the DNA single strands to create the duplex. The excited state oxidation and reduction potentials of the complex are estimated to be 1.7 and -0.9 V vs. NHE, respectively, indicating that it is competent for both oxidative HT to guanine and reductive ET to thymine or cytosine. Because this single complex can be used to probe both DNA HT and DNA ET, the mechanisms and efficiencies of these processes can be directly compared in the same duplex.

We conducted these studies by taking advantage of the fast ring-opening kinetics of cyclopropylamine-modified nucleobases. When non-covalent Ir complex was added to duplexes containing ^{CP}G, only ten minutes of irradiation were needed to achieve complete degradation of the CP rings. The reaction was less efficient in the case of ^{CP}C: after twenty minutes of irradiation, the yield of ring opening was 86%.[96] The mechanism of ^{CP}G ring-opening in this construct is oxidative, while that of ^{CP}C ring-opening is reductive. If the ^{CP}C ring-opening reaction were to occur by an oxidative mechanism, substitution of inosine for guanine opposite ^{CP}C should result in more efficient damage due to the decreased competition for holes. This effect was not observed. Further experiments involving covalently tethered Ir-DNA conjugates support these observations.[97] When ^{CP}G was incorporated into an adenine tract several bases away from the Ir complex intercalation site, the ^{CP}G ring-opening yield after one hour of irradiation was 46%. When ^{CP}C was incorporated into the duplex at the same site, the ring-opening yields were 31% when ^{CP}C was base paired with inosine and only 10% when ^{CP}C was base paired with guanine. These results suggest that within an adenine tract, ^{CP}C decomposition is an oxidative process, and that HT through an adenine tract is preferred over ET. When the modified bases were incorporated into thymine tracts instead, the results turned out differently. In these duplexes, the ^{CP}G ring-opening yield was very similar: 55% after one hour of irradiation. However, the ring-opening yields for ^{CP}C embedded within thymine tracts were much lower. The yields were 5% when ^{CP}C was paired with guanine and only 2% when ^{CP}C was paired with inosine. In this case, the yield was lower for the inosine-containing duplex, suggesting that ^{CP}C had been reduced and that ET is the preferred mechanism of charge transport through pyrimidines. Thus, the mechanism of ^{CP}C ring-opening depends strongly on the sequence context.

By systematically varying the distance between the intercalation site of the tethered Ir complex and the electron or hole acceptor in these assemblies, it is possible to compare the distance dependences of hole and electron transport directly, from the same probe and within the same sequence context. Experiments of this type were carried out utilizing ^{CP}A as a kinetically fast hole trap and 5-bromouridine (^{Br}U) as a fast, irreversible electron trap.[98] In order to reduce ^{Br}U, excited Ir was first reduced by ascorbate via the flash-quench technique. The distance dependence of each process was characterized by the parameter β, which serves as a proxy for the resistivity of the sequence and is a measure of the exponential decay in CT yield with distance. For HT, $\beta = 0.05$, while for ET, $\beta = 0.10$ or 0.12, depending on whether ^{Br}U was embedded within an adenine tract or a thymine tract, respectively. The shallow distance dependence observed in both cases suggests that HT and ET occur by similar mechanisms. Importantly, the amount of attenuation in CT yield upon the incorporation of a mismatch or abasic site at the position in the bridge neighboring the CT trap was identical for the ^{CP}A and ^{Br}U strands, indicating that successful charge migration along the duplex is less strongly affected by a change in the redox potential of the bridge than it is by perturbations in base stacking.

The ability of $[Ir(ppy)_2(dppz')]^+$ to participate in both electron and hole transfer within DNA allows for a two-step CT process, dubbed the "ping-pong" reaction, shown in Figure 1.5 on page 31. In this reaction, the complex is first reduced by DNA-mediated HT, then subsequently reoxidized by DNA-mediated ET, following a single photoexcitation event. The ping-pong reaction was utilized in a series of experiments involving HT to ^{CP}A followed by ET to either ^{Br}U or ^{CP}C, in order to understand more fully the similarities and differences between DNA HT and ET.[99] In one experiment, the distance between the ^{CP}A and the Ir binding site was increased while the distance between the ^{Br}U and the Ir binding site remained the same. As the ^{CP}A was moved further from the Ir binding site, both the ^{CP}A ring-opening yield and the ^{Br}U decomposition yield decreased, but the ratio of the decomposition yield to the ring-opening yield remained at about 40%. Importantly, very little ^{Br}U decomposition was observed in the absence of either ^{CP}A or the Ir complex. Strikingly, when ^{CP}C was substituted for ^{Br}U, ^{CP}C ring-opening was stoichiometric with

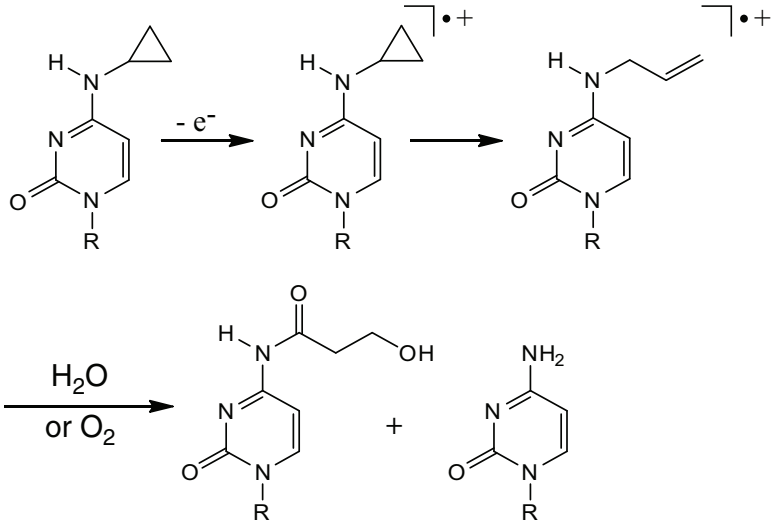

Scheme 1.3: The ^{CP}C ring-opening mechanism

^{CP}A ring-opening even though ^{CP}A and ^{CP}C ring-opening yields decreased as the ^{CP}A distance increased. Base pairing ^{CP}C with inosine rather than guanine had no effect, suggesting that ^{CP}C is opened reductively in this sequence context. These results show that the ping-pong reaction is generalizable and very efficient. Importantly, by using a single probe to trigger both HT and ET under the same experimental conditions, we have shown that the two mechanisms have similar characteristics, and that DNA CT, whether reductive or oxidative, is a general reporter for the integrity of the DNA base stack.

1.3 DNA Charge Transport in a Biological Context

Given the remarkable ability of DNA to mediate CT reactions over long molecular distances and the exquisite sensitivity of this process to perturbations in the base stack, we have begun to explore the biological implications of this chemistry. Below, we consider several cellular processes in which DNA-mediated CT may be utilized, including funneling of damage to particular sites of the genome and the participation of metalloproteins in DNA-mediated redox chemistry.

1.3.1 Generation of Mitochondrial DNA Mutations

DNA-mediated CT experiments have revealed that one-electron oxidation reactions, initiated using covalently tethered or intercalative metal complexes, can occur over distances as large as 200 Å.[63] This observation suggests that DNA CT can act in a physiological context, where CT over such long molecular distances may serve as a strategy to protect the genome from incessant oxidative stress. Experimental observations are in line with this proposal. Using ligation-mediated PCR to identify lesions, we have utilized $[Rh(phi)_2(bpy)]^{3+}$ to probe DNA CT in nuclei isolated from HeLa cells. The patterns of oxidative damage observed in this system are the same as those observed for guanine oxidation by $[Rh(phi)_2(bpy)]^{3+}$ *in vitro*; damage occurs at the 5′-G of 5′-GG-3′ sites. This result suggests that guanine oxidation occurs via DNA-mediated CT even in the presence of constitutively bound proteins.[56,100]

Hallmarks of DNA-mediated oxidation are observed in other cellular environments

such as mitochondria. These organelles contain their own DNA (mtDNA), making them particularly interesting systems in which to examine the possibility of DNA-mediated CT *in vivo*. Such experiments were carried out using mitochonria from HeLa cells. Oxidative damage was introduced by incubating HeLa cells with $[Rh(phi)_2(bpy)]^{3+}$, which is readily absorbed, and then irradiating them.[101] Sites of DNA-mediated oxidation were revealed by a primer extension assay. Base oxidation resulting from DNA-mediated hole migration was observed primarily in conserved sequence block II of mtDNA, a critical regulatory element involved in DNA replication.[102–104] Mutations within this region of mtDNA are associated with tumor formation and other disease conditions.[105]

Remarkably, sites of oxidation within the mitochondria occur as far as 70 bases from the intercalated metal complex, suggesting that DNA-mediated CT plays a role in the regulation of oxidative damage in mtDNA.[102] Conserved sequence block II, which contains seven consecutive guanines, is a site of very low oxidation potential, and could therefore act as a sink for lesions such as 8-oxo-dG.[100] Presumably, funneling damage to this region via DNA-mediated CT halts replication of a damaged mitochondrial genome, preventing the propagation of genetic errors (Figure 1.6). Nevertheless, replication of DNA containing lesions ultimately leads to mutations within conserved sequence block II such as G-to-T transversions. These mutations ultimately reduce the amount of guanine in the regulatory region, eliminating the checkpoint and funneling functions of the site, and decreasing mitochondrial efficiency. Tumor cells, which do not necessarily depend on respiration, could survive by utilizing alternative energy pathways despite mitochondrial malfunction.[101]

1.3.2 DNA-Mediated CT with Metalloproteins: Establishing DNA-Bound Redox Potentials

1.3.2.1 Base Excision Repair Enzymes

Base excision repair (BER) proteins identify and remove oxidized bases from DNA. Several of these enzymes, such as MutY and endonuclease III (EndoIII) from *E. coli*, are known to contain redox-active $[4Fe\text{-}4S]^{2+}$ clusters. However, a distinct role for these cofactors has been investigated only recently. Interestingly, although MutY is capable of folding in the absence

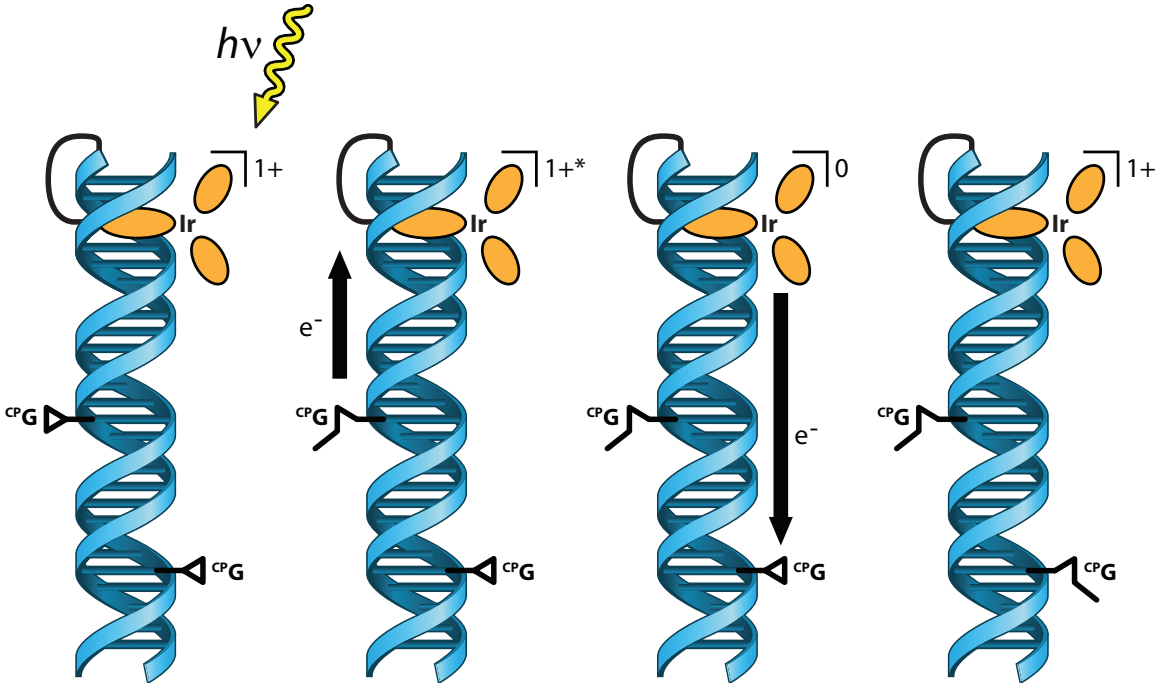

Figure 1.5: Ping-pong electron transfer. From left to right: photoexcitation of the Ir complex results in DNA-mediated ET from the ^{CP}G base. Subsequent ET from the Ir complex reduces the ^{CP}C base.

of the cluster, the cluster is required for DNA binding.[106] Experiments with EndoIII showed that the solvent-accessible cluster undergoes decomposition when treated with oxidizing ferricyanide. The protein is resistant to reduction, having an estimated $[4Fe{-}4S]^{2+/1+}$ couple midpoint potential of less than -600 mV.[107,108] Notably, initial measurements of the redox potentials of these proteins were performed in the absence of DNA.

Experiments on DNA-modified electrodes were conducted to determine whether DNA binding might alter the redox properties of the [4Fe-4S] cluster (Figure 1.7). Cyclic voltammetry of MutY at the DNA-modified surface yielded a midpoint potential of +90 mV vs. NHE, an appropriate potential for a physiologically active redox switch.[109] In the absence of DNA, or when the electrode was modified with duplex DNA containing an abasic site, no signal was observed, proving that electron transfer occurs through the DNA base stack to the redox cofactor of bound MutY. In similar experiments, the redox potentials of EndoIII and the *Archeoglobus fulgidus* uracil DNA glycosylase (AfUDG) were measured as 59 mV vs. NHE and 95 mV vs. NHE, respectively.[109]

In order to compare the redox potential of EndoIII in the absence and presence of DNA directly, electrochemical experiments were conducted using highly oriented pyrolytic graphite (HOPG) electrodes.[110] On a bare electrode, oxidative scans of EndoIII yielded an irreversible anodic peak at ~ 250 mV and loss of the yellow solution color, indicating degradation of the $[4Fe\text{-}4S]^{2+}$ cluster to form the $[3Fe\text{-}4S]^{+}$ cluster. Consecutive positive scans showed broad, irregular signals at -80 and -710 mV vs. NHE, consistent with degradation. In contrast, on electrodes modified with pyrenated DNA, a reversible midpoint potential of ~ 20 mV vs. NHE was observed. DNA is thus necessary for the stable oxidation of EndoIII. By comparing the oxidation potential of EndoIII in the absence and presence of DNA, it was determined that EndoIII in the 3+ oxidation state binds DNA at least 1000 times more tightly than the reduced 2+ form, suggesting that iron-sulfur cluster-containing proteins become activated upon oxidation.

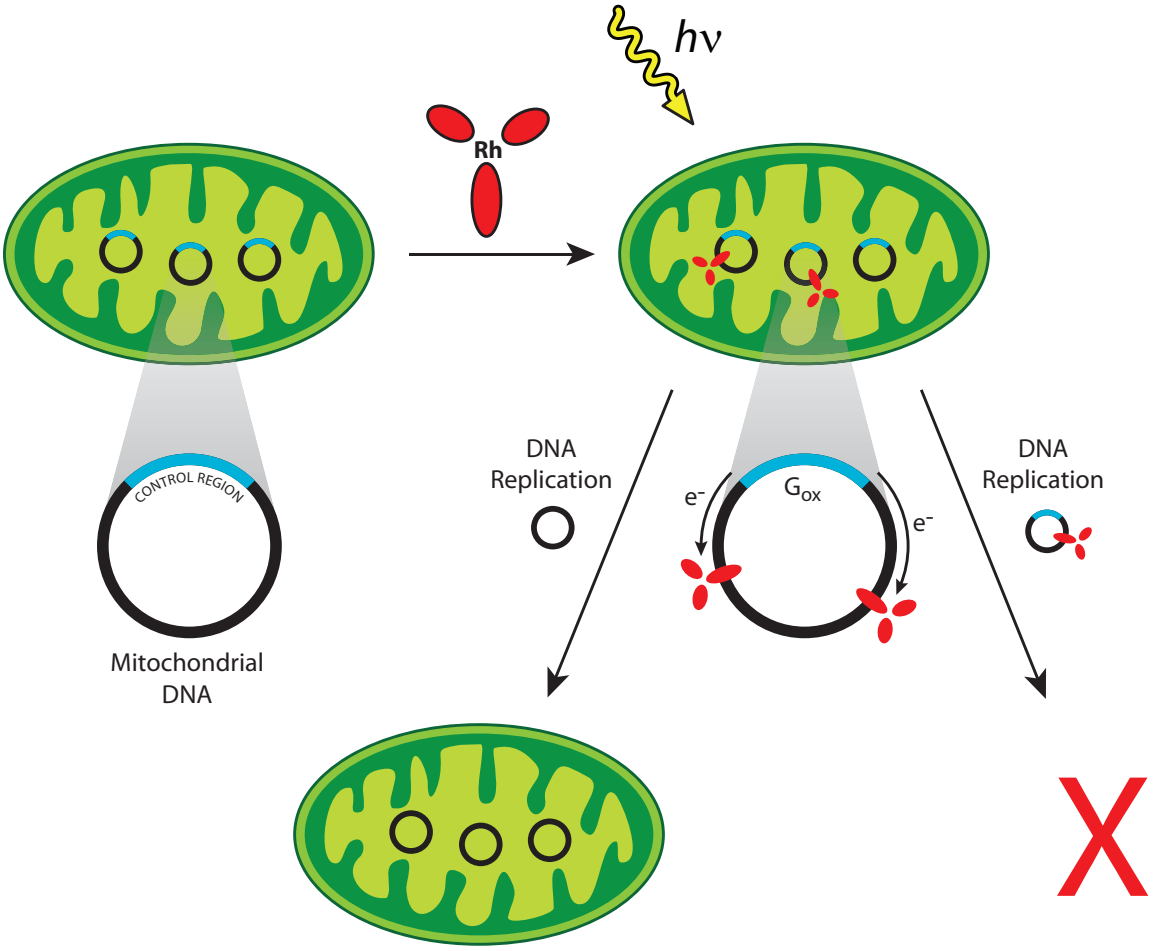

Figure 1.6: Damage of mitochondrial DNA via DNA-mediated CT. Multiple copies of mitochondrial DNA (black) are found in mitochondria (green) within the cell. Following incubation with $[Rh(phi)_2(bpy)]^{3+}$, irradiation of the cells results in oxidation at low potential guanine sites (G_{ox}). Damage in the genome is funneled (curved arrows) via DNA-mediated CT to the control region (blue), preventing replication of the lesion-filled plasmid (bottom right). In the absence of Rh, mitochondrial replication occurs as normal (bottom left).

1.3.2.2 The SoxR Transcription Factor

Other redox-active proteins may also become activated upon oxidation. The SoxR transcription factor regulates the response to superoxide within the cell. SoxR binds DNA as a dimer and contains two [2Fe-2S] clusters (one in each monomer) that are not required for protein folding.[111–114] The oxidation of SoxR leads to the expression of the SoxS transcription factor, which controls expression of genes involved in protecting the cell from stress. Interestingly, the oxidized and reduced forms of the protein show equal affinities for the SoxR promoter.[115] The redox potential of SoxR in the absence of DNA, however, is approximately -290 mV.[113,116,117] This value, much lower than the potential within the cell, is inconsistent with the proposed mechanism of SoxR; a redox sensor for oxidation cannot function if it is always switched on. Determination of the DNA-bound redox potential of SoxR provides insight into the activation mechanism of the protein. On HOPG surfaces modified with pyrenated DNA, a quasi-reversible electrochemical signal was observed for the [2Fe-2S] cluster of SoxR at +200 mV vs. NHE.[115] Similar potentials were observed for SoxR extracted from several different organisms. Thus, DNA binding shifts the redox potential of SoxR by $\sim +500$ mV. It is likely that this shift in potential provides the energy for the torquing of DNA by oxidized SoxR, activating transcription. Critically, we see the importance of performing redox measurements of DNA binding proteins in the presence of DNA, as the DNA polyanion alters the protein environment and the potential. MutY, EndoIII, and SoxR show redox activity in a physiologically relevant regime only when bound to DNA.

1.3.3 DNA-Mediated Cross-Linking and Oxidation of MutY

The methods used to probe long-range DNA-mediated oxidation of 5′-GG-3′ have also aided in the study of DNA/protein interactions, allowing us to gain insight into how these metalloproteins might take advantage of the unique property of DNA to conduct charge. It has been shown that photoactivation of metallointercalators in the presence of DNA-bound protein can lead to the formation of protein-DNA cross-links. Experiments harnessing DNA-mediated CT to generate such cross-links have provided a more detailed look at the

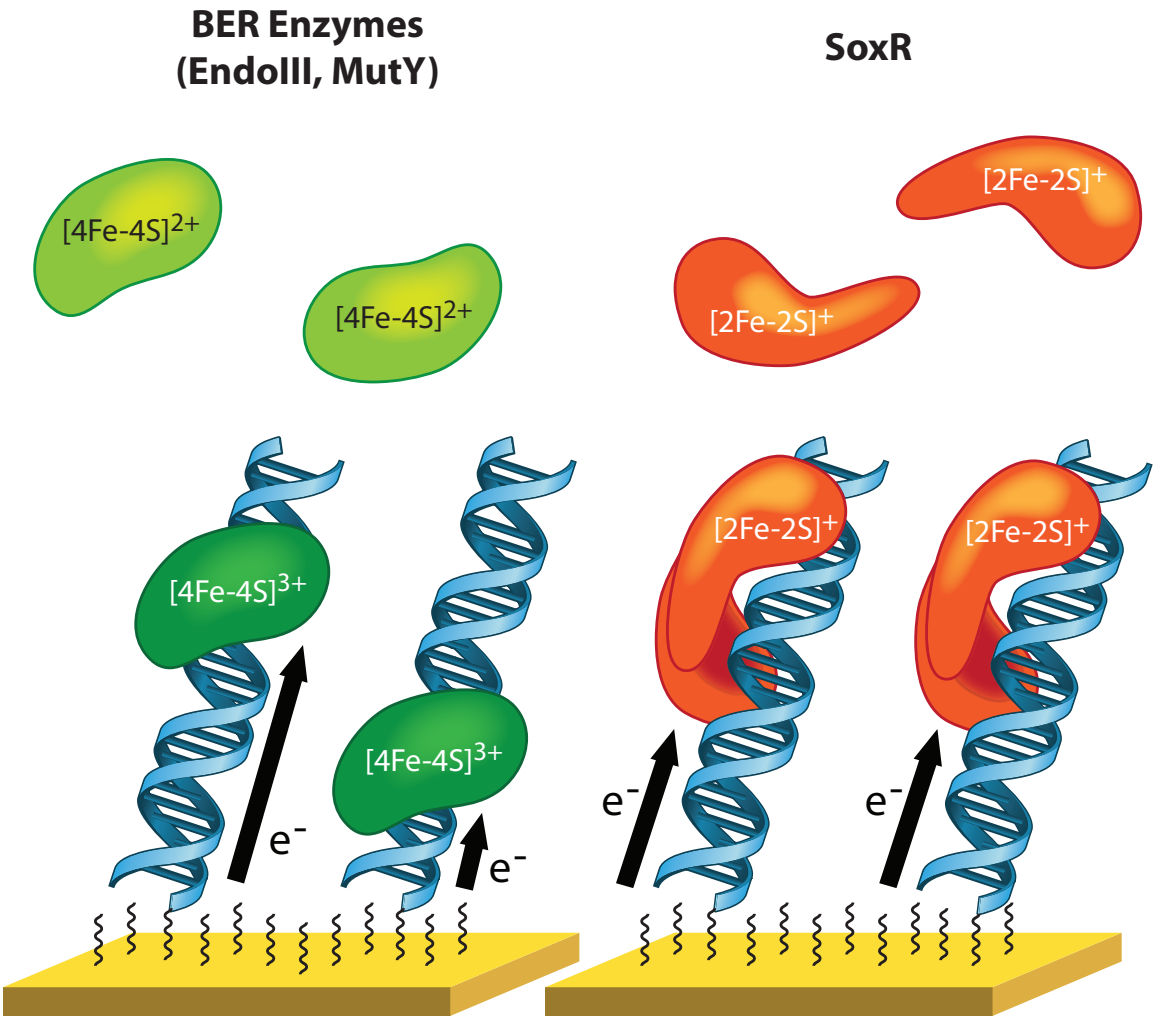

Figure 1.7: Illustration of surfaces used for DNA-protein electrochemistry of BER proteins (left) and SoxR (right). DNA duplexes are attached to the gold surface via a 5′ thiol linker. Mercaptohexanol (curved lines) is used as a backfilling agent, preventing direct contact between the redox probe and the electrochemical surface. Electrons travel (arrow) from the gold surface to the bound protein. DNA binding activates EndoIII and MutY toward oxidation to the 3+ state, and SoxR binds as a dimer.

amino acid/DNA interface.[118–126]

DNA photooxidation and protein cross-linking experiments were performed in the presence of MutY to better understand the factors affecting the detection of its target lesion, adenine mispaired with 8-oxo-dG. In these experiments, $[Rh(phi)_2(bpy')]^{3+}$, covalently tethered to the DNA strand, was used to generate oxidative damage.[126] Early models suggested that MutY searches for damage by flipping bases out of the DNA duplex one by one for interrogation. In our experiments, protein binding decreased the oxidation yield, but it did not affect the oxidation pattern, even at high concentrations.[127] This result suggests that MutY binding does not perturb the DNA structure, but that MutY may act as a hole sink in addition to guanine. It also indicates that the protein might use a mechanism other than base flipping to search for damage. In cross-linking experiments, adducts were observed to form between 8-oxo-dG and lysine 142 of MutY, even though the protein binding site was separated from the Rh photooxidant binding site by more than 20 Å. It should be noted that lysine 142 in MutY was thought to play a large mechanistic role during the repair of 8-oxo-dG:A lesions based on early cross-linking and NMR investigations.[50,119,128] This result indicates that protein/DNA cross-links can be formed by long-range DNA-mediated CT.[126]

Several experiments have shown that the strategies used to oxidize guanine can also be used to oxidize DNA-bound MutY. For example, low-temperature EPR measurements of samples including $[Ru(phen)_2dppz]^{2+}$, the quencher $[Co(NH_3)_5Cl]^{2+}$, and poly(dG-dC) or poly(dA-dT) in the absence or presence of MutY revealed a primary g value of 2.02. This signal was attributed to the $[3Fe\text{-}4S]^{+}$ cluster, formed upon oxidative degradation of the $[4Fe\text{-}4S]^{2+}$ cluster. Smaller signals at g values of 2.08 and 2.06 were assigned to the stable oxidized cluster, $[4Fe\text{-}4S]^{3+}$.[129,130] Interestingly, these latter signals were of significantly lower intensity in the poly(dA-dT) sample than in the poly(dG-dC) sample. This result suggests that the oxidation of MutY occurs more efficiently when transient charge occupation on guanine is possible. This reaction is described in Scheme 1.4.

The DNA-mediated oxidation of MutY was also investigated by time-resolved spectroscopy using the flash-quench technique.[129] In the absence of protein, the transient ab-

sorption decay corresponded to decay of the guanine radical. In the presence of protein, the transient absorption decays showed two phases: a fast phase due to decay of the guanine radical and a slow phase with a spectral profile characteristic of the $[4Fe\text{-}4S]^{3+/2+}$ difference spectrum. Thus, the DNA-mediated oxidation of MutY can be observed directly. Importantly, these experiments established that guanine radical formation can directly lead to the oxidation of bound protein.

Collectively, biochemical experiments, EPR, and transient absorption spectroscopy indicate that MutY can be oxidized by a DNA-mediated mechanism. Considering the function of this enzyme, it is reasonable that, within the cell, DNA-mediated CT initiated by oxidative stress may serve as a means to activate repair. Further, considering that the redox potentials of BER proteins lie in a physiologically relevant regime only when the proteins are bound to DNA, and that mismatches and lesions block DNA-mediated CT,[88,131,132] it is even possible that DNA-binding redox active proteins may scan large stretches of the genome for damage by passing charge between them.[109,110,115,127,133]

Our model for DNA-mediated signaling between redox-active proteins is described for MutY as follows.[127] Binding to DNA shifts the potential of the MutY $[4Fe\text{-}4S]^{2+}$ cluster toward oxidation. In the absence of oxidative stress, the cluster remains in the 2+ state. Guanine cation radicals, formed endogenously under conditions of oxidative stress, can oxidize the cluster from the 2+ to the 3+ state. This reaction neutralizes the guanine radical and increases the affinity of MutY for the duplex by three orders of magnitude. If a second MutY protein is bound in the 2+ state at a distant site, charge can be transferred through the duplex from the first to the second protein. The first protein, now in the 2+ state, loses affinity for DNA and is free to relocate to another site. This process comprises a scan of the region of DNA between the proteins for damage. However, in the event that a lesion known to attenuate charge transfer, such as a base pair mismatch or an oxidized base, intervenes between the bound enzymes, DNA-mediated CT cannot proceed. If this occurs, the proteins remain in the vicinity of the damage, slowly processing to the site of damage.

Interestingly, this process is not limited to pairs of the same protein, or even to iron-

sulfur cluster proteins; any redox-active protein with a potential in the vicinity of 100 mV is expected to participate in the search process. The ability of MutY to help EndoIII find its target lesions has already been reported.[133] In addition, experiments are currently being conducted in our laboratory to determine the extent to which iron-sulfur cluster-containing helicase enzymes, such as XPD and DinG, can assist in the search for damage.

1.3.4 Transcriptional Activation in SoxR by DNA-Mediated Oxidation

In light of our findings regarding the role that DNA-mediated CT may play in the BER pathway, we have examined the DNA-mediated oxidation of SoxR, an iron-sulfur cluster-containing transcription factor. SoxR is activated in the presence of oxidative stress; however, the identity of the specific oxidant is unknown. *In vivo* studies using redox-cyclers such as paraquat to induce oxidative stress show that superoxide is not the direct activator of SoxR. Rather, the redox-cyclers deplete cellular NADPH, which is normally required to keep SoxR in a reduced form. The redox-cyclers then undergo autooxidation, losing an electron to dioxygen and producing superoxide. In laboratory experiments, the protein can be reversibly reduced with dithionite, or it can be reversibly oxidized with plumbagin and phenazine methosulfate.[113] Electrochemistry of SoxR shows a redox signal for the [2Fe-2S] cluster at +200 mV vs. NHE, indicating that the protein undergoes one-electron oxidation when bound to DNA.[115] Due to the redox shift observed upon DNA binding, it is reasonable that the DNA-bound form of SoxR might be the missing oxidative switch. In a process similar to that observed for MutY, guanine radicals generated by ROS may activate SoxR. Once oxidized, SoxR can then promote transcription to combat oxidative stress.

To test this theory, SoxR oxidation experiments were recently conducted in our laboratory using $[Ru(phen)(dppz)(bpy')]^{2+}$ and the flash-quench technique.[134] In these studies, $[Co(NH_3)_5Cl]^{2+}$ was used as the quencher, eliminating back electron transfer. Similarly to the MutY oxidation experiments described earlier, the yield of 5′-GG-3′ oxidation products decreased in the presence of reduced (activatable) SoxR. This indicates that SoxR is able to donate an electron to the oxidized guanine, filling the radical hole with its own lost electron, and being oxidized itself. Conversely, in the absence of SoxR, or when fully

oxidized SoxR was included in solution, no attenuation in damage was observed. These results clearly show that SoxR is able to interact with the DNA base stack and participate in DNA-mediated CT. Further, the SoxR response to guanine radicals generated in DNA suggests that oxidative damage can initiate protein activation.

In order to examine the SoxR response to DNA damage within the cell, *E. coli* cultures were treated with $[Rh(phi)_2bpy]^{3+}$. This intercalator, upon photoactivation, was previously shown to generate guanine damage in the mitochondria of HeLa cells.[101,102,135] In our experiment, transcription of the *soxS* RNA product, observed using reverse transcription PCR, indicated activation of SoxR. Bacteria irradiated in the presence of the Rh photooxidant showed much higher *soxS* product levels than non-irradiated bacteria. Additionally, expression levels of *soxS* in the presence of $[Rh(phi)_2bpy]^{3+}$ were similar to those measured when methyl viologen, a redox-cycler, was used instead. Since the complex cannot oxidize SoxR in the absence of DNA, it is assumed that SoxR oxidation takes place through a guanine radical intermediate. To determine whether SoxR can be activated over a distance by long-range DNA-mediated CT, $[Rh(phi)_2bpy]^{3+}$ was tethered to a 180-mer duplex of DNA containing the SoxR binding site and the -10 and -35 promoter regions of *soxS* (Figure 1.8).[61,134] Following irradiation, gene products were monitored with an anaerobic abortive transcription assay. The abortive transcription product, a 4-mer, was only observed in samples containing reduced SoxR and Rh-tethered DNA. Importantly, there was no direct photooxidation of SoxR by $[Rh(phi)_2bpy]^{3+}$ in the absence of DNA. These results indicate that DNA-mediated transcriptional activation of SoxR can occur over a distance of 270 Å. DNA CT has therefore emerged not only as an indicator of oxidative damage, but also as a signal to metalloproteins in the genome to initiate repair.

1.4 Conclusions

Initially used as general probes to understand the nature of DNA-mediated CT, the utility of metal complexes increased greatly. Precise tuning of reactivity and specificity has resulted in complexes that are capable of generating damage *in vivo*. Probe design has become more nuanced, taking into account characteristics including ligand sterics, DNA binding modes,

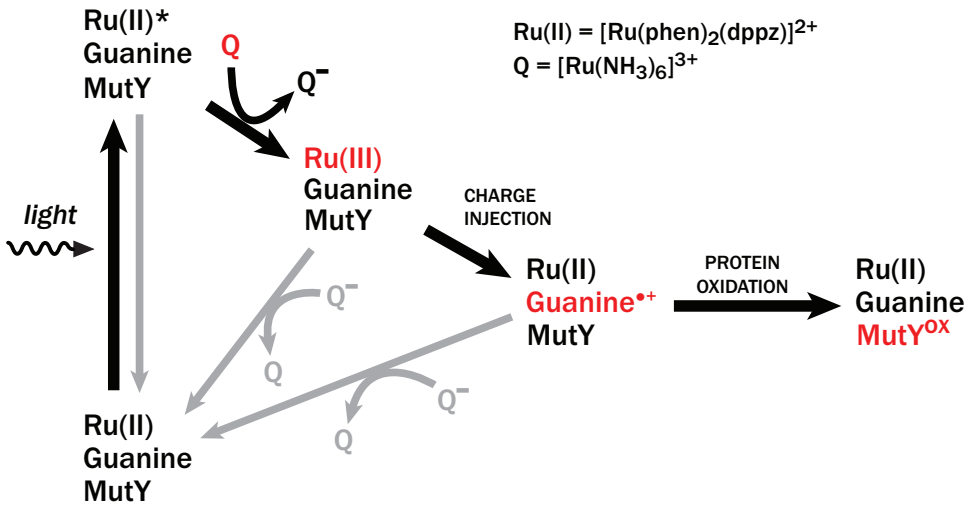

Scheme 1.4: The flash-quench technique can be used to generate Ru(III) and subsequently oxidize DNA-bound MutY. Following photoexcitation, Ru(II)* is quenched, forming the powerful ground state oxidant Ru(III). This species proceeds to oxidize guanine within the base stack. The guanine radical can form oxidation products or it can oxidize a bound protein such as MutY. Back electron transfer reactions, which decrease the yield of oxidized protein, are shown in gray. The species that holds the moving charge at each step is shown in red.

the extent of electronic coupling to DNA, and stereospecificity. Metallointercalators such as $[Rh(phi)_2bpy]^{3+}$ initiate electron transfer in DNA upon photoactivation, resulting in observable damage to guanine, which is the most easily oxidized nucleobase. Charge transport through DNA can occur over extremely long molecular distances. The rich photophysical properties of these complexes in particular have facilitated spectroscopic characterization of the mechanism of DNA-mediated CT, and experiments with cyclopropyl-modified bases have allowed for direct comparison between hole and electron transfer.

Experiments conducted *in vivo* also depend on our understanding of the photophysical mechanics of metal complexes since these photooxidants are used to trigger DNA damage within cells. Utilizing metal complexes as photooxidants, the funneling of damage to specific regulatory sites in the mitochondrial genome has been observed. Metal complexes have also been used to activate repair proteins and to initiate transcription. In these latter applications, we have also observed DNA-mediated redox chemistry to metal centers, but here the coordination scaffolds are the amino acid backbones of metalloproteins. Using early experiments with simple coordination complexes to guide our investigations, our goal is now shifting from the understanding of DNA-mediated CT as a fundamental physical process to the recognition of this fascinating chemistry in cellular sensing and signalling.

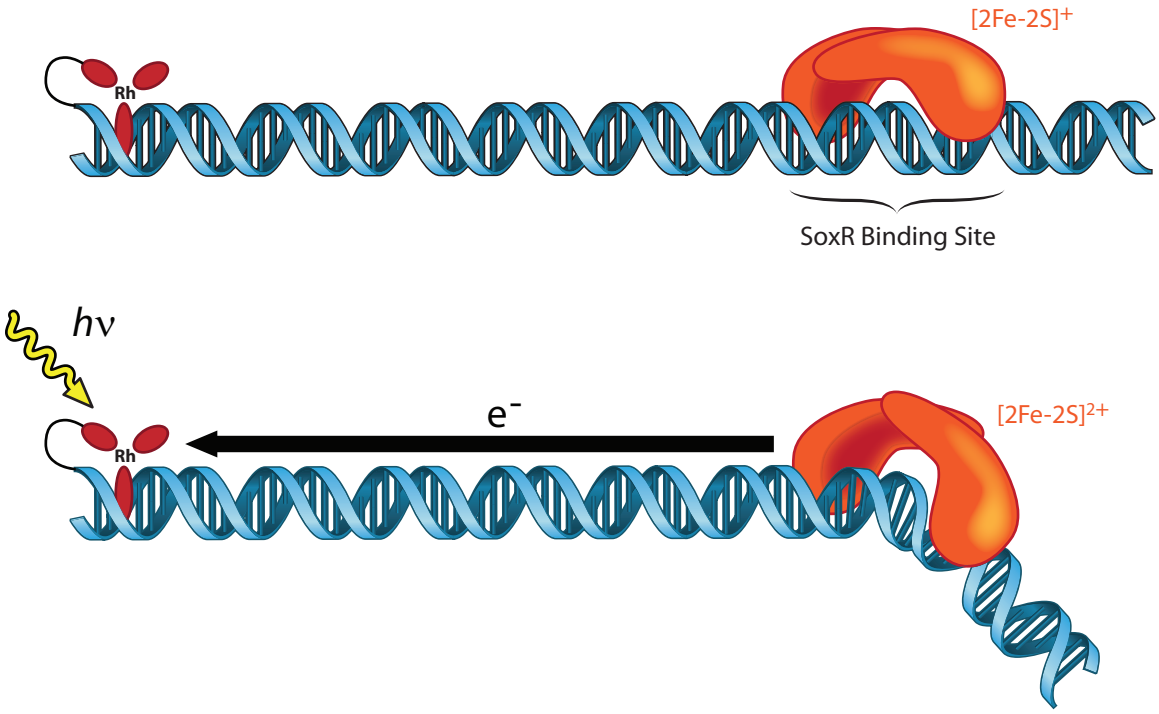

Figure 1.8: A model for the transcriptional activation of SoxR via DNA-mediated oxidation. Top: SoxR is bound to a DNA duplex at a position well removed from the covalently bound photooxidant $[Rh(phi_2)(bpy')]^{3+}$. SoxR initially binds in the reduced (+1) state. Bottom: Photoactivation of the metal complex triggers electron transfer, resulting in the oxidation of SoxR to the (2+) state and a structural change in the protein. The structural change induces kinking of DNA at the SoxR binding site, which signals recruitment of transcription machinery such as RNA polymerase.

References

[1] van Loon, B., Markkanen, E., and Hübscher, U. "Oxygen as a friend and enemy: How to combat the mutational potential of 8-oxo-guanine." *DNA Repair* **9**, 604–616 (2010).

[2] David, S. S., O'Shea, V. L., and Kundu, S. "Base-excision repair of oxidative DNA damage." *Nature* **447**, 941–950 (2007).

[3] Møller, P., Folkmann, J. K., Forchhammer, L., Bräuner, E. V., Danielsen, P. H., Risom, L., and Loft, S. "Air pollution, oxidative damage to DNA, and carcinogenesis." *Cancer Lett.* **266**, 84–97 (2008).

[4] Cooke, M. S., Evans, M. D., Dizdaroglu, M., and Lunec, J. "Oxidative DNA damage: mechanisms, mutation, and disease." *FASEB J.* **17**, 1195–1214 (2003).

[5] Nishikawa, M. "Reactive oxygen species in tumor metastasis." *Cancer Lett.* **266**, 53–59 (2008).

[6] Klaunig, J. E., and Kamendulis, L. M. "The role of oxidative stress in carcinogenesis." *Annu. Rev. Pharmacol. Toxicol.* **44**, 239–267 (2004).

[7] Kopelevich, Y., and Esquinazi, P. "Graphene Physics in Graphite." *Adv. Mat.* **19**, 4559–4563 (2007).

[8] Lerman, L. "Structural Considerations in the Interaction of DNA and Acridines." *J. Mol. Biol.* **3**, 18–30 (1961).

[9] Berman, H. M., and Young, P. R. "The Interaction of Intercalating Drugs with Nucleic Acids." *Ann. Rev. Biophys. Bioeng.* **10**, 87–114 (1981).

[10] Kielkopf, C., Erkkila, K., Hudson, B., Barton, J. K., and Rees, D. "Structure of a photoactive rhodium complex intercalated into DNA." *Nat. Struct. Molec. Biol.* **7**, 117–121 (2000).

[11] Pierre, V. C., Kaiser, J. T., and Barton, J. K. "Insights into finding a mismatch through the structure of a mispaired DNA bound by a rhodium intercalator." *Proc. Natl. Acad. Sci. USA* **104**, 429–434 (2007).

[12] Zeglis, B. M., Pierre, V. C., and Barton, J. K. "Metallo-intercalators and metallo-insertors." *Chem. Commun.* **7345**, 4565–4579 (2007).

[13] Zeglis, B. M., Pierre, V. C., Kaiser, J. T., and Barton, J. K. "A bulky rhodium complex bound to an adenosine-adenosine DNA mismatch: general architecture of the metalloinsertion binding mode." *Biochemistry* **48**, 4247–4253 (2009).

[14] Barton, J. K., Kumar, C. V., and Turro, N. J. "DNA-mediated photoelectron transfer reactions." *J. Am. Chem. Soc.* **108**, 6391–6393 (1986).

[15] Murphy, C. J., and Barton, J. K. "Ruthenium complexes as luminescent reporters of DNA." *Methods Enzymol.* **226**, 576–594 (1993).

[16] Friedman, A. E., Chambron, J.-C., Sauvage, J.-P., Turro, N. J., and Barton, J. K. "Molecular 'Light Switch' for DNA: $Ru(bpy)_2(dppz)^{2+}$." *J. Am. Chem. Soc.* **112**, 4960–4962 (1990).

[17] Hartshorn, R. M., and Barton, J. K. "Novel Dipyridophenazine Complexes of Ruthenium(II): Exploring Luminescent Reporters of DNA." *J. Am. Chem. Soc.* **114**, 5919–5925 (1992).

[18] Jenkins, Y., Friedman, A. E., Turro, N. J., and Barton, J. K. "Characterization of dipyridophenazine complexes of ruthenium(II): the light switch effect as a function of nucleic acid sequence and conformation." *Biochemistry* **31**, 10809–10816 (1992).

[19] Turro, C., Bossmann, S. H., Jenkins, Y., Barton, J. K., and Turro, N. J. "Proton Transfer Quenching of the MLCT Excited State of $Ru(phen)_2dppz^{2+}$ in Homogeneous Solution and Bound to DNA." *J. Am. Chem. Soc.* **117**, 9026–9032 (1995).

[20] Olson, E. J. C., Hu, D., Hörmann, A., Jonkman, A. M., Arkin, M. R., Stemp, E. D. A., Barton, J. K., and Barbara, P. F. "First Observation of the Key Intermediate

in the "Light-Switch" Mechanism of $[Ru(phen)_2dppz]^{2+}$." *J. Am. Chem. Soc.* **119**, 11458–11467 (1997).

[21] Chang, I.-J., Gray, H. B., and Winkler, J. R. "High-Driving-Force Electron Transfer in Metalloproteins: Intramolecular Oxidation of Ferrocytochrome c by $Ru(2,2'\text{-bpy})_2(im)(his\text{-}33)^{3+}$." *J. Am. Chem. Soc.* **113**, 7056–7057 (1991).

[22] Barton, J. K., Dannenberg, J. J., and Raphael, A. L. "Enantiomeric Selectivity in Binding Tris(phenanthroline)zinc(II) to DNA." *J. Am. Chem. Soc.* **104**, 4967–4969 (1982).

[23] Barton, J. K., Basile, L. A., Danishefsky, A., and Alexandrescu, A. "Chiral probes for the handedness of DNA helices: enantiomers of tris(4,7-diphenylphenanthroline)ruthenium(II)." *Proc. Natl. Acad. Sci. USA* **81**, 1961–1965 (1984).

[24] Barton, J. K., Danishefsky, A., and Goldberg, J. "Tris(phenanthroline)ruthenium(II): Stereoselectivity in Binding to DNA." *J. Am. Chem. Soc.* **106**, 2172–2176 (1984).

[25] Barton, J. K., and Raphael, A. L. "Photoactivated stereospecific cleavage of double-helical DNA by cobalt(III) complexes." *J. Am. Chem. Soc.* **106**, 2466–2468 (1984).

[26] Barton, J. K., and Lolis, E. "Chiral Discrimination in the Covalent Binding of Bis(phenanthroline)dichlororuthenium(II) to B-DNA." *J. Am. Chem. Soc.* **107**, 708–709 (1985).

[27] Kumar, C. V., Barton, J. K., and Turro, N. J. "Photophysics of ruthenium complexes bound to double helical DNA." *J. Am. Chem. Soc.* **107**, 5518–5523 (1985).

[28] Westerlund, F., Pierard, F., Eng, M. P., Nordén, B., and Lincoln, P. "Enantioselective luminescence quenching of DNA light-switch $[Ru(phen)_2dppz]^{2+}$ by electron transfer to structural homologue $[Ru(phendione)_2dppz]^{2+}$." *J. Phys. Chem. B* **109**, 17327–17332 (2005).

[29] Barton, J. K. "Metals and DNA: Molecular Left-Handed Complements." *Science* **233**, 727–734 (1986).

[30] Barton, J. K., Goldberg, J. M., Kumar, C. V., and Turro, N. J. "Binding Modes and Base Specificity of Tris(phenanthroline)ruthenium(II) Enantiomers with Nucleic Acids: Tuning the Stereoselectivity." *J. Am. Chem. Soc.* **108**, 2081–2088 (1986).

[31] Jenkins, Y., and Barton, J. K. "A Sequence-Specific Molecular Light Switch: Tethering of an Oligonucleotide to a Dipyridophenazine Complex of Ruthenium(II)." *J. Am. Chem. Soc.* **114**, 8736–8738 (1992).

[32] Holmlin, R. E., Dandliker, P. J., and Barton, J. K. "Synthesis of Metallointercalator-DNA Conjugates on a Solid Support." *Bioconj. Chem.* **10**, 1122–1130 (1999).

[33] Zeglis, B. M., and Barton, J. K. "A Mismatch-Selective Bifunctional Rhodium-Oregon Green Conjugate: A Fluorescent Probe for Mismatched DNA." *J. Am. Chem. Soc.* **128**, 5654–5655 (2006).

[34] Puckett, C. A., and Barton, J. K. "Fluorescein redirects a ruthenium-octaarginine conjugate to the nucleus." *J. Am. Chem. Soc.* **131**, 8738–8739 (2009).

[35] Puckett, C. A., and Barton, J. K. "Targeting a ruthenium complex to the nucleus with short peptides." *Bioorg. Med. Chem.* **18**, 3564–3569 (2010).

[36] Krotz, A. H., Kuo, L. Y., Shields, T. P., and Barton, J. K. "DNA recognition by rhodium(III) polyamine intercalators: considerations of hydrogen bonding and van der Waals interactions." *J. Am. Chem. Soc.* **115**, 3877–3882 (1993).

[37] Krotz, A. H., Hudson, B. P., and Barton, J. K. "Assembly of DNA Recognition Elements on an Octahedral Rhodium Intercalator: Predictive Recognition of 5′-TGCA-3′ by cap Δ-[Rh [(R, R)-Me_2trien] phi]$^{3+}$." *J. Am. Chem. Soc.* **115**, 12577–12577 (1993).

[38] Sitlani, A., and Barton, J. K. "Sequence-specific recognition of DNA by phenanthrenequinone diimine complexes of rhodium(III): importance of steric and van der Waals interactions." *Biochemistry* **33**, 12100–12108 (1994).

[39] Shields, T. P., and Barton, J. K. "Structural examination of enantioselective intercalation: ^{1}H NMR of Rh$(en)_2$phi^{3+} isomers bound to d$(GTGCAC)_2$." *Biochemistry* **34**, 15049–15056 (1995).

[40] Hudson, B. P., and Barton, J. K. "Solution Structure of a Metallointercalator Bound Site Specifically to DNA." *J. Am. Chem. Soc.* **120**, 6877–6888 (1998).

[41] Sardesai, N. Y., Zimmermann, K., and Barton, J. K. "DNA Recognition by Peptide Complexes of Rhodium(III): Example of a Glutamate Switch." *J. Am. Chem. Soc.* **116**, 7502–7508 (1994).

[42] Sardesai, N. Y., and Barton, J. K. "DNA recognition by metal-peptide complexes containing the recognition helix of the phage 434 repressor." *J. Biol. Inorg. Chem.* **2**, 762–771 (1997).

[43] Hastings, C. A., and Barton, J. K. "Perturbing the DNA sequence selectivity of metallointercalator-peptide conjugates by single amino acid modification." *Biochemistry* **38**, 10042–10051 (1999).

[44] Terbrueggen, R. H., and Barton, J. K. "Sequence-specific DNA binding by a rhodium complex: recognition based on sequence-dependent twistability." *Biochemistry* **34**, 8227–8234 (1995).

[45] Terbrueggen, R. H., Johann, T. W., and Barton, J. K. "Functionalized Rhodium Intercalators for DNA Recognition." *Inorg. Chem.* **37**, 6874–6883 (1998).

[46] Franklin, S. J., and Barton, J. K. "Differential DNA recognition by the enantiomers of 1-Rh(MGP)$_2$phi: a combination of shape selection and direct readout." *Biochemistry* **37**, 16093–16105 (1998).

[47] Odom, D. T., Parker, C. S., and Barton, J. K. "Site-specific inhibition of transcription factor binding to DNA by a metallointercalator." *Biochemistry* **38**, 5155–5163 (1999).

[48] Fitzsimons, M. P., and Barton, J. K. "Design of a Synthetic Nuclease: DNA Hydrolysis by a Zinc-Binding Peptide Tethered to a Rhodium Intercalator." *J. Am. Chem. Soc.* **119**, 3379–3380 (1997).

[49] Purugganan, M. D., Kumar, C. V., Turro, N. J., and Barton, J. K. "Accelerated electron transfer between metal complexes mediated by DNA." *Science* **241**, 1645–1649 (1988).

[50] Murphy, C. J., Arkin, M. R., Ghatlia, N. D., Bossmann, S. H., Turro, N. J., and Barton, J. K. "Fast photoinduced electron transfer through DNA intercalation." *Proc. Natl. Acad. Sci. USA* **91**, 5315–5319 (1994).

[51] Murphy, C. J., Arkin, M. R., Jenkins, Y., Ghatlia, N. D., Bossmann, S. H., Turro, N. J., and Barton, J. K. "Long-range photoinduced electron transfer through a DNA helix." *Science* **262**, 1025–1029 (1993).

[52] Stemp, E. D. A., Arkin, M. R., and Barton, J. K. "Electron transfer between metallointercalators bound to DNA: Spectral identification of the transient intermediate." *J. Am. Chem. Soc.* **117**, 2375–2376 (1995).

[53] Holmlin, R. E., Stemp, E. D. A., and Barton, J. K. "$Os(phen)_2dppz^{2+}$ in Photoinduced DNA-Mediated Electron Transfer Reactions." *J. Am. Chem. Soc.* **118**, 5236–5244 (1996).

[54] Holmlin, R. E., and Barton, J. K. "$Os(phen)_2(dppz)^{2+}$: A Red-Emitting DNA Probe." *Inorg. Chem.* **34**, 7–8 (1995).

[55] Steenken, S., and Jovanovic, S. V. "How Easily Oxidizable Is DNA? One-Electron Reduction Potentials of Adenosine and Guanosine Radicals in Aqueous Solution." *J. Am. Chem. Soc.* **119**, 617–618 (1997).

[56] Saito, I., Takayama, M., Sugiyama, H., Nakatani, K., Tsuchida, A., and Yamamoto, M. "Photoinduced DNA Cleavage via Electron Transfer: Demonstration that Guanine Residues Located $5'$ to Guanine are the Most Electron-Donating Sites." *J. Am. Chem. Soc.* **117**, 6406–6407 (1995).

[57] Kelley, S. O., and Barton, J. K. "Electron Transfer Between Bases in Double Helical DNA." *Science* **283**, 375–381 (1999).

[58] Stemp, E. D. A., Arkin, M. R., and Barton, J. K. "Oxidation of Guanine in DNA by $Ru(phen)_2(dppz)^{3+}$ Using the Flash-Quench Technique." *J. Am. Chem. Soc.* **119**, 2921–2925 (1997).

[59] Candeias, L. P., and Steenken, S. "Structure and Acid-Base Properties of One-Electron-Oxidized Deoxyguanosine, Guanosine, and 1-Methylguanosine." *J. Am. Chem. Soc.* **111**, 1094–1099 (1989).

[60] Shibutani, S., Takeshita, M., and Grollman, A. P. "Insertion of specific bases during DNA synthesis past the oxidation-damaged base 8-oxodG." *Nature* **349**, 431–434 (1991).

[61] Hall, D. B., Holmlin, R. E., and Barton, J. K. "Oxidative DNA damage through long-range electron transfer." *Nature* **382**, 731–735 (1996).

[62] Arkin, M. R., Stemp, E. D. A., Coates Pulver, S., and Barton, J. K. "Long-range oxidation of guanine by Ru(III) in duplex DNA." *Chem. Biol.* **4**, 389–400 (1997).

[63] Núñez, M. E., Hall, D. B., and Barton, J. K. "Long-range oxidative damage to DNA: effects of distance and sequence." *Chem. Biol.* **6**, 85–97 (1999).

[64] Williams, T. T., Odom, D. T., and Barton, J. K. "Variations in DNA Charge Transport with Nucleotide Composition and Sequence." *J. Am. Chem. Soc.* **122**, 9048–9049 (2000).

[65] Bhattacharya, P. K., and Barton, J. K. "Influence of intervening mismatches on long-range guanine oxidation in DNA duplexes." *J. Am. Chem. Soc.* **123**, 8649–8656 (2001).

[66] Hall, D. B., Kelley, S. O., and Barton, J. K. "Long-range and short-range oxidative damage to DNA: photoinduced damage to guanines in ethidium-DNA assemblies." *Biochemistry* **37**, 15933–15940 (1998).

[67] Kelley, S. O., Holmlin, R. E., Stemp, E. D. A., and Barton, J. K. "Photoinduced Electron Transfer in Ethidium-Modified DNA Duplexes: Dependence on Distance and Base Stacking." *J. Am. Chem. Soc.* **119**, 9861–9870 (1997).

[68] Kelley, S. O., and Barton, J. K. "DNA-mediated electron transfer from a modified base to ethidium: π-stacking as a modulator of reactivity." *Chem. Biol.* **5**, 413–425 (1998).

[69] Wan, C., Fiebig, T., Kelley, S. O., Treadway, C. R., Barton, J. K., and Zewail, A. H. "Femtosecond dynamics of DNA-mediated electron transfer." *Proc. Natl. Acad. Sci. USA* **96**, 6014–6019 (1999).

[70] Kanvah, S., and Schuster, G. B. "Oxidative damage to DNA: Inhibition of guanine damage." *Pure Appl. Chem.* **78**, 2297–2304 (2006).

[71] Williams, T. T., Dohno, C., Stemp, E. D. A., and Barton, J. K. "Effects of the photooxidant on DNA-mediated charge transport." *J. Am. Chem. Soc.* **126**, 8148–8158 (2004).

[72] O'Neill, M. A., and Barton, J. K. "2-Aminopurine: a probe of structural dynamics and charge transfer in DNA and DNA:RNA hybrids." *J. Am. Chem. Soc.* **124**, 13053–13066 (2002).

[73] O'Neill, M. A., and Barton, J. K. "Effects of strand and directional asymmetry on base-base coupling and charge transfer in double-helical DNA." *Proc. Natl. Acad. Sci. USA* **99**, 16543–16550 (2002).

[74] O'Neill, M. A., Becker, H.-C., Wan, C., Barton, J. K., and Zewail, A. H. "Ultrafast Dynamics in DNA-Mediated Electron Transfer: Base Gating and the Role of Temperature." *Angew. Chem. Int. Ed.* **42**, 5896–5900 (2003).

[75] Genereux, J. C., and Barton, J. K. "Mechanisms for DNA charge transport." *Chem. Rev.* **110**, 1642–1662 (2010).

[76] Nakatani, K., Dohno, C., and Saito, I. "Design of a Hole-Trapping Nucleobase: Termination of DNA-Mediated Hole Transport at *N*-Cyclopropyldeoxyguanosine." *J. Am. Chem. Soc.* **123**, 9681–9682 (2001).

[77] Shao, F., O'Neill, M. A., and Barton, J. K. "Long-range oxidative damage to cytosines in duplex DNA." *Proc. Natl. Acad. Sci. USA* **101**, 17914–17919 (2004).

[78] Dohno, C., Stemp, E. D. A., and Barton, J. K. "Fast back electron transfer prevents guanine damage by photoexcited thionine bound to DNA." *J. Am. Chem. Soc.* **125**, 9586–9587 (2003).

[79] Musa, O., Horner, J., Shahin, H., and Newcomb, M. "A Kinetic Scale for Dialkylaminyl Radical Reactions." *J. Am. Chem. Soc.* **118**, 3862–3868 (1996).

[80] Shaffer, C. L., Morton, M. D., and Hanzlik, R. P. "Enzymatic *N*-Dealkylation of an *N*-Cyclopropylamine: An Unusual Fate for the Cyclopropyl Group." *J. Am. Chem. Soc.* **123**, 349–350 (2001).

[81] O'Neill, M. A., Dohno, C., and Barton, J. K. "Direct chemical evidence for charge transfer between photoexcited 2-aminopurine and guanine in duplex DNA." *J. Am. Chem. Soc.* **126**, 1316–1317 (2004).

[82] O'Neill, M. A., and Barton, J. K. "DNA charge transport: conformationally gated hopping through stacked domains." *J. Am. Chem. Soc.* **126**, 11471–11483 (2004).

[83] Shao, F., Augustyn, K. E., and Barton, J. K. "Sequence dependence of charge transport through DNA domains." *J. Am. Chem. Soc.* **127**, 17445–17452 (2005).

[84] Augustyn, K. E., Genereux, J. C., and Barton, J. K. "Distance-Independent DNA Charge Transport Across an Adenine Tract." *Angew. Chem. Int. Ed.* **46**, 5731–5733 (2007).

[85] Genereux, J. C., Augustyn, K. E., Davis, M. L., Shao, F., and Barton, J. K. "Back-Electron Transfer Suppresses the Periodic Length Dependence of DNA-Mediated Charge Transport Across Adenine Tracts." *J. Am. Chem. Soc.* **130**, 15150–15156 (2008).

[86] Genereux, J. C., Wuerth, S. M., and Barton, J. K. "Single-Step Charge Transport through DNA over Long Distances." *J. Am. Chem. Soc.* **133**, 3863–3868 (2011).

[87] Kelley, S. O., Barton, J. K., Jackson, N. M., and Hill, M. G. "Electrochemistry of methylene blue bound to a DNA-modified electrode." *Bioconj. Chem.* **8**, 31–37 (1997).

[88] Kelley, S. O., Jackson, N. M., Hill, M. G., and Barton, J. K. "Long-Range Electron Transfer through DNA Films." *Angew. Chem. Int. Ed.* **38**, 941–945 (1999).

[89] Boon, E. M., Salas, J. E., and Barton, J. K. "An electrical probe of protein-DNA interactions on DNA-modified surfaces." *Nat. Biotech.* **20**, 282–286 (2002).

[90] Boon, E. M., and Barton, J. K. "DNA electrochemistry as a probe of base pair stacking in A-, B-, and Z-form DNA." *Bioconj. Chem.* **14**, 1140–1147 (2003).

[91] Boal, A. K., and Barton, J. K. "Electrochemical detection of lesions in DNA." *Bioconj. Chem.* **16**, 312–321 (2005).

[92] Gorodetsky, A. A., Buzzeo, M. C., and Barton, J. K. "DNA-Mediated Electrochemistry." *Bioconj. Chem.* **19**, 2285–2296 (2008).

[93] Genereux, J. C., and Barton, J. K. "DNA charges ahead." *Nature Chem.* **1**, 106–107 (2009).

[94] Drummond, T. G., Hill, M. G., and Barton, J. K. "Electron transfer rates in DNA films as a function of tether length." *J. Am. Chem. Soc.* **126**, 15010–15011 (2004).

[95] Lu, W., Vicic, D. a., and Barton, J. K. "Reductive and oxidative DNA damage by photoactive platinum(II) intercalators." *Inorg. Chem.* **44**, 7970–7980 (2005).

[96] Shao, F., Elias, B., Lu, W., and Barton, J. K. "Synthesis and characterization of iridium(III) cyclometalated complexes with oligonucleotides: insights into redox reactions with DNA." *Inorg. Chem.* **46**, 10187–10199 (2007).

[97] Shao, F., and Barton, J. K. "Long-range electron and hole transport through DNA with tethered cyclometalated iridium(III) complexes." *J. Am. Chem. Soc.* **129**, 14733–14738 (2007).

[98] Elias, B., Shao, F., and Barton, J. K. "Charge migration along the DNA duplex: hole versus electron transport." *J. Am. Chem. Soc.* **130**, 1152–1153 (2008).

[99] Elias, B., Genereux, J. C., and Barton, J. K. "Ping-pong electron transfer through DNA." *Angew. Chem. Int. Ed.* **47**, 9067–9070 (2008).

[100] Merino, E. J., Boal, A. K., and Barton, J. K. "Biological contexts for DNA charge transport chemistry." *Curr. Opin. Chem. Biol.* **12**, 229–237 (2008).

[101] Merino, E. J., Davis, M. L., and Barton, J. K. "Common mitochondrial DNA mutations generated through DNA-mediated charge transport." *Biochemistry* **48**, 660–666 (2009).

[102] Merino, E. J., and Barton, J. K. "DNA oxidation by charge transport in mitochondria." *Biochemistry* **47**, 1511–1517 (2008).

[103] Xu, B., and Clayton, D. A. "RNA-DNA hybrid formation at the human mitochondrial heavy-strand origin ceases at replication start sites: an implication for RNA-DNA hybrids serving as primers." *EMBO J.* **15**, 3135–3143 (1996).

[104] Pham, X. H., Farge, G., Shi, Y., Gaspari, M., Gustafsson, C. M., and Falkenberg, M. "Conserved Sequence Box II Directs Transcription Termination and Primer Formation in Mitochondria." *J. Biol. Chem.* **281**, 24647–24652 (2006).

[105] Tan, D.-J., Bai, R.-K., and Wong, L.-J. C. "Comprehensive Scanning of Somatic Mitochondrial DNA Mutations in Breast Cancer." *Cancer Res.* **62**, 972–976 (2002).

[106] Porello, S. L., Cannon, M. J., and David, S. S. "A substrate recognition role for the [4Fe-4S]^2+ cluster of the DNA repair glycosylase MutY." *Biochemistry* **37**, 6465–6475 (1998).

[107] Cunningham, R. P., Asahara, H., Bank, J. F., Scholes, C. P., Salerno, J. C., Surerus, K., Munck, E., McCracken, J., Peisach, J., and Emptage, M. H. "Endonuclease III is an iron-sulfur protein." *Biochemistry* **28**, 4450–4455 (1989).

[108] Fu, W., O'Handley, S., Cunningham, R. P., and Johnson, M. K. "The Role of the Iron-Sulfur Cluster in *Escherichia coli* Endonuclease III: A Resonance Raman Study." *J. Biol. Chem.* **267**, 16135–16137 (1992).

[109] Boal, A. K., Yavin, E., Lukianova, O. A., O'Shea, V. L., David, S. S., and Barton, J. K. "DNA-bound redox activity of DNA repair glycosylases containing [4Fe-4S] clusters." *Biochemistry* **44**, 8397–8407 (2005).

[110] Gorodetsky, A. A., Boal, A. K., and Barton, J. K. "Direct electrochemistry of endonuclease III in the presence and absence of DNA." *J. Am. Chem. Soc.* **128**, 12082–12083 (2006).

[111] Pomposiello, P. J., and Demple, B. "Redox-operated genetic switches: the SoxR and OxyR transcription factors." *Trends Biotechnol.* **19**, 109–114 (2001).

[112] Hidalgo, E., and Demple, B. "An iron-sulfur center essential for transcriptional activation by the redox-sensing SoxR protein." *EMBO J.* **13**, 138–146 (1994).

[113] Gaudu, P., and Weiss, B. "SoxR, a [2Fe-2S] Transcription Factor, is Active Only in its Oxidized Form." *Proc. Natl. Acad. Sci. USA* **93**, 10094–10098 (1996).

[114] Ding, H., Hidalgo, E., and Demple, B. "The redox state of the [2Fe-2S] clusters in SoxR protein regulates its activity as a transcription factor." *J. Biol. Chem.* **271**, 33173–33175 (1996).

[115] Gorodetsky, A. A., Dietrich, L. E. P., Lee, P. E., Demple, B., Newman, D. K., and Barton, J. K. "DNA binding shifts the redox potential of the transcription factor SoxR." *Proc. Natl. Acad. Sci. USA* **105**, 3684–3689 (2008).

[116] Ding, H., and Demple, B. "In vivo Kinetics of a Redox-Regulated Transcriptional Switch." *Proc. Natl. Acad. Sci. USA* **94**, 8445–8449 (1997).

[117] Kobayashi, K., and Tagawa, S. "Activation of SoxR-dependent transcription in Pseudomonas aeruginosa." *J. Biochem.* **136**, 607–615 (2004).

[118] Burrows, C. J., and Muller, J. G. "Oxidative Nucleobase Modifications Leading to Strand Scission." *Chem. Rev.* **98**, 1109–1152 (1998).

[119] Hickerson, R. P., Chepanoske, C. L., Williams, S. D., David, S. S., and Burrows, C. J. "Mechanism-Based DNAProtein Cross-Linking of MutY via Oxidation of 8-Oxoguanosine." *J. Am. Chem. Soc.* **121**, 9901–9902 (1999).

[120] Chakrabarti, S. K., Bai, C., and Subramanian, K. S. "DNA-Protein Crosslinks Induced by Nickel Compounds in Isolated Rat Renal Cortical Cells and its Antagonism

by Specific Amino Acids and Magnesium Ion." *Toxicol. Appl. Pharmacol.* **154**, 245–255 (1999).

[121] Gavin, I. M., Melnik, S. M., Yurina, N. P., Khabarova, M. I., and Bavykin, S. G. "Zero-Length Protein±Nucleic Acid Crosslinking by Radical-Generating Coordination Complexes as a Probe for Analysis of Protein±DNA Interactions *in Vitro* and *in Vivo*." *Analyt. Biochem.* **263**, 26–30 (1998).

[122] Zhitkovich, A., Lukanova, A., Popov, T., Taioli, E., Cohen, H., Costa, M., and Toniolo, P. "DNA-protein crosslinks in peripheral lymphocytes of individuals exposed to hexavalent chromium compounds." *Biomarkers* **1**, 86–93 (1996).

[123] Izzotti, A., Bagnasco, M., Camoirano, A., Orlando, M., and De Flora, S. "DNA fragmentation, DNA-protein crosslinks, ^{32}P postlabeled nucleotidic modifications, and 8-hydroxy-2′-deoxyguanosine in the lung but not in the liver of rats receiving intratracheal instillations of chromium(VI). Chemoprevention by oral *N*." *Mut. Res.* **400**, 233–244 (1998).

[124] Villanueva, A., Cañete, M., Trigueros, C., Rodriguez-Borlado, L., and Juarranz, A. "Photodynamic induction of DNAprotein cross-linking in solution by several sensitizers and visible light." *Biopolymers* **33**, 239–244 (1993).

[125] Nguyen, K. L., Steryo, M., Kurbanyan, K., Nowitzki, K. M., Butterfield, S. M., Ward, S. R., and Stemp, E. D. A. "DNAProtein Cross-Linking from Oxidation of Guanine via the FlashQuench Technique." *J. Am. Chem. Soc.* **122**, 3585–3594 (2000).

[126] Boon, E. M., Pope, M. A., Williams, S. D., David, S. S., and Barton, J. K. "DNA-Mediated Charge Transport as a Probe of MutY/DNA Interaction." *Biochemistry* **41**, 8464–8470 (2002).

[127] Boon, E. M., Livingston, A. L., Chmiel, N. H., David, S. S., and Barton, J. K. "DNA-mediated charge transport for DNA repair." *Proc. Natl. Acad. Sci. USA* **100**, 12543–12547 (2003).

[128] House, P. G., Volk, D. E., Thiviyanathan, V., Manuel, R. C., Luxon, B. A., Gorenstein, D. G., and Lloyd, R. S. "Potential double-flipping mechanism by *E. coli* MutY." *Prog. Nucl. Acids Res. Mol. Biol.* **68**, 349–364 (2001).

[129] Yavin, E., Boal, A. K., Stemp, E. D. A., Boon, E. M., Livingston, A. L., O'Shea, V. L., David, S. S., and Barton, J. K. "Protein-DNA charge transport: redox activation of a DNA repair protein by guanine radical." *Proc. Natl. Acad. Sci. USA* **102**, 3546–3551 (2005).

[130] Dilg, A. W., Mincione, G., Achterhold, K., Iakovleva, O., Mentler, M., Luchinat, C., Bertini, I., and Parak, F. G. "Simultaneous interpretation of Mössbauer, EPR and ^{57}Fe ENDOR spectra of the [Fe_4S_4] cluster in the high-potential iron protein I from *Ectothiorhodospira halophila*." *J. Biol. Inorg. Chem.* **4**, 727–741 (1999).

[131] Boon, E. M., Ceres, D. M., Drummond, T. G., Hill, M. G., and Barton, J. K. "Mutation detection by electrocatalysis at DNA-modified electrodes." *Nat. Biotech.* **18**, 1096–1100 (2000).

[132] Kelley, S. O., Boon, E. M., Barton, J. K., Jackson, N. M., and Hill, M. G. "Single-base mismatch detection based on charge transduction through DNA." *Nucl. Acids Res.* **27**, 4830–4837 (1999).

[133] Boal, A. K., Genereux, J. C., Sontz, P. A., Gralnick, J. A., Newman, D. K., and Barton, J. K. "Redox signaling between DNA repair proteins for efficient lesion detection." *Proc. Natl. Acad. Sci. USA* **106**, 15237–15242 (2009).

[134] Lee, P. E., Demple, B., and Barton, J. K. "DNA-mediated redox signaling for transcriptional activation of SoxR." *Proc. Natl. Acad. Sci. USA* **106**, 13164–13168 (2009).

[135] Merino, E. J., and Barton, J. K. "Oxidation by DNA charge transport damages conserved sequence block II, a regulatory element in mitochondrial DNA." *Biochemistry* **46**, 2805–2811 (2007).

Chapter 2

Synthesis and Characterization of Tricarbonyl Rhenium Complexes*

*Adapted from E. D. Olmon et al. *J. Am. Chem. Soc.* **133**, 13718–13730 (2011), and E. D. Olmon, M. G. Hill, and J. K. Barton, *Inorg. Chem.* **Accepted** (2011).

2.1 Introduction

The rich photophysical, photochemical, and redox properties of polypyridyl transition metal complexes make them useful in a wide range of fields, including energy conversion[1,2], medicine[3–5], cellular imaging,[6–9] and DNA sensing.[10–13] The utility of these metal complexes stems from their stability in many different chemical environments, as well as their rich photophysical behavior and potent redox reactivity. In addition, the general synthetic flexibility and modularity of such molecules allows for easy and systematic modification of these properties.

Re complexes of the family *fac*-[Re(CO)$_3$(diimine)(L)]^n, where L is usually a cyclic imine or a halide, have been used as probes in time-resolved infrared (TRIR) spectroscopy. Vibrational modes involving the tricarbonyl ligand set provide three unique and specific transition moments that are well removed energetically from those of organic carbonyl groups. These are the totally symmetric in-phase ν(CO) vibration A$'$(1), which appears in ground state vibrational spectra near 2030 cm^{-1}, and the totally symmetric out-of-phase A$'$(2) and equatorial asymmetric A$''$ modes, which appear near 1920 cm^{-1}.[14] Elaborate photophysical and photochemical pathways can be elucidated by monitoring changes in the energies of these modes following electronic excitation of the complex.[15–20]

Because the carbonyl ligand stretching frequencies are energetically isolated from most organic vibrational modes, these complexes are especially suitable for use in the study of biomolecular photophysics and redox chemistry. For example, by coordinating Re$^{\mathrm{I}}$(CO)$_3$(4,7-dimethyl-1,10-phenanthroline) to histidine 124 in *Pseudomonas Aeruginosa* azurin, researchers were able to follow the kinetics of charge transfer from the Re photooxidant to the Cu(I) center of the protein by observing changes in the vibrational frequencies of the Re CO ligands.[21,22] This work has shown that an intervening aromatic residue such as tryptophan can serve as an intermediate in a multistep tunneling mechanism between the photooxidant and the Cu center, increasing the rate of charge transfer by several orders of magnitude. Similarly, early studies have appeared in which tricarbonyl Re complexes were used to trigger the oxidation of DNA.[23,24] In such experiments, changes in the vibrational stretching frequencies of the CO ligands and the formation of oxidized guanine products

can be observed simultaneously.

Here, we report the synthesis and characterization of a pair of related tricarbonyl Re complexes, $[Re(CO)_3(dppz)(py'\text{-}OH)]^+$ and $[Re(CO)_3(dppz)(py'\text{-}OEt)]^+$ (dppz = dipyrido[3,2-*a*:2′,3′-*c*]phenazine; py′-OH = 3-(pyridin-4-yl)propanoic acid; py′-OEt = ethyl 3-(pyridin-4-yl)propanoate), (Scheme 2.1) designed for use as DNA photooxidants. These complexes share many photophysical characteristics with other tricarbonyl Re complexes that bear dppz, including an increase in luminescence in the presence of DNA. In addition, we show that the excited state reduction potential of these complexes is sufficiently strong to oxidize guanine.

2.2 Experimental Section

2.2.1 Materials

Unless indicated otherwise, all reagents and solvents were of reagent grade or better and were used as received without further purification. The ligand 3-(pyridin-4-yl)propanoic acid (py′-OH) was purchased from Chess GmbH (Mannheim, Germany).

2.2.2 Synthesis of $[Re(CO)_3(dppz)(py'\text{-}OR)]^+$

The synthesis of [*fac*-$Re(CO)_3$(dppz)(py′-OH)]Cl closely followed the procedure of Stoeffler, et al.[25] A mixture of 253 mg (0.7 mmol) $Re(CO)_5Cl$ and 147 mg (0.7 mmol) 1,10-phenanthroline-5,6-dione in 7 mL toluene was refluxed (110 °C) for 4.5 h. The crude solid product was collected by suction filtration, purified by silica gel using THF as an eluent, and dried under vacuum to yield $Re(CO)_3Cl$(1,10-phenanthroline-5,6-dione) as an orange microcrystalline solid. $Re(CO)_3Cl$(dppz) was formed by heating 160 mg (0.31 mmol) $Re(CO)_3Cl$(1,10-phenanthroline-5,6-dione) in 15 mL EtOH to reflux (85 °C), adding 55 mg (0.6 mmol) *o*-phenylenediamine, and refluxing the mixture for 1 h. The yellow-ochre solid product was collected by suction filtration. ^{1}H NMR (300 MHz) in DMSO indicated the presence of the dppz ligand: δ 8.22 (q, 2H), 8.31 (m, 2H), 8.55 (q, 2H), 9.58 (d, 2H), 9.88 (d, 2H). The desired product was obtained following substitution for the Cl ligand. A sus-

pension of 160 mg (0.27 mmol) $Re(CO)_3Cl(dppz)$ was heated under Ar to 50 °C in 25 mL dry DMF. After addition of 280 mg (1.1 mmol) $AgPF_6$, the reaction mixture was heated at 50 °C for 5 min, then 250 mg (1.7 mmol) py′-OH was added and the mixture was refluxed at 70 °C under Ar for 6 h. The reaction was cooled, and the AgCl precipitate was removed by gravity filtration, yielding an orange-yellow solution. The crude product was purified by silica gel using 5% methanol in chloroform as the eluent, and then dried under vacuum to yield $[Re(CO)_3(dppz)(py'\text{-}OR)](PF_6)$. The PF_6 counter ion was exchanged for chloride using Sephadex QAE A-25 anion exchange resin, and the resulting solution was concentrated using a C18 Sep-Pak to yield *fac*-$[Re(CO)_3(dppz)(py'\text{-}OR)]Cl$ as a bright yellow solid. ^{1}H NMR (PF_6 salt, 300 MHz, CD_3CN): δ 9.79 (dd, 2H), 9.65 (dd, 2H), 8.37 (dd, 2H), 8.23 (m, 4H), 8.09 (dd, 2H), 7.13 (d, 2H), 2.73 (t, 2H), 2.44 (t, 2H). ^{13}C NMR (PF_6 salt, 300 MHz, CD_3CN): δ 155.3, 155.0, 151.3, 149.0, 142.4, 136.5, 132.4, 129.3, 128.2, 126.3, 32.3, 28.9. ESI: calcd 703.7 for $C_{29}H_{19}N_5O_5Re$ (M^+), found 703.9.

The related ethyl ester was prepared in the same way following the Fischer esterification of py′-OH. ^{1}H NMR (PF_6 salt, 300 MHz, CD_3CN): δ 9.90 (dd, 2H), 9.65 (dd, 2H), 8.45 (dd, 2H), 8.26 (dd, 2H), 8.20 (dd, 2H), 8.13 (dd, 2H), 7.09 (d, 2H), 3.88 (q, 2H), 2.72 (t, 2H), 2.41 (t, 2H), 0.99 (t, 3H). ESI: calcd 731.8 for $C_{31}H_{23}N_5O_5Re$ (M^+), found 732.0.

2.2.3 Electrochemistry

Electrochemical measurements were carried out using an electrochemical workstation (CH Instruments 650A). Cyclic voltammetry (CV) was performed at ambient temperature using a standard three electrode apparatus with a glassy carbon working electrode, a Pt auxiliary electrode, and a Ag/AgCl reference electrode. The use of an internal ferrocene/ferrocenium standard for CV measurements facilitated conversion of the potentials referenced against Ag/AgCl to NHE. Immediately prior to measurement, samples were degassed rigorously with N_2. All samples were measured in the presence of 0.1 M tetra-n-butylammonium hexafluorophosphate electrolyte. All redox potentials are reported herein vs. NHE.

2.2.4 Spectroscopy

Steady-state absorption spectra were recorded on a Beckman DU 7400 diode array spectrophotometer. Steady-state emission spectra were recorded on a Fluorolog-3 spectrofluorometer (Jobin Yvon) using 2 mm slits. Scattered light was rejected from the detector by appropriate filters. Reported emission and excitation spectra are the average of at least five consecutive measurements. Low volume 1 cm path-length quartz cells were used for both spectrophotometric and luminescence experiments.

Fourier Transform Infrared (FT-IR) spectroscopy experiments were carried out on a Thermo-Nicolet NEXUX 670 FT-IR spectrometer. Samples were held in a 100 μm-path-length cell between two CaF_2 plates. Samples concentrations were approximately 1 mM in acetonitrile. Samples were degassed thoroughly before introduction into the sample cell.

2.3 Results and Discussion

2.3.1 Metal Complex Design

The Re complexes described here were designed specifically for use in TRIR experiments involving DNA. This intention led to the incorporation of two structural elements that facilitate interactions with the DNA duplex. The first of these is the polycyclic heteroaromatic ligand dppz, which allows the complex to bind to DNA by intercalation. In this binding mode, the intercalating ligand slides into the base stack, sandwiching itself between two neighboring bases.[26] Structural changes to the DNA duplex include a slight unwinding to accommodate the intercalator and a corresponding increase in length. Intercalation increases the binding affinity of the complex due to favorable π stacking interactions and hydrophobic forces. Because of the large surface area of dppz, these effects can be quite strong; the binding affinity of $[Ru(phen)_2(dppz)]^{2+}$ is on the order of 10^7 M^{-1}, whereas that of $[Ru(phen)_3]^{2+}$ is closer to 10^4 M^{-1}.[27] Intercalation also facilitates strong electronic coupling between the metal complex and the base stack. It is this coupling that enables charge transport to occur through the DNA base stack over long distances[28] The second structural element is a carboxyalkyl chain, which is introduced via functionalization at the

4 position of a pyridine ligand. This modification allows for covalent attachment of the complex at specific sites on the DNA strand. By controlling the site of incorporation and intercalation, it is possible to determine the distance between the Re charge donor and the charge acceptor.

2.3.2 Metal Complex Synthesis

The synthetic strategy used for the preparation of $[Re(CO)_3(dppz)(py'\text{-}OR)]^+$ was based on the high-yielding and highly extensible methodology of Stoeffler et al.[25] The synthesis is outlined in Scheme 2.2. The first step involves substitution of 1,10-phenanthroline-5,6-dione for two carbonyl ligands of $Re(CO)_5Cl$. Due to the trans effect, addition of the bidentate ligand results in the generation of only the *facial* stereoisomer. Following purification of the product by silica gel chromatography, formation of dppz is effected by condensation of *o*-phenylenediamine with the dione. The desired product is formed by substitution of the Cl ligand for pyridine or a derivative of pyridine in the presence of $AgPF_6$. If the pyridine ligand is functionalized with a hydrophilic group such as a carboxylate, purification of the crude product by silica gel chromatography can be difficult due to the high retention of the species on the solid phase. In such cases, it is advisable to protect the carboxylate with an ester prior to ligation of the ligand at the metal center. Pure, dry product forms a bright yellow powder that is insoluble in water. Salt metathesis on an anion exchange column can be used to generate the chloride salt, which is slightly more soluble in aqueous solution.

The entire synthesis takes only a few days. In addition, the modular nature of the procedure allows for the rapid synthesis of a large number of related species. For example, by using 4- or 5-substituted *o*-phenylenediamine, it is possible to generate dppz ligands functionalized at the 11 and 12 positions. Similarly, any number of ligands, not just pyridine derivatives, can fill the last coordination site. Such strategies have been used to tease out the subtle photophysics of tricarbonyl Re complexes.[14,17,20,29–31]

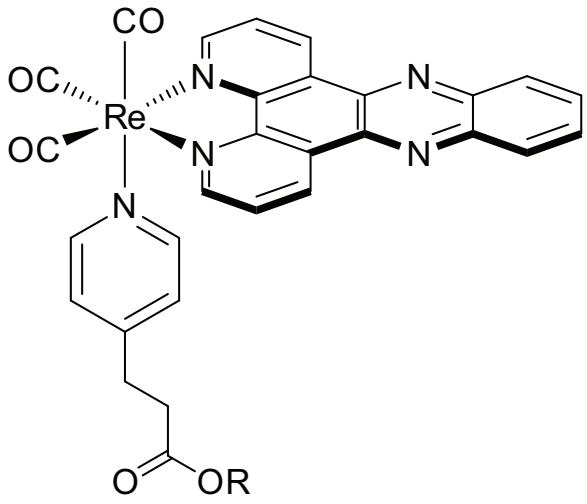

Scheme 2.1: $[Re(CO)_3(dppz)(py'\text{-}OR)]^+$

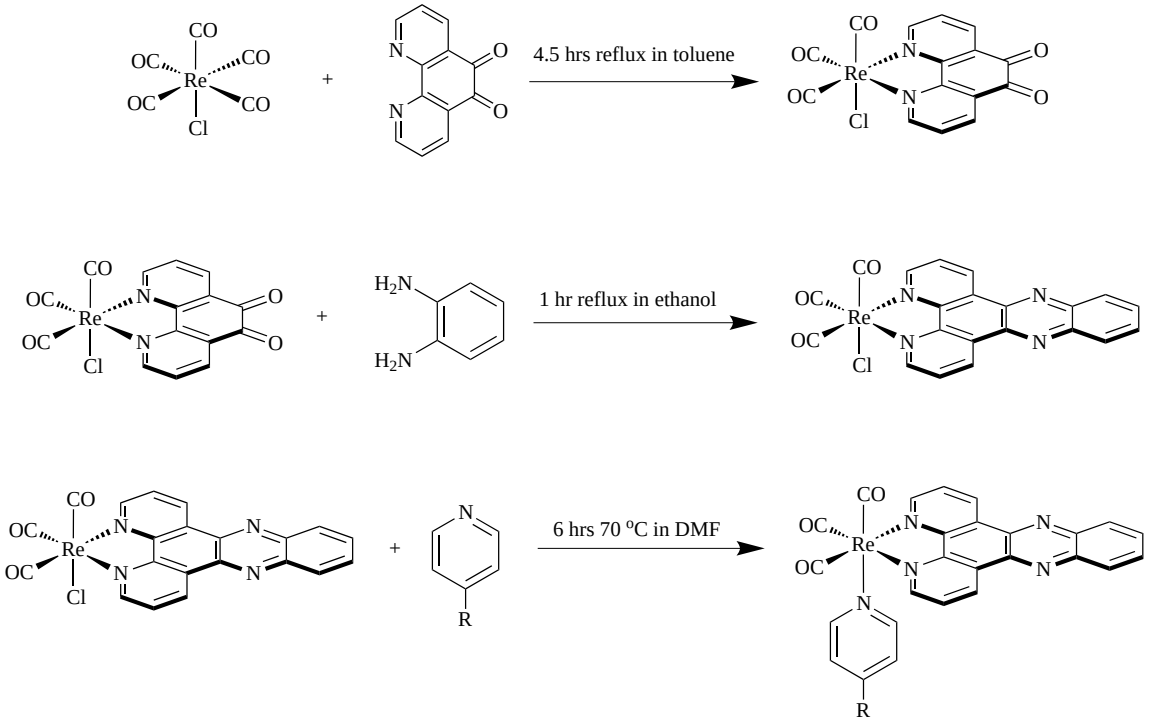

Scheme 2.2: Synthesis of $[Re(CO)_3(dppz)(py')]^+$

2.3.3 Photophysical Characterization of $[Re(CO)_3(dppz)(py'\text{-}OR)]^+$

Spectroscopically, the Re complexes resemble other dppz-bearing tricarbonyl Re complexes (Figure 2.1).[19,25,29,31–38] The complex displays absorption maxima at 364 nm and 382 nm ($\epsilon_{388} \approx 11\,000\ M^{-1}\ cm^{-1}$),[25,34] with a weak tail extending into the visible region. The emission spectrum ($\lambda_{ex} = 355$ nm) in acetonitrile is bifurcated, exhibiting maxima at 555 nm and 595 nm. The excitation spectrum of $[Re(CO)_3(dppz)(py'\text{-}OEt)]^+$ in acetonitrile ($\lambda_{em} =$ 550 nm) indicates the evolution of prominent luminescence at 570 nm upon excitation between 300 nm and 370 nm, with less emission at higher excitation wavelengths.

The high degree of similarity between the absorption spectra of complexes of the type *fac*-$[Re(CO)_3(dppz)(L)]^{n+}$ and the free dppz ligand suggests that the absorption maxima observed near 360 nm and 380 nm result from a $\pi \rightarrow \pi^*$ (dppz) intraligand (IL) transition.[19,25] However, the long, low-intensity tail into the visible region, as well as a slight red shift of these bands compared to the free dppz ligand, indicates the presence of an underlying $d\pi(Re) \rightarrow \pi^*$ (dppz) metal-to-ligand charge transfer (MLCT) transition.[19,32] The complexes $[Re(CO)_3(dppz)(py'\text{-}OR)]^+$ share these characteristics, suggesting that irradiation with light in the near-UV populates several excited states in this species, namely MLCT states and IL transitions centered on the phenanthrene (IL_{phen}) and phenazine (IL_{phz}) parts of dppz.[18,19,31,35,36] Over time, the initially excited singlet states are expected to decay to ^3MLCT, $^3IL_{phen}$ and $^3IL_{phz}$ states.[19]

The FT-IR spectrum of $[Re(CO)_3(dppz)(py'\text{-}OEt)]^+$ is shown in Figure 2.2 on page 68. The spectrum consists of two strong bands. The band at 2036 cm^{-1} corresponds to absorbance of the A′(1) mode, and the band at 1932 cm^{-1} corresponds to overlapping absorption of the A′(2) and A″ modes. The low intensity shoulders at 2025 cm^{-1} and 1905 cm^{-1} are likely due to impurities.

2.3.4 Interactions with DNA

Addition of DNA to a solution of $[Re(CO)_3(dppz)(py'\text{-}OEt)]^+$ results in a decrease and slight redshift of the IL absorption bands near 360 and 390 nm. This change is illustrated in Figure 2.3 for the addition of 30-mer duplexes containing only A·T or only G·C base

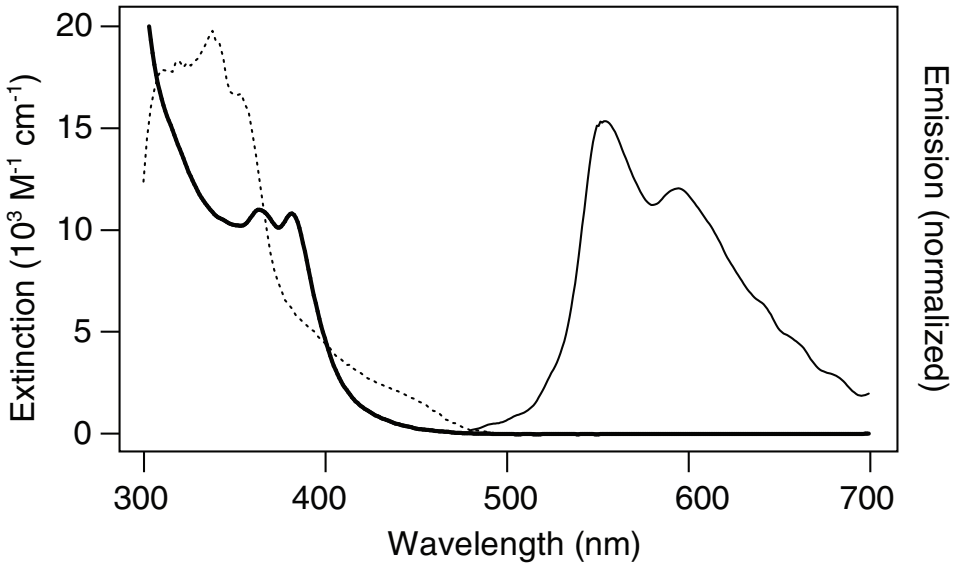

Figure 2.1: UV/visible steady-state characteristics of $[Re(CO)_3(dppz)(py')]^+$. The absorbance spectrum (bold), emission spectrum (λ_{ex} = 355 nm; solid), and excitation spectrum (λ_{em} = 570 nm; dotted) of the complex (18 μM) in degassed acetonitrile are shown.

pairs. Hypochromicity is observed in both sequence contexts, showing that the identity of the bases has a negligible effect on binding. The change in absorption observed upon the addition of DNA is common for transition metal complexes that contain polycyclic aromatic ligands and is indicative of intercalative binding.[26,39–43]

Emission measurements also show evidence of intercalative binding. In aqueous solution, complexes of the type $[Re(CO)_3(dppz)(L)]^{n+}$ behave as a DNA light switches,[44] emitting only in the presence of DNA.[18,19,25,29,31,33,35,36] This phenomenon is a result of a decrease in solvent accessibility to the intercalated dppz ligand. In solution, hydrogen bonding between water and the phenazine nitrogens of the dppz ligand enable a facile non-radiative decay pathway for excited state relaxation, shutting off luminescence. Upon intercalation, solvent is excluded from interactions with dppz, and fluorescence is restored.[45] Changes in the luminescence of $[Re(CO)_3(dppz)(py'\text{-}OEt)]^+$ upon binding to DNA are shown in Figure 2.3. When the complex is bound to a DNA sequence containing only A·T pairs or a mixed sequence, its luminescence spectrum displays a maximum at 570 nm and a shoulder near 610 nm. This spectrum is typical of dppz-containing tricarbonyl Re complexes. By comparison with the emission of $[Ru(bpy)_3]^{2+}$ in deaerated acetonitrile, the emission quantum yield of $[Re(CO)_3(dppz)(py'\text{-}OEt)]^+$ in the presence of the A·T 30-mer in buffer is 0.008 (compared to 0.062 for $[Ru(bpy)_3]^{2+}$).[46] Interestingly, when bound to a 30-mer consisting of only G·C base pairs, or to DNA with high GC content, emission of the complexes is almost completely quenched, and the maximum is shifted to 585 nm.[47] This dependence of emission on GC content has been observed before. In early experiments, the origin of this effect was unknown. It was suggested that dppz complexes of Re bind more strongly to A·T sequences than to G·C sequences due to more facile propeller twisting of the A and T bases. This flexibility was presumed to decrease unfavorable steric interactions between the DNA backbone and the ancillary (non-intercalating) ligands of the metal complex.[33] More recently, it was suggested that the difference in luminescence in the two sequence contexts is instead due to quenching of the Re* excited state by guanine.[32] This more straightforward explanation is supported by biochemical and spectroscopic experiments.[23,24,47]

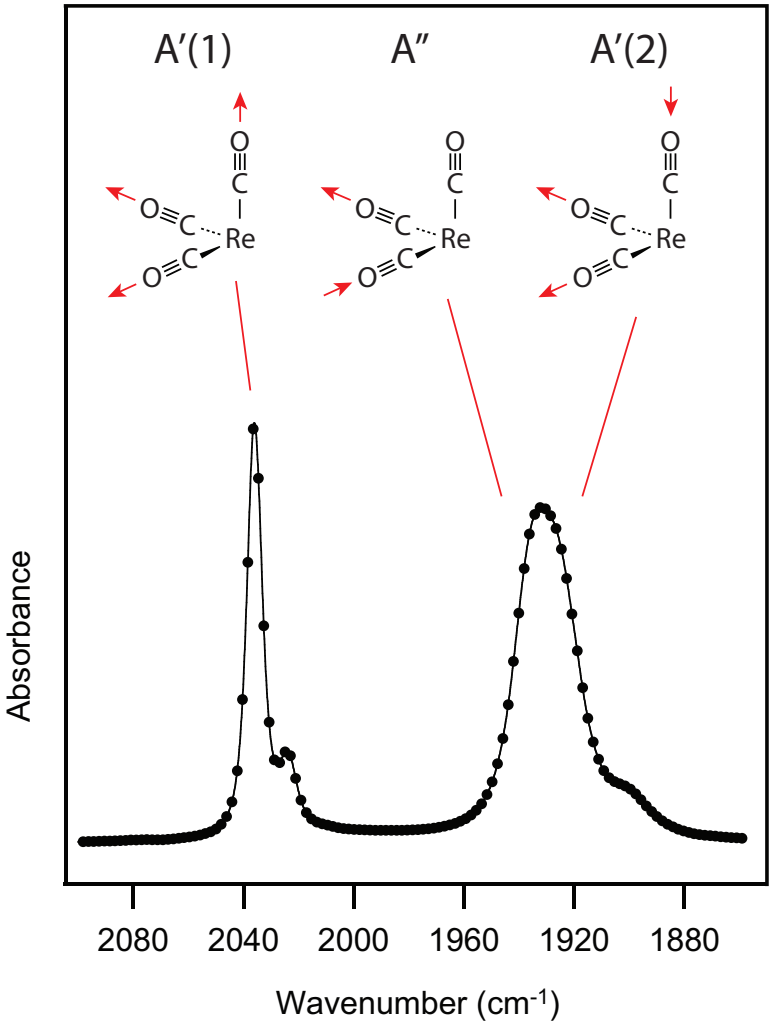

Figure 2.2: FT-IR spectrum of $[Re(CO)_3(dppz)(py'\text{-}OEt)]^+$ saturated in degassed acetonitrile. The solid line shows a cubic spline fit to the data points. Vibrational assignments are based on those of Vlček.[14] For this complex, the A″ and A′(2) bands overlap.

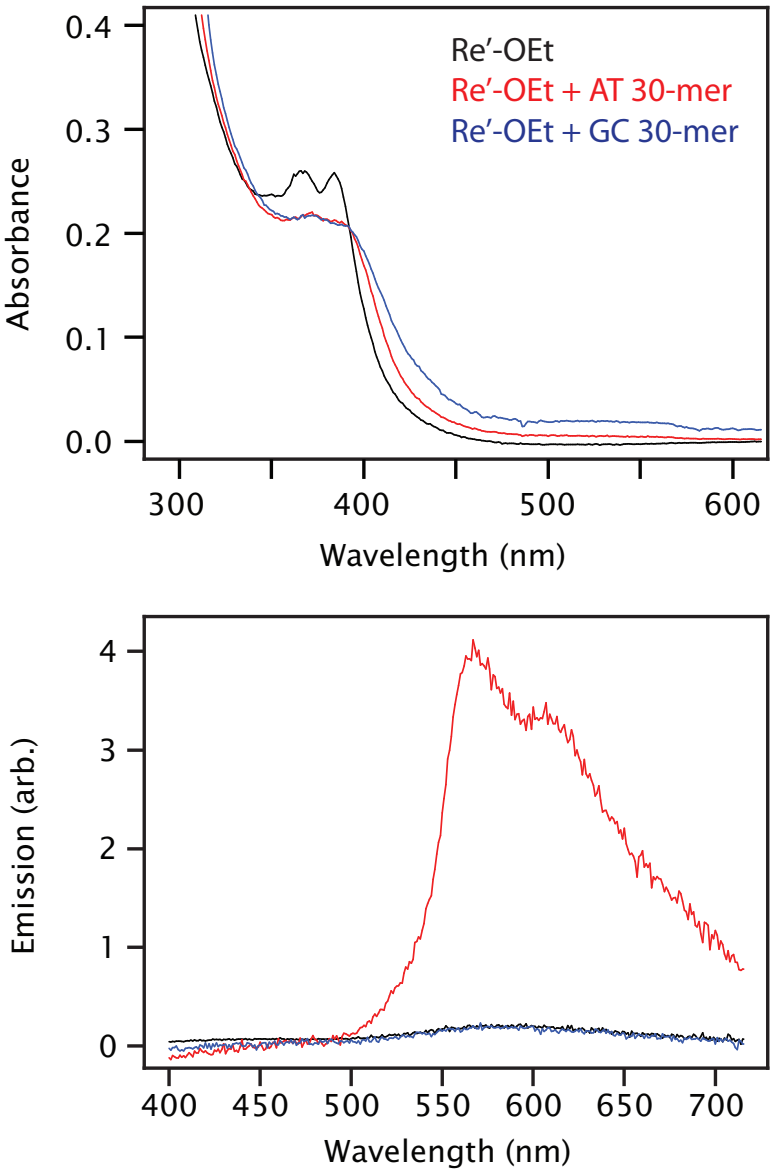

Figure 2.3: Steady-state optical absorption and emission spectra of 25 μM $[Re(CO)_3(dppz)(py'\text{-}OEt)]^+$ and 25 μM DNA 30-mer in D_2O buffer (10 mM NaP_i, 50 mM NaCl; pD 7.0). Top: optical absorption of the Re complex without (black) and with AT-30 (red) or GC-30 (blue). Bottom: emission of Re without (black) or with AT-30 (red) or GC-30 (blue) following excitation at 355 nm. Luminescence spectra have been corrected for emission from DNA alone.

2.3.5 Electrochemistry

In order to understand the redox properties of the Re complexes, their electrochemical behavior was studied by CV. The CV trace of $[Re(CO)_3(dppz)(py'\text{-}OH)]^+$ shows several overlapping peaks upon reduction and one sharp peak upon reoxidation, indicating aggregation of the complex at the electrode surface, while the CV of $[Re(CO)_3(dppz)(py'\text{-}OEt)]^+$ is much cleaner, showing one reversible redox wave at -850 mV (Figure 2.4). Because the carboxylate functionality is so far removed from the metal center, the ground state redox properties of the ester are expected to be identical to those of the carboxylic acid. Further reduction of $[Re(CO)_3(dppz)(py'\text{-}OEt)]^+$ to -1.8 V shows several additional irreversible reduction waves. The excited state reduction potential of $[Re(CO)_3(dppz)(py'\text{-}OEt)]^+$, $E^\circ(Re^{+*}/Re^0)$, was estimated using the formula

$$E^\circ(Re^{+*}/Re^0) = E_{00} + E^\circ(Re^+/Re^0),$$

where E_{00} is the zero-zero excited-state energy and $E^\circ(Re^+/Re^0)$ is the ground state reduction potential.[48] Since DNA-mediated CT may occur from several excited states in these Re complexes, depending on the relative rates of CT and conversion between excited states,[19] E_{00} is best approximated as a range of values. The lower bound for E_{00} can be estimated as the emission maximum (570 nm in aqueous solution, or 2.18 eV), and the upper bound can be estimated as the crossover point between the emission and excitation spectra (480 nm, or 2.58 eV). Thus, for $E^\circ(Re^+/Re^0) = -850$ mV, $E^\circ(Re^{+*}/Re^0)$ is estimated to lie between 1.33 V and 1.73 V. Considering the redox potentials of the base nucleosides ($E^\circ[G^{\bullet+}/G]$ = 1.29 V; $E^\circ[A^{\bullet+}/A]$ = 1.42 V; $E^\circ[T^{\bullet+}/T]$ = 1.6 V; $E^\circ[C^{\bullet+}/C]$ = 1.7 V),[49] the oxidation strength of excited $[Re(CO)_3(dppz)(py'\text{-}OR)]^+$ is indeed sufficient to oxidize guanine.

Since the only difference between samples that showed aggregation at the electrode and samples that did not is the presence of a carboxylic acid functionality instead of a protective ethyl ester at the same position, it is clear that the ethyl ester improves the solubility of the complex in some way. In aqueous solution, the carboxylic acid may become deprotonated, leading to the formation of a zwitterionic species that is has no net charge. In this case, π-stacking interactions between dppz ligands and a lack of electrostatic repulsion between neighboring molecules may lead to dimerization or aggregation of the complexes.

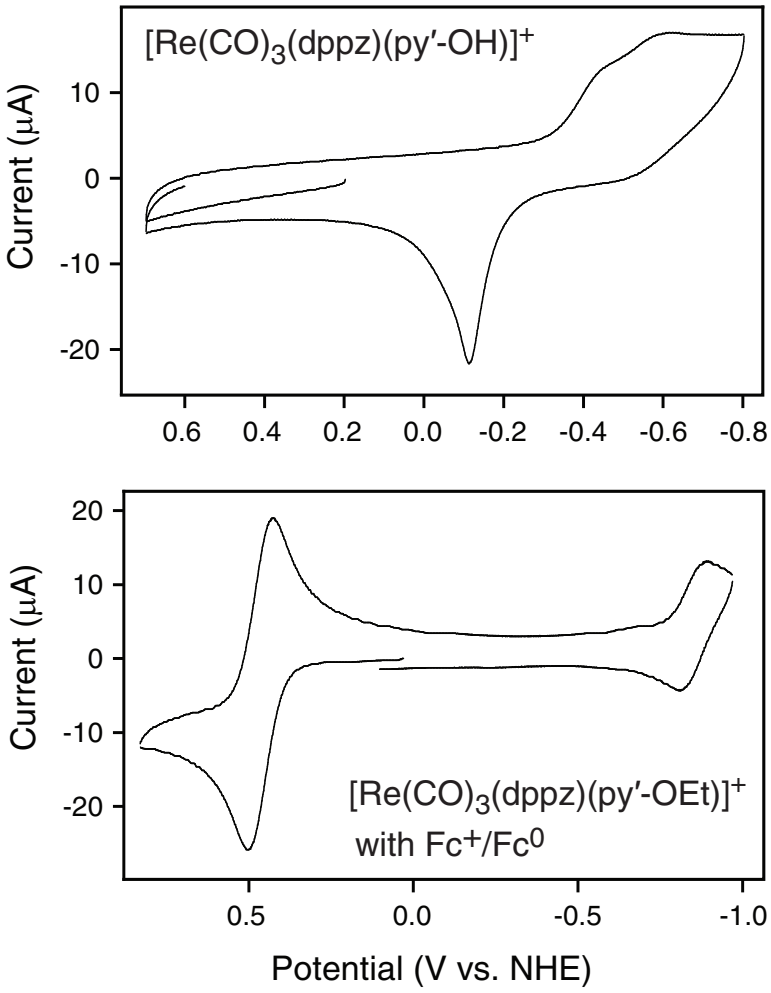

Figure 2.4: Cyclic voltammograms for 20 μM $[Re(CO)_3(dppz)(py'\text{-}OH)]^+$ (top) and 20 μM $[Re(CO)_3(dppz)(py'\text{-}OEt)]^+$ (bottom) in acetonitrile. Samples were thoroughly degassed with N_2 prior to measurement. Measurements were made using a glassy carbon working electrode, a Pt auxiliary electrode, and a Ag/AgCl reference electrode. $[Re(CO)_3(dppz)(py'\text{-}OEt)]^+$ was measured in the presence of a ferrocene/ferrocenium (Fc^+/Fc^0) internal standard. A scan rate of 0.2 V/s was used.

It is unclear whether the aggregation at the electrode is due to a similar process, but it cannot be ruled out.

2.4 Conclusions

Well-tested techniques were employed to synthesize the complexes $[Re(CO)_3(dppz)(py'\text{-}OH)]^+$ and $[Re(CO)_3(dppz)(py'\text{-}OEt)]^+$. The ease and speed with which these syntheses can be carried out verifies the generality of the procedure. The properties of the new complexes are consistent with those of similar complexes: they bind to DNA by intercalation, they exhibit light switch behavior, they have two strong, well-resolved IR absorption bands, and they are strong enough oxidants from the excited state to oxidize guanine. These characteristics ensure that the Re complexes synthesized will be valuable probes for the study of DNA-mediated CT.

References

[1] Polo, A. S., Itokazu, M. K., and Murakami Iha, N. Y. "Metal complex sensitizers in dye-sensitized solar cells." *Coord. Chem. Rev.* **248**, 1343–1361 (2004).

[2] Hagfeldt, A., Boschloo, G., Sun, L., Kloo, L., and Pettersson, H. "Dye-sensitized solar cells." *Chem. Rev.* **110**, 6659–6663 (2010).

[3] Clarke, M. J. "Ruthenium metallopharmaceuticals." *Coord. Chem. Rev.* **236**, 209–233 (2003).

[4] Eryazici, I., Moorefield, C. N., and Newkome, G. R. "Square-planar Pd(II), Pt(II), and Au(III) terpyridine complexes: their syntheses, physical properties, supramolecular constructs, and biomedical activities." *Chem. Rev.* **108**, 1834–1895 (2008).

[5] Abu-Surrah, A. S., and Kettunen, M. "Platinum group antitumor chemistry: design and development of new anticancer drugs complementary to cisplatin." *Curr. Med. Chem.* **13**, 1337–1357 (2006).

[6] Puckett, C. A., and Barton, J. K. "Targeting a ruthenium complex to the nucleus with short peptides." *Bioorg. Med. Chem.* **18**, 3564–3569 (2010).

[7] Neugebauer, U., Pellegrin, Y., Devocelle, M., Forster, R. J., Signac, W., Moran, N., and Keyes, T. E. "Ruthenium polypyridyl peptide conjugates: membrane permeable probes for cellular imaging." *Chem. Commun.* **2**, 5307–5309 (2008).

[8] Cosgrave, L., Devocelle, M., Forster, R. J., and Keyes, T. E. "Multimodal cell imaging by ruthenium polypyridyl labelled cell penetrating peptides." *Chem. Commun.* **46**, 103–105 (2010).

[9] Gill, M. R., Garcia-Lara, J., Foster, S. J., Smythe, C., Battaglia, G., and Thomas, J. A. "A ruthenium(II) polypyridyl complex for direct imaging of DNA structure in living cells." *Nature Chem.* **1**, 662–667 (2009).

[10] Lim, M. H., Song, H., Olmon, E. D., Dervan, E. E., and Barton, J. K. "Sensitivity of Ru(bpy)2dppz2+ luminescence to DNA defects." *Inorg. Chem.* **48**, 5392–5397 (2009).

[11] Marti, A., Puckett, C. A., Dyer, J., Stevens, N., Jockusch, S., Ju, J., Barton, J. K., and Turro, N. J. "Inorganic-Organic Hybrid Luminescent Binary Probe for DNA Detection Based on Spin-Forbidden Resonance Energy Transfer." *J. Am. Chem. Soc.* **129**, 8680–8681 (2007).

[12] Zeglis, B. M., and Barton, J. K. "A Mismatch-Selective Bifunctional Rhodium-Oregon Green Conjugate: A Fluorescent Probe for Mismatched DNA." *J. Am. Chem. Soc.* **128**, 5654–5655 (2006).

[13] Rüba, E., Hart, J. R., and Barton, J. K. "[Ru(bpy)2(L)]Cl2: luminescent metal complexes that bind DNA base mismatches." *Inorg. Chem.* **43**, 4570–4578 (2004).

[14] Vlček, A. "Ultrafast Excited-State Processes in Re(I) Carbonyl-Diimine Complexes: From Excitation to Photochemistry." *Top. Organomet. Chem.* **29**, 73–114 (2010).

[15] Turner, J. J., George, M. W., Johnson, F. P. A., and Westwell, J. R. "Time-resolved Infrared Spectroscopy of Excited States of Transition Metal Species." *Coord. Chem. Rev.* **125**, 101–114 (1993).

[16] George, M. W., and Turner, J. J. "Excited states of transition metal complexes studied by time-resolved infrared spectroscopy." *Coord. Chem. Rev.* **177**, 201–217 (1998).

[17] Stufkens, D. J., and Vlček, A. "Ligand-dependent excited state behaviour of Re(I) and Ru(II) carbonyl-diimine complexes." *Coord. Chem. Rev.* **177**, 127–179 (1998).

[18] Kuimova, M. K., Alsindi, W. Z., Dyer, J., Grills, D. C., Jina, O. S., Matousek, P., Parker, A. W., Porius, P., Sun, X. Z., Towrie, M., Wilson, C., Yang, J., and George, M. W. "Using picosecond and nanosecond time-resolved infrared spectroscopy for the investigation of excited states and reaction intermediates of inorganic systems." *Dalton Trans.* 3996–4006 (2003).

[19] Dyer, J., Blau, W. J., Coates, C. G., Creely, C. M., Gavey, J. D., George, M. W., Grills, D. C., Hudson, S., Kelly, J. M., Matousek, P., McGarvey, J. J., McMaster, J., Parker, A. W., Towrie, M., and Weinstein, J. A. "The photophysics of *fac*-$[Re(CO)_3(dppz)(py)]^+$ in CH_3CN: a comparative picosecond flash photolysis, transient

infrared, transient resonance Raman and density functional theoretical study." *Photochem. Photobiol. Sci.* **2**, 542–554 (2003).

[20] Vlček, A., and Busby, M. "Ultrafast ligand-to-ligand electron and energy transfer in the complexes fac-[Re^{I}(L)$(CO)_3$(bpy)]$^{n+}$." *Coord. Chem. Rev.* **250**, 1755–1762 (2006).

[21] Shih, C., Museth, A. K., Abrahamsson, M., Blanco-Rodríguez, A. M., Di Bilio, A. J., Sudhamsu, J., Crane, B. R., Ronayne, K. L., Towrie, M., Vlček, A., Richards, J. H., Winkler, J. R., and Gray, H. B. "Tryptophan-accelerated electron flow through proteins." *Science* **320**, 1760–1762 (2008).

[22] Blanco-Rodríguez, A. M., Di Bilio, A. J., Shih, C., Museth, A. K., Clark, I. P., Towrie, M., Cannizzo, A., Sudhamsu, J., Crane, B. R., Sýkora, J., Winkler, J. R., Gray, H. B., Záliš, S., and Vlček, A. "Phototriggering Electron Flow through Re^{I}-modified *Pseudomonas aeruginosa* Azurins." *Chem. Eur. J.* **17**, 5350–5361 (2011).

[23] Cao, Q., Creely, C. M., Davies, E. S., Dyer, J., Easun, T. L., Grills, D. C., McGovern, D. A., McMaster, J., Pitchford, J., Smith, J. A., Sun, X.-Z., Kelly, J. M., and George, M. W. "Excited state dependent electron transfer of a rhenium-dipyridophenazine complex intercalated between the base pairs of DNA: a time-resolved UV-visible and IR absorption investigation into the photophysics of *fac*-[$Re(CO)_3(F_2dppz)(py)]^+$ b." *Photochem. Photobiol. Sci.* **10**, 1355–1364 (2011).

[24] Smith, J. A., George, M. W., and Kelly, J. M. "Transient spectroscopy of dipyridophenazine metal complexes which undergo photo-induced electron transfer with DNA." *Coord. Chem. Rev.* **In Press**, (2011).

[25] Stoeffler, H. D., Thornton, N. B., Temkin, S. L., and Schanze, K. S. "Unusual Photophysics of a Rhenium(I) Dipyridophenazine Complex in Homogeneous Solution and Bound to DNA." *J. Am. Chem. Soc.* **117**, 7119–7128 (1995).

[26] Pyle, A., Rehmann, J., Meshoyrer, R., Kumar, C., Turro, N., and Barton, J. K. "Mixed-ligand Complexes of Ruthenium(II): Factors Governing Binding to DNA." *J. Am. Chem. Soc.* **111**, 3051–3058 (1989).

[27] Jenkins, Y., Friedman, A. E., Turro, N. J., and Barton, J. K. "Characterization of dipyridophenazine complexes of ruthenium(II): the light switch effect as a function of nucleic acid sequence and conformation." *Biochemistry* **31**, 10809–10816 (1992).

[28] Genereux, J. C., Boal, A. K., and Barton, J. K. "DNA-Mediated Charge Transport in Redox Sensing and Signaling." *J. Am. Chem. Soc.* **132**, 891–905 (2010).

[29] Dyer, J., Grills, D. C., Matousek, P., Parker, A. W., Towrie, M., Weinstein, J. A., and George, M. W. "Revealing the photophysics of *fac*-[(dppz-12-NO_2)Re$(CO)_3$(4-Me_2Npy)]$^+$: a picosecond time-resolved IR study." *Photochem. Photobiol. Sci.* 872–873 (2002).

[30] Kuimova, M. K., Gill, P. M. W., Lin, C.-Y., Matousek, P., Towrie, M., Sun, X. Z., George, M. W., and Parker, A. W. "Picosecond time-resolved infrared study of 2-aminopurine ionisation in solution." *Photochem. Photobiol. Sci.* **6**, 949–955 (2007).

[31] Kuimova, M. K., Alsindi, W. Z., Blake, A. J., Davies, E. S., Lampus, D. J., Matousek, P., McMaster, J., Parker, A. W., Towrie, M., Sun, X.-Z., Wilson, C., and George, M. W. "Probing the solvent dependent photophysics of *fac*-[Re$(CO)_3$(dppz-X_2)Cl] (dppz-X_2 = 11,12-X_2-dipyrido[3,2-*a*:2′,3′-*c*]phenazine); X = CH_3, H, F, Cl, CF_3)." *Inorg. Chem.* **47**, 9857–9869 (2008).

[32] Ruiz, G. T., Juliarena, M. P., Lezna, R. O., Wolcan, E., Feliz, M. R., and Ferraudi, G. "Intercalation of *fac*-[(4,4′-bpy)$Re^I(CO)_3$(dppz)]$^+$, dppz = dipyridyl[3,2-*a*:2′3′-*c*]phenazine, in polynucleotides. On the UV-vis photophysics of the Re(I) intercalator and the redox reactions with pulse radio." *Dalton Trans.* **3**, 2020–2029 (2007).

[33] Yam, V. W.-W., Lo, K. K.-W., Cheung, K.-K., and Kong, R. Y.-C. "Deoxyribonucleic acid binding and photocleavage studies of rhenium(I) dipyridophenazine complexes." *J. Chem. Soc., Dalton Trans.* **14**, 2067–2072 (1997).

[34] Yam, V. W.-W., Lo, K. K.-W., Cheung, K.-K., and Kong, R. Y.-C. "Synthesis, photophysical properties and DNA binding studies of novel luminescent rhenium(I) com-

plexes. X-Ray crystal structure of [Re(dppn)$(CO)_3$(py)](OTf)." *J. Chem. Soc., Chem. Commun.* **3**, 1191–1193 (1995).

[35] Dyer, J., Creely, C. M., Penedo, J. C., Grills, D. C., Hudson, S., Matousek, P., Parker, A. W., Towrie, M., Kelly, J. M., and George, M. W. "Solvent dependent photophysics of fac-[Re$(CO)_3$(11,12-X_2dppz)(py)]$^+$(X = H, F or Me)." *Photochem. Photobiol. Sci.* **6**, 741–748 (2007).

[36] Kuimova, M. K., Sun, Z., Matousek, P., Grills, D. C., Parker, A. W., Towrie, M., and George, M. W. "Probing intraligand and charge transfer excited states of *fac*-[Re(R)$(CO)_3(CO_2$Et-dppz)]$^+$ (R = py, 4-Me_2N-py; CO_2Et-dppz = dipyrido[3,2-a:2′,3′-c]phenazine-11-carboxylic ethyl ester) using time-resolved infrared spectroscopy." *Photochem. Photobiol. Sci.* **6**, 1158–1163 (2007).

[37] Waterland, M. R., Gordon, K. C., McGarvey, J. J., and Jayaweera, P. M. "Spectroscopic and electrochemical studies of a series of copper(I) and rhenium(I) complexes with substituted dipyrido[3,2-*a*:2,3-*c*]phenazine ligands." *J. Chem. Soc., Dalton Trans.* **10**, 609–616 (1998).

[38] Waterland, M. R., and Gordon, K. C. "Electronic absorption, resonance Raman and excited-state resonance Raman spectroscopy of rhenium(I) and copper(I) complexes , with substituted dipyrido[3,2-*a*:2′,3′-*c*]phenazine ligands, and their electron reduced products." *J. Raman Spec.* **31**, 243–253 (2000).

[39] Sitlani, A., and Barton, J. K. "Sequence-specific recognition of DNA by phenanthrenequinone diimine complexes of rhodium(III): importance of steric and van der Waals interactions." *Biochemistry* **33**, 12100–12108 (1994).

[40] Barton, J. K., Danishefsky, A., and Goldberg, J. "Tris(phenanthroline)ruthenium(II): Stereoselectivity in Binding to DNA." *J. Am. Chem. Soc.* **106**, 2172–2176 (1984).

[41] Sitlani, A., Long, E. C., Pyle, A. M., and Barton, J. K. "DNA Photocleavage by Phenanthrenequinone Diimine Complexes of Rhodium(III): Shape-Selective Recognition and Reaction." *J. Am. Chem. Soc.* **114**, 2303–2312 (1992).

[42] Kirsch-De Mesmaeker, A., Orellana, G., Barton, J. K., and Turro, N. J. "Ligand-dependent interaction of ruthenium(II) polypyridyl complexes with DNA probed by emission spectroscopy." *Photochem. Photobiol.* **52**, 461–472 (1990).

[43] Shao, F., Elias, B., Lu, W., and Barton, J. K. "Synthesis and characterization of iridium(III) cyclometalated complexes with oligonucleotides: insights into redox reactions with DNA." *Inorg. Chem.* **46**, 10187–10199 (2007).

[44] Friedman, A. E., Chambron, J.-C., Sauvage, J.-P., Turro, N. J., and Barton, J. K. "Molecular 'Light Switch' for DNA: $Ru(bpy)_2(dppz)^{2+}$." *J. Am. Chem. Soc.* **112**, 4960–4962 (1990).

[45] Turro, C., Bossmann, S. H., Jenkins, Y., Barton, J. K., and Turro, N. J. "Proton Transfer Quenching of the MLCT Excited State of $Ru(phen)_2dppz^{2+}$ in Homogeneous Solution and Bound to DNA." *J. Am. Chem. Soc.* **117**, 9026–9032 (1995).

[46] Caspar, J. V., and Meyer, T. J. "Photochemistry of $Ru(\ bpy)_3^{2+}$. Solvent Effects." *J. Am. Chem. Soc.* **105**, 5583–5590 (1983).

[47] Olmon, E. D., Sontz, P. A., Blanco-Rodríguez, A. M., Towrie, M., Clark, I. P., Vlček, A., and Barton, J. K. "Charge Photoinjection in Intercalated and Covalently Bound $[Re(CO)_3(dppz)(py)]^+$-DNA Constructs Monitored by Time-Resolved Visible and Infrared Spectroscopy." *J. Am. Chem. Soc.* **133**, 13718–13730 (2011).

[48] Juris, A., Balzani, V., Barigelletti, F., Campagna, S., Belser, P., and Von Zelewsky, A. "Ru(II) polypyridine complexes: photophysics, photochemistry, electrochemistry, and chemiluminescence." *Coord. Chem. Rev.* **84**, 85–277 (1988).

[49] Steenken, S., and Jovanovic, S. V. "How Easily Oxidizable Is DNA? One-Electron Reduction Potentials of Adenosine and Guanosine Radicals in Aqueous Solution." *J. Am. Chem. Soc.* **119**, 617–618 (1997).

Chapter 3

DNA-Mediated CT in Re-DNA Constructs Monitored by Time Resolved Infrared Spectroscopy*

*Adapted from E. D. Olmon, P. A. Sontz, A. M. Blanco-Rodríguez, M. Towrie, I. P. Clark, A. Vlček, and J. K. Barton, *J. Am. Chem. Soc.* **133**, 13718–13730 (2011).

3.1 Introduction

The ability of DNA to mediate charge transport (CT) has been established using a variety of redox-active probes and in a great diversity of experimental systems.[1–3] The efficiency of DNA-mediated CT is affected by several factors, including the extent of electronic coupling between the probe and the DNA base stack, coupling within the base stack itself, the driving force of the CT reaction, and the base sequence. DNA CT has been observed over long molecular distances with little attenuation,[4–6] suggesting its utility in molecular-scale devices[7–9] and in biological systems.[2,10–13] Many of the properties of DNA CT have been elucidated in experiments involving the slow accumulation of oxidative damage at low potential guanine sites. While such methods remain useful in the investigation of DNA CT, a general probe for direct, time-resolved monitoring of these processes remains elusive.

Time-resolved infrared (TRIR) spectroscopy offers several advantages over other time-resolved methods for the study of CT events.[14] With the proper choice of IR-active probe and solvent medium, changes in the absorption pattern of well-resolved, transient IR bands provide kinetic information on specific photophysical, chemical, and biochemical processes, together with structural characterization of the excited states and reaction intermediates involved. One common family of probes are coordination complexes of the type $[\mathrm{Re(CO)_3}(N,N)(\mathrm{L})]^n$, where *N*,*N* stands for an α-diimine ligand such as 2,2′-bipyridine (bpy), phenanthroline (phen), or dppz (dipyrido[3,2-*a*:2′,3′-*c*]phenazine) and L represents an axial ligand, often Cl ($n = 0$) or functionalized pyridine ($n = 1+$).[15–23] Photophysical or photochemical reactions involving these Re complexes are manifested in TRIR spectra as changes in the intensities and positions (energies) of absorption bands due to CO stretching vibrations of the $\mathrm{Re(CO)_3}$ group, ν(C≡O). Variation of the *N*,*N* and L ligands affords fine control over the excited-state characters and energetics.[16,18–20,22–27] These complexes have also proven useful as biochemical probes for fluorescence imaging,[28] for monitoring the dynamics of structural fluctuations,[29,30] and especially, for triggering photoinduced electron transfer (ET).[31] Information on ET kinetics and intermediates provided by TRIR is more direct than that obtained using UV/visible time-resolved spectroscopic methods due to the low specificity of the latter. Recently, the presence of tryptophan along the ET

pathway in $Re(CO)_3(4,7\text{-dimethyl-}1,10\text{-phenanthroline})$-modified azurin was shown to increase the rate of ET.[32–34] Although other coordination complexes, such as dicarbonyl Ru species, $W(CO)_5$(4-cyanopyridine), and $[Ru(bpy)(CN)_4]^{2-}$ have been employed as TRIR probes, tricarbonyl Re complexes have been studied much more extensively.[14,16,35] TRIR can also be used to monitor changes in the vibrational frequencies and IR band intensities of organic functionalities in ET assemblies.[36] Of particular interest, TRIR spectra were recorded following the 267 nm excitation of the four canonical nucleotides and of poly(dG-dC)·poly(dG-dC) and poly(dA-dT)·poly(dA-dT).[37] In that work, the lifetimes of the transient states of the free nucleotides ranged from 2.2 to 4.7 ps, while those of the polymers were an order of magnitude longer. Upon 200 nm photoionization of 5′-dGMP and poly(dG-dC)·poly(dG-dC), evidence for the formation of the guanine radical was observed by TRIR as the growth of a transient band at 1702 cm^{-1}.[38] In other experiments, TRIR was used to observe the triplet state of thymine and of 2′-dT,[39] as well as to unravel the pH-dependent photophysics of 5′-G, 5′-GMP, and poly(G).[40] Importantly, these studies indicate that TRIR can be used to monitor photoinduced changes of DNA and of $[Re(CO)_3(N,N)(L)]^n$ simultaneously, making it possible to investigate both the donor and the acceptor sites of Re–DNA CT assemblies. Although interactions between Re complexes and DNA have been studied by UV/visible spectroscopy,[41,42] these interactions had not been investigated by vibrational methods until very recently.[43,44]

Here, TRIR spectroscopy is used in conjunction with other methods to observe the DNA-mediated oxidation of guanine in DNA by photoexcited $[Re(CO)_3(dppz)(py'\text{-OR})]^+$, where py′-OR represents pyridine functionalized at the 4 position (Scheme 3.1). The influence of guanine on the photochemical behavior of the Re complex bound to DNA is investigated by comparing results obtained in four different DNA contexts, including two in which the complex is covalently tethered to specific locations on the duplex. The data presented show that the photoexcited Re complex can oxidize guanine at a distance of several bases away by DNA-mediated CT and that this process can be monitored on the ps to μs timescale by TRIR. The results of this study, in which TRIR is used for the first time to observe DNA-mediated CT between photooxidants and guanine in well-defined covalent

constructs, shows that the DNA sequence surrounding the metal complex binding site has a large influence on the photophysics and photochemistry of the system.

3.2 Experimental Section

3.2.1 Materials

Most reagents for metal complex synthesis and coupling were purchased from Sigma-Aldrich unless otherwise indicated. 3-(pyridin-4-yl)propanoic acid (py′-OH) was purchased from Chess GmbH (Mannheim, Germany). Reagents for DNA synthesis were purchased from Glen Research (Sterling, VA). All reagents were used as received.

3.2.2 Complex and Conjugate Synthesis

Preparation of $[Re(CO)_3(dppz)(py'\text{-}OH)](PF_6)$ was adapted from previously described methods.[41] Following the synthesis, the PF_6^- counter anion was exchanged (QAE Sephadex A-25 resin, GE Healthcare) for chloride ion in order to increase the solubility of the complex in aqueous media. Because facile proton loss from the carboxylic acid-modified pyridine ligand results in an overall neutral zwitterionic species, altering the extent of electrostatic repulsion between complex molecules and of electrostatic attraction to DNA, the protected ethyl ester version of the complex, $[Re(CO)_3(dppz)(py'\text{-}OEt)]^+$ (py′-OEt = ethyl 3-(pyridin-4-yl)propanoate), was used for some experiments.

3.2.3 Oligonucleotide Synthesis and Modification

Oligonucleotides were synthesized using standard solid-phase phosphoramidite chemistry on an Applied Biosystems 3400 DNA synthesizer. Covalent tethers were appended to the 5′-OH termini of resin-bound oligonucleotides as described by Holmlin.[45] The alkyl tether was added to the DNA strand by successive treatment with carbonyldiimidazole and diaminononane. Agitation of the resin-bound, amine-modified DNA strands in the presence of excess (5 mg) $[Re(CO)_3(dppz)(py'\text{-}OH)]Cl$, *O*-(benzotriazol-1-yl)-*N*,*N*,*N*′,*N*′-tetramethyluronium hexafluorophosphate (HBTU), 1-hydroxybenzotriazole hydrate (HOBT),

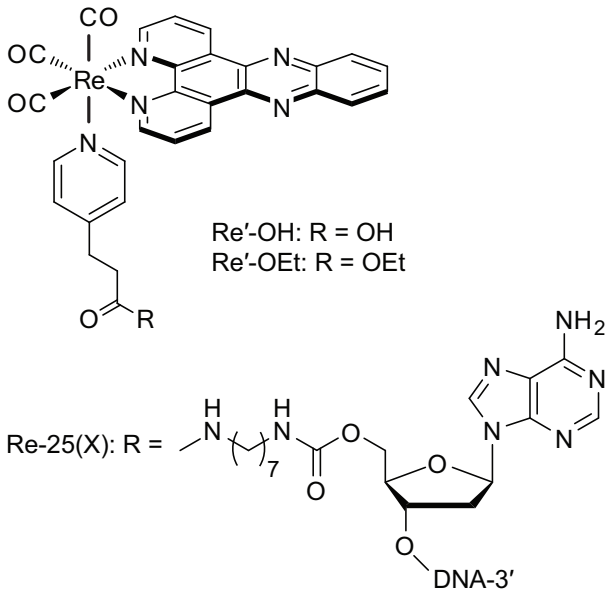

AT-30

```
5′-TTTATATTATTAAATAAATTTTATATATTT-3′
3′-AAATATAATAATTTATTTAAAATATATAAA-5′
```

GC-30

```
5′-CCCGCGCCGCCGGGCGGGCCCCGCGCGCCC-3′
3′-GGGCGCGGCGGCCCGCCCGGGGCGCGCGGG-5′
```

Re-25(X), X = G, I

Scheme 3.1: Schematic illustration of $[Re(CO)_3(dppz)(py'\text{-}OR)]^+$, the covalent linker, and the DNA sequences used for studies of guanine oxidation. Experiments involving AT-30 and GC-30 were conducted in the presence of the free complex Re′-OH. In the covalent assemblies Re-25(G) and Re-25(I), the Re photooxidant is tethered to the 5′ end of one strand via a peptide linkage.

and diisopropylethylamine (DIEA) in anhydrous DMF for 24 hours resulted in covalent attachment of the metal complex to the DNA. Cleavage from the resin was effected by incubation in NH_4OH at 60 °C for 6 hours. Oligonucleotides were purified by reversed-phase HPLC and characterized by MALDI-TOF mass spectrometry. Oligonucleotide concentrations were determined by UV/visible spectrophotometry (Beckman DU 7400). Annealing was accomplished by incubating solutions containing equimolar amounts of complementary strands in buffer (10 mM NaP_i, 50 mM NaCl buffer; pH 7.0) at 90 °C for 5 minutes followed by slow cooling over 90 minutes to ambient temperature.

3.2.4 Assay for Oxidative DNA Damage

Oxidative DNA cleavage experiments were performed using a protocol adapted from Zeglis and Barton[46] with the following adjustments. Oligonucleotides were labeled at the 3′-end by incubating a mixture of 2 μL single-stranded DNA (100 μM), 5 μL [α-^{32}P]-dTTP (Perkin Elmer), 2 μL terminal transferase (TdT; New England Biolabs), 5 μL $CoCl_2$ solution (included with TdT), and 5 μL terminal transferase reaction buffer (included with TdT) for 2 hours at 37 °C. Before gel purification, strands were incubated at 90 °C for 20 minutes in 100 μL 10% aqueous piperidine to induce cleavage of damaged strands. Following purification and annealing, samples (10 μL, 2 μM) were irradiated in parallel for 2 hours using a solar simulator (Oriel Instruments) fitted with a 340 nm internal long pass filter. Samples were then treated with 0.2 units calf thymus DNA and 10% piperidine (v/v), heated for 30 minutes at 90 °C, and dried *in vacuo*. After gel electrophoresis, oxidative damage was quantified by phosphorimagery (ImageQuant). Sample counts are reported as % of total counts per lane and were corrected by subtracting the dark control.

3.2.5 Spectroelectrochemistry

IR spectroelectrochemistry was carried out using a custom-built, optically transparent, thin-layer electrode (OTTLE) cell (path length = 0.1 mm) consisting of vapor-deposited platinum working and pseudoreference electrodes and a Pt-wire auxiliary electrode.[47] The potential of the cell was controlled by a potentiostat (CH Instruments Model 650A electrochemical

workstation). Samples consisted of saturated solutions of metal complexes in dry acetonitrile with 0.1 M Bu_4NPF_6 electrolyte. Samples were degassed by bubbling argon and introduced into the optical cell using a gas-tight syringe prior to measurement. The cell was held at a reducing potential, and spectra were acquired on a Thermo-Nicolet NEXUX 670 FT-IR spectrometer every 4 seconds until the sample was fully reduced.

3.2.6 UV/Visible Emission and Transient Absorption Spectroscopy

Steady-state emission spectra were recorded on a Fluorolog-3 spectrofluorometer (Jobin Yvon) using 2 mm slits. Scattered excitation light was rejected from the detector by appropriate filters. Reported spectra are averages of at least five consecutive measurements.

All time-resolved UV/visible spectroscopic measurements were carried out at the Beckman Institute Laser Resource Center. Nanosecond luminescence decay measurements and transient absorption (TA) measurements were performed using the third harmonic (355 nm) of a 10 Hz, Q-switched Nd:YAG laser (Spectra-Physics Quanta-Ray PRO-Series) as the excitation source (8 ns pulse width, 5 mJ/pulse). Probe light was provided by a synchronized, pulsed 75 W Hg-Xe arc lamp (PTI model A 1010), and detection was accomplished using a photomultiplier tube (Hamamatsu R928) following wavelength selection by a double monochromator (Instruments SA DH-10). Scattered light was rejected using suitable filters. The samples were held in 1-cm-path-length quartz cuvettes (Starna) equipped with stir bars. TA measurements were made with and without excitation, and were corrected for background light, scattering, and fluorescence.

Picosecond emission decay measurements[48–51] were performed using the third harmonic of a regeneratively amplified mode-locked Nd:YAG laser (355 nm, 1 ps pulse width after amplification) as the excitation source and a picosecond streak camera (Hamamatsu C5680, photon-counting mode) as the detector. Emission was observed under magic angle conditions using a 550 nm long-pass cutoff filter.

3.2.7 TRIR Spectroscopy

The ULTRA instrument at the STFC Rutherford Appleton Laboratory was used. The instrument is described in detail elsewhere.[52] Briefly, a titanium sapphire laser-based regenerative amplifier (Thales) produces 800 nm, ∼50 fs pulses at a 10 kHz repetition rate. The laser output is split in two parts, one of which is either frequency doubled or is used to drive an OPA (Light Conversion, TOPAS) equipped with SHG and SFG units to produce a pump beam at 400 or 355 nm, respectively. The second pumps a TOPAS OPA, yielding signal and idler beams that are difference frequency mixed to generate ∼400 cm^{-1} broad mid IR probe pulses. An optical delay line is used to introduce a delay between the pump and probe beams, and the mid IR probe spectrum is recorded at a given time delay using two 128 element HgCdTe detectors (Infrared Associates). For ns–μs measurements, the sample was pumped with 355 nm, 0.7 ns FWHM pulses (AOT, AOT-YVO-20QSP/MOPO), and probed with electronically synchronized 50 fs IR pulses.[53] The sample solutions were placed in a round dip 0.75 mm deep, drilled into a CaF_2 plate, and tightly covered with a polished CaF_2 window. The cell was scanned-rastered across the area of the dip in two dimensions to prevent laser heating and decomposition of the sample. FTIR spectra measured before and after the experiment demonstrated sample stability.

3.2.8 Fitting Methods

TRIR data were simulated at each time delay as a series of Gaussian terms in order to extract kinetic data from overlapping transient bands. The area of each Gaussian was calculated, and kinetic decays were constructed as the change in area with delay time. Nanosecond time-resolved emission, TRIR, and TA data were fit by nonlinear least-squares analysis using IGOR Pro software (Wavemetrics). Model functions consisted of a linear series of exponential terms of the form

$$y(t) = \sum a_i \exp(-t/\tau_i),$$

where a_i and τ_i are the pre-exponential factor and lifetime, respectively, of the ith term. Up to three exponential terms were included until reasonable fits were obtained. For time-resolved emission data, the percent relative contribution reported in Table 3.1 on page 88 represents the number of photons emitted at the probe wavelength by each emissive population, and is calculated as

$$\% \text{ Relative Contribution (emission)} = a_n\tau_n \Big/ \sum a_i\tau_i$$

(the area under the decay for the nth exponential term normalized to the total area under the decay curve). For TRIR and TA data, the percent relative contribution represents the change in absorbance of species n extrapolated to time $t = 0$, and is calculated as

$$\% \text{ Relative Contribution (absorption)} = a_n \Big/ \sum a_i \, .$$

Picosecond emission data were collected at 1 ns, 5 ns, and 50 ns time ranges and spliced together before fitting. Data were compressed logarithmically in time prior to fitting in order to decrease the bias of long time data on the fit. These data could not be fit well to a series of exponential terms and were instead analyzed by the maximum entropy method using a MATLAB (MathWorks) routine written at Caltech.[48–51]

3.3 Results

3.3.1 Research Strategy and Design of Re-DNA CT Assemblies

With the aim to establish DNA oxidation by electronically excited rhenium tricarbonyl-diimine complexes, we have employed a newly developed sensitizer, $[Re(CO)_3(dppz)(py'\text{-}OR)]^+$ (R = H, Re′−OH; or R = CH_2CH_3, Re'-OEt), that can be covalently linked to DNA (Figure 3.1). Three design elements make this a promising probe for the study of DNA-mediated CT. The first is the incorporation of TRIR-active carbonyl ligands. Re carbonyl-diimine complexes are useful probes in TRIR spectroscopic experiments due to the intense and well-resolved bands corresponding to carbonyl stretching modes. These modes are

Table 3.1: Least-Squares Fit Parameters for TRIR Decays of $[Re(CO)_3(dppz)(py'\text{-}OR)]^+$ in the Presence of DNA ($\lambda_{ex} = 355$ nm)

Technique	Detail	Sample	Lifetime, seconds (% Relative Contribution[a])					
			10^{-9}	10^{-8}	10^{-7}	10^{-6}	10^{-5}	$> 10^{-5}$ [b]
TRIR[c]	$R(CO)_3$ Bleach Recovery	AT-30 + Re′-OH		1.4 (28)	3.0 (31)		2.5 (41)	
		GC-30 + Re′-OH		6.3 (43)	5.5 (49)		1.1 (8)	
		Re-25(I)		2.6 (16)	4.8 (30)		2.8 (54)	
		Re-25(G)	4.8[d]		2.9 (65)	9.1 (35)		
	MLCT (2071 cm^{-1})	AT-30 + Re′-OH	8.8 (38)		5.6 (38)			Long (23)
		Re-25(I)		3.2 (36)	8.9 (44)			Long (20)
	IL (2030 cm^{-1})	AT-30 + Re′-OH			1.5 (31)		2.4 (69)	
		GC-30 + Re′-OH			1.8 (51)	1.0 (42)	2.2 (7)	
		Re-25(I)				3.0 (34)		Long (66)
		Re-25(G)	4.0[d]		3.0 (58)	9.2 (42)		
	$G^{\bullet+}/G^{\bullet}$ (1702 cm^{-1})	GC-30 + Re′-OH			2.1[d]	5.8		
	DNA Bleach Recovery	AT-30 + Re′-OH			1.4 (48)	5.0 (18)		Long (35)
		GC-30 + Re′-OH		5.9 (31)	9.6 (69)			
		Re-25(I)			3.1 (88)			Long (12)
		Re-25(G)		2.9[d]	8.4 (53)	1.0 (47)		
ns Visible TA[e]	$\lambda_{probe} = 475$ nm	AT-30 + Re′-OH			4.9 (17)		2.7 (83)	
		GC-30 + Re′-OH			2.7 (42)	2.0 (58)		
		Re-25(I)			9.6 (42)		2.0 (58)	
		Re-25(G)			4.4 (37)		1.4 (63)	
ns Emission[e,f]	$\lambda_{probe} = 570$ nm	AT-30 + Re′-OH	2.9 (34)	2.4 (23)	5.7 (43)			
		GC-30 + Re′-OH	3.2 (39)	2.7 (35)	2.4 (26)			
		Re-25(I)	5.3 (17)	2.6 (21)	5.4 (62)			
		Re-25(G)	3.9 (42)	2.1 (30)	4.5 (28)			

[a] Determined by different methods for absorption and emission; see Experimental Section
[b] "Long" indicates incomplete decay.
[c] Uncertainty estimated as 20%
[d] These values reflect an increase in intensity.
[e] Uncertainty estimated as 10%
[f] Processes faster than 8 ns are convoluted with instrument response.

extremely sensitive to changes in electron density distribution, molecular structure, and environment.[17,24,30,32,54,55] The second design element is the inclusion of the planar dppz ligand. By incorporating dppz on the metal center, we ensure effective electronic coupling with the DNA base stack. Indeed, the binding constants for intercalating dppz complexes such as $[Ru(bpy)_2(dppz)]^{2+}$ and $[Ru(phen)_2(dppz)]^{2+}$ are greater than 10^6 M^{-1}.[56] While the binding of complexes like $[Re(CO)_3(dppz)(py'\text{-}OR)]^+$ is weaker (10^5 M^{-1})[41,42,57] due to its lower electrostatic charge, the decrease of the molar absorptivity of its near-UV absorption band (i.e., hypochromicity) upon incubation with DNA, as well as an increase in the melting temperature of the bound DNA duplex by approximately 5 °C (depending on the sequence), indicate that this Re complex indeed binds by intercalation. The third design element is the ability to covalently attach the complex to DNA via carboxyalkyl-modified pyridine incorporated at the axial coordination site. The covalent link between the complex and the DNA strand, while flexible, restricts diffusion of the unbound complex, ensuring a higher percentage bound than if the complex were allowed to diffuse freely. In addition, the covalent link enables us to define the DNA sequence at the binding region, eliminating sequence effects as a variable. Physical models suggest that in the equilibrium geometry, tethering restricts binding to the region within three base pairs from the end of the duplex.

The DNA duplexes used were designed to test for the effect of the DNA sequence on the efficiency of DNA oxidation. For systems in which guanine, an effective hole trap, is placed near the expected binding site of the Re complex, charge injection may be followed by facile back electron transfer (BET). Such nonproductive reactions are competitive with permanent charge trapping at guanine sites.[58–60] The frequency of nonproductive events can be reduced by replacing guanine at the Re binding site with inosine (I), a base analog that has a higher oxidation potential than guanine ($E^\circ[I^{\bullet+}/I] \approx 1.5$ V vs. NHE; $E^\circ[G^{\bullet+}/G] = 1.29$ V vs. NHE).[60–63] With these considerations in mind, four DNA sequences were designed (Scheme 3.1). Two of them contain only adenine and thymine (AT-30) or guanine and cytosine (GC-30) and are expected to reveal the effect of the absence or presence, respectively, of strong guanine thermodynamic hole traps on DNA oxidation by noncovalently bound $[Re(CO)_3(dppz)(py'-OH)]^+$. Two DNA sequences were also designed to test for the

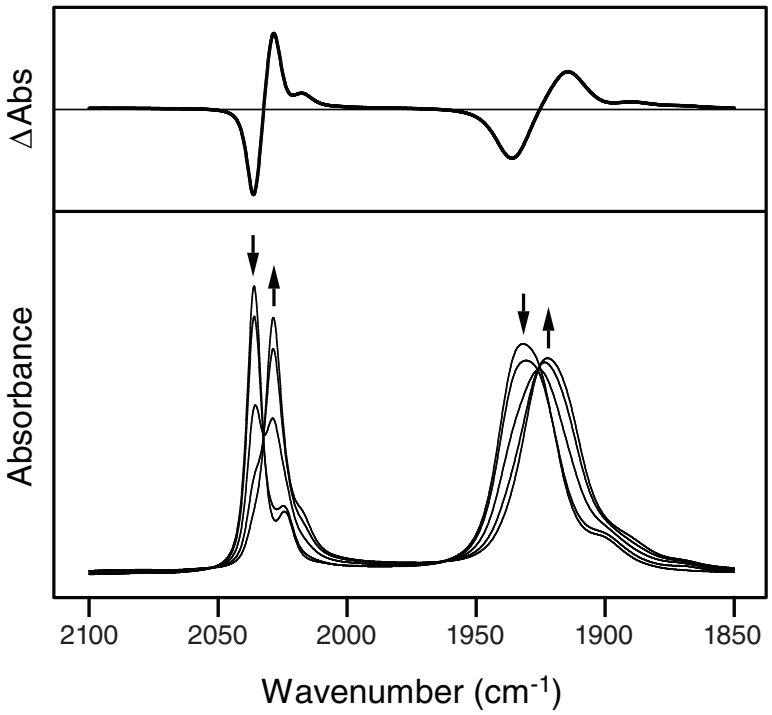

Figure 3.1: Steady-state FTIR spectra (bottom) of saturated Re′−OEt in acetonitrile recorded during bulk reduction using an OTTLE cell. Arrows indicate spectral changes that occur upon reduction. The difference in absorbance between the fully reduced species and the initial species is also shown (top).

effect of neighboring guanine on the efficiency of long range DNA oxidation by covalently-bound Re. These are Re-25(G), which contains guanine next to the Re binding site, and Re-25(I), in which guanine is replaced by inosine.

3.3.2 Sensitizer Characterization

The photophysics of $[Re(CO)_3(dppz)(py'\text{-}OH)]^+$ and $[Re(CO)_3(dppz)(py'\text{-}OEt)]^+$ are very similar, suggesting that modification at the py′ carbonyl has little effect on the energetics of the complex. For example, each complex exhibits absorption maxima at 364 and 382 nm ($\epsilon \approx 11,000\ M^{-1}\ cm^{-1}$),[41,64] with a tail that extends into the visible region.[65] The emission spectra of both complexes show maxima at 554 and 595 nm. At 570 nm, Re′-OH and Re′-OEt each show a biexponential emission decay in acetonitrile, with lifetimes on the order of 200 ns (∼10%) and 10 μs (∼90%), tentatively attributed to emission from different ^{3}IL states.[65] Tethering the Re species to DNA, therefore, is expected to have negligible influence on the energetics of the complex.

The reduction potential of the emissive ^{3}IL state(s), $E^\circ(Re^{+}*/Re^0)$, of the Re label can be estimated as the sum of the ground state reduction potential, $E^\circ(Re^+/Re^0)$, and the zero-zero excited-state energy, E_{00}.[66] The exact value of E_{00} is unknown, but it is estimated to lie between the energy at which the excitation and emission spectra coincide (480 nm, 2.58 eV) and the energy of the emission maximum in aqueous solution (570 nm, 2.18 eV). For Re′-OEt in acetonitrile, $E^\circ(Re^+/Re^0)$ was reported as −850 mV vs. NHE,[65] predicting the excited-state reduction potential to lie between 1.33 and 1.73 eV. As an oxidant, electronically excited Re′-OEt is clearly strong enough to oxidize guanine, and it may be strong enough to oxidize adenine ($E^\circ[A^{\bullet+}/A] = 1.42$ V vs. NHE).[67] The latter reaction, however, is expected to be slower due to the lower driving force. Note that the redox potentials of the canonical bases described here were determined by pulse radiolysis of the free nucleosides and are therefore estimates of the potentials of the bases in the DNA polymer environment. For a summary of experimentally-determined guanine redox potentials in different contexts, see Genereux and Barton (2010).[1]

Hole injection into the DNA base stack must coincide with reduction of the metal com-

plex. In order to characterize this reduced state independently, IR spectroelectrochemical reduction of saturated Re′-OEt in acetonitrile was carried out (Figure 3.1). Before reduction, the spectrum exhibits a band at 2036 cm^{-1} assigned to the totally symmetric in-phase ν(C≡O) vibration A′(1), and a band at 1932 cm^{-1} due to quasidegenerate totally symmetric out-of-phase A′(2) and equatorial antisymmetric A″ ν(C≡O) vibrations.[17,54,68] Reduction results in a bathochromic shift of these bands to 2029 cm^{-1} and 1922 cm^{-1}, respectively. This shift is similar to that observed previously[23] upon reduction of [$ReCl(CO)_3$(dppz)] and its small magnitude is consistent with occupation of the phenazine π^* orbital of the dppz ligand in the [$Re^{I}(CO)_3$(dppz$^{\bullet-}$)(py′-OEt)] reduction product.[24] Subsequent regeneration of the initial species via reoxidation was 95% complete, suggesting partial irreversible decomposition of the electrogenerated product; however, these decomposition products are not expected to interfere in time-resolved spectroscopic experiments employing fast photocycles. An attempt was made to duplicate the experiment in D_2O buffer (10 mM NaP_i, 50 mM NaCl, pD 7.0) in order to generate spectra that would be more directly comparable to TRIR measurements conducted in D_2O buffer. Although the low solubility of the complex and the strong background absorbance of the solvent in this energy region prevented precise analysis, band positions, widths, and relative intensities were similar to those observed in acetonitrile solutions.

3.3.3 Oxidative Damage Pattern of Re-25(G) and Re-25(I) Observed by PAGE

Figure 3.2 shows DNA-mediated oxidative damage in 2 μM solutions of Re-25(G) and Re-25(I) observed after 2 hours of broadband ($\lambda_{ex} > 340$ nm) irradiation and 20% PAGE analysis. Damage occurs as base radicals, formed following hole injection by the excited Re complex, react with solution species such as H_2O or O_2 to form irreversible products.[69,70] Subsequent treatment of the 3′-[^{32}P]-labeled DNA with piperidine induces cleavage at damage sites. For both Re-25(G) and Re-25(I), damage is observed primarily at the 5′-G site of the 5′-GG-3′ doublet, several bases distant from the Re complex binding site predicted from physical models. Importantly, the low concentrations used in these experiments preclude in-

terstrand damage (i.e., it is unlikely that the Re moiety of one construct will intercalate into the base stack of another). The observation of damage at the 5′-GG-3′ site indicates that long-range photoinduced hole injection from the Re label to DNA indeed occurs, consistent with results obtained for a similar Re-DNA conjugate.[65] However, the extent of damage is consistently greater in the case of Re-25(I) than Re-25(G).

3.3.4 Emission Measurements

Many Re tricarbonyl complexes of dppz behave as DNA light switches,[18–23,41,42] much like their Ru counterparts,[71] and the complexes studied here are no exception. In the absence of DNA, negligible emission is observed from an aqueous solution of Re′-OH or Re′-OEt; however, in the presence of AT-30 and in the Re-25(I) sample, a prominent emission band is observed that exhibits a maximum at 570 nm and a shoulder near 600 nm, resembling the emission spectrum seen for similar Re complexes in organic solvents.[19,21,22,41,42,57,64] In the presence of GC-30 and in the Re-25(G) sample, the emission is much less intense, the maxima are shifted to 585 nm, and no shoulder is observed. Steady-state emission spectra of AT-30 alone and in the presence of Re′-OEt are shown in Figure 3.3. Interestingly, the DNA oligomers used in this study are themselves emissive under 355 nm excitation, giving rise to a broad band near 450 nm that tails into the visible region. All efforts were made to ensure that this is not an effect of the instrument, solvent, scattering, or impurities. Such emission, ascribed to excitons or charge transfer excited states, has previously been observed in DNA oligomers but not in calf thymus DNA.[72–74] The Re-loaded AT-30 sample shows overlapping DNA and Re′-OEt emission. By scaling and subtracting the emission band due to DNA alone, it is possible to isolate emission from only the intercalated complexes. Significantly, emission from Re′-OEt becomes strongly quenched on going from AT-30 to GC-30 (Figure 3.3). A similar decrease is observed for Re-25(G) compared to Re-25(I). The concentrations of DNA and of the Re complex are the same in all of the samples, but the intensity of emission decreases as AT-30 $\approx$ Re-25(I) $>$ Re-25(G) $\approx$ GC-30.

Differences in emission intensity are also observed in time-resolved measurements carried out on the nanosecond timescale with a PMT detector (response time 8 ns) and on

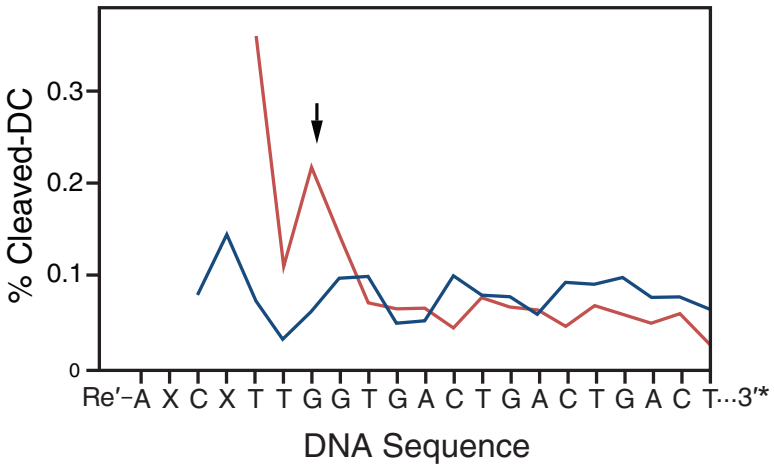

Figure 3.2: Quantification of oxidative damage observed for Re-25(I) (X = I; red) or Re-25(G) (X = G; blue) by PAGE analysis. Aqueous samples containing 3′-[α-^{32}P]-radiolabelled (indicated by *) Re-DNA constructs (2 μM) were irradiated for 2 hrs and treated with piperidine to induce cleavage at damaged bases. Cleavage products were separated by 20% PAGE and imaged by phosphorimagery. Quantitation was accomplished by normalizing counts at each site to total counts per lane. Traces were corrected for false positives by subtracting the dark control (DC). The arrow indicates the 5′-guanine of a 5′-GG-3′ doublet. Re is expected to bind 2–3 bases in from the 5′-end of the duplex.

the picosecond timescale using a streak camera (response time 55 ps). On the nanosecond timescale, the time-integrated emission intensity of Re-25(G) at 570 nm is 14% that of Re-25(I), and the intensity of GC-30 is 12% that of AT-30, following the trend observed in stationary spectra. Even on the picosecond timescale, the instantaneous emission intensity extrapolated to $t = 0$ is lower in the GC-30 and Re-25(G) samples than in the AT-30 and Re-25(I) samples, respectively. In addition, on this timescale the time-integrated emission intensity of Re-25(G) is 79% that of Re-25(I), and the intensity of GC-30 is 69% that of AT-30. These observations clearly indicate reaction(s) between electronically excited Re complex and DNA occurring on the picosecond-to-nanosecond timescale. Based on results of the PAGE experiment, hole transfer from Re* to G is most likely a prominent contributing reaction pathway.

The emission decay of the four DNA samples is highly multiexponential, with lifetimes varying over four orders of magnitude, from ∼100 ps to ∼500 ns. The present data do not allow us to attribute individual emission decay components to particular species present in the solution, although steady-state results suggest that DNA excimer emission contributes significantly (∼20%) to the total decay. After accounting for DNA excimer emission, which decays with a lifetime of only a few ns,[74] about half of the Re emission decays within 50 ns, and the remainder persists for hundreds of ns. Maximum entropy fitting of the emission decays yields several distributions of rate constants (Figure 3.4). The lifetime distributions vary only slightly between samples, and in every sample, the majority component has a lifetime of less than 1 ns. Notably, while most of the lifetimes are shortened slightly on going from AT-30 to GC-30 and from Re-25(I) to Re-25(G), no decay component is observed that corresponds to quenching of the excited Re sensitizer by guanine. Considering the significant quenching in steady-state measurements of the GC-30 and Re-25(G) samples, it seems that quenching at the reactive binding site(s) is ultrafast, probably tens of picoseconds or faster, but involves only a fraction of the excited population.

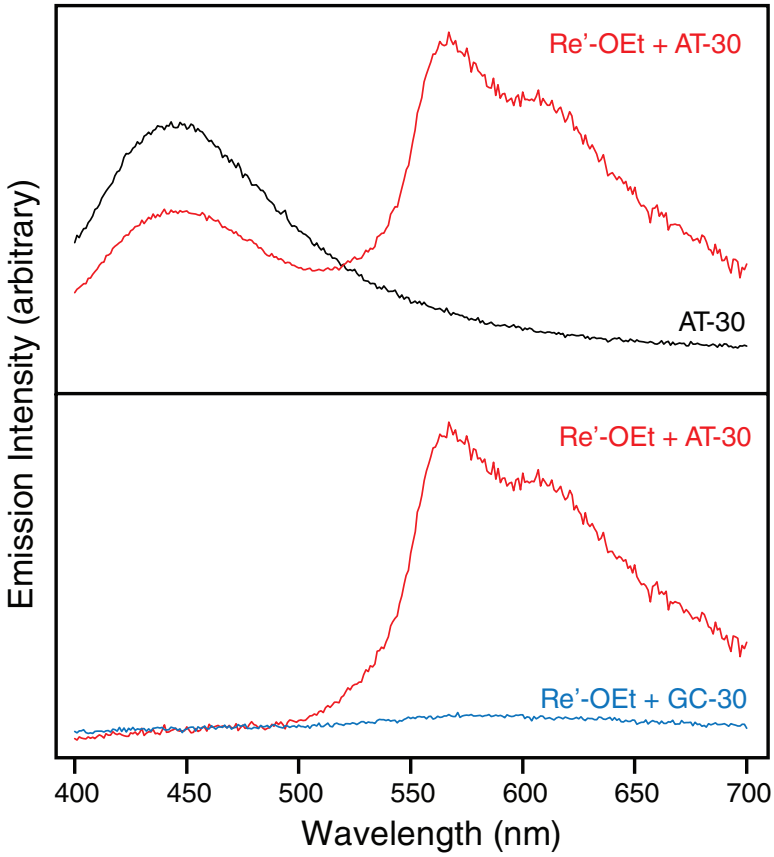

Figure 3.3: Steady-state emission spectra of 25 μM Re′-OEt and 0.5 mM DNA (base pairs) in D_2O buffer (10 mM NaP_i, 50 mM NaCl; pD 7.0) solution following excitation at 355 nm. Emission spectra of Re′-OEt with AT-30 (red) or GC-30 (blue) have been corrected for emission from DNA alone.

3.3.5 Time-Resolved Infrared (TRIR) Spectra

Whereas emission spectra provide evidence for ultrafast hole injection from electronically excited Re into the GC-30 and Re-25(G) samples, TRIR has the potential to characterize the reacting state(s) of the Re complex and to detect products and intermediates. To this effect, TRIR spectra were investigated in the picosecond (1–100 ps) and nanosecond-to-microsecond time domains in the regions of the $Re(CO)_3$ $\nu(C{\equiv}O)$ and DNA organic carbonyl vibrations.

Typical picosecond TRIR spectra obtained in the (C≡O) region after 355 nm excitation are shown in Figure 3.5 for AT-30 and GC-30. The spectra measured 1 ps after excitation show negative bands due to bleaching of the ground state absorption (2036 and 1939 cm^{-1}) and broad transient bands at 2026 and 1908 cm^{-1}. Over the course of time, both features decay in intensity while a sharp band grows in at 2031 cm^{-1} (overlapping with the 2036 cm^{-1} bleach) together with a broad band between 1915 and 1935 cm^{-1}. These new transients partially overlap with the parent bleaches at 2036 and 1939 cm^{-1}; hence, the growth of the transients is accompanied by a decrease in the intensities of both bleaches and a distortion of the band shape of the 1939 cm^{-1} bleach. The down-shift in the energies of the transient bands from the ground-state positions is typical of $\pi \rightarrow \pi^*$ ^{3}IL(dppz) excited states.[19–23,26,27,54] Tentatively, we attribute the initially formed 2026 and 1908 cm^{-1} transient bands to a hot ^{3}IL state localized at the phen part of the dppz ligand, ^{3}IL(phen). Subsequent electron density reorganization and cooling produce another ^{3}IL state localized predominantly at the phenazine part, ^{3}IL(phz), manifested as the sharp 2036 cm^{-1} band. The ^{3}IL(phz) IR spectrum is more similar to that of the ground states than to the ^{3}IL(phen) spectrum since the electronic changes in ^{3}IL(phz) occur further away from the Re center. The excited-state conversion is largely completed in the first 100 ps. The spectra measured at 100 and 500 ps also show a shoulder at ∼2020 cm^{-1} that probably corresponds to a residual population of the IL(phen) state. The ps spectra do not show any bands attributable to Re→dppz MLCT states, which are expected to occur at higher energies.

The GC-30 sample shows very similar behavior (Figure 3.5, bottom); however, there

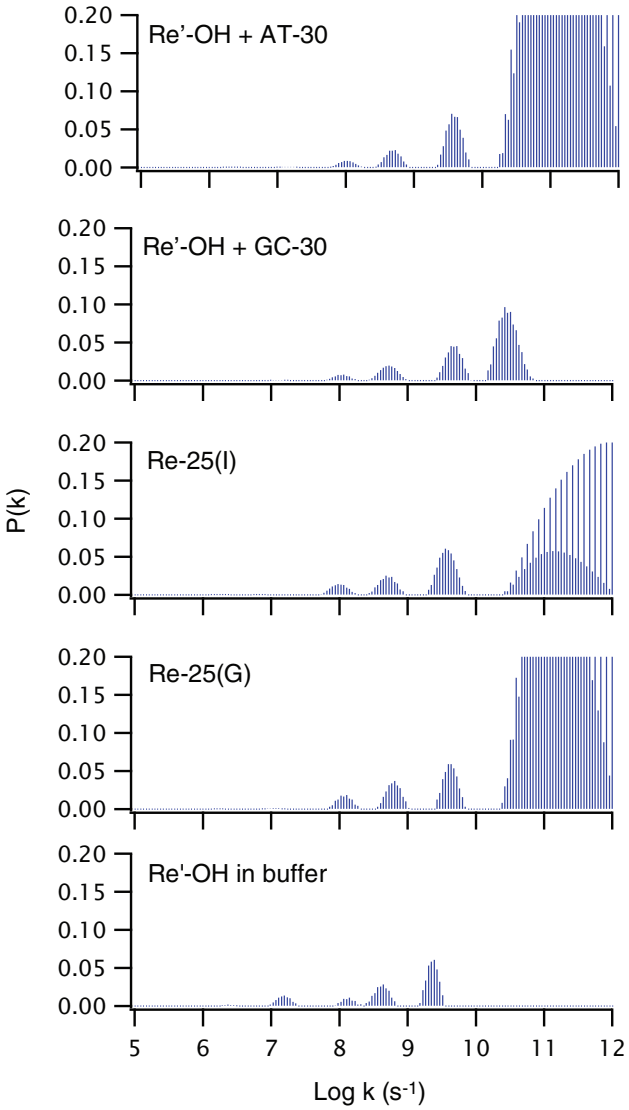

Figure 3.4: Lifetime distributions from maximum entropy analysis of emission from (64 μM) Re$'-$OH in the presence of 1.6 mM (base pairs) DNA and of 64 μM Re-25(I) or Re-25(G) measured on the picosecond timescale (λ_{ex} = 355 nm, 1 ps pulse width). Samples were prepared in D_2O buffer 10 mM NaP_i, 50 mM NaCl; pD 7.0) and were irradiated at 355 nm. Probability P is plotted as a function of rate k. Large distributions at $k = 10^{11} - -10^{12}$ s^{-1} are caused by convolution of the measurement signal with instrumental noise. The emission decay from Re$'$-OH in buffer is expected to be monoexponential; the complex distribution of rates observed here may be due to the formation of aggregates (solubility is quite low) or it may simply be an effect of the low emission intensity observed for this sample.

is one important difference: the ∼2031 cm^{-1} ^{3}IL(phz) feature at longer time delays (> 50 ps) is much weaker relative to the initially formed transient than in the case of AT-30. In accordance with the ultrafast GC-30 emission intensity quenching, we attribute this deficiency to a partial picosecond quenching of the ^{3}IL state(s) by CT with guanine to produce [$Re^I(CO)_3$(dppz$^{\bullet-}$)(py′-OH)] and $G^{\bullet+}$. The lack of IR features in the TRIR spectra due to the reduced Re complex is likely caused by two factors. The first is very close similarity with the spectrum of the ^{3}IL(phz) state (compare with Figure 3.1); the second is very fast BET that regenerates the ground state and keeps the concentration of the reduced state low. The persistence of the 2031 cm^{-1} band of GC-30 into the nanosecond-to-microsecond domain (see below) demonstrates that the relaxed ^{3}IL(phz) state of Re′-OEt shows little reactivity, if any. This spectral feature could also correspond to a population of Re complexes that are protected from solvent quenching by DNA binding but are not well coupled to the base stack.

The picosecond TRIR spectrum of AT-30 in the DNA region is very similar to that measured in the nanosecond time domain (Figure 3.6). The spectra show instantaneous formation of bleach bands at 1618 (weak), 1635, 1660, and 1690 (weak) cm^{-1} that are not accompanied by the formation of transients. These bleaches originate from a decrease in the intensity of the nucleobase carbonyl IR bands upon excitation, rather than band shifts, and they compare well with bleaches observed upon direct 267 nm photoexcitation of nucleic acid polymers.[37] The GC-30 sample shows strong bleaches at about 1577, 1619 (weak), 1648 and 1679 cm^{-1}, again without the formation of transients. Notably, on the picosecond timescale there is no evidence of a transient due to oxidized $G^{\bullet+}$ or $G^{\bullet}$, which would be expected at ∼1700 cm^{-1}.[38,43,44] The absence of such a transient is consistent with the ultrafast BET proposed above.

Picosecond TRIR spectra (Figure 3.5) of the Re-25(I) and Re-25(G) samples in both the Re(CO)3 ν(C≡O) and the DNA carbonyl regions closely resemble those of the AT-30 and GC-30 samples, respectively. Importantly, the ^{3}IL(phz) band intensity at 100–500 ps is much lower for Re-25(G) than Re-25(I) relative to the initial transient, again indicating ultrafast Re*→G CT. Absence of any [$Re^I(CO)_3$(dppz$^{\bullet-}$)(py′-OH)] or $G^{\bullet+}$/$G^{\bullet}$ IR features

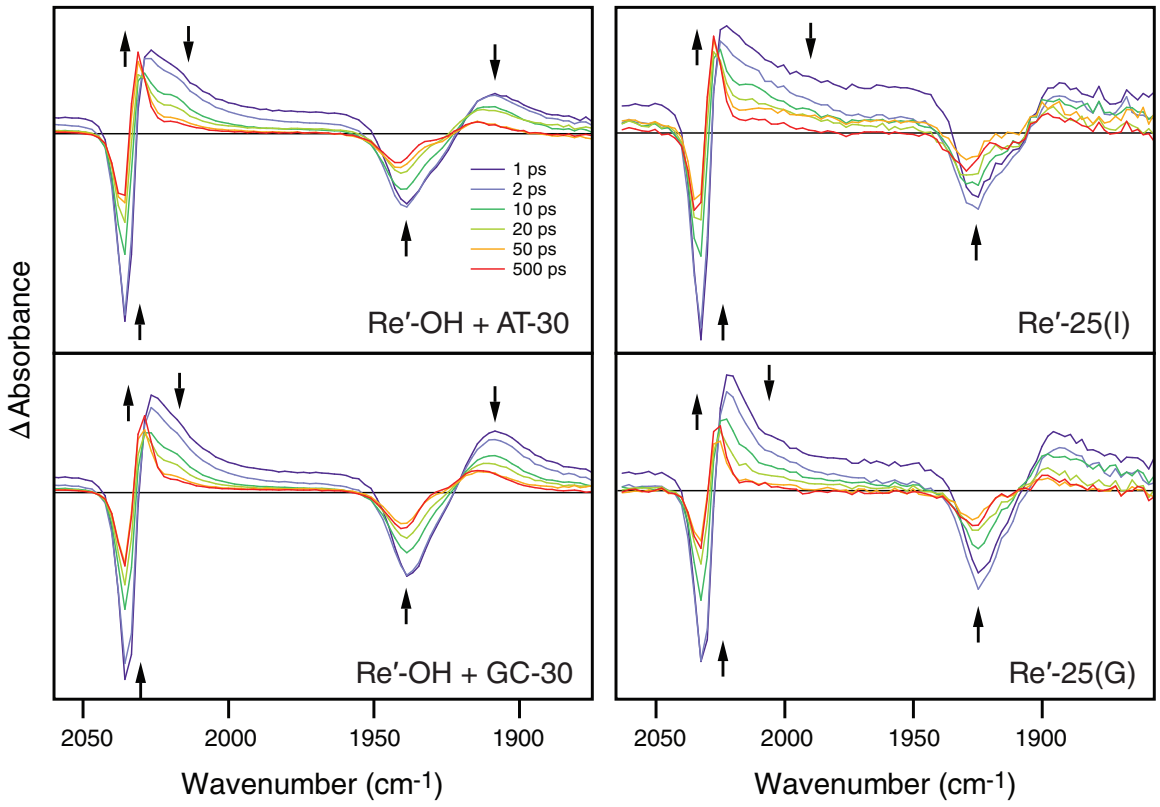

Figure 3.5: Picosecond-timescale TRIR difference spectra of Re/DNA systems measured at specified time delays after 355 nm, 50 fs excitation. Left: 4.8 mM (base pairs) AT-30 (top) or GC-30 (bottom) with 0.5 mM Re′-OH. Right: 100 μM Re-25(I) (top) or Re-25(G) (bottom). Each probe data point is separated by ca. 2.1 cm^{-1}. Arrows indicate changes in the spectra with time. Delay times displayed are a subset of the data collected.

suggests ultrafast BET, as in the case of GC-30.

TRIR spectra recorded between 1 ns and 10 μs after photoexcitation are shown in Figure 3.6. The spectral patterns are very similar to those obtained in picosecond experiments at 100 ps and longer: The IL(phz) bands, as well as the bleaches in the DNA region, appear prominently in all four samples. Despite these similarities, closer examination reveals several important spectral differences. The AT-30 and Re-25(I) samples both show a weak isolated positive band at 2070 cm^{-1} and a broad, positive absorbance near 1980 cm^{-1}. The 2070 cm^{-1} band can be assigned definitively to the MLCT excited state based on analyses of related complexes.[19–23,25–27,54,68,75] This assignment predicts two additional low-intensity absorption bands near 2015 cm^{-1} and 1960 cm^{-1} due to hypsochromic shift of the A′(2) and A″ modes upon excitation of the complex into the MLCT state. These features are probably encompassed by the broad unresolved absorption between 1960 cm^{-1} and 1990 cm^{-1} and eclipsed by the much stronger absorption of IL states at higher energies. The MLCT features are absent in the GC-30 and Re-25(G) spectra. The AT-30 and Re-25(I) samples also exhibit a pronounced shoulder near 2020 cm^{-1} that is weaker for GC-30 and nearly absent in the Re-25(G) sample. This shoulder grows in intensity with increasing sample irradiation during the experiment, so it is in part related to transient absorption of a side photoproduct. However, its greater intensity in the AT-30 and Re-25(I) samples may be due to the presence of an underlying MLCT band or residual population of the ^{3}IL(phen) state, as observed in the picosecond experiments (see above). Importantly, on the nanosecond timescale, TRIR spectra of GC-30 in the DNA region show a growing band at ∼1700 cm^{-1} attributable to the oxidized guanine radical, $G^{\bullet+}$ or $G^{\bullet}$. This transient is very similar to that observed at 1702 cm^{-1} in both 5′-dGMP and poly(dG-dC)·poly(dG-dC) upon 200 nm photoionization, which was assigned to oxidized guanine (although the particular ionic state of this radical was not determined).[38,43,44]

The nanosecond kinetic behavior of the four samples differs substantially in several ways (Table 3.1). (i) The bleach recoveries and ^{3}IL(phz) decays of the AT-30 and Re-25(I) are largely composed of long-lived components (≈20 μs) with smaller contributions on the timescale of tens to hundreds of nanoseconds. The occurrence of such slow microsecond

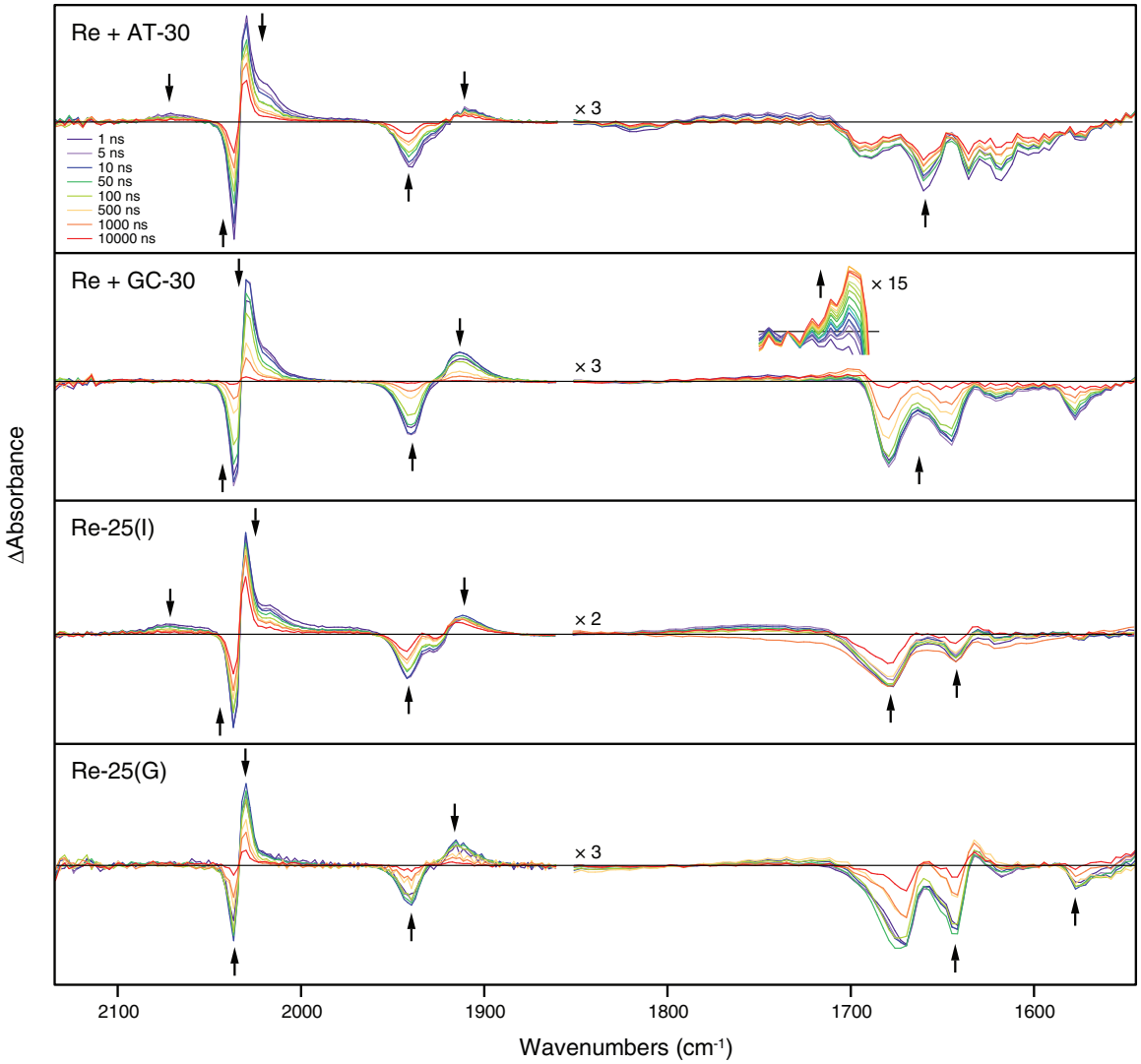

Figure 3.6: Nanosecond-timescale TRIR difference spectra showing changes in the IR absorbance of systems containing 0.5 mM $[Re(CO)_3(dppz)(py'\text{-}OR)]^+$ and 4.8 mM DNA (base pairs) following 355 nm excitation. Both the $Re(CO)_3$ $\nu(C{\equiv}O)$ (1860–2150 cm^{-1}) and the DNA C=O stretching (1550–1850 cm^{-1}) regions are shown. Arrows indicate changes in the spectra with time. Delay times displayed are a subset of the data collected. The growth of the signal at ∼1700 cm^{-1} in the GC-30 sample is shown in the inset.

processes, which have no counterparts in emission decays, indicates the presence of long-lived, non-emissive ^{3}IL excited states or transient species. (ii) The AT-30 and Re-25(I) MLCT band at $\sim$2070 cm^{-1} is fully formed in the 1 ns spectra and decays monotonically over time with lifetimes of 9 and 32 ns, respectively. In general, the lifetimes of the MLCT bands are significantly different than those of the IL bands, showing that the ^{3}IL and ^{3}MLCT states are not equilibrated. Importantly, the 2070 cm^{-1} MLCT band is completely absent in the spectra of the GC-30 and Re-25(G) samples, probably due to very fast quenching of the ^{3}MLCT excited state by guanine. (iii) Compared with AT-30 and Re-25(I), both GC-30 and Re-25(G) show faster ^{3}IL decay and bleach recovery. (iv) Direct IR evidence for $G^{\bullet+}/G^{\bullet}$ formation was obtained for the GC-30 sample, where a band appears with a lifetime of 210 ns in the DNA spectral region at $\sim$1700 cm^{-1} and then decays over $\sim$20 μs with a lifetime estimated roughly as 6 μs (Figure 3.7).

As in the picosecond TRIR spectra, we do not see any distinct signals attributable to the reduced Re sensitizer $[Re^{I}(CO)_3(dppz^{\bullet-})(py'\text{-OH})]$ in any of the samples. This again is because its IR spectrum is nearly identical with that of the ^{3}IL(phz) state; moreover, the yield of reduced Re species is low due to efficient BET.

3.3.6 Visible TA

Transient absorption decay in the visible spectral range at 475 nm was investigated in order to compare the TRIR kinetics specific to the $Re(CO)_3$ moiety with those of the dppz part of the chromophore. A single exponential term was a poor model for the transient decay, indicating that more than one transient species exists during the course of the measurement. Biexponential fit parameters for the transient decays are shown in Table 3.1 on page 88. It should be noted that the TA experiments were performed with a time resolution of about 10 ns, so they only provide information on the slower kinetics and longer-lived intermediates. Still, the TA decay lifetimes for each sample are comparable to the decay of the TRIR band near 2030 cm^{-1}, including the lifetime shortening upon guanine incorporation near the Re binding site. It follows that the same states and processes are monitored by both methods. In a similar system, the TA spectrum of the reduced state following 355 nm excitation of

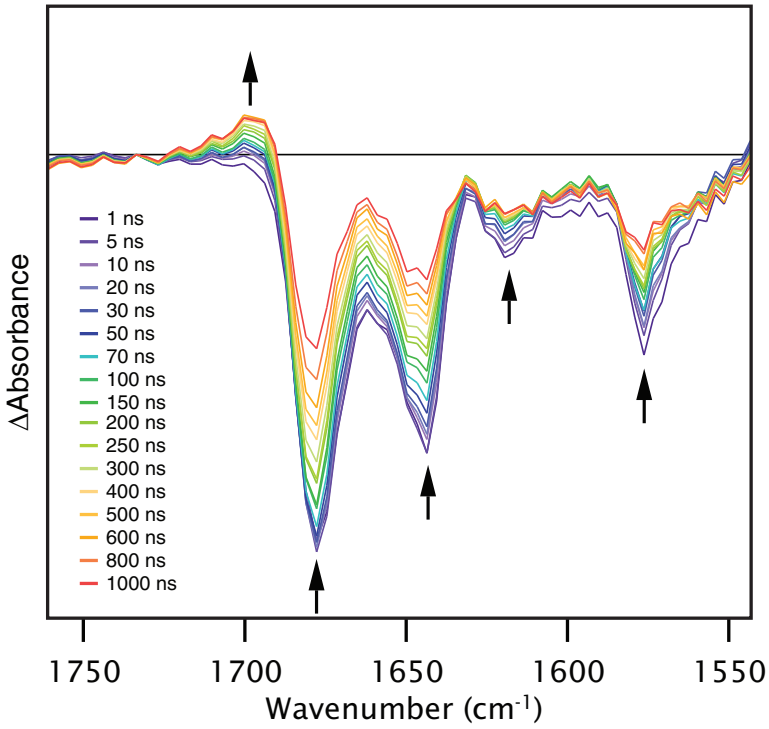

Figure 3.7: Nanosecond-timescale TRIR difference spectra showing changes in the IR absorbance of 4.8 mM (base pairs) GC-30 in the presence of 0.5 mM Re′-OH following excitation at 355 nm. Arrows indicate changes in the spectra with time. The increase in absorbance at ∼1700 cm^{-1} is clearly displayed.

a Re-DNA conjugate could not be distinguished from the spectrum of the excited state, presumably due to the greater concentration of the excited state and the strong similarity between the two spectra.[65] However, a change in the lifetime of the transient upon DNA binding suggested that DNA-mediated quenching by guanine was taking place. A similar effect is expected for the conjugates studied here.

3.4 Discussion

3.4.1 Interactions Between $[Re(CO)_3(dppz)(py'\text{-}OR)]^+$ and DNA

Strong interactions between intercalating metal complexes and DNA are well known. As observed with several other dppz-bearing cationic metal complexes, incubation with DNA results in hypochromicity of the electronic spectrum and increased luminescence of the complex.[76–78] Certainly, the light switch effect is a strong indicator of intercalative binding. Biexponential emission decays observed for other light switch complexes bound to DNA, such as dppz complexes of Ru, have been attributed to the existence of two different intercalative binding modes: a perpendicular mode, in which the metal-phenazine axis of the dppz ligand lies along the DNA dyad axis, and a side-on mode, in which the metal-phenazine axis lies along the long axis of the base pairs.[79] In a similar way, the multiexponential emission decays observed for the Re complexes are probably due in part to the existence of several binding modes. Emission decay lifetimes of intercalated complexes are also affected by the DNA sequence to which they are bound.[80–82] Although the range of DNA binding sites in the tethered complexes is limited, the tether is flexible enough to allow for binding at any of several locations, each of which may have a different effect on the luminescence lifetime. Similarly, for non-tethered samples, slight variations in the sequence at the binding site may contribute differently to the overall decay. DNA sequence effects, therefore, also contribute to the multiexponential emission decay kinetics of bound complexes.

The bleaches observed in the organic carbonyl stretching region of the TRIR spectra (1600 cm^{-1} to 1700 cm^{-1}) could be another indication of the strong interaction between the complexes and DNA. It is possible that such bleach signals arise from direct photoexcitation of DNA, but excited states thus generated are expected to persist for only a

few nanoseconds.[74] On the contrary, the μs DNA bleach recovery lifetimes, commensurate with the Re excited-state lifetimes observed herein, indicate that the bleached signals originate from perturbation of the bases upon photoexcitation of the electronically coupled Re chromophore. A similar effect was observed previously upon 400 nm photoexcitation of $[Ru(dppz)(tap)_2]^{2+}$ intercalated nonspecifically into poly(dG-dC)·poly(dG-dC).[83] In that work, a series of overlapping bleach and transient signals in the organic carbonyl stretching region at short times (2 ps to 2 ns) was attributed to guanine oxidation by excited Ru via a proton-coupled electron transfer (PCET) mechanism. Such a mechanism seems unlikely in our system because of the absence of TRIR transients that could be assigned to changes in cytosine carbonyl stretching frequency.

3.4.2 Guanine Oxidation by $[Re(CO)_3(dppz)(py'\text{-}OR)]^+$*

Previous work has shown that extended irradiation of mixtures of $[Re(CO)_3(dppz)(py)]^+$ and supercoiled plasmid DNA at $\lambda_{ex} > 350$ nm results in nicks in the DNA backbone.[42] In that work, the yield of cleavage did not depend on the concentration of singlet oxygen, suggesting that cleavage is the result of direct oxidation of guanine by the excited complex. The experimental results described here provide further evidence for the oxidation of guanine in DNA duplexes by photoexcited $[Re(CO)_3(dppz)(py'\text{-}OR)]^+$. In PAGE experiments, oxidation was observed preferentially at the the 5′-guanine of the 5′-GG-3′ doublet. Importantly, the observation of oxidation at this site, at least three base pairs removed from the Re binding site, indicates that long-range DNA-mediated CT has occurred. The preferential oxidation of the 5′-guanine of the doublet is typical for long-range DNA-mediated CT processes.[84,85] This pattern is due to localization of the injected hole at guanine, the site of lowest oxidation potential.[67] Once localized on guanine, proton transfer with base-paired cytosine results in the formation of the neutral guanine radical ($k > 10^7$ s^{-1}).[38] In this state, the radical is quite stable, and can persist for > 1 ms.[86] In the present study, a greater yield of guanine damage was observed by PAGE at the guanine doublet in Re-25(I) than in Re-25(G). This result can be attributed to the effect of the flanking guanines in Re-25(G). For each photon absorbed, CT may occur to any low potential guanine site that

is well-coupled to the probe. Statistically, transfer to and trapping at the guanine doublet is more probable in Re-25(I) than in Re-25(G) since CT to inosine is expected to be thermodynamically less favorable.[60,65] The long-range DNA-mediated oxidation of guanine observed in the gel experiment is not surprising, given the favorable driving force and strong electronic coupling between the complex and DNA.

The spectroscopic data are also consistent with guanine oxidation. By both steady-state and time-resolved emission, the luminescence intensity of each AT-30 and Re-25(I) is greater than that for GC-30 and Re-25(G), respectively. In early work, a similar disparity in the emission intensity of $[Re(CO)_3(dppz)(py)]^+$, a known DNA light-switch complex, bound to poly(dA)·poly(dT) versus poly(dG)·poly(dC) was ascribed to steric inhibition of binding to the latter duplex.[42] Such an interpretation falls short on several accounts. First, it cannot explain the difference in emission intensity observed between Re-25(I) and Re-25(G); exchanging guanine for inosine at the Re binding site is expected to present a negligible change in steric interactions between the complex and the duplex. Second, it is not consistent with the equal degree of hypochromicity observed in the electronic spectrum of a similar Re complex when bound to either poly(dG-dC)·poly(dG-dC) or poly(dA-dT)·poly(dA-dT).[57] Finally, it contradicts the strong luminescence observed from the bulkier light switch complex $[Ru(bpy)_2(dppz)]^{2+}$ bound to poly(dG-dC)·poly(dG-dC).[71] A more consistent explanation involves facile quenching of the Re excited state by guanine.[43,44,57] CT from excited Re to guanine accounts well for our observation that the Re-25(G) and GC-30 samples, in which guanine neighbors the intercalation site, show less emission than the Re-25(I) and AT-30 samples, in which direct interaction between the complex and guanine is prevented.

TRIR spectra reported above provide further information on the rate and mechanism of guanine oxidation in GC-30 and Re-25(G). The reduced yield of the IL(phz) state relative to AT-30 and Re-25(I) suggests that Re*→G CT involves the IL(phen) state and occurs on a comparable timescale as the IL(phen)→IL(phz) conversion, namely a few tens of picoseconds. In addition, the absence of MLCT features in spectra observed on the nanosecond timescale shows that parallel CT involving the MLCT state occurs with a subnanosecond lifetime. Under some circumstances, IL(phz) could be reactive as well, but

we have no direct evidence for a process involving this state. The rate of Re*→G CT cannot be determined exactly by TRIR because the spectral patterns of the IL-excited and reduced states cannot be distinguished. Nevertheless, the picosecond-timescale CT rates are further corroborated by comparison of the instantaneous ($t = 0$) emission intensity between samples. On the nanosecond timescale, the four samples give similar emission decay rates, although the integrated emission intensity is much less for Re-25(G) and GC-30 than for Re-25(I) and AT-30.

The reason for the absence of a guanine oxidation signal in TRIR spectra of Re-25(G) and Re-25(I) is unclear, but it may be an effect of the mixed base sequence used in these constructs. In previous studies of guanine oxidation by $[Ru^{III}(phen)_2(dppz)]^{3+}$, a strong transient was observed in the visible region that was attributed to the neutral guanine radical when the complex was intercalated in poly(dG)·poly(dG) or poly(dG-dA)·poly(dC-dT), but no signal was seen when the complex was intercalated in poly(dG-dT)·poly(dC-dA).[86] This difference was attributed to sequence-dependent variations in the redox potential of guanine or to structural variations, which would alter the coupling in the system.

3.4.3 Long-Lived Transient States

In addition to the reactive Re states, TRIR and TA measurements indicate that one or more non-emissive transient states persists long after the emissive species has been depleted. We have established that the long-lived transients are composed primarily of mixtures of Re in the ^{3}IL(phz) excited state and in the reduced state, $[Re(CO)_3(dppz^{\bullet-})(py'\text{-}OR)]$. The long-lifetime decay processes observed by these absorption methods therefore contain contributions from the decay of these two states. From the ^{3}IL(phz) state, the decay is likely due to internal conversion to the ground state. From the reduced state, the decay is caused by charge recombination, i.e., BET. The observation of long-lived transients in the AT-30 sample and the possibility for the oxidation of adenine by excited Re indicate that some amount of charge injection may occur in the absence of guanine. However, the lack of evidence for the formation of $A^{\bullet+}$ and the relatively strong emission observed in the AT-30 system suggest that if CT with adenine occurs, it is slow, minimally competitive

with emission, and followed by fast BET.

3.4.4 Suggested Mechanism of DNA-Mediated Guanine Oxidation

Based on spectroscopic evidence, a model can be generated for the oxidation of guanine by excited $[Re(CO)_3(dppz)(py'\text{-}OR)]^+$ (Scheme 3.2). Photoexcitation of the complex populates a mixture of close-lying IL(phen), IL(phz), and MLCT excited states, presumably spin-triplets, that are clearly observed by TRIR. (Such a mixture of states has been observed experimentally in several rhenium tricarbonyl complexes and has been verified in computational models.[17,19,26,87]) Based on our TRIR results, it appears that different excited states are more or less likely to participate in DNA-mediated CT. The MLCT state in particular, which is not observed in samples where the excited complex is in direct contact with guanine, seems to be more easily quenched than the IL states. The CT reactivity appears to decrease in the order MLCT > IL(phen) > IL(phz). It is also possible that conversion between excited states affects the apparent rates and yields observed for charge injection or emission. The reaction pathways from the excited state are also governed by the extent of electronic coupling in the system, which itself is determined by the dynamics of the probe and of the bases themselves.[65] At the instant of excitation, two major populations exist. The first involves complexes which are poorly bound or which are bound to DNA in orientations that are not conducive to electron transfer. In this population, the mechanism of relaxation involves either quenching by water, as is observed for dppz complexes of Ru in polar, protic solvents,[56,88] or emission. Emission is expected to occur primarily from the ^{3}IL state, as reported for $[Re(CO)_3(dppz)(py)]^+$ in acetonitrile.[19] In the second population, the excited complex is well coupled to the DNA. Here, excited state quenching via positive charge (i.e., hole) injection into the DNA duplex is the preferred reaction pathway. Indeed, primarily coherent CT at a distance of ten base pairs was observed in systems utilizing 2-aminopurine as a hole donor.[60] Such processes are rapid. In systems involving DNA-bound ethidium, DNA-mediated CT over distances of several bases was observed to occur in 5 ps.[89] Further, emission quenching is not limited to the population that exists in a CT-active configuration at the moment of excitation; reorientation of the

bound oxidant to generate such a configuration may occur within the lifetime of the excited state. The rate of reorientation for DNA-bound ethidium is 75 ps,[89] although for a larger molecule such as $[Re(CO)_3(dppz)(py'\text{-}OR)]^+$, this rate may be slower. Following charge separation, charge recombination (BET) may occur. After all, the ground state oxidation of $[Re^I(CO)_3(dppz^{\bullet-})(py'\text{-}OH)]^0$ ($E^\circ[Re^+/Re^0] = -0.85$ V vs. NHE) by $G^{\bullet+}$ ($E^\circ[G^{\bullet+}/G] = 1.29$ V vs. NHE)[67] is thermodynamically favorable, and immediately after charge separation, the system exists in a CT-active state. Back reaction along this pathway is consistent with the absence of a guanine signal at short times in TRIR experiments. While this non-productive reaction pathway can be invoked to explain some of the experimental observations, additional pathways must be operative; quantitative deactivation of the charge separated state via short-range BET would prevent the eventual formation of permanent oxidative damage. A third population, then, involves molecules that are well coupled during charge injection, but that lose coupling before BET can take place due to reorientational motion of either the probe or the bases. The holes thus isolated within the base stack are quite stable and can migrate away from the site of injection, further reducing the probability for BET to occur and increasing the yield of permanent oxidative damage.[60] Charge migration is limited in rate by stacking and destacking motions of the duplex, which form transient delocalized electronic domains.[90,91] The 210 ns rate of formation for the guanine radical signal observed at $\sim$1700 cm^{-1} by TRIR in the GC-30 sample may therefore reflect the rate of this conformational gating.

3.5 Concluding Remarks

Complexes that contain IR-active moieties show promise as probes for the study of DNA CT. In this work, we have used PAGE and time-resolved spectroscopy to observe the oxidation of guanine in DNA by photoexcited $[Re(CO)_3(dppz)(py'\text{-}OR)]^+$. Although no direct evidence for this reaction is afforded by UV/visible methods, fast excited-state quenching by guanine provides indirect evidence that oxidation is taking place. Direct evidence for the formation of guanine oxidation products is observed biochemically by PAGE analysis and spectroscopically by TRIR following photoexcitation of Re′-OEt in the presence of GC-30.

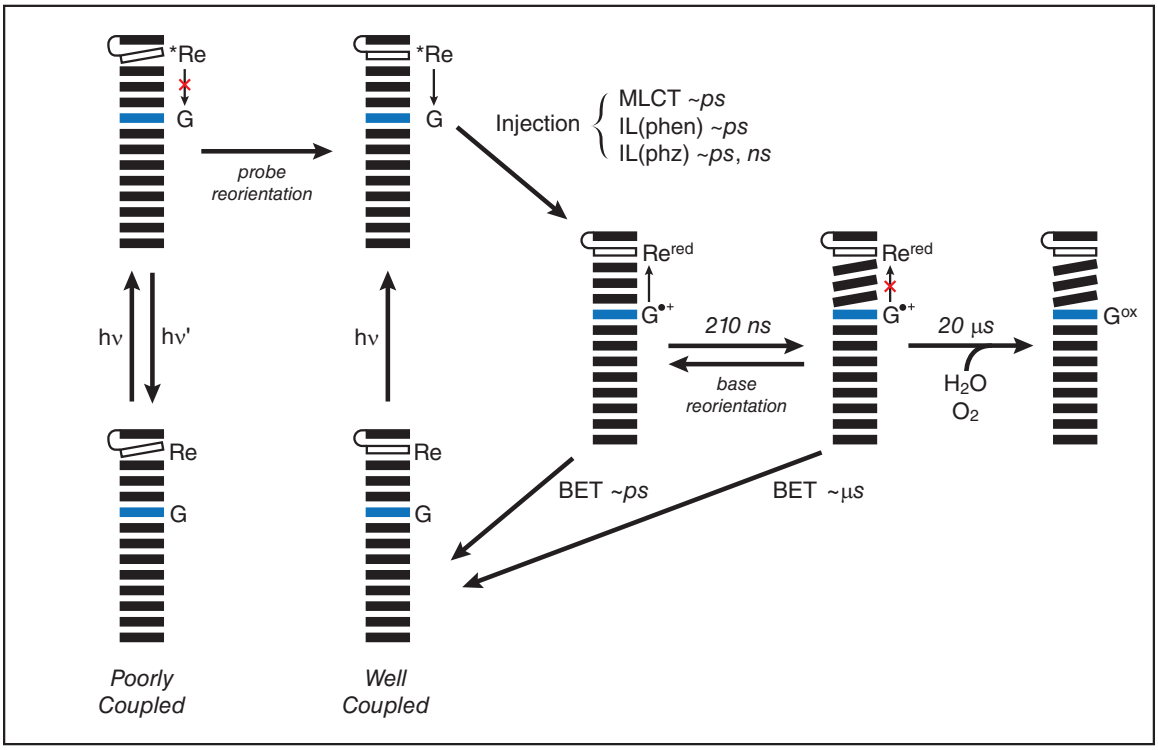

Scheme 3.2: The proposed model for the oxidation of guanine by photoexcited $[Re(CO)_3(dppz)(py'\text{-}OR)]^+$. Photoexcitation in the poorly coupled system results in emission ($h\nu'$) or non-radiative decay to the ground state. Photoexcitation in the well-coupled system results in charge injection over an arbitrary distance to form reduced $[Re(CO)_3(dppz^{\bullet-})(py'\text{-}OR)]^0$ (Re^{red}) and the guanine radical cation ($G^{\bullet+}$). During the excited state lifetime of the complex, the poorly coupled system may undergo reorientation, allowing charge injection. From the charge-separated state, facile back electron transfer (BET) competes with charge migration and trapping, resulting either in no reaction or the formation of permanent oxidation products. Base motions may result in isolation of the injected charge, favoring the trapping pathway.

Similarities between the spectral features and kinetics of this system with those of other DNA sequences containing guanine allow us to conclude that the photochemical processes observed in the GC-30 sample are general. In these systems, the rate of guanine oxidation (herein 210 ns) is dictated largely by motions of the bases, which allow for long-range charge separation and prevent BET, rather than by the intrinsic photophysics of the photosensitizer complex. In this respect, the role of Re′-OEt is similar to that of other photooxidants that have been used in DNA CT studies.[60,90,91]

Unlike the well-known $[Ru(phen)_2(dppz)]^{2+}$ DNA "light-switch", Re(I) tricarbonyl-dppz complexes are strong enough photooxidants to inject positive charge into DNA directly from their electronically excited state(s), i.e., without the use of an external quencher and involvement of diffusion-controlled steps. This allows for ultrafast charge injection, with possible applications in mechanistic studies of DNA-mediated CT and in development of DNA-based photonic devices. However, the present study indicates that charge injection by $[Re(CO)_3(dppz)(py'\text{-}OR)]^+$ preferentially involves the initially populated IL(phen) and the minor MLCT states, with the long-lived ^{3}IL(phz) state showing little reactivity, if any. This, together with fast BET, limits the reaction yield. From the experimental point of view, Re tricarbonyl-diimines have the advantage of being both ET phototriggers and probes by virtue of their sensitive IR spectral responses to changes in the electron density distribution.[32,34] However, in the particular case of dppz complexes, the TRIR spectral analysis is complicated by the close resemblance of ^{3}IL(phz) and reduced-state spectral patterns that renders the two species indistinguishable. It is suggested that optimization of the Re-photooxidant structure will improve both the charge injection efficiency and the IR spectral response.

A complete picture of DNA CT requires the observation of processes on very different timescales. At the instant of photoexcitation, the extent of coupling between the probe and the base stack, and between the bases themselves, defines two populations of DNA: one that is CT-active and one that is CT-inactive. The outcomes of fast processes, such as fluorescence and charge injection, are determined based on the relative sizes of these populations. At longer times, base motions change the energetic landscape, offering alternative reaction

pathways, such as charge migration and trapping, that were not available immediately after excitation. TRIR allows for the observation of processes at all of these timescales, making it a valuable addition to the methods employed for the study of DNA-mediated CT.

References

[1] Genereux, J. C., and Barton, J. K. "Mechanisms for DNA charge transport." *Chem. Rev.* **110**, 1642–1662 (2010).

[2] Barton, J. K., Olmon, E. D., and Sontz, P. A. "Metal complexes for DNA-mediated charge transport." *Coord. Chem. Rev.* **255**, 619–634 (2011).

[3] Schuster, G. B., Ed. *Topics in Current Chemistry: Long-Range Charge Transfer in DNA I*; Springer-Verlag: New York, 2004.

[4] Núñez, M. E., Hall, D. B., and Barton, J. K. "Long-range oxidative damage to DNA: effects of distance and sequence." *Chem. Biol.* **6**, 85–97 (1999).

[5] Slinker, J. D., Muren, N. B., Renfrew, S. E., and Barton, J. K. "DNA charge transport over 34 nm." *Nature Chem.* **3**, 228–233 (2011).

[6] Augustyn, K. E., Genereux, J. C., and Barton, J. K. "Distance-Independent DNA Charge Transport Across an Adenine Tract." *Angew. Chem. Int. Ed.* **46**, 5731–5733 (2007).

[7] Gorodetsky, A. A., Buzzeo, M. C., and Barton, J. K. "DNA-Mediated Electrochemistry." *Bioconj. Chem.* **19**, 2285–2296 (2008).

[8] Guo, X., Gorodetsky, A. A., Hone, J., Barton, J. K., and Nuckolls, C. "Conductivity of a single DNA duplex bridging a carbon nanotube gap." *Nat. Nanotech.* **3**, 163–167 (2008).

[9] Slinker, J. D., Muren, N. B., Gorodetsky, A. A., and Barton, J. K. "Multiplexed DNA-modified electrodes." *J. Am. Chem. Soc.* **132**, 2769–2774 (2010).

[10] Genereux, J. C., Boal, A. K., and Barton, J. K. "DNA-Mediated Charge Transport in Redox Sensing and Signaling." *J. Am. Chem. Soc.* **132**, 891–905 (2010).

[11] Boal, A. K., Genereux, J. C., Sontz, P. A., Gralnick, J. A., Newman, D. K., and Barton, J. K. "Redox signaling between DNA repair proteins for efficient lesion detection." *Proc. Natl. Acad. Sci. USA* **106**, 15237–15242 (2009).

[12] Lee, P. E., Demple, B., and Barton, J. K. "DNA-mediated redox signaling for transcriptional activation of SoxR." *Proc. Natl. Acad. Sci. USA* **106**, 13164–13168 (2009).

[13] Augustyn, K. E., Merino, E. J., and Barton, J. K. "A role for DNA-mediated charge transport in regulating p53: Oxidation of the DNA-bound protein from a distance." *Proc. Natl. Acad. Sci. USA* **104**, 18907–18912 (2007).

[14] Turner, J. J., George, M. W., Johnson, F. P. A., and Westwell, J. R. "Time-resolved Infrared Spectroscopy of Excited States of Transition Metal Species." *Coord. Chem. Rev.* **125**, 101–114 (1993).

[15] Kumar, A., Sun, S.-S., and Lees, A. J. "Photophysics and Photochemistry of Organometallic Rhenium Diimine Complexes." *Top. Organomet. Chem.* **29**, 1–35 (2010).

[16] Stufkens, D. J., and Vlček, A. "Ligand-dependent excited state behaviour of Re(I) and Ru(II) carbonyl-diimine complexes." *Coord. Chem. Rev.* **177**, 127–179 (1998).

[17] Vlček, A. "Ultrafast Excited-State Processes in Re(I) Carbonyl-Diimine Complexes: From Excitation to Photochemistry." *Top. Organomet. Chem.* **29**, 73–114 (2010).

[18] Dyer, J., Grills, D. C., Matousek, P., Parker, A. W., Towrie, M., Weinstein, J. A., and George, M. W. "Revealing the photophysics of *fac*-[(dppz-12-NO_2)$Re(CO)_3$(4-Me_2Npy)]$^+$: a picosecond time-resolved IR study." *Photochem. Photobiol. Sci.* 872–873 (2002).

[19] Dyer, J., Blau, W. J., Coates, C. G., Creely, C. M., Gavey, J. D., George, M. W., Grills, D. C., Hudson, S., Kelly, J. M., Matousek, P., McGarvey, J. J., McMaster, J., Parker, A. W., Towrie, M., and Weinstein, J. A. "The photophysics of *fac*-[$Re(CO)_3$(dppz)(py)]$^+$ in CH_3CN: a comparative picosecond flash photolysis, transient infrared, transient resonance Raman and density functional theoretical study." *Photochem. Photobiol. Sci.* **2**, 542–554 (2003).

[20] Kuimova, M. K., Alsindi, W. Z., Dyer, J., Grills, D. C., Jina, O. S., Matousek, P., Parker, A. W., Porius, P., Sun, X. Z., Towrie, M., Wilson, C., Yang, J., and

George, M. W. "Using picosecond and nanosecond time-resolved infrared spectroscopy for the investigation of excited states and reaction intermediates of inorganic systems." *Dalton Trans.* 3996–4006 (2003).

[21] Kuimova, M. K., Sun, Z., Matousek, P., Grills, D. C., Parker, A. W., Towrie, M., and George, M. W. "Probing intraligand and charge transfer excited states of *fac*-[Re(R)(CO)$_3$(CO$_2$Et-dppz)]$^+$ (R = py, 4-Me$_2$N-py; CO$_2$Et-dppz = dipyrido[3,2-a:2′,3′-c]phenazine-11-carboxylic ethyl ester) using time-resolved infrared spectroscopy." *Photochem. Photobiol. Sci.* **6**, 1158–1163 (2007).

[22] Dyer, J., Creely, C. M., Penedo, J. C., Grills, D. C., Hudson, S., Matousek, P., Parker, A. W., Towrie, M., Kelly, J. M., and George, M. W. "Solvent dependent photophysics of fac-[Re(CO)$_3$(11,12-X$_2$dppz)(py)]$^+$(X = H, F or Me)." *Photochem. Photobiol. Sci.* **6**, 741–748 (2007).

[23] Kuimova, M. K., Alsindi, W. Z., Blake, A. J., Davies, E. S., Lampus, D. J., Matousek, P., McMaster, J., Parker, A. W., Towrie, M., Sun, X.-Z., Wilson, C., and George, M. W. "Probing the solvent dependent photophysics of *fac*-[Re(CO)$_3$(dppz-X$_2$)Cl] (dppz-X$_2$ = 11,12-X$_2$-dipyrido[3,2-*a*:2′,3′-*c*]phenazine); X = CH$_3$, H, F, Cl, CF$_3$)." *Inorg. Chem.* **47**, 9857–9869 (2008).

[24] Vlček, A., and Záliš, S. "Modeling of charge-transfer transitions and excited states in d^6 transition metal complexes by DFT techniques." *Coord. Chem. Rev.* **251**, 258–287 (2007).

[25] George, M. W., and Turner, J. J. "Excited states of transition metal complexes studied by time-resolved infrared spectroscopy." *Coord. Chem. Rev.* **177**, 201–217 (1998).

[26] Vlček, A., and Busby, M. "Ultrafast ligand-to-ligand electron and energy transfer in the complexes fac-[Re^I(L)(CO)$_3$(bpy)]$^{n+}$." *Coord. Chem. Rev.* **250**, 1755–1762 (2006).

[27] Busby, M., Matousek, P., Towrie, M., and Vlček, A. "Ultrafast excited-state dynamics of photoisomerizing complexes *fac*-[Re(Cl)(CO)$_3$(papy)$_2$] and *fac*-

[Re(papy)$(CO)_3$(bpy)]$^+$ (papy=trans-4-phenylazopyridine)." *Inorg. Chim. Acta* **360**, 885–896 (2007).

[28] Lo, K. K.-W., Louie, M.-W., and Zhang, K. Y. "Design of luminescent iridium(III) and rhenium(I) polypyridine complexes as in vitro and in vivo ion, molecular and biological probes." *Coord. Chem. Rev.* **254**, 2603–2622 (2010).

[29] Blanco-Rodríguez, A. M., Busby, M., Grdinaru, C., Crane, B. R., Di Bilio, A. J., Matousek, P., Towrie, M., Leigh, B. S., Richards, J. H., Vlček, A., and Gray, H. B. "Excited-State Dynamics of Structurally Characterized aeruginosa Azurins in Aqueous Solution." *J. Am. Chem. Soc.* **3**, 3552–3557 (2006).

[30] Blanco-Rodríguez, A. M., Busby, M., Ronayne, K., Towrie, M., Grdinaru, C., Sudhamsu, J., Sýkora, J., Hof, M., Záliš, S., Di Bilio, A. J., Crane, B. R., Gray, H. B., and Vlček, A. "Relaxation Dynamics of Pseudomonas aeruginosa $Re^{I}(CO)_3(\alpha$-diimine)$(HisX)^+$ (X= 83, 107, 109, 124, 126) Cu^{II} Azurins." *J. Am. Chem. Soc.* **3**, 11788–11800 (2009).

[31] Gray, H. B., and Winkler, J. R. "Electron Flow through Proteins." *Chem. Phys. Lett.* **483**, 1–9 (2009).

[32] Blanco-Rodríguez, A. M., Di Bilio, A. J., Shih, C., Museth, A. K., Clark, I. P., Towrie, M., Cannizzo, A., Sudhamsu, J., Crane, B. R., Sýkora, J., Winkler, J. R., Gray, H. B., Záliš, S., and Vlček, A. "Phototriggering Electron Flow through Re^{I}-modified *Pseudomonas aeruginosa* Azurins." *Chem. Eur. J.* **17**, 5350–5361 (2011).

[33] Connick, W. B., Di Bilio, A. J., Hill, M. G., Winkler, J. R., and Gray, H. B. "Tricarbonyl(1,10-phenanthroline)(imidazole) rhenium(I): a powerful photooxidant for investigations of electron tunneling in proteins." *Inorg. Chim. Acta* **240**, 169–173 (1995).

[34] Shih, C., Museth, A. K., Abrahamsson, M., Blanco-Rodríguez, A. M., Di Bilio, A. J., Sudhamsu, J., Crane, B. R., Ronayne, K. L., Towrie, M., Vlček, A., Richards, J. H.,

Winkler, J. R., and Gray, H. B. "Tryptophan-accelerated electron flow through proteins." *Science* **320**, 1760–1762 (2008).

[35] Encinas, S., Morales, A. F., Barigelletti, F., Barthram, A. M., White, C. M., Couchman, S. M., Jeffery, J. C., Ward, M. D., Grills, D. C., and George, M. W. "Derivatives of the $[Ru(bipy)(CN)_4]^{2-}$ chromophore with pendant pyridyl-based binding sites: synthesis, pH dependent-luminescence, and time-resolved infrared spectroscopic studies." *J. Chem. Soc., Dalton Trans.* 3312–3319 (2001).

[36] Towrie, M., Doorley, G. W., George, M. W., Parker, A. W., Quinn, S. J., and Kelly, J. M. "ps-TRIR covers all the bases–recent advances in the use of transient IR for the detection of short-lived species in nucleic acids." *Analyst* **134**, 1265–1273 (2009).

[37] Kuimova, M. K., Dyer, J., George, M. W., Grills, D. C., Kelly, J. M., Matousek, P., Parker, A. W., Sun, X. Z., Towrie, M., and Whelan, A. M. "Monitoring the effect of ultrafast deactivation of the electronic excited states of DNA bases and polynucleotides following 267 nm laser excitation using picosecond time-resolved infrared spectroscopy." *Chem. Commun.* 1182–1184 (2005).

[38] Kuimova, M. K., Cowan, A. J., Matousek, P., Parker, A. W., Sun, X. Z., Towrie, M., and George, M. W. "Monitoring the direct and indirect damage of DNA bases and polynucleotides by using time-resolved infrared spectroscopy." *Proc. Natl. Acad. Sci. USA* **103**, 2150–2153 (2006).

[39] Hare, P. M., Middleton, C. T., Mertel, K. I., Herbert, J. M., and Kohler, B. "Time-resolved infrared spectroscopy of the lowest triplet state of thymine and thymidine." *Chem. Phys.* **347**, 383–392 (2008).

[40] McGovern, D. A., Doorley, G. W., Whelan, A. M., Parker, A. W., Towrie, M., Kelly, J. M., and Quinn, S. J. "A study of the pH dependence of electronically excited guanosine compounds by picosecond time-resolved infrared spectroscopy." *Photochem. Photobiol. Sci.* **8**, 542–548 (2009).

[41] Stoeffler, H. D., Thornton, N. B., Temkin, S. L., and Schanze, K. S. "Unusual Photophysics of a Rhenium(I) Dipyridophenazine Complex in Homogeneous Solution and Bound to DNA." *J. Am. Chem. Soc.* **117**, 7119–7128 (1995).

[42] Yam, V. W.-W., Lo, K. K.-W., Cheung, K.-K., and Kong, R. Y.-C. "Deoxyribonucleic acid binding and photocleavage studies of rhenium(I) dipyridophenazine complexes." *J. Chem. Soc., Dalton Trans.* **14**, 2067–2072 (1997).

[43] Smith, J. A., George, M. W., and Kelly, J. M. "Transient spectroscopy of dipyridophenazine metal complexes which undergo photo-induced electron transfer with DNA." *Coord. Chem. Rev.* **In Press**, (2011).

[44] Cao, Q., Creely, C. M., Davies, E. S., Dyer, J., Easun, T. L., Grills, D. C., McGovern, D. A., McMaster, J., Pitchford, J., Smith, J. A., Sun, X.-Z., Kelly, J. M., and George, M. W. "Excited state dependent electron transfer of a rhenium-dipyridophenazine complex intercalated between the base pairs of DNA: a time-resolved UV-visible and IR absorption investigation into the photophysics of *fac*-$[Re(CO)_3(F_2dppz)(py)]^+$ b." *Photochem. Photobiol. Sci.* **10**, 1355–1364 (2011).

[45] Holmlin, R. E., Dandliker, P. J., and Barton, J. K. "Synthesis of Metallointercalator-DNA Conjugates on a Solid Support." *Bioconj. Chem.* **10**, 1122–1130 (1999).

[46] Zeglis, B. M., and Barton, J. K. "DNA base mismatch detection with bulky rhodium intercalators: synthesis and applications." *Nat. Protoc.* **2**, 357–371 (2007).

[47] Boyle, P. D., Boyd, D. C., Mueting, A. M., and Pignolet, L. H. "Redox and Acid-Base Chemistry of $[Au_2Re_2(H)_6(PPh_3)_6]PF_6$ and Related Cluster Compounds." *Inorg. Chem.* **27**, 4424–4429 (1988).

[48] Pletneva, E. V., Gray, H. B., and Winkler, J. R. "Many Faces of the Unfolded State: Conformational Heterogeneity in Denatured Yeast Cytochrome *c*." *J. Mol. Biol.* **345**, 855–867 (2005).

[49] Pletneva, E. V., Gray, H. B., and Winkler, J. R. "Snapshots of cytochrome *c* folding." *Proc. Natl. Acad. Sci. USA* **102**, 18397–18402 (2005).

[50] Kimura, T., Lee, J. C., Gray, H. B., and Winkler, J. R. "Site-specific collapse dynamics guide the formation of the cytochrome c' four-helix bundle." *Proc. Natl. Acad. Sci. USA* **104**, 117–122 (2007).

[51] Kimura, T., Lee, J. C., Gray, H. B., and Winkler, J. R. "Folding energy landscape of cytochrome cb_{562}." *Proc. Natl. Acad. Sci. USA* **106**, 7834–7839 (2009).

[52] Greetham, G. M., Burgos, P., Cao, Q., Clark, I. P., Codd, P. S., Farrow, R. C., George, M. W., Kogimtzis, M., Matousek, P., Parker, A. W., Pollard, M. R., Robinson, D. A., Xin, Z.-J., and Towrie, M. "ULTRA: A Unique Instrument for Time-Resolved Spectroscopy." *Appl. Spectrosc.* **64**, 1311–1319 (2010).

[53] Towrie, M., Gabrielsson, A., Matousek, P., Parker, A. W., Blanco-Rodríguez, A. M., and Vlček, A. "A High-Sensitivity Femtosecond to Microsecond Time-Resolved Infrared Vibrational Spectrometer." *Appl. Spectrosc.* **59**, 467–473 (2005).

[54] Dattelbaum, D. M., Omberg, K. M., Hay, P. J., Gebhart, N. L., Martin, R. L., Schoonover, J. R., and Meyer, T. J. "Defining Electronic Excited States Using Time-Resolved Infrared Spectroscopy and Density Functional Theory Calculations." *J. Phys. Chem. A* **108**, 3527–3536 (2004).

[55] Gamelin, D. R., George, M. W., Glyn, P., Grevels, F.-W., Johnson, F. P. A., Klotzbücher, W., Morrison, S. L., Russell, G., Schaffner, K., and Turner, J. J. "Structural Investigation of the Ground and Excited States of $ClRe(CO)_3(4,4'\text{-bipyridyl})_2$ Using Vibrational Spectroscopy." *Inorg. Chem.* **33**, 3246–3250 (1994).

[56] Turro, C., Bossmann, S. H., Jenkins, Y., Barton, J. K., and Turro, N. J. "Proton Transfer Quenching of the MLCT Excited State of $Ru(phen)_2dppz^{2+}$ in Homogeneous Solution and Bound to DNA." *J. Am. Chem. Soc.* **117**, 9026–9032 (1995).

[57] Ruiz, G. T., Juliarena, M. P., Lezna, R. O., Wolcan, E., Feliz, M. R., and Ferraudi, G. "Intercalation of *fac*-$[(4,4'\text{-bpy})Re^{I}(CO)_3(dppz)]^+$, dppz = dipyridyl[3,2-$a$:2′3′-$c$]phenazine, in polynucleotides. On the UV-vis photophysics of the Re(I) intercalator and the redox reactions with pulse radio." *Dalton Trans.* **3**, 2020–2029 (2007).

[58] Dohno, C., Stemp, E. D. A., and Barton, J. K. "Fast back electron transfer prevents guanine damage by photoexcited thionine bound to DNA." *J. Am. Chem. Soc.* **125**, 9586–9587 (2003).

[59] Williams, T. T., Dohno, C., Stemp, E. D. A., and Barton, J. K. "Effects of the photooxidant on DNA-mediated charge transport." *J. Am. Chem. Soc.* **126**, 8148–8158 (2004).

[60] Genereux, J. C., Wuerth, S. M., and Barton, J. K. "Single-Step Charge Transport through DNA over Long Distances." *J. Am. Chem. Soc.* **133**, 3863–3868 (2011).

[61] Yoo, J., Delaney, S., Stemp, E. D. A., and Barton, J. K. "Rapid radical formation by DNA charge transport through sequences lacking intervening guanines." *J. Am. Chem. Soc.* **125**, 6640–6641 (2003).

[62] O'Neill, M. A., Dohno, C., and Barton, J. K. "Direct chemical evidence for charge transfer between photoexcited 2-aminopurine and guanine in duplex DNA." *J. Am. Chem. Soc.* **126**, 1316–1317 (2004).

[63] Genereux, J. C., Augustyn, K. E., Davis, M. L., Shao, F., and Barton, J. K. "Back-Electron Transfer Suppresses the Periodic Length Dependence of DNA-Mediated Charge Transport Across Adenine Tracts." *J. Am. Chem. Soc.* **130**, 15150–15156 (2008).

[64] Yam, V. W.-W., Lo, K. K.-W., Cheung, K.-K., and Kong, R. Y.-C. "Synthesis, photophysical properties and DNA binding studies of novel luminescent rhenium(I) complexes. X-Ray crystal structure of $[Re(dppn)(CO)_3(py)](OTf)$." *J. Chem. Soc., Chem. Commun.* **3**, 1191–1193 (1995).

[65] Olmon, E. D., Hill, M. G., and Barton, J. K. "Using Metal Complex Reduced States to Monitor the Oxidation of DNA." *Inorg. Chem.* **Submitted**, (2011).

[66] Juris, A., Balzani, V., Barigelletti, F., Campagna, S., Belser, P., and Von Zelewsky, A. "Ru(II) polypyridine complexes: photophysics, photochemistry, electrochemistry, and chemiluminescence." *Coord. Chem. Rev.* **84**, 85–277 (1988).

[67] Steenken, S., and Jovanovic, S. V. "How Easily Oxidizable Is DNA? One-Electron Reduction Potentials of Adenosine and Guanosine Radicals in Aqueous Solution." *J. Am. Chem. Soc.* **119**, 617–618 (1997).

[68] Dattelbaum, D. M., Omberg, K. M., Schoonover, J. R., Martin, R. L., and Meyer, T. J. "Application of Time-Resolved Infrared Spectroscopy to Electronic Structure in Metal-to-Ligand Charge-Transfer Excited States." *Inorg. Chem.* **41**, 6071–6079 (2002).

[69] Burrows, C. J., and Muller, J. G. "Oxidative Nucleobase Modifications Leading to Strand Scission." *Chem. Rev.* **98**, 1109–1152 (1998).

[70] Williams, T. T., Odom, D. T., and Barton, J. K. "Variations in DNA Charge Transport with Nucleotide Composition and Sequence." *J. Am. Chem. Soc.* **122**, 9048–9049 (2000).

[71] Friedman, A. E., Chambron, J.-C., Sauvage, J.-P., Turro, N. J., and Barton, J. K. "Molecular 'Light Switch' for DNA: $Ru(bpy)_2(dppz)^{2+}$." *J. Am. Chem. Soc.* **112**, 4960–4962 (1990).

[72] Kwok, W.-M., Ma, C., and Phillips, D. L. "'Bright' and 'dark' excited states of an alternating at oligomer characterized by femtosecond broadband spectroscopy." *J. Phys. Chem. B* **113**, 11527–11534 (2009).

[73] Markovitsi, D., Gustavsson, T., and Vaya, I. "Fluorescence of DNA Duplexes: From Model Helices to Natural DNA." *J. Phys. Chem. Lett.* **1**, 3271–3276 (2010).

[74] Banyasz, A., Vaya, I., Changenet-Barret, P., Gustavsson, T., Douki, T., and Markovitsi, D. "Base Pairing Enhances Fluorescence and Favors Cyclobutane Dimer Formation Induced upon Absorption of UVA Radiation by DNA." *J. Am. Chem. Soc.* **133**, 5163–5165 (2011).

[75] Kuimova, M. K., Gordon, K. C., Howell, S. L., Matousek, P., Parker, A. W., Sun, X.-Z., Towrie, M., and George, M. W. "Picosecond time-resolved infrared spectroscopic investigation into electron localisation in the excited states of Re(I) polypyridyl complexes with bridging ligands." *Photochem. Photobiol. Sci.* **5**, 82–87 (2006).

[76] Hiort, C., Lincoln, P., and Nordén, B. "DNA binding of Δ- and Λ-$[Ru(phen)_2DPPZ]^{2+}$." *J. Am. Chem. Soc.* **115**, 3448–3454 (1993).

[77] Holmlin, R. E., and Barton, J. K. "$Os(phen)_2(dppz)^{2+}$: A Red-Emitting DNA Probe." *Inorg. Chem.* **34**, 7–8 (1995).

[78] Shao, F., Elias, B., Lu, W., and Barton, J. K. "Synthesis and characterization of iridium(III) cyclometalated complexes with oligonucleotides: insights into redox reactions with DNA." *Inorg. Chem.* **46**, 10187–10199 (2007).

[79] Hartshorn, R. M., and Barton, J. K. "Novel Dipyridophenazine Complexes of Ruthenium(II): Exploring Luminescent Reporters of DNA." *J. Am. Chem. Soc.* **114**, 5919–5925 (1992).

[80] Jenkins, Y., Friedman, A. E., Turro, N. J., and Barton, J. K. "Characterization of dipyridophenazine complexes of ruthenium(II): the light switch effect as a function of nucleic acid sequence and conformation." *Biochemistry* **31**, 10809–10816 (1992).

[81] Holmlin, R. E., Stemp, E. D. A., and Barton, J. K. "$Ru(phen)_2dppz^{2+}$ Luminescence: Dependence on DNA Sequences and Groove-Binding Agents." *Inorg. Chem.* **37**, 29–34 (1998).

[82] Stemp, E. D. A., Holmlin, R. E., and Barton, J. K. "Electron transfer between metal complexes bound to DNA: variations in sequence, donor, and metal binding mode." *Inorg. Chim. Acta* **297**, 88–97 (2000).

[83] Elias, B., Creely, C., Doorley, G. W., Feeney, M. M., Moucheron, C., Kirsch-DeMesmaeker, A., Dyer, J., Grills, D. C., George, M. W., Matousek, P., Parker, A. W., Towrie, M., and Kelly, J. M. "Photooxidation of guanine by a ruthenium dipyridophenazine complex intercalated in a double-stranded polynucleotide monitored directly by picosecond visible and infrared transient absorption spectroscopy." *Chem. Eur. J.* **14**, 369–375 (2008).

[84] Saito, I., Takayama, M., Sugiyama, H., Nakatani, K., Tsuchida, A., and Yamamoto, M. "Photoinduced DNA Cleavage via Electron Transfer: Demonstration that Guanine

Residues Located 5′ to Guanine are the Most Electron-Donating Sites." *J. Am. Chem. Soc.* **117**, 6406–6407 (1995).

[85] Hall, D. B., Holmlin, R. E., and Barton, J. K. "Oxidative DNA damage through long-range electron transfer." *Nature* **382**, 731–735 (1996).

[86] Stemp, E. D. A., Arkin, M. R., and Barton, J. K. "Oxidation of Guanine in DNA by $Ru(phen)_2(dppz)^{3+}$ Using the Flash-Quench Technique." *J. Am. Chem. Soc.* **119**, 2921–2925 (1997).

[87] MacQueen, D. B., and Schanze, K. S. "Free energy and solvent dependence of intramolecular electron transfer in donor-substituted rhenium(I) complexes." *J. Am. Chem. Soc.* **113**, 7470–7479 (1991).

[88] Olson, E. J. C., Hu, D., Hörmann, A., Jonkman, A. M., Arkin, M. R., Stemp, E. D. A., Barton, J. K., and Barbara, P. F. "First Observation of the Key Intermediate in the "Light-Switch" Mechanism of $[Ru(phen)_2dppz]^{2+}$." *J. Am. Chem. Soc.* **119**, 11458–11467 (1997).

[89] Wan, C., Fiebig, T., Kelley, S. O., Treadway, C. R., Barton, J. K., and Zewail, A. H. "Femtosecond dynamics of DNA-mediated electron transfer." *Proc. Natl. Acad. Sci. USA* **96**, 6014–6019 (1999).

[90] O'Neill, M. A., Becker, H.-C., Wan, C., Barton, J. K., and Zewail, A. H. "Ultrafast Dynamics in DNA-Mediated Electron Transfer: Base Gating and the Role of Temperature." *Angew. Chem. Int. Ed.* **42**, 5896–5900 (2003).

[91] Shao, F., O'Neill, M. A., and Barton, J. K. "Long-range oxidative damage to cytosines in duplex DNA." *Proc. Natl. Acad. Sci. USA* **101**, 17914–17919 (2004).

Chapter 4

Using Metal Complex Reduced States to Monitor the Oxidation of DNA*

*Adapted from E. D. Olmon, M. G. Hill, and J. K. Barton, *Inorg. Chem.* **Accepted** (2011).

4.1 Introduction

Cellular DNA is continually under the threat of oxidation from a host of sources.[1–4] Left unrepaired, oxidative damage to DNA leads to health problems, including cancer.[5–7] In order to improve our understanding of the chemical mechanisms underlying oxidative damage, as well as the biological factors affecting the prevalence, detection, and repair of such damage, it is necessary to utilize a wide variety of chemical and biological tools and techniques.

One especially useful tool for the study of oxidative damage in DNA is DNA-mediated charge transport (CT). Due to orbital overlap between the π systems of neighboring nucleobases, DNA can serve as a bridge in long-range electron transfer (ET) reactions. Unlike photocleavage mechanisms, many of which result in the formation of nonspecific damage by reactive oxygen species,[8–10] or photoligation mechanisms, which lead to the formation of unnatural adducts between metal complexes and DNA,[11] DNA-mediated CT results in preferential damage at sites of low oxidation potential. Oxidative events at low potential guanine sites ($E^{\circ}[G^{\bullet+}/G]$ = 1.29 V vs. NHE)[12] can be initiated by many different DNA-bound oxidants, including organic molecules, transition metal complexes, and DNA base analogues,[13–18] allowing for the study of DNA oxidation in a wide variety of environments and sequence contexts. Additionally, oxidative probes are capable of inducing damage in regions far from the site of charge injection. In solution studies, damage at guanine sites was observed almost 200 Å away from a DNA-bound oxidant.[19] Recently, our laboratory observed the propagation of robust redox signals over a distance of 100 base pairs, or 340 Å, in DNA monolayers on gold electrodes.[20] DNA CT may fulfill biological roles as well. The observed funneling of oxidative damage to regions of mitochondrial DNA that contain genes necessary for replication may serve as a check against the propagation of damaged genetic material in situations of high oxidative stress.[21] DNA CT also may be involved in other capacities within the cell,[22] for example, to activate transcription[23,24] and to perform long-range signaling.[25]

In order to study such reactions in the laboratory, it is necessary to have a convenient method for initiating DNA CT reactions.[26] Transition metal complexes have proven especially amenable for use as oxidants in the study of DNA damage due to their synthetic

versatility and the ability to tune their redox properties. In addition, an appropriate ligand set enables metal complexes to interact strongly with DNA through intercalative binding, allowing for the initiation of long-range DNA-mediated oxidation by optical excitation of the bound complex. Complexes of the type $[Rh(phi)_2(L)]^{3+}$ (phi = 9,10-phenanthrenequinone diimine), where L = bpy (2,2′-bipyridine) or phen (phenanthroline), are especially strong photooxidants. These complexes, which bind DNA through intercalation of the phi ligand, were used to establish the ability of DNA to propagate charge.[27] Photoexcitation of DNA-bound $[Rh(phi)_2(L)]^{3+}$ at 365 nm leads to injection of a positive charge into the DNA base stack, which then equilibrates at sites of low redox potential (guanine and guanine repeats).[19,28] Iridium complexes have also been used to initiate DNA-mediated CT processes. The complex $[Ir(ppy)_2(dppz)]^+$ (ppy = 2-phenylpyridine; dppz = dipyrido[2,3-*a*:2′,3′-*c*]phenazine) intercalates into DNA via the dppz ligand. Interestingly, from the excited state, the complex is a strong enough reductant and oxidant to promote both the reduction and the oxidation of DNA.[29] This remarkable ability has enabled characterization of DNA-mediated electron transfer and DNA-mediated hole transfer in identical sequence contexts, showing that both have a shallow distance dependence.[30,31] Tricarbonyl rhenium complexes are of interest due to the strong infrared absorption of the carbonyl ligands. Excitation and reduction of such complexes can be followed temporally by observing dynamic changes in the stretching frequencies of the carbonyl ligands.[32–34] In addition, complexes such as $[Re(CO)_3(dppz)(L)]^{n+}$ act as "light switches",[35] luminescing only when bound to DNA.[36–39] Such interesting photophysical properties provide additional means of monitoring DNA CT events.

Due to the large number of factors that affect the relative efficiency of DNA CT, such as DNA binding strengths, redox properties, and photophysical behavior of various metal complexes, it is necessary to compare DNA oxidants in identical environments. In the present study, we have examined the ability of three metal complexes to report on DNA-mediated oxidation events through the appearance of their reduced states. We have focused on investigation of the reduced states of $[Rh(phi)_2(bpy')]^{3+}$, $[Ir(ppy)_2(dppz')]^+$, and $[Re(CO)_3(dppz)(py')]^+$ [**Rh**, **Ir**, and **Re**, respectively; bpy′ = 4-methyl-4′-(butyric

acid)-2,2′-bipyridine; dppz′ = 6-(dipyrido[3,2-*a*:2′,3′-*c*]phenazin-11-yl)hex-5-ynoic acid; py′ = 3-(pyridin-4-yl)-propanoic acid] and their DNA-conjugates (**Rh-DNA**, **Ir-DNA**, and **Re-DNA**) in aqueous and organic solutions, as well as their efficiencies of DNA photooxidation. The structures of the complexes and conjugates are shown in Scheme 4.1. We have used steady-state spectroelectrochemistry and nanosecond transient absorption (TA) spectroscopy to record the electronic spectra of the reduced states of the metal complexes and the charge transfer products of the metal-DNA conjugates, respectively. In addition, we have compared these spectral profiles with the redox properties and efficiency of DNA photooxidation of the three complexes.

4.2 Experimental Section

4.2.1 Materials

Unless indicated otherwise, all reagents and solvents were of reagent grade or better and were used as received without further purification. All reagents for DNA synthesis were purchased from Glen Research (Sterling, VA).

4.2.2 Synthesis of Metal Complexes

The synthesis of [*fac*−$Re(CO)_3$(dppz)(py′)]Cl is described completely in Section 2.2.2 on Page 59. The complexes $[Ir(ppy)_2(dppz')]Cl$ and $[Rh(phi)_2(bpy')]Cl_3$ were gifts from coworkers or were prepared using established protocols.[29,40]

4.2.3 DNA Synthesis and Modification

Oligonucleotides were prepared using standard solid-phase phosphoramidite chemistry on an Applied Biosystems 3400 DNA synthesizer. Covalent tethers were appended to the 5′-ends of resin-bound oligonucleotides in two ways. For the **Ir-DNA** conjugate, an amino-terminated C_6-alkyl phosphoramidite was added in the last step of the automated synthesis; for the **Rh**- and **Re-DNA** conjugates, a diaminononane linker was added as previously described.[41] Agitation of the amine modified strands in the presence of metal complex, *O*-(benzotriazol-1-yl)-*N*,*N*,*N*′,*N*′-tetramethyluronium hexafluorophosphate (HBTU),

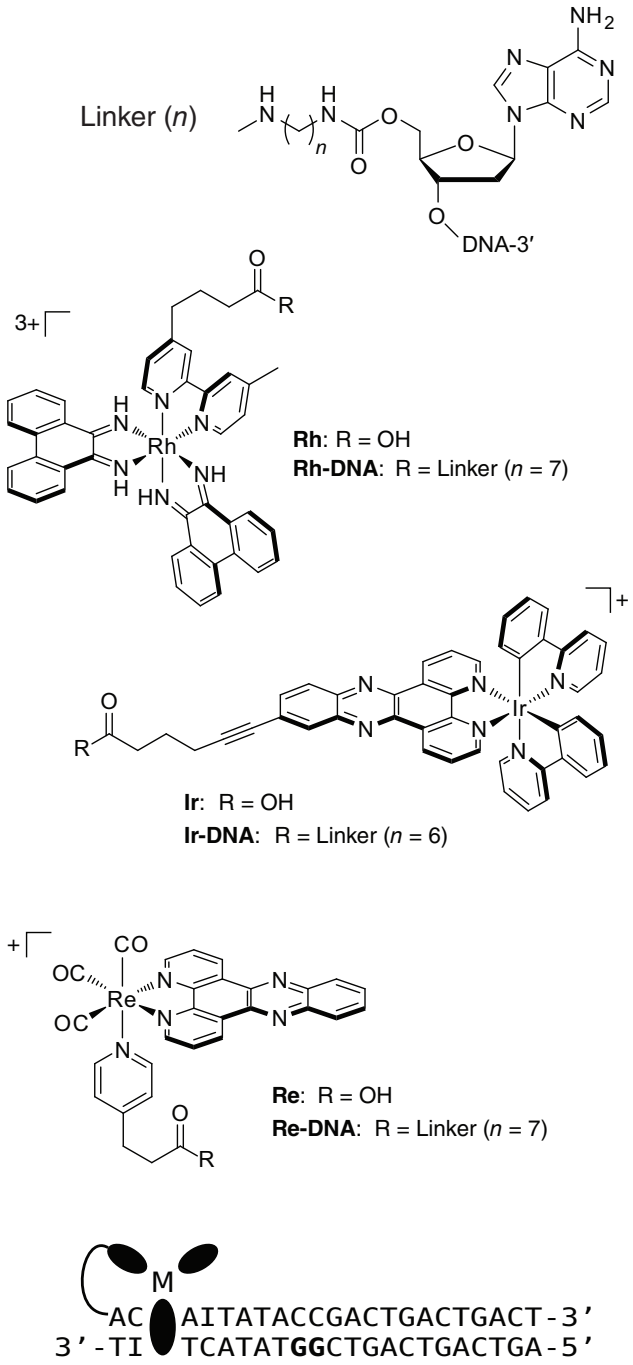

Scheme 4.1: Structures of complexes and DNA sequences used in biochemical and spectroscopic experiments. The complexes were used free in solution or were covalently attached to the DNA sequence shown via an alkyl linker ($n = 6$ or 7). The 5′-GG-3′ site is shown in bold. Physical models suggest that the tethered complexes intercalate 1–3 bases from the end of the duplex.

1-hydroxybenzotriazole hydrate (HOBT), and diisopropylethylamine (DIEA) in anhydrous DMF resulted in covalent attachment of the metal complexes to the DNA. Cleavage from the resin was effected by incubation in NH_4OH at 60 °C for 6 h. Strands were purified by reversed-phase HPLC (50 mM aqueous ammonium acetate/acetonitrile gradient) using a Clarity 5μ Oligo-RP column (Phenomenex). Oligonucleotides were characterized by MALDI-TOF mass spectrometry and quantitated by UV/visible spectroscopy. Annealing was accomplished by incubating solutions containing equimolar amounts of complementary strands in buffer (10 mM sodium phosphate, 50 mM NaCl buffer; pH 7.5) at 90 °C for 5 min followed by slow cooling over 90 min to ambient temperature. The melting temperature (T_m) of each duplex was determined by monitoring the 260 nm absorbance of a dilute sample while heating slowly (1 °C min^{-1}) from ambient temperature to 100 °C; the T_m is taken as the inflection point of the melting curve.

4.2.4 Gel Electrophoresis

Polyacrylamide gel electrophoresis (PAGE) experiments were performed based on published procedures.[42] Briefly, DNA strands were radioactively labeled on the 5′-end with [α-^{32}P]-ATP (MP Biomedicals), treated with 10% piperidine for 25 min at 90 °C, and purified by 20% PAGE. Duplexes were formed by heating a mixture of the purified, labeled strands (8 pmol), unlabeled strands of the same sequence (192 pmol), and complement strands bearing tethered metal complexes (200 pmol) at 90 °C for 5 min followed by slow cooling over 90 min to ambient temperature. Irradiation of 2 μM (duplex) samples for various times was carried out using an Oriel Instruments solar simulator (300–440 nm) equipped with a 355 nm long-pass filter. Samples were treated with 0.2 units calf thymus DNA to improve sample recovery and 10% piperidine (v/v) to induce strand cleavage at damaged sites, heated for 30 min at 90 °C, and dried *in vacuo*. Following separation by 20% PAGE, gels were developed using a Molecular Dynamics Storm 820 phosphorimager and Molecular Dynamics phosphorimaging screens. Gels were visualized and quantified using ImageQuant software (Molecular Dynamics). Damage at specific sites is determined as percent counts relative to the total counts per lane.

4.2.5 Spectroelectrochemistry

UV-visible spectroelectrochemistry was carried out using a custom-built, optically transparent, thin-layer electrode (OTTLE) cell (path length = 0.1 mm) consisting of vapor-deposited platinum working and pseudoreference electrodes and a Pt-wire auxiliary electrode.[43] The potential of the cell was controlled by an electrochemical workstation (CH Instruments 650A). Samples consisted of saturated solutions of metal complexes in dry organic solvents that were degassed under N_2 and introduced into the optical cell using a gastight syringe. The cell was held at a reducing potential, and spectra were acquired every 4 s until the sample was fully reduced using a spectrophotometer (Hewlett Packard 8452A).

4.2.6 Time-Resolved Spectroscopy

Steady-state emission spectra were recorded on a Fluorolog-3 spectrofluorometer (Jobin Yvon) using 2 mm slits. Scattered light was rejected from the detector by appropriate filters.

Time-resolved spectroscopic measurements were carried out at the Beckman Institute Laser Resource Center. Time-resolved emission and TA measurements were conducted using instrumentation that has been described.[44] Briefly, the third harmonic (355 nm) of a 10 Hz, Q-switched Nd:YAG laser (Spectra-Physics Quanta-Ray PRO-Series) was used as an excitation source (pump pulse duration ≈8 ns). For the measurement of transient absorbance spectra, a white light flashlamp of ∼15 ns duration was employed as the probe lamp, and two photodiode arrays (Ocean Optics S1024DW Deep Well Spectrometer) detected the measurement and reference beams. For the measurement of transient kinetics, the probe light was provided by a pulsed 75 W arc lamp (PTI model A 1010) and detected with a photomultiplier tube (Hamamatsu R928) following wavelength selection by a double monochromator (Instruments SA DH-10). For both spectral and kinetic measurements, the pump and probe beams were collinear, and scattered laser light was rejected from the detectors using suitable filters. The samples were held in 1 cm path length quartz cuvettes (Starna) equipped with stir bars and irradiated at 355 nm with 500–1000 laser pulses at 5 mJ pulse^{-1}. Samples were monitored for degradation by UV/visible absorbance

and exchanged for fresh sample when necessary. Samples were prepared with a maximum absorbance of 0.7 in order to achieve high signal-to-noise ratios in TA experiments. TA measurements were made with and without excitation, and were corrected for background light, scattering, and fluorescence. Transient spectra were smoothed using a boxcar algorithm to reduce the effect of instrumental noise.

Kinetic traces were fit to exponential equations of the form

$$I(t) = a_0 + \sum_n a_n \exp(-t/\tau_n),$$

where $I(t)$ is the signal intensity as a function of time, a_0 is the intensity at long time, a_n is a pre-exponential factor that represents the relative contribution from the nth component to the trace, and τ_n is the lifetime of the nth component. Up to two exponential terms were used in the model function to obtain acceptable fits. Kinetic traces were smoothed logarithmically prior to fitting in order to decrease the weight of long time data on the fit.

4.3 Results

4.3.1 Metal Complex Characteristics

The **Rh** and **Ir** metal complexes each contain one intercalating ligand (phi in **Rh** and dppz in **Ir**) and two ancillary ligands, resulting in the formation of Δ and Λ stereoisomers. The efficiency of DNA CT depends strongly on the extent of coupling between the DNA base stack and the bound metal complex, so the stronger binding Δ-isomer is preferred for CT experiments.[41] While the diastereomers of Rh-DNA conjugates are easily resolved by reversed-phase HPLC, those of Ir-DNA conjugates are not. For this reason, only the Δ-isomer of **Rh-DNA** was used in experiments involving metal complex-DNA conjugates, while **Ir-DNA** was used as an isomeric mixture. For experiments involving free metal complexes, isomeric mixtures were used. The Re complex was synthesized using the published protocol for the analogous complex, *fac*-$[Re(CO)_3(dppz)(4\text{-methylpyridine})]^+$.[37] Only the facial stereoisomer is expected to form during synthesis, so enantiomeric separation was not a consideration during purification.

The photophysical properties of **Rh** and **Ir** have been described.[29,45] Optical absorbance spectra for all three complexes are shown in Figure 4.1. Importantly, the three complexes absorb at very different strengths throughout the near-UV region. The weakest absorber is bf, with an extinction coefficient at 384 nm of only 11 000 $M^{-1}cm^{-1}$.[37,39] The spectra of **Rh** and **Ir** are more intense, with extinction coefficients of $\epsilon_{390} = 19\,000$ M^{-1} cm^{-1} and $\epsilon_{405} = 30\,600$ M^{-1} cm^{-1}, respectively.[29,41] **Re-DNA** is also unlike **Rh-DNA** and **Ir-DNA** in that is exhibits luminescence. The luminescence is persistent, suggesting that quenching by guanine is competitive with emissive decay in this sequence context.

4.3.2 Spectroelectrochemistry

Absorbance spectra of the reduced metal complexes were determined using spectroelectrochemistry. Spectra of metal complexes saturated in organic solvents were recorded at regular time intervals during reduction. For **Rh** and **Ir** in 0.1 M TBAH/DMF, the potential was held at < -1.0 V vs. Ag/AgCl. For **Re** in 0.1 M TBAH/CH_3CN, the potential was held at -1.25 V vs. Ag/AgCl. These potentials are sufficient for single-electron reduction of the complexes. Figure 4.2 shows the initial ground state spectrum of each sample, as well as the spectrum resulting from exhaustive reduction. For all three samples, reduction causes a decrease in the intensity of the most prominent near-UV band, with the concomitant appearance of broad bands at lower energies. In the spectra of **Ir** and **Re**, absorption bands also appear at higher energies. For **Ir**, subsequent oxidation at 0 V resulted in quantitative regeneration of the initial species, but **Rh** and **Re** showed only incomplete ($\sim$95%) recovery. These results indicate that the reduction of **Ir**, but not that of **Rh** or **Re**, is completely reversible on the timescale of the experiment ($\sim$10 s). Even so, electrogenerated side products observed in spectroelectrochemistry experiments are not expected to interfere in time-resolved spectroscopic experiments employing fast laser pulses.

4.3.3 Design and Synthesis of Metal Complex-DNA Conjugates

In order to better understand the interactions between metal complexes and DNA, and the ability of metal complexes to oxidize DNA, three metal complex-DNA conjugates were

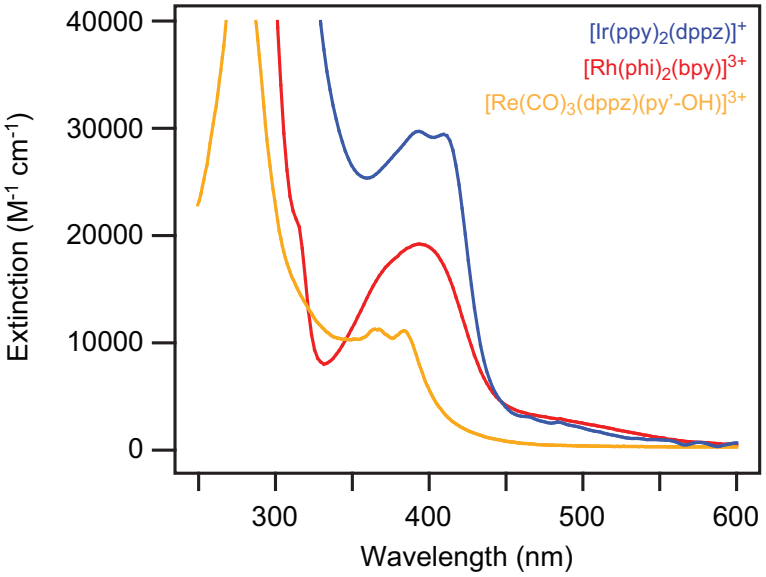

Figure 4.1: UV/visible spectra of **Rh**, **Ir**, and **Re** in acetonitrile. The spectra have been plotted in terms of molar extinction in order to facilitate comparison between the spectra.

synthesized. The three conjugates contain identical DNA sequences, and the metal complex in each conjugate is covalently tethered to one end of the duplex via a long alkyl linker. The structures of the complexes and conjugates are shown in Scheme 4.1. The tether in each case is designed to provide considerable conformational flexibility, allowing the complexes to bind DNA as they would in the absence of the covalent linker. However, the tether is not sufficiently long to allow for binding at sites past three base pairs from the end of the duplex, assuming that intercalation occurs from the major groove.[46] By limiting the position at which each complex is free to bind, it is possible to control the distance between the photooxidant and the low potential 5′-GG-3′ hole trap, negating possible effects of differential distance on the yield and kinetics of DNA CT. Notably, the metal binding site and the 5′-GG-3′ trap are separated by at least five base pairs (17 Å), so oxidation at the guanine doublet is presumed to be DNA mediated. Since identical DNA sequences are used in all three conjugates, each complex experiences a similar electronic environment when bound. In order to increase the yield of long-range oxidative damage, inosine, rather than guanine, has been incorporated at the metal binding site. Due to its relatively low redox potential (1.29 V vs. NHE)[12], guanine is easily oxidized, and the radical formed can participate in facile back electron transfer (BET) to regenerate the initial state of the system.[47] Inosine, although structurally similar to guanine, has a higher redox potential (1.5 V vs. NHE)[18] and is not oxidized as readily. These considerations ensure that the distance of DNA CT and the environment of the metal complex are the same in the three conjugates.

Previous experiments have shown that all three complexes bind DNA by intercalation, as evidenced by hypochromism and a red shift in the near-UV absorption upon addition of DNA.[29,37,40] Support for this binding mode is also provided by an increase in the DNA duplex melting temperature in the presence of the metal complexes (Table 4.1), since π-stacking interactions between the bases and the intercalating ligands are expected to stabilize the duplexes. Interestingly, the presence of the covalent linker on the intercalating ligand of **Ir** does not inhibit intercalation of this complex. Presumably, the complex interacts with the DNA bases during annealing, so that when the duplex is formed, the

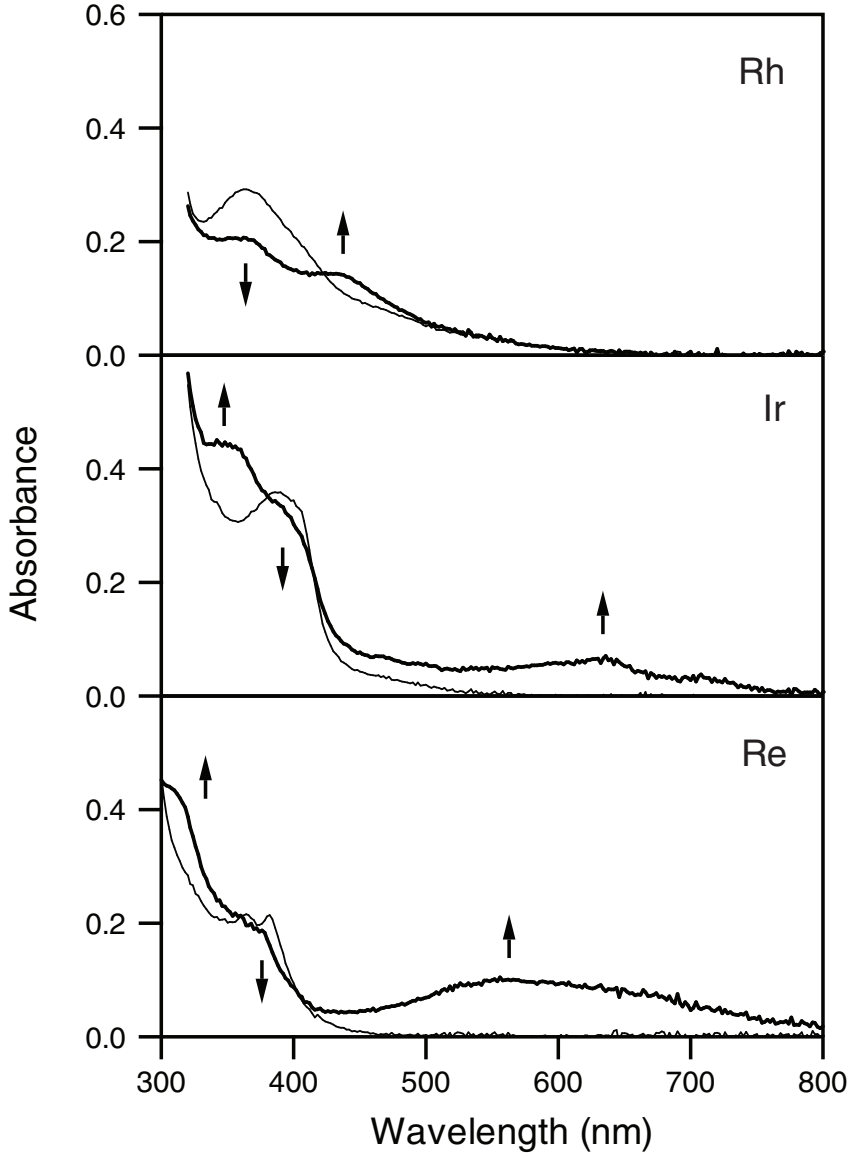

Figure 4.2: Steady-state UV/visible absorbance spectra of metal complexes before (thin line) and after (thick line) reduction by bulk electrolysis. Top: 16 μM $[Rh(phi)_2(bpy')]^{3+}$ in DMF; middle: 12 μM $[Ir(ppy)_2(dppz')]^{+}$ in DMF; bottom: 20 μM $[Re(CO)_3(dppz)(py'-OEt)]^{+}$ in acetonitrile. Arrows indicate changes in the spectra upon reduction.

construct resembles a threaded needle, with the metal center on one side of the duplex, the tether on the other, and the intercalated dppz ligand connecting them.[29]

4.3.4 Guanine Oxidation Observed by PAGE

An assay for guanine damage was carried out in order to establish directly the ability of **Re** to oxidize guanine and to enable comparison between the yield of oxidation observed upon excitation of each of the three metal complexes. Figure 4.4 shows the result of the photodamage experiment. Irradiation of DNA in the presence of each metal complex results in damage, although to varying degrees. Most prominently, extensive damage at the 5′-G of the 5′-GG-3′ doublet in **Rh-DNA** appears after only 30 minutes of irradiation. At this time point, damage in **Ir-DNA** is undetectable, and damage in **Re-DNA** is faint. Damage accrues linearly in all three samples with increasing irradiation time (Figure 4.3). After 120 minutes of irradiation, damage in **Ir-DNA** has accumulated beyond the baseline, and damage in **Re-DNA** has become pronounced. The damage yield at both guanines of the 5′-GG-3′ site increases as **Ir-DNA** < **Re-DNA** < **Rh-DNA** (Table 4.1). The absolute quantum yield of damage could not be determined accurately due to the nature of the sample geometry, but these values are expected to be comparable to those observed in similar conjugates between DNA and $[Rh(phi)_2(bpy')]^{3+}$ (2×10^{-6}).[17] Interestingly, the amount of damage does not correlate with the number of photons absorbed per sample. Based only on absorbance, **Ir**, which has a higher extinction coefficient than **Rh** and **Re**, and which has better spectral overlap with the excitation source (Figure 4.1), would be expected to be the most efficient photooxidant. Additionally, the pattern of damage differs in the three conjugates. While the **Rh-DNA** sample shows damage mainly at the 5′-G of the guanine doublet, the **Re-DNA** sample shows comparable damage at both guanines of the doublet, as well as pronounced damage close to the presumed complex binding site. This pattern of cleavage for **Re-DNA** does not appear to be the result of sensitization of singlet oxygen, given the lack of damage at thymine and the absence of damage enhancement in D_2O reported elsewhere.[38] Importantly, at the duplex concentrations used in these experiments (2 μM), interduplex guanine oxidation is not expected to be significant at the concentrations

Table 4.1: Melting Temperatures and Guanine Oxidation Yields for Metal Complex-DNA Conjugates

Species	T_m, $°C^a$	G^{ox} yield^b
Unmodified DNA	51	—
Rh-DNA	59	1.00
Ir-DNA	58	0.06
Re-DNA	52	0.57

[a] Measured using 2 μM duplexes in buffer (10 mM sodium phosphate, 50 mM NaCl; pH 7.5); uncertainty in T_m estimated as 1 °C

[b] Guanine oxidation yield determined via PAGE analysis; reported as the combined counts at both guanine sites of the 5′-GG-3′ doublet after 120 min irradiation relative to counts per lane, and normalized to the amount of damage observed for **Rh-DNA**

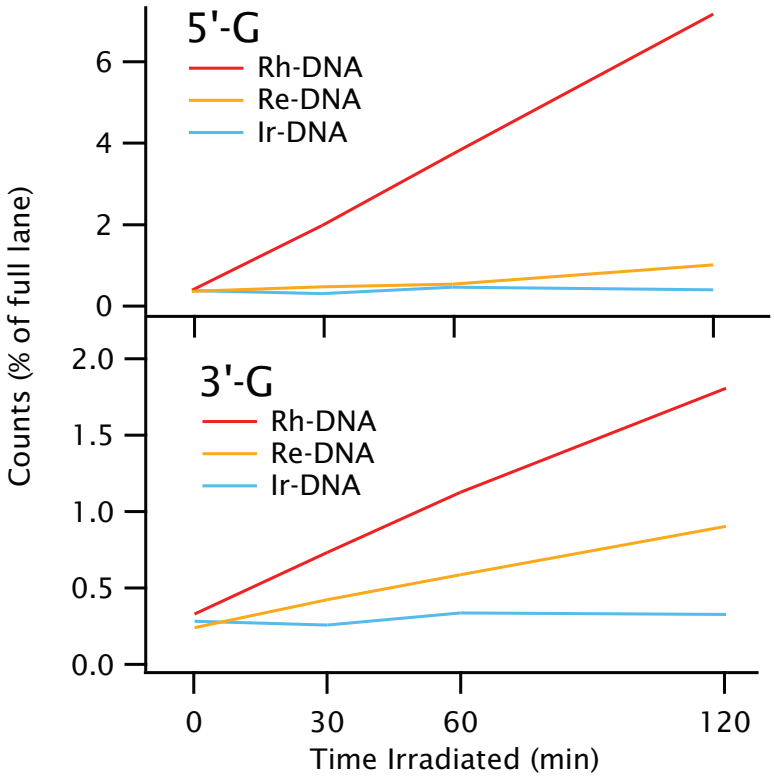

Figure 4.3: Accumulation of guanine damage with irradiation time. Damage at the 3′ and 5′ sites of the guanine doublet was quantified as the number of counts at those sites relative to the counts per lane from the PAGE gel (Figure 4.4). Sample conditions are described in the text.

used here.[19] These results indicate that although each complex has the ability to carry out guanine oxidation at long range from the excited state, competing reaction pathways operate differently in the three systems.

4.3.5 Transient Absorption Spectra

TA spectra of the three conjugates are shown in Figure 4.5. The spectra illustrate the difference in absorbance observed 60 ns after 355 nm excitation of 15 μM aqueous buffered samples (10 mM sodium phosphate, 50 mM NaCl; pH 7.5). In general, the three conjugates display similar difference spectra. **Rh-DNA** shows a strong bleach near 390 nm due to depletion of the ground state, as well as a positive transient centered at 460 nm with a long tail extending into the red. This is similar to the TA spectrum obtained for $[Rh(phi)_2(bpy)]^{3+}$ in water 30 ns after 420 nm excitation, except that in the latter case, an additional broad transient was observed centered near 680 nm.[48] **Ir-DNA** also shows a strong transient that is red-shifted from the ground state absorbance. However, in the case of **Ir-DNA**, the band is quite broad and featureless, extending into the near-IR region. No bleach was observed in the transient spectrum of **Ir-DNA** at 405 nm. An attempt to observe the excited state difference spectrum of $[Ir(ppy)_2(dppz)]^+$ in DMF after 355 nm ($\sim$10 ns pulse duration) yielded only broad absorption throughout the visible region. Finally, **Re-DNA** shows a strong, broad absorption throughout the visible region with a maximum near 460 nm and a shoulder near 550 nm, similar to what was observed for the excitation of $[Re(CO)_3(dppz)(py)]^+$ in acetonitrile upon 400 nm excitation.[49] While the intensity of the TA signal is comparable for **Rh-DNA** and **Ir-DNA**, the signal for **Re-DNA** at 60 ns is over twice as strong.

Difference spectra between the reduced and non-reduced metal complexes in organic solvents, measured by spectroelectrochemistry, are also shown in Figure 4.5. Interestingly, there are several similarities between these difference spectra and those obtained by TA. For example, while the spectroelectrochemistry difference spectrum of **Rh** does not show the extended tail to long wavelengths observed in the TA spectrum of **Rh-DNA**, the positions of the bleaches and of the absorbance maxima are roughly the same. Similarly, while the

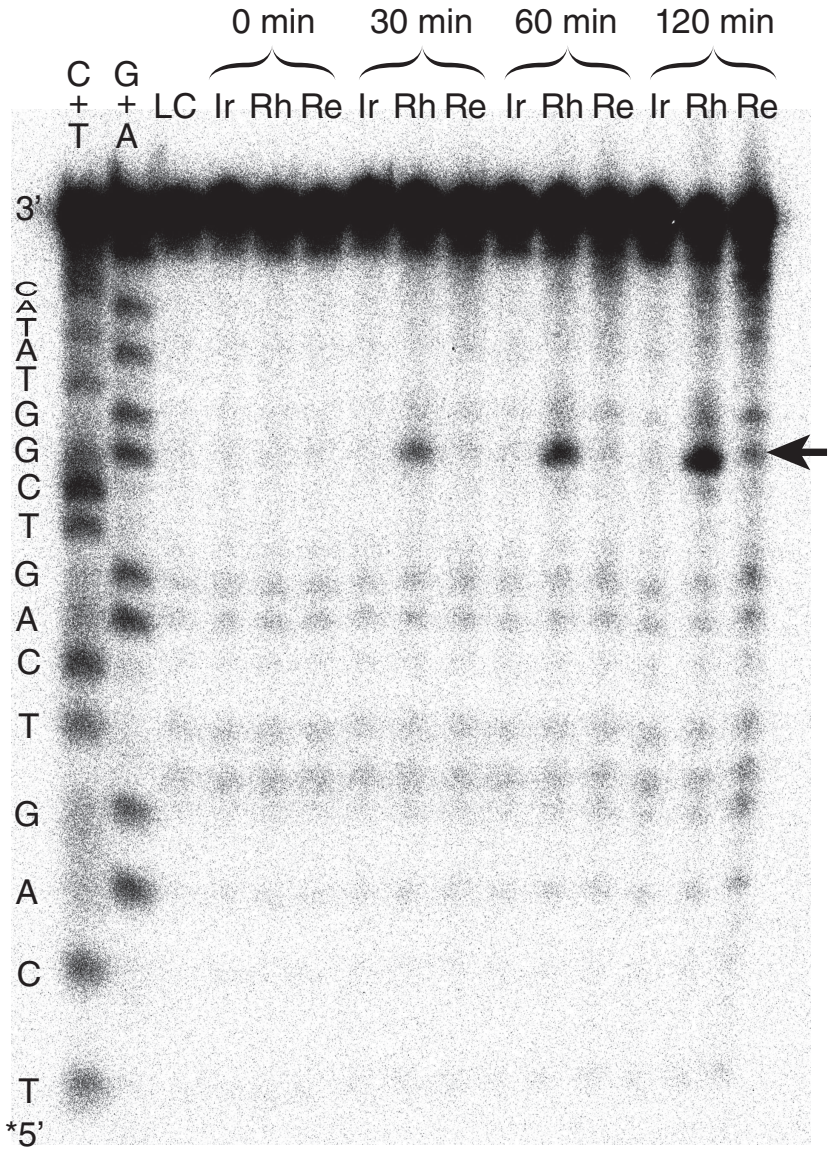

Figure 4.4: PAGE analysis following photooxidation of guanine by $[Rh(phi)_2(bpy')]^{3+}$, $[Ir(ppy)_2(dppz')]^{+}$, and $[Re(CO)_3(dppz)(py')]^{+}$ covalently bound to DNA. Metal-DNA conjugates (2 μM in buffer: 10 mM sodium phosphate, 50 mM NaCl, pH 7.5) were irradiated for 0, 30, 60, or 120 min. DNA strand cleavage at sites of oxidation was achieved by treatment with 10% piperidine. Cleavage products were separated by 20% PAGE and visualized by phosphorimagery. C+T and G+A: Maxam-Gilberts sequencing lanes; LC: light control (no metal complex); Ir, Rh, Re: the corresponding metal-DNA conjugates, irradiated for the indicated times. The DNA sequence is shown along the left edge of the gel. The position of the radiolabel is indicated by *. The 5′-G of the 5′-GG-3′ doublet is indicated by an arrow.

spectroelectrochemistry difference spectrum of **Ir** shows a bleach at 405 nm and the TA difference spectrum of **Ir-DNA** does not, bands in both spectra exhibit a sharp increase in absorbance near 420 nm and are relatively flat throughout the visible region. Finally, although the electrochemical difference spectrum of **Re** exhibits a bleach near 390 nm while the TA difference spectrum of **Re-DNA** does not, and although their band shapes are different, both absorb strongly into the near-IR. Although the spectra of metal complexes bound to DNA are not expected to be completely analogous to those observed in organic solvents due to differences in the solvation environments, the spectroelectrochemistry difference spectra and the TA difference spectra show remarkable similarities. This result suggests that both techniques probe similar molecular states.

4.3.6 Kinetics

The emission and TA lifetimes of the metal complexes in acetonitrile are quite different from those of the DNA conjugates in aqueous solution. Kinetic parameters obtained from least-squares analysis are shown in Table 4.2. In general, lifetimes of the three complexes differ by several orders of magnitude. In acetonitrile, **Rh** and **Ir** are non-emissive upon excitation at 355 nm, but **Re** shows strong emission at 570 nm that decays biexponentially with lifetimes of 180 ns and 17 μs. The behavior of Re-OEt is similar, although its emission decay lifetime is consistently observed to be shorter than that of **Re**, even after exhaustive degassing of the solvent via the freeze-pump-thaw method. The lifetimes of non-emissive excited states can be inferred from TA measurements. Excitation of **Rh** in acetonitrile at 355 nm results in a weak transient signal at 460 nm (the TA maximum) with a lifetime of 81 ns. Similarly, excitation of **Ir** gives a transient at 540 nm that decays with a lifetime of 270 ns. Presumably, the 19 μs decay observed by TA for **Re** corresponds to the 17 μs decay observed through emission.

TA decays for the three metal complex-DNA conjugates are shown in Figure 4.6. Again, the lifetimes of the transients differ greatly between the conjugates. In particular, transient signals measured for systems containing DNA-conjugated **Rh** and **Re** have much longer lifetimes than those observed in organic solvents. For **Rh-DNA**, the best fit gives

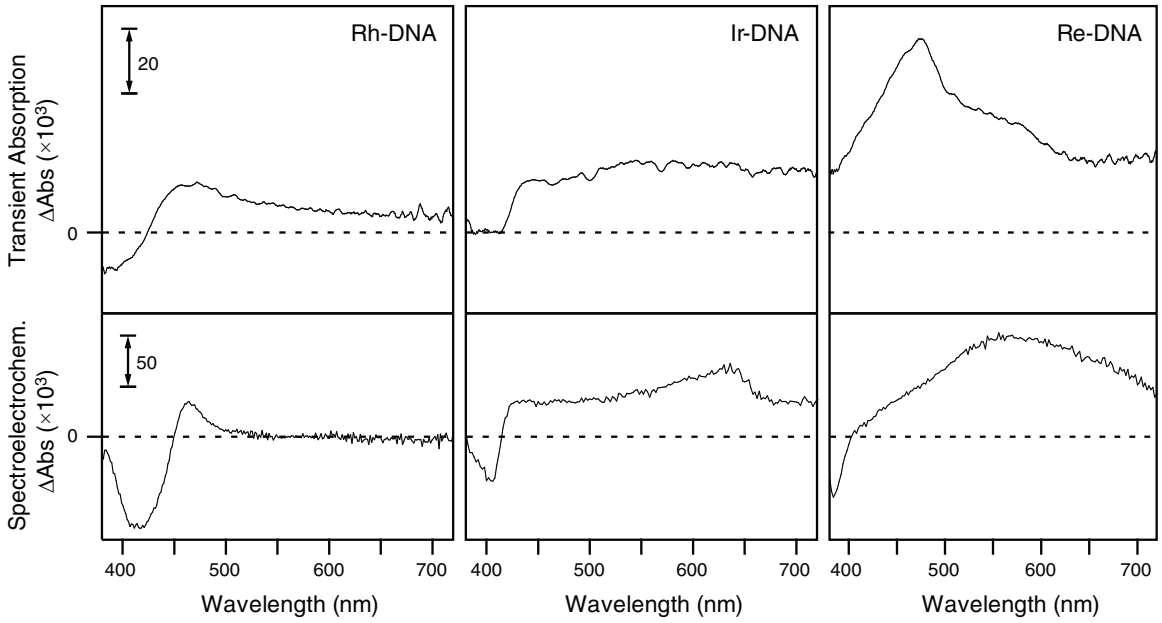

Figure 4.5: Comparison between transient absorption difference spectra and spectroelectrochemical difference spectra. Top: TA spectra obtained 60 ns after excitation at 355 nm of 15 μM $[Rh(phi)_2(bpy')]^{3+}$, $[Ir(ppy)_2(dppz')]^{+}$, and $[Re(CO)_3(dppz)(py')]^{+}$ covalently bound to DNA. Bottom: spectroelectrochemistry difference spectra for (from left to right) 16 μM $[Rh(phi)_2(bpy')]^{3+}$ in DMF, 12 μM $[Ir(ppy)_2(dppz')]^{+}$ in DMF, and 20 μM $[Re(CO)_3(dppz)(py')]^{+}$ in acetonitrile.

Table 4.2: Least-Squares Parameters for Time-Resolved Emission and Transient Absorption Decay Lifetimes for Metal Complexes and Metal Complex-DNA Conjugates

Species[a]	Emission		Transient Absorption	
	λ_{probe}, nm	τ, ns (% contribution)[b]	λ_{probe}, nm	τ, ns (% contribution)[b]
Rh	—	—	460	81
Ir	—	—	540	270
Re	570	180 (12), 17 000 (88)	475	19 000
Re-OEt	570	210 (11), 7 600 (89)	475	8 000
Rh-DNA	—	—	460	73 (79), 1 100 (21)
Ir-DNA	—	—	540	5.9 (94), 280 (6)
Re-DNA	570	265	475	3 200 (37), 35 000 (63)

[a] Complexes were dissolved in deaerated acetonitrile; metal complex-DNA conjugates were prepared in buffer (10 mM sodium phosphate, 50 mM NaCl; pH 7.5).
[b] Uncertainty in lifetimes estimated as 10%; values in parentheses correspond to the pre-exponential coefficients a_n following normalization of the signal.

lifetimes of 73 ns and 1.1 μs. For **Re-DNA**, photoexcitation yields a more persistent transient signal, with lifetimes of 3.2 μs and 35 μs. **Ir-DNA**, on the other hand, exhibits a very prominent (94%), short-lived component with a lifetime on the order of 6 ns and a longer-lived component with a lifetime of 280 ns. The spectroscopic differences observed between the three conjugates underscore the diversity of their photophysical behavior and the differences in their interactions with DNA.

4.4 Discussion

4.4.1 Excited State Assignments

The steady-state photophysical properties of **Rh**, **Ir**, and **Re** resemble those of analogous complexes. For example, good agreement between the TA spectra of several phi-containing complexes following excitation at 420 nm has enabled assignment of the 390 nm absorption band in $[Rh(phi)_2(phen)]^{3+}$ to a combination of $\pi \rightarrow \pi^*$ (phen) and $\pi \rightarrow \pi^*$ (phi) transitions, which quickly relax (< 60 ns) to an intraligand charge transfer (ILCT) state in which electron density has shifted to the phenanthrene portion of the phi ligand.[48] Due to the similarities between the photophysics of $[Rh(phi)_2(phen)]^{3+}$ and $[Rh(phi)_2(bpy)]^{3+}$, a similar process is expected in the latter complex and in its tether-functionalized analogue, **Rh**. The absorption profiles of **Re** and **Ir** are also attributed to a mixture of several transitions. For example, tricarbonyl Re complexes bearing dppz are known to populate several singlet excited states upon photon absorption, including metal-to-ligand charge transfer (MLCT) states and ILCT states centered on the dppz ligand.[49–53] Over time, intersystem crossing and internal conversion leads to population of the emissive ^{3}IL states.[49] Similarly, **Ir** exhibits a strong absorption band in the near-UV in acetonitrile, as well as a weak, broad band centered near 450 nm.[29] As in **Re**, the higher energy bands are likely due to an IL transition on dppz, while the lower energy band is probably MLCT in character. Thus, in all three complexes, a molecular orbital of the intercalating ligand is populated upon excitation.

4.4.2 Reduced Metal Complexes

The electronic structure of reduced **Rh** may be determined by comparing it with the reduced states of other phi complexes. For example, $E^{\circ}(Ru^{2+}/Ru^{+})$ in $[Ru(bpy)_2(phi)]^{2+}$ appears at a more positive potential than in $[Ru(bpy)_3]^{2+}$, indicating that in complexes with mixed bpy and phi ligands, phi is reduced more readily than bpy.[54] The product of single-electron reduction of **Rh** can therefore be assigned as $[Rh^{III}(phi)(phi^{\bullet -})(bpy')]^{2+}$. The reduced states of **Re** and **Ir** can be assigned based on analogy to other complexes ligated by dppz. It has been shown that electrochemical reduction of dppz results in addition of an electron to the phenazine-centered orbital of dppz rather than to the α-diimine-centered orbitals that are populated upon excitation to the MLCT state.[55] Spectroscopically, reduction of dppz is manifested as the appearance of an absorption band centered near 570 nm that absorbs throughout the visible spectral range.[55] The resemblance between the difference spectrum of reduced dppz and that of reduced **Re** and **Ir** suggests that reduction of **Re** and **Ir** results in addition of an electron to the phenazine-centered orbital of the dppz ligand as well. These assignments are consistent with those of reduced $[Os(phen)_2(dppz)]^{2+}$ and $[Ru(dppz)_3]^{2+}$, which show similar spectral behavior.[56] The reduced states of the three complexes, therefore, also involve the intercalating ligand. The participation in photophysical and electrochemical process of the intercalating ligand, which is intimately associated with the DNA base stack, may be necessary for efficient DNA-mediated CT to proceed.[57]

4.4.3 Comparison of Spectroelectrochemical and TA Difference Spectra

The TA difference spectra of **Rh-DNA** and **Re-DNA** are similar to spectra observed upon photoexcitation of $[Rh(phi)_2(bpy)]^{3+}$ in water[48,58] and $[Re(CO)_3(dppz)(py)]^{+}$ in acetonitrile,[49] respectively. However, the TA spectra of the three conjugates also exhibit features in common with the reduced state spectra observed by spectroelectrochemistry. Considering the favorable driving force for guanine oxidation by excited **Rh**, **Ir**, and **Re**, the oxidative damage observed in PAGE experiments, and numerous reports in the literature confirming the ability of similar complexes to oxidize guanine from a distance,[19,28,30,58–60] the observation of reduced states in the TA spectra is expected. In each system, oxidation of guanine

by the photoexcited metal complex must result in the reduction of the metal complex. The observed TA spectra, therefore, likely consist of mixtures of excited and reduced states.

Analysis of the TA lifetimes supports the formation of a mixture of states. In all three samples, DNA-mediated CT is expected to occur at a rate faster than the time resolution of the instrument.[27,61,62] In **Rh-DNA**, the TA decay exhibits two lifetimes, the shorter of which is within error of the TA lifetime of **Rh** in acetonitrile and can therefore be ascribed to decay from the excited state of complex molecules that are not well coupled to the DNA base stack at the time of excitation. However, as is apparent by gel analysis, **Rh-DNA** shows the highest level of guanine damage. This supports the idea that DNA-mediated CT is fast compared to the TA instrumentation; eighty percent of the decay appears from the excited state as unquenched and uncoupled, but a faster static quenching must occur. This static quenching component reflects DNA-mediated CT that gives rise to the guanine damage. The second lifetime component, which is over an order of magnitude slower, is not observed in the absence of DNA, and is attributed to absorption of the reduced state.

The TA decay of **Ir-DNA** is also biexponential; however, in this case, it is the lifetime of the longer-lived component that shares similarity with the lifetime of **Ir** in acetonitrile. Here, the interpretation is slightly different. Considering the driving force for guanine oxidation, it is still probable that the reduced state of the complex is formed in **Ir-DNA**, but that its lifetime is much shorter in **Ir-DNA** than the lifetime of the reduced state in **Rh-DNA**. The longer lifetime in **Rh-DNA** and the shorter lifetime in **Ir-DNA**, then, reflect the rates of BET in these systems. Importantly, this interpretation is consistent with the results of the PAGE experiment: the low yield of guanine damage in **Ir-DNA** is due to fast BET in that system.

In **Re-DNA**, no component is observed that matches the excited state lifetime of **Re** or Re-OEt, suggesting that the DNA environment affects the photodynamics of this complex. However, excitation in the presence of DNA does lead to formation of a long-lived transient. A similar result was observed for $[Re(CO)_3(dppz)(4\text{-methylpyridine})]^+$ in the presence of calf thymus DNA.[37] Interestingly, in that case, the transient decay was also biphasic in the presence of DNA, and as the DNA concentration was increased, the longer

time component became more dominant. Both phases were assigned to formation of the ^{3}IL(dppz) excited state, while the ten fold difference in lifetime between the two phases was attributed to two different binding modes or differences in solvent accessibility. While these factors can influence excited state lifetimes, it is probable that excited state quenching by guanine to form the reduced metal complex also occurs, similar to what we propose for **Ir-DNA** and **Rh-DNA**.

4.4.4 A Model for DNA-Mediated Guanine Oxidation

From these considerations, a model for the DNA-mediated oxidation of guanine by intercalating photooxidants can be constructed (Figure 4.2 on page 154). Prior to excitation, the system exists as an equilibrium of two populations: one in which the metal complex is poorly coupled to the base stack (not shown in Scheme 4.2) and one in which the complex is well coupled. Excitation of the metal complex may be followed by luminescent or non-radiative relaxation, or (in the well-coupled system) by charge injection to form the reduced metal complex and the guanine radical cation. From the charge-separated state, the formation of permanent guanine oxidation products by reaction with water or oxygen competes with BET. If charge injection is slow (due to poor coupling between the oxidant and the DNA base stack), decay to the ground state will preclude the eventual formation of guanine damage. If charge injection is fast, the yield of permanent damage may still be attenuated by facile BET. This mechanism combines the results observed by PAGE and transient absorption, and it is expected to be general for any intercalating metal complex photooxidant.

4.4.5 Factors Affecting the Efficiency of Guanine Oxidation

According to the model, the quantum yield of guanine damage, $\Phi_{G_{ox}}$, can be expressed as:

$$\Phi_{G_{ox}} = \Phi_{CT} \frac{k_{trap}}{k_{trap} + k_{BET}}, \tag{4.1}$$

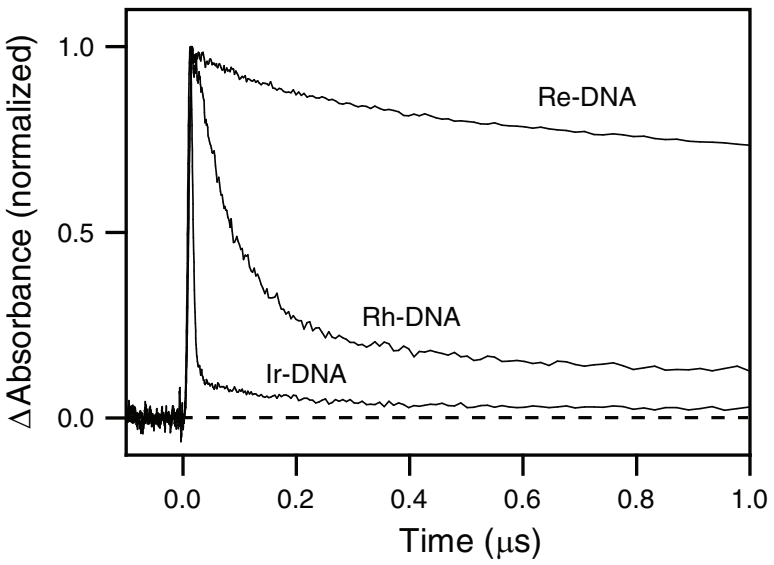

Figure 4.6: Transient absorption decay traces for 15 μM $[Rh(phi)_2(bpy')]^{3+}$ (460 nm), $[Ir(ppy)_2(dppz')]^{+}$ (540 nm), and $[Re(CO)_3(dppz)(py')]^{+}$ (475 nm) covalently bound to DNA following excitation at 355 nm.

where Φ_{CT} is the quantum yield of CT, k_{trap} and k_{BET} are the rates of hole trapping (to form permanent guanine products) and BET, respectively; and

$$\Phi_{CT} = F\frac{k_{CT}}{k_{CT} + k_{em} + k_{nr}} \tag{4.2}$$

depends on F, the fraction of conjugates that achieves a CT-active conformation within the excited state lifetime, and the rates of CT (k_{CT}), emission (k_{em}, if applicable), and non-radiative decay processes (k_{nr}). Here, k_{CT} refers to the intrinsic rate of CT through DNA, assuming a maximally coupled system. Using the definition of quantum yield, the amount of damage observed, $N_{G_{ox}}$, can be expressed as a function of N_{abs}, the number of photons absorbed:

$$N_{G_{ox}} = N_{abs} \times F\left(\frac{k_{CT}}{k_{CT} + k_{em} + k_{nr}}\right)\left(\frac{k_{trap}}{k_{trap} + k_{BET}}\right). \tag{4.3}$$

This function nicely summarizes the many factors that affect the yield of guanine damage. A greater number of photons absorbed, a greater fraction of the population in a CT-active conformation, and faster rates of CT and trapping increase the yield; conversely, faster rates of emission, non-radiative decay, and BET decrease the yield.

The extent of electronic coupling between the photooxidant and the hole acceptor is expected to have a strong influence on the amount of damage observed. Intercalation confers superior coupling between the oxidant and the DNA base stack. Functionally, the intercalated ligand "becomes" an additional base, linking the electronic system of the metal complex to that of the base stack. Poor coupling, therefore, disrupts this linkage and decreases the rate of charge injection. Factors that affect the degree of coupling between the oxidant and the base stack include the planarity and size of the intercalating ligand,[57,63] the charge of the complex, the dynamics of the oxidant within the intercalation site,[62] and the size, shape, and hydrophobicity of the ancillary ligands.[58,64,65] Experimentally, the extent of coupling of the metal complex to the base stack is reflected in part by the increase in DNA melting temperature in the presence of the intercalator and by the extent of hypochromism associated with binding. From melting temperature data (Table 4.1),

coupling in the conjugates increases as **Re-DNA** < **Ir-DNA** < **Rh-DNA**. The stronger coupling observed in **Rh-DNA** is likely due to its higher charge (+3 for **Rh**, compared to +1 for **Ir** and **Re**), as well as the use of only the diastereomer bearing the tighter binding Δ-isomer.

In general, the extent of coupling between the bases themselves also affects the yield of damage. Indeed, the efficiency of DNA CT depends on the DNA sequence[66–68] and base motions,[69,70] and examination of DNA CT in solution[71] and through DNA monolayers on gold surfaces[72–74] has illustrated the acute sensitivity of DNA CT to intervening mismatches and lesions. In our tethered systems, such sequence-dependent and dynamic effects are not expected to cause differences in the guanine oxidation yield, since they will have equal bearing on the results for each of the three conjugates. Variations in CT associated with distance were not determined in these experiments, but they are expected to be comparable for the three assemblies. Not only do the tethered binding positions appear to be comparable based on model building, but more importantly, for well-coupled probes the distance dependence of DNA-mediated CT is shallow, independent of the probe.[19,31,75,76]

The rate of any CT process is related to the thermodynamic driving force according to Marcus theory.[77] For the CT reaction, thermodynamic analysis predicts that **Rh*** should be the strongest oxidant ($E^{\circ}[Rh^{3+}*/Rh^{2+}]$ = 2.0 V vs. NHE)[48], while **Ir*** ($E^{\circ}[Ir^{+}*/Ir^{0}]$ = 1.7 V vs. NHE,[29] with E_{00} calculated as the crossover point between the absorbance and emission spectra) is expected to yield a similar amount of damage as **Re*** ($E^{\circ}[Re^{+}*/Re^{0}]$ = 1.73 V, calculated in a similar way), but this trend is not observed. One factor that contributes to the greater yield in **Re-DNA** is the much longer lifetime (slower k_{em} and k_{nr}) observed for the excited state of **Re** (Table 4.2). Besides decreasing the denominator in Eq. 4.3, a longer excited state lifetime will increase F, since more conformational states of DNA can be sampled prior to relaxation of the excited state. This increases the probability of achieving a CT-active conformation within the excited state lifetime. Another contributing factor is facile BET in **Ir-DNA**, which deactivates the charge-separated precursor before damage can occur. TA experiments have shown that in the absence of BET, the lifetime of the guanine radical extends into the millisecond regime.[47] Any process that

neutralizes the radical within its lifetime will decrease the yield of permanent damage.[17] As an extreme example, BET completely prevents the formation of oxidative guanine damage when thionine is used as an intercalating photooxidant, despite the favorable driving force for this reaction (∼0.7 eV).[78] The driving force for BET in each of the conjugates increases approximately as **Rh-DNA** (1.29 eV)[48] < **Ir-DNA** (1.99 eV)[29] < **Re-DNA** (2.14 eV). Due to the large free-energy changes associated with BET, these processes are expected to lie in the Marcus inverted region.[79] From these considerations alone, the rate of BET is therefore predicted to be fastest in **Rh-DNA** and slowest in **Re-DNA**. The observation of faster BET in **Ir-DNA** than in **Rh-DNA** by TA spectroscopy indicates that other factors, such as reorganization energy, may affect the rate of BET. Interestingly, effective coupling is needed for efficient BET as well as CT. In **Re-DNA**, poorer coupling to the base stack could decrease the efficiency of BET, further enhancing the yield of guanine damage in this conjugate.

The trend observed in the guanine oxidation assay can be explained by the interplay of these many factors. The higher yield of damage in the **Rh-DNA** sample is likely due to the strong driving force for guanine oxidation. For **Rh**, this value is 0.71 eV, compared to 0.51 eV for **Ir-DNA** and 0.54 eV for **Re-DNA**. This strong driving force leads to a fast k_{CT}. The high yield in the **Rh-DNA** sample is also due to strong coupling, evidenced by the high melting temperature differential observed for **Rh-DNA**: (8 °C, compared to 7 °C for **Ir-DNA** and 1 °C for **Re-DNA**). Presumably, BET in **Rh-DNA** is offset by these factors. In comparing **Ir-DNA** and **Re-DNA**, which have the same intercalating ligand, the same charge, and show a similar driving force for guanine oxidation, other factors become important. In these conjugates, the stronger coupling of **Ir** to the base stack results in faster rates of CT and BET, decreasing the yield of damage, while the longer excited-state lifetime and strongly inverted BET in **Re-DNA** increase damage.

4.5 Conclusions

The electrochemical and photophysical properties of three metal complexes and their DNA conjugates have been observed in the same sequence context. All of the complexes have

high excited state reduction potentials, and gel electrophoresis experiments indicate that guanine oxidation by the excited complexes can occur via DNA CT. Comparison between spectroelectrochemical difference spectra and TA difference spectra suggests that photoexcitation of metal complex-DNA conjugates results in a mixture of excited and reduced metal states, allowing for the observation of charge-separated intermediates and measurement of the relative rates of charge recombination (BET). The ability to oxidize guanine indicates effective coupling of all of the complexes to the DNA base stack, signifying that these or similar complexes could be useful for triggering oxidation in more complex experimental systems.

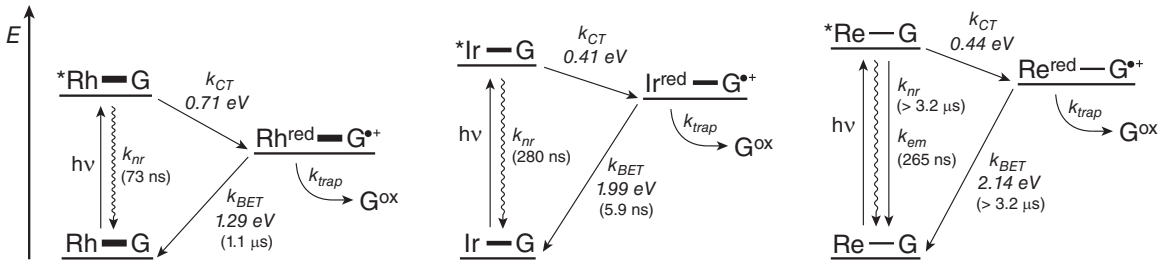

Scheme 4.2: Proposed model for the DNA-mediated oxidation of guanine by metallointercalating photooxidants. Conjugates are represented as M-G, where the thickness of the line connecting M and G represents the extent of coupling between the metal complex and the base stack. Wavy arrows represent non-radiative decay from the excited state (**Rh***, **Ir***, or **Re***). Reduced metal complex states are represented as M^{red}. The guanine radical cation ($G^{\bullet+}$) is distinguished from permanent guanine oxidation products (G^{ox}). Energy level differences are to scale. Thermodynamic driving forces are shown for charge injection and back electron transfer (BET), and lifetimes are shown in parentheses. In each scheme, the equilibrium with the poorly coupled system is omitted for clarity.

References

[1] Møller, P., Folkmann, J. K., Forchhammer, L., Bräuner, E. V., Danielsen, P. H., Risom, L., and Loft, S. "Air pollution, oxidative damage to DNA, and carcinogenesis." *Cancer Lett.* **266**, 84–97 (2008).

[2] Cooke, M. S., Evans, M. D., Dizdaroglu, M., and Lunec, J. "Oxidative DNA damage: mechanisms, mutation, and disease." *FASEB J.* **17**, 1195–1214 (2003).

[3] Klaunig, J. E., and Kamendulis, L. M. "The role of oxidative stress in carcinogenesis." *Annu. Rev. Pharmacol. Toxicol.* **44**, 239–267 (2004).

[4] Nishikawa, M. "Reactive oxygen species in tumor metastasis." *Cancer Lett.* **266**, 53–59 (2008).

[5] van Loon, B., Markkanen, E., and Hübscher, U. "Oxygen as a friend and enemy: How to combat the mutational potential of 8-oxo-guanine." *DNA Repair* **9**, 604–616 (2010).

[6] Lovell, M. A., and Markesbery, W. R. "Oxidative Damage in Mild Cognitive Impairment and Early Alzheimers Disease." *J. Neurosci. Res.* **85**, 3036–3040 (2007).

[7] David, S. S., O'Shea, V. L., and Kundu, S. "Base-excision repair of oxidative DNA damage." *Nature* **447**, 941–950 (2007).

[8] Joyce, L. E., Aguirre, J. D., Angeles-Boza, A. M., Chouai, A., Fu, P. K.-L., Dunbar, K. R., and Turro, C. "Photophysical Properties, DNA Photocleavage, and Photocytotoxicity of a Series of Dppn Dirhodium(II,II) Complexes." *Inorg. Chem.* **49**, 5371–5376 (2010).

[9] Sasmal, P. K., Saha, S., Majumdar, R., Dighe, R. R., and Chakravarty, A. R. "Photocytotoxic oxovanadium(IV) complexes showing light-induced DNA and protein cleavage activity." *Inorg. Chem.* **49**, 849–859 (2010).

[10] Hussain, A., Saha, S., Majumdar, R., Dighe, R. R., and Chakravarty, A. R. "Photocytotoxicity and DNA photocleavage activity of La(III) and Gd(III) complexes of phenanthroline bases." *Ind. J. Chem.* **50**, 519–530 (2011).

[11] Le Gac, S., Foucart, M., Gerbaux, P., Defrancq, E., Moucheron, C., and Kirsch-De Mesmaeker, A. "Photo-reactive Ru(II)-oligonucleotide conjugates: influence of an intercalating ligand on the inter- and intra-strand photo-ligation processes." *Dalton Trans.* **39**, 9672–9683 (2010).

[12] Steenken, S., and Jovanovic, S. V. "How Easily Oxidizable Is DNA? One-Electron Reduction Potentials of Adenosine and Guanosine Radicals in Aqueous Solution." *J. Am. Chem. Soc.* **119**, 617–618 (1997).

[13] Delaney, S., and Barton, J. K. "Long-range DNA Charge Transport." *J. Org. Chem.* **68**, 6475–6483 (2003).

[14] Schuster, G. B., Ed. *Topics in Current Chemistry: Long-Range Charge Transfer in DNA I*; Springer-Verlag: New York, 2004.

[15] Valis, L., Wang, Q., Raytchev, M., Buchvarov, I., Wagenknecht, H.-A., and Fiebig, T. "Base pair motions control the rates and distance dependencies of reductive and oxidative DNA charge transfer." *Proc. Natl. Acad. Sci. USA* **103**, 10192–10195 (2006).

[16] Sanii, L., and Schuster, G. B. "Long-Distance Charge Transport in DNA: Sequence-Dependent Radical Cation Injection Efficiency." *J. Am. Chem. Soc.* **122**, 11545–11546 (2000).

[17] Williams, T. T., Dohno, C., Stemp, E. D. A., and Barton, J. K. "Effects of the photooxidant on DNA-mediated charge transport." *J. Am. Chem. Soc.* **126**, 8148–8158 (2004).

[18] Kelley, S. O., and Barton, J. K. "Electron Transfer Between Bases in Double Helical DNA." *Science* **283**, 375–381 (1999).

[19] Núñez, M. E., Hall, D. B., and Barton, J. K. "Long-range oxidative damage to DNA: effects of distance and sequence." *Chem. Biol.* **6**, 85–97 (1999).

[20] Slinker, J. D., Muren, N. B., Renfrew, S. E., and Barton, J. K. "DNA charge transport over 34 nm." *Nature Chem.* **3**, 228–233 (2011).

[21] Merino, E. J., and Barton, J. K. "DNA oxidation by charge transport in mitochondria." *Biochemistry* **47**, 1511–1517 (2008).

[22] Genereux, J. C., Boal, A. K., and Barton, J. K. "DNA-Mediated Charge Transport in Redox Sensing and Signaling." *J. Am. Chem. Soc.* **132**, 891–905 (2010).

[23] Augustyn, K. E., Merino, E. J., and Barton, J. K. "A role for DNA-mediated charge transport in regulating p53: Oxidation of the DNA-bound protein from a distance." *Proc. Natl. Acad. Sci. USA* **104**, 18907–18912 (2007).

[24] Lee, P. E., Demple, B., and Barton, J. K. "DNA-mediated redox signaling for transcriptional activation of SoxR." *Proc. Natl. Acad. Sci. USA* **106**, 13164–13168 (2009).

[25] Boal, A. K., Genereux, J. C., Sontz, P. A., Gralnick, J. A., Newman, D. K., and Barton, J. K. "Redox signaling between DNA repair proteins for efficient lesion detection." *Proc. Natl. Acad. Sci. USA* **106**, 15237–15242 (2009).

[26] Barton, J. K., Olmon, E. D., and Sontz, P. A. "Metal complexes for DNA-mediated charge transport." *Coord. Chem. Rev.* **255**, 619–634 (2011).

[27] Murphy, C. J., Arkin, M. R., Jenkins, Y., Ghatlia, N. D., Bossmann, S. H., Turro, N. J., and Barton, J. K. "Long-range photoinduced electron transfer through a DNA helix." *Science* **262**, 1025–1029 (1993).

[28] Hall, D. B., Holmlin, R. E., and Barton, J. K. "Oxidative DNA damage through long-range electron transfer." *Nature* **382**, 731–735 (1996).

[29] Shao, F., Elias, B., Lu, W., and Barton, J. K. "Synthesis and characterization of iridium(III) cyclometalated complexes with oligonucleotides: insights into redox reactions with DNA." *Inorg. Chem.* **46**, 10187–10199 (2007).

[30] Shao, F., and Barton, J. K. "Long-range electron and hole transport through DNA with tethered cyclometalated iridium(III) complexes." *J. Am. Chem. Soc.* **129**, 14733–14738 (2007).

[31] Elias, B., Shao, F., and Barton, J. K. "Charge migration along the DNA duplex: hole versus electron transport." *J. Am. Chem. Soc.* **130**, 1152–1153 (2008).

[32] Turner, J. J., George, M. W., Johnson, F. P. A., and Westwell, J. R. "Time-resolved Infrared Spectroscopy of Excited States of Transition Metal Species." *Coord. Chem. Rev.* **125**, 101–114 (1993).

[33] George, M. W., and Turner, J. J. "Excited states of transition metal complexes studied by time-resolved infrared spectroscopy." *Coord. Chem. Rev.* **177**, 201–217 (1998).

[34] Vlček, A. "Ultrafast Excited-State Processes in Re(I) Carbonyl-Diimine Complexes: From Excitation to Photochemistry." *Top. Organomet. Chem.* **29**, 73–114 (2010).

[35] Friedman, A. E., Chambron, J.-C., Sauvage, J.-P., Turro, N. J., and Barton, J. K. "Molecular 'Light Switch' for DNA: $Ru(bpy)_2(dppz)^{2+}$." *J. Am. Chem. Soc.* **112**, 4960–4962 (1990).

[36] Ruiz, G. T., Juliarena, M. P., Lezna, R. O., Wolcan, E., Feliz, M. R., and Ferraudi, G. "Intercalation of *fac*-$[(4,4'\text{-bpy})Re^{I}(CO)_3(dppz)]^{+}$, dppz = dipyridyl[3,2-*a*:2′3′-*c*]phenazine, in polynucleotides. On the UV-vis photophysics of the Re(I) intercalator and the redox reactions with pulse radio." *Dalton Trans.* **3**, 2020–2029 (2007).

[37] Stoeffler, H. D., Thornton, N. B., Temkin, S. L., and Schanze, K. S. "Unusual Photophysics of a Rhenium(I) Dipyridophenazine Complex in Homogeneous Solution and Bound to DNA." *J. Am. Chem. Soc.* **117**, 7119–7128 (1995).

[38] Yam, V. W.-W., Lo, K. K.-W., Cheung, K.-K., and Kong, R. Y.-C. "Deoxyribonucleic acid binding and photocleavage studies of rhenium(I) dipyridophenazine complexes." *J. Chem. Soc., Dalton Trans.* **14**, 2067–2072 (1997).

[39] Yam, V. W.-W., Lo, K. K.-W., Cheung, K.-K., and Kong, R. Y.-C. "Synthesis, photophysical properties and DNA binding studies of novel luminescent rhenium(I) complexes. X-Ray crystal structure of $[Re(dppn)(CO)_3(py)](OTf)$." *J. Chem. Soc., Chem. Commun.* **3**, 1191–1193 (1995).

[40] Sitlani, A., Long, E. C., Pyle, A. M., and Barton, J. K. "DNA Photocleavage by Phenanthrenequinone Diimine Complexes of Rhodium(III): Shape-Selective Recognition and Reaction." *J. Am. Chem. Soc.* **114**, 2303–2312 (1992).

[41] Holmlin, R. E., Dandliker, P. J., and Barton, J. K. "Synthesis of Metallointercalator-DNA Conjugates on a Solid Support." *Bioconj. Chem.* **10**, 1122–1130 (1999).

[42] Zeglis, B. M., and Barton, J. K. "DNA base mismatch detection with bulky rhodium intercalators: synthesis and applications." *Nat. Protoc.* **2**, 357–371 (2007).

[43] Boyle, P. D., Boyd, D. C., Mueting, A. M., and Pignolet, L. H. "Redox and Acid-Base Chemistry of $[Au_2Re_2(H)_6(PPh_3)_6]PF_6$ and Related Cluster Compounds." *Inorg. Chem.* **27**, 4424–4429 (1988).

[44] Dempsey, J. L., Winkler, J. R., and Gray, H. B. "Kinetics of electron transfer reactions of H_2-evolving cobalt diglyoxime catalysts." *J. Am. Chem. Soc.* **132**, 1060–1065 (2010).

[45] Pyle, A. M., Chiang, M. Y., and Barton, J. K. "Synthesis and characterization of physical, electronic, and photochemical aspects of 9,10-phenanthrenequinonediimine complexes of ruthenium(II) and rhodium(III)." *Inorg. Chem.* **29**, 4487–4495 (1990).

[46] Dupureur, C. M., and Barton, J. K. "Structural Studies of Λ- and Δ-$[Ru(phen)_2dppz]^{2+}$ Bound to $d(GTCGAC)_2$: Characterization of Enantioselective Intercalation." *Inorg. Chem.* **36**, 33–43 (1997).

[47] Stemp, E. D. A., Arkin, M. R., and Barton, J. K. "Oxidation of Guanine in DNA by $Ru(phen)_2(dppz)^{3+}$ Using the Flash-Quench Technique." *J. Am. Chem. Soc.* **119**, 2921–2925 (1997).

[48] Turro, C., Evenzahav, A., Bossmann, S. H., Barton, J. K., and Turro, N. J. "Excited state properties of $Rh(phi)_2(phen)^{3+}$ and related complexes: a strong photooxidant." *Inorg. Chim. Acta* **243**, 101–108 (1996).

[49] Dyer, J., Blau, W. J., Coates, C. G., Creely, C. M., Gavey, J. D., George, M. W., Grills, D. C., Hudson, S., Kelly, J. M., Matousek, P., McGarvey, J. J., McMas-

ter, J., Parker, A. W., Towrie, M., and Weinstein, J. A. "The photophysics of *fac*-$[Re(CO)_3(dppz)(py)]^+$ in CH_3CN: a comparative picosecond flash photolysis, transient infrared, transient resonance Raman and density functional theoretical study." *Photochem. Photobiol. Sci.* **2**, 542–554 (2003).

[50] Dyer, J., Creely, C. M., Penedo, J. C., Grills, D. C., Hudson, S., Matousek, P., Parker, A. W., Towrie, M., Kelly, J. M., and George, M. W. "Solvent dependent photophysics of fac-$[Re(CO)_3(11,12\text{-}X_2dppz)(py)]^+$(X = H, F or Me)." *Photochem. Photobiol. Sci.* **6**, 741–748 (2007).

[51] Kuimova, M. K., Alsindi, W. Z., Blake, A. J., Davies, E. S., Lampus, D. J., Matousek, P., McMaster, J., Parker, A. W., Towrie, M., Sun, X.-Z., Wilson, C., and George, M. W. "Probing the solvent dependent photophysics of *fac*-$[Re(CO)_3(dppz\text{-}X_2)Cl]$ (dppz-X_2 = 11,12-X_2-dipyrido[3,2-*a*:2′,3′-*c*]phenazine); X = CH_3, H, F, Cl, CF_3)." *Inorg. Chem.* **47**, 9857–9869 (2008).

[52] Kuimova, M. K., Sun, Z., Matousek, P., Grills, D. C., Parker, A. W., Towrie, M., and George, M. W. "Probing intraligand and charge transfer excited states of *fac*-$[Re(R)(CO)_3(CO_2Et\text{-}dppz)]^+$ (R = py, 4-Me_2N-py; CO_2Et-dppz = dipyrido[3,2-a:2′,3′-c]phenazine-11-carboxylic ethyl ester) using time-resolved infrared spectroscopy." *Photochem. Photobiol. Sci.* **6**, 1158–1163 (2007).

[53] Kuimova, M. K., Alsindi, W. Z., Dyer, J., Grills, D. C., Jina, O. S., Matousek, P., Parker, A. W., Porius, P., Sun, X. Z., Towrie, M., Wilson, C., Yang, J., and George, M. W. "Using picosecond and nanosecond time-resolved infrared spectroscopy for the investigation of excited states and reaction intermediates of inorganic systems." *Dalton Trans.* 3996–4006 (2003).

[54] Belser, P., von Zelewsky, A., and Zehnder, M. "Synthesis and Properties of Ruthenium(II) Ccomplexes with *o*-Quinodiimine Ligands. Crystal and Molecular Structure of $Ru(bpy)_2(C_6H_4(NH)_2)(PF_6)_2$." *Inorg. Chem.* **20**, 3098–3103 (1981).

[55] Fees, J., Kaim, W., Moscherosch, M., Matheis, W., Klíma, J., Krejčík, M., and Záliš, S.

"Electronic Structure of the 'Molecular Light Switch' $[Ru(bpy)_2(dppz)]^{2+}$ (dppz = Dipyrido[3,2-*a*:2′,3′-*c*]phenazine). Cyclic Voltammetric, UV/Vis, and EPR/ENDOR Study of Multiply Reduced Complexes and Ligands." *Inorg. Chem.* **32**, 166–174 (1993).

[56] Fees, J., Ketterle, M., Klein, A., Fiedler, J., and Kaim, W. "Electrochemical, spectroscopic and EPR study of transition metal complexes of dipyrido[3,2-*a*:2,3-*c*]phenazine." *J. Chem. Soc., Dalton Trans.* 2595–2600 (1999).

[57] Delaney, S., Pascaly, M., Bhattacharya, P. K., Han, K., and Barton, J. K. "Oxidative damage by ruthenium complexes containing the dipyridophenazine ligand or its derivatives: a focus on intercalation." *Inorg. Chem.* **41**, 1966–1974 (2002).

[58] Turro, C., Hall, D. B., Chen, W., Zuilhof, H., Barton, J. K., and Turro, N. J. "Solution Photoreactivity of Phenanthrenequinone Diimine Complexes of Rhodium and Correlations with DNA Photocleavage and Photooxidation." *J. Phys. Chem. A* **102**, 5708–5715 (1998).

[59] Hall, D. B., and Barton, J. K. "Sensitivity of DNA-Mediated Electron Transfer to the Intervening π-Stack: A Probe for the Integrity of the DNA Base Stack." *J. Am. Chem. Soc.* **119**, 5045–5046 (1997).

[60] Elias, B., Creely, C., Doorley, G. W., Feeney, M. M., Moucheron, C., Kirsch-DeMesmaeker, A., Dyer, J., Grills, D. C., George, M. W., Matousek, P., Parker, A. W., Towrie, M., and Kelly, J. M. "Photooxidation of guanine by a ruthenium dipyridophenazine complex intercalated in a double-stranded polynucleotide monitored directly by picosecond visible and infrared transient absorption spectroscopy." *Chem. Eur. J.* **14**, 369–375 (2008).

[61] Arkin, M. R., Stemp, E. D. A., Holmlin, R. E., Barton, J. K., Hörmann, A., Olson, E. J. C., and Barbara, P. F. "Rates of DNA-mediated electron transfer between metallointercalators." *Science* **273**, 475–480 (1996).

[62] Wan, C., Fiebig, T., Kelley, S. O., Treadway, C. R., Barton, J. K., and Zewail, A. H.

"Femtosecond dynamics of DNA-mediated electron transfer." *Proc. Natl. Acad. Sci. USA* **96**, 6014–6019 (1999).

[63] Ren, J., Jenkins, T. C., and Chaires, J. B. "Energetics of DNA Intercalation Reactions." *Biochemistry* **39**, 8439–8447 (2000).

[64] Terbrueggen, R. H., Johann, T. W., and Barton, J. K. "Functionalized Rhodium Intercalators for DNA Recognition." *Inorg. Chem.* **37**, 6874–6883 (1998).

[65] Ernst, R. J., Song, H., and Barton, J. K. "DNA Mismatch Binding and Antiproliferative Activity of Rhodium Metalloinsertors." *J. Am. Chem. Soc.* **131**, 2359–2366 (2009).

[66] Stemp, E. D. A., Holmlin, R. E., and Barton, J. K. "Electron transfer between metal complexes bound to DNA: variations in sequence, donor, and metal binding mode." *Inorg. Chim. Acta* **297**, 88–97 (2000).

[67] Williams, T. T., Odom, D. T., and Barton, J. K. "Variations in DNA Charge Transport with Nucleotide Composition and Sequence." *J. Am. Chem. Soc.* **122**, 9048–9049 (2000).

[68] Shao, F., Augustyn, K. E., and Barton, J. K. "Sequence dependence of charge transport through DNA domains." *J. Am. Chem. Soc.* **127**, 17445–17452 (2005).

[69] O'Neill, M. A., and Barton, J. K. "DNA-mediated charge transport requires conformational motion of the DNA bases: elimination of charge transport in rigid glasses at 77 K." *J. Am. Chem. Soc.* **126**, 13234–13235 (2004).

[70] O'Neill, M. A., and Barton, J. K. "DNA charge transport: conformationally gated hopping through stacked domains." *J. Am. Chem. Soc.* **126**, 11471–11483 (2004).

[71] Bhattacharya, P. K., and Barton, J. K. "Influence of intervening mismatches on long-range guanine oxidation in DNA duplexes." *J. Am. Chem. Soc.* **123**, 8649–8656 (2001).

[72] Kelley, S. O., Boon, E. M., Barton, J. K., Jackson, N. M., and Hill, M. G. "Single-base mismatch detection based on charge transduction through DNA." *Nucl. Acids Res.* **27**, 4830–4837 (1999).

[73] Boon, E. M., Ceres, D. M., Drummond, T. G., Hill, M. G., and Barton, J. K. "Mutation detection by electrocatalysis at DNA-modified electrodes." *Nat. Biotech.* **18**, 1096–1100 (2000).

[74] Boal, A. K., and Barton, J. K. "Electrochemical detection of lesions in DNA." *Bioconj. Chem.* **16**, 312–321 (2005).

[75] Pascaly, M., Yoo, J., and Barton, J. K. "DNA mediated charge transport: characterization of a DNA radical localized at an artificial nucleic acid base." *J. Am. Chem. Soc.* **124**, 9083–9092 (2002).

[76] Augustyn, K. E., Genereux, J. C., and Barton, J. K. "Distance-Independent DNA Charge Transport Across an Adenine Tract." *Angew. Chem. Int. Ed.* **46**, 5731–5733 (2007).

[77] Clark, C. D., and Hoffman, M. Z. "Effect of solution medium on the rate constants of excited-state electron-transfer quenching reactions of ruthenium(II)-diimine photosensitizers." *Coord. Chem. Rev.* **159**, 359–373 (1997).

[78] Dohno, C., Stemp, E. D. A., and Barton, J. K. "Fast back electron transfer prevents guanine damage by photoexcited thionine bound to DNA." *J. Am. Chem. Soc.* **125**, 9586–9587 (2003).

[79] Gray, H. B., Winkler, J. R., and Wiedenfeld, D. "Effects of driving force on the rates of intramolecular and bimolecular electron-transfer reactions." *Coord. Chem. Rev.* **200-202**, 875–886 (2000).

Chapter 5

Oxidation of Proteins by DNA-Mediated Charge Transport

5.1 Introduction

5.1.1 DNA-mediated CT in a Biological Context

Studies of DNA-mediated Charge Transport (CT) in well-defined molecular assemblies have been enlightening. A large body of work involving metal complex probes bound to short DNA oligomers shapes our current understanding of the factors that affect the efficiency of CT, including the extent of electronic coupling of the probe to the DNA base stack, the thermodynamic driving force for the forward CT reaction to occur, and the probability for the reverse reaction (back electron transport, BET) to take place.[1] These studies have also led to the development of a mechanistic model for CT: injected charge exists within the base stack as a delocalized molecular orbital spanning several neighboring DNA bases, and translocation of the charge through the base stack to low potential redox targets depends on the transient formation of these delocalized domains, defined by conformational fluctuations of the duplex.[1]

Because the motion of charge relies on the stable formation of orbitals spanning several stacked bases, any structural disruption intervening between a charge donor and a charge acceptor decreases the efficiency of DNA-mediated CT. For example, experiments conducted at DNA monolayers on gold surfaces have shown that most base pair mismatches and many naturally occuring base lesions attenuate CT.[2–4] Biochemical and electrochemical experiments have also illustrated the effects that protein binding has on DNA-mediated CT. Proteins that can disrupt the DNA base stack decrease the yield of CT upon binding. Examples include the methyltransferase M.*Hha*I, which flips its target base out of the base stack during methylation, replacing it with glutamine 237, and the restriction endonuclease R.*Pvu*II, a TATA binding protein that severely kinks DNA.[5–9] Alternatively, binding of the transcription factor Antennapedia homeodomain protein, which does not distort the base stack upon binding and promotes a slight increase in long-range DNA-mediated CT, most likely due to compaction and rigidification of the bases.[6] Significantly, mutation of glutamine 237 to tryptophan in M.*Hha*I restores long-range CT, proving that protein-induced structural perturbations to the base stack can attenuate DNA-mediated CT.[5,10]

While *in vitro* experiments involving DNA-binding proteins can illustrate the varied

effects of macromolecule binding on DNA-mediated CT, their inclusion does not properly model the plethora of interactions encountered by DNA within the cellular milieu. Several experiments were conducted to study CT in such environments. In particular, a series of experiments were carried out to show that DNA-mediated CT is not inhibited by nucleosome packing and that it can occur over biologically relevant distances. In one such experiment, $[Rh(phi)_2(bpy)]^{3+}$ (phi = phenanthrenequinone diimine; bpy = 2,2′-bipyridine) was tethered to the end of a 146 base pair strand of DNA that was wrapped around a histone core. Excitation of the Rh complex resulted in oxidative DNA damage at low potential 5′-GG-3′ sites over a distance of 24 base pairs, indicating that nucleosome formation does not inhibit DNA-mediated CT.[11] In another set of experiments, nuclei isolated from HeLa cells were treated with the non-covalent Rh complex and irradiated. In this case, damage was primarily observed at the 5′-G of 5′-GG-3′ and 5′-GGG-3′ sites, even in protein-bound regions that are not accessible to Rh.[12] In a set of related experiments, oxidative damage in mitochonrial DNA generated by nonspecifically-bound Rh complex was found mainly in conserved sequence block II, a region of the mitochondrial genome responsible for transcriptional regulation.[13–15] Funneling of damage to this particular site is presumed to be evolutionarily advantageous; under conditions of oxidative stress, highly damaged mitochondria cease reproduction. This prevents the propagation of genetic errors, thus maintaining proper metabolic function within the cell. DNA-mediated CT is therefore not only possible within a cell, but it may also be advantageous.

5.1.2 Evidence for DNA-Mediated Protein Oxidation

The experiments discussed above show that DNA-mediated CT can occur over long distances and in complex cellular environments. It is therefore not unreasonable that nature could utilize this remarkable phenomenon to perform long-range redox chemistry. Early experiments supporting this proposition involved the use of the flash-quench technique to generate tryptophan cation radicals in DNA-bound tripeptides.[16,17] The flash-quench technique involves the generation of a strong Ru(III) ground state oxidant *in situ* following oxidative quenching of the Ru(II)* excited state by a diffusable quencher. When this

method is used with $[Ru(bpy)_2(dppz)]^{2+}$ or $[Ru(phen)_2(dppz)]^{2+}$ (dppz = dipyrido[3,2-*a*:2′,3′-*c*]phenazine; phen = 1,10-phenanthroline), the resulting Ru(III) species is strong enough to oxidize guanine or tryptophan. In solutions of Ru(II), quencher, DNA, and the tripeptide Lys-Trp-Lys, photoexcitation of the Ru complex resulted in oxidation of intercalated tryptophan, which was observed by transient absorption (TA) spectroscopy. A similar experiment was carried out with wild-type M.*Hha*I and the Q237W mutant in place of the tripeptide. When the wild-type protein was added to solution, the only transient absorption signal observed belonged to the Ru(III) species. When the mutant was used instead, a transient signal appeared that was assigned to formation of the intercalated tryptophan cation radical.[10] DNA-mediated oxidation of bound proteins is possible even in the absence of an intercalating moiety. In a guanine oxidation assay involving the covalently-bound DNA photooxidant anthraquinone and the DNA-binding cell cycle regulator p53, protein oxidation was attenuated with the introduction of a disruptive base pair mismatch intervening between anthraquinone and p53.[18] In addition, mass spectra of the protein are consistent with the oxidative formation of disulfide bonds generated as a result of DNA-mediated CT. These results show that long-range redox reactions can occur through DNA to form highly reactive amino acid radicals and disulfide bonds within proteins.

Proteins that are known to be redox active can also be oxidized via DNA-mediated CT. In particular, the redox reactivities of the iron-sulfur cluster-containing base excision repair (BER) proteins MutY and endonuclease III (EndoIII) have been studied electrochemically on DNA-modified electrodes. In the absence of DNA, oxidation of the $[4Fe\text{-}4S]^{2+}$ cluster of EndoIII can be effected by addition of ferricyanide or by application of a +250 mV electrochemical potential. Under these conditions, oxidation of the cluster is irreversible and degradative, resulting in formation of the $[3Fe\text{-}4S]^{+}$ product.[19,20] In the presence of DNA, reversible oxidation occurs at a potential of ∼50 mV vs. NHE, forming the $[4Fe\text{-}4S]^{3+}$ cluster.[20,21] DNA binding, therefore, stabilizes the 3+ form of the cluster. The behavior of MutY, which is highly homologous to EndoIII and also contains a $[4Fe\text{-}4S]^{2+}$ cluster, is similar. Oxidation of this protein on a DNA-modified gold electrode gives a redox potential of 90 mV vs. NHE.[21,22] DNA binding was also observed to dramatically shift the

redox potential of the transcription factor SoxR.[23] In the absence of DNA, the oxidation potential of the protein is −290 mV vs. NHE. In the presence of DNA, this potential shifts by over +450 mV to +200 mV vs. NHE. These results indicate that DNA binding greatly influences the reactivity of these redox-active enzymes. For the BER proteins, the DNA binding affinity is expected to increase by several orders of magnitude upon oxidation of the [4Fe-4S] cluster from the 2+ to the 3+ state.[20] These proteins therefore bind more tightly to DNA in an oxidizing environment, where oxidative base lesions are more likely to form. In the case of SoxR, the shift in potential may instead provide the energy to bend DNA. Such a conformational change induced by SoxR binding has been observed in copper phenanthroline footprinting experiments.[23] In photooxidation experiments involving SoxR and $[Rh(phi)_2(bpy)]^{3+}$ tethered to DNA, activation of transcription could be accomplished *in vitro* by long-range DNA-mediated CT over a distance of 80 base pairs (270 Å).[24] The results of these experiments indicate that oxidation of redox-active enzymes may serve to direct the biological functions of BER protein activation and transcriptional activation.

5.1.3 Evidence Supporting Redox Signaling by DNA-mediated CT

Mounting experimental evidence suggests that DNA-mediated CT may play another role in the mechanism of action of BER enzymes, namely, as the method by which these enzymes detect genetic damage. The observation of long-range CT in guanine oxidation experiments[25], the physiologically relevant redox potentials of DNA-bound BER proteins, the elimination of DNA-mediated CT in strands containing base mismatches or lesions, and the ability of these iron-sulfur proteins to participate in DNA-mediated CT systems as oxidative traps suggest that these proteins could scan large stretches of the genome for damage simply and efficiently by passing a charge through it.

A model has been proposed to illustrate the mechanism of lesion detection by BER enzymes (Figure 5.1).[22] First, one protein with a $[4Fe\text{-}4S]^{2+}$ cluster binds to DNA and becomes oxidized, perhaps via hole transfer from a nearby guanine radical generated by ROS. The protein, now with an oxidized $[4Fe\text{-}4S]^{3+}$ cluster, remains tightly bound to the duplex. If a second protein with a $[4Fe\text{-}4S]^{2+}$ cluster binds nearby, CT can occur through

the base stack between the two bound proteins. This CT event comprises a scan of the genomic region for base lesions. Following CT, the first protein, now bearing a 2+ cluster, can dissociate, and the process repeats. In the event that a mismatch or lesion intervenes between two bound proteins, CT cannot occur. In this case, both proteins will remain bound, precessing more slowly to the damage site.

Importantly, this DNA-mediated search for damage can be performed coorperatively between any two proteins with redox potentials of approximately 100 mV. Support for cooperative searching has been established using a number of different approaches.[26] First, computational models show that if 20% of BER enzymes are oxidized and CT is allowed over distances of 200 base pairs, a search of the full *E. coli* genome would take only 8 minutes. As a comparison, a simpler model involving only facilitated diffusion requires 46 minutes. Considering that the doubling time of *E. coli* is only 20 minutes, it is clear that facilitated diffusion is inadequate; many lesions would be left unrepaired. Second, atomic force microscopy experiments show that proteins are bound more often to DNA strands containing a mismatch than to well-matched strands. Remarkably, this effect is statistically significant even when mismatch strands are used that contain only one mismatched base pair out of 3,800. Third, a transversion assay was used to test the ability of different BER enzymes to help one another search for lesions. In *E. coli* EndoIII knockouts, repair of the target lesion of MutY was only 50% as efficient as in the fully functional reporter strain. These results collectively strengthen the argument for a cooperative DNA-mediated search mechanism involving redox active proteins.

5.1.4 Time-Resolved Spectroscopy with Redox-Active Proteins

While biochemical and electrochemical experiments have been useful in elucidating the role that DNA-mediated CT may play in biological processes, these methods cannot be used to characterize the rates or absolute efficiencies of such processes. Spectroscopic methods, however, can be used to observe specific products as they form. By monitoring the emission or absorption of a sample over time, it is often possible to observe short-lived reactive or unstable chemical species. Such techniques have already been used to observe the guanine

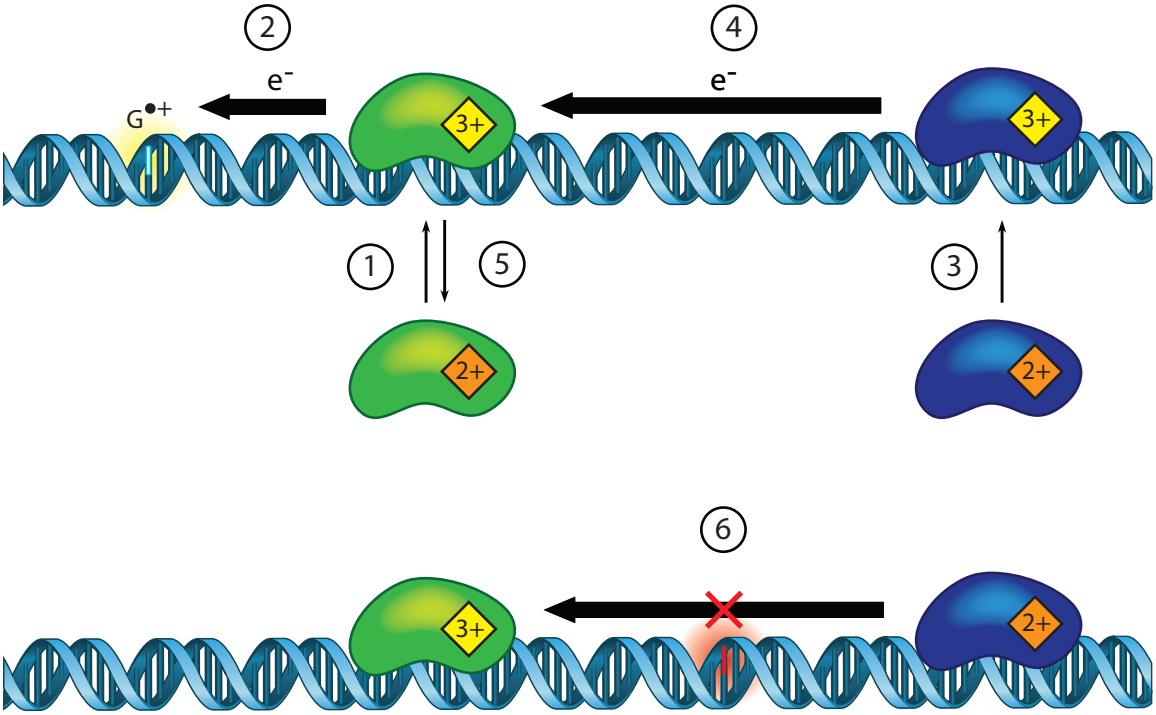

Figure 5.1: A model for the DNA-mediated detection of lesions. 1) A protein containing a $[4Fe\text{-}4S]^{2+}$ cluster binds to DNA. 2) Electron transfer to a nearby guanine cation radical results in formation of the $[4Fe\text{-}4S]^{3+}$ cluster. The protein is now strongly bound to the DNA strand. 3) A second protein, which contains a $[4Fe\text{-}4S]^{2+}$ cluster, binds nearby. 4) CT between the two proteins comprises a scan of the region for DNA damage. 5) The protein now bearing the 2+ cluster dissociates and the process repeats. 6) If a lesion intervenes between the proteins, CT cannot occur, and the proteins precess to the location of the damage.

cation radical, formed in poly(dG-dC) using the flash-quench technique.[27] In this experiment, the guanine radical persisted for milliseconds, depending on the quencher employed. The DNA-mediated oxidation of metalloproteins has also been observed spectroscopically. In the presence of DNA and ferricytochrome *c*, excitation of $[Ru(phen)_2(dppz)]^{2+}$ results in the formation of the reduced protein.[28] Similarly, the flash-quench technique can be used to oxidize MutY. In this experiment, the formation of a long-lived, positive transient absorption band near 410 nm was assigned to the oxidized $[4Fe\text{-}4S]^{3+}$ cluster of the protein.[29] Importantly, the guanine cation radical was an intermediate in the protein oxidation reaction in both cases. This similarity suggests that the guanine radical may play a general role as a redox intermediate in biochemical pathways involving DNA-mediated oxidation. In addition, it should be stressed that formation of the oxidized proteins in both experiments was observed directly as the reaction was occuring. The ability to directly observe these transient species makes time-resolved spectroscopy the best tool to characterize the DNA-mediated oxidation of redox-active proteins.

Here, we describe several lines of work that share a common goal: to observe the DNA-mediated oxidation of redox-active proteins spectroscopically. Various experimental strategies, detailed below, were employed to this end. Observations in p53 systems are very promising. Although spectra obtained under conditions designed for p53 oxidation are of low intensity and were difficult to reproduce, they compare favorably to transient spectra obtained upon oxidation of tyrosine in Lys-Tyr-Lys tripeptides. Measurements in SoxR systems were hindered by the presence of dithionite. This reducing agent, included to keep the protein in the reduced form, greatly complicated the kinetics of the system. Some evidence suggests that dithionite can serve as a reductive quencher of Ru(II)* luminescence. The third protein studied is EndoIII. Although no direct evidence for its oxidation was obtained, experiments involving metal complex photooxidants suggest that the addition of EndoIII does introduce an additional sink for oxidative DNA-mediated CT. These results together highlight experimental challenges faced in bioinorganic spectroscopy and provide a foundation on which to base further experiments.

5.2 Experimental Section

5.2.1 Materials

All materials were purchased from commercial sources and used as received unless otherwise indicated. DNA synthesis reagents were purchased from Glen Research (Sterling, VA). The synthesis of $[Re(CO)_3(dppz)(py')]Cl$ is described completely in Section 2.2.2 on Page 59. The complexes $[Ir(ppy)_2(dppz')]Cl$ and $[Rh(phi)_2(bpy')]Cl_3$ were gifts from coworkers or were prepared using established protocols.[30,31]

5.2.2 Synthesis of DNA and Tethered Conjugates

Oligonucleotides were prepared using standard solid-phase phosphoramidite chemistry on an Applied Biosystems 3400 DNA synthesizer. Covalent tethers were appended to the 5′-ends of resin-bound oligonucleotides as described in Section 4.2.3 on page 128. Annealing was accomplished by incubating solutions containing equimolar amounts of complementary strands in buffer (10 mM NaP_i, 50 mM NaCl buffer; pH 7.5) at 90 °C for 5 min followed by slow cooling over 90 min to ambient temperature. The melting temperature (T_m) of each duplex was determined by monitoring the 260 nm absorbance of a dilute sample while heating slowly (1 °C min^{-1}) from ambient temperature to 100 °C; the T_m is taken as the inflection point of the melting curve.

5.2.3 Protein Expression and Purification

The proteins p53 and SoxR were expressed, purified, and kindly supplied by Wendy Mercer and Paul Lee, respectively. EndoIII was expressed from the pNTH10 expression vector and purified as described.[32] Briefly, pNTH10 was transformed into JM101 cells by electroporation at 1.7 kV. Following selection on LB+ampicillin plates, a large-scale culture was grown to OD_{600} = 0.6–0.8. EndoIII expression was induced by the addition of 0.5 mL 1 M isopropyl-β-D-thiogalactopyranoside and incubated at 37 °C for 4 hours. Cells were pelleted, washed, and lysed with lysozyme in the presence of phenylmethylsulfonyl fluoride. Nucleic acids were degraded with DNaseI and RNaseA. Anion exchange on quaternary methylammonium resin (Sigma) and cation exchange on sulfopropyl sepharose resin (Sigma) were

performed at 4 °C to remove nucleic acids and other impurities. The protein was precipitated with ammonium sulfate, resuspended, and purified by size exclusion chromatography (AcA54 resin, Sigma). Purity was determined by SDS-PAGE. Protein solutions were concentrated by reverse dialysis with polyethylene glycol in buffer. Concentrated solutions were dialyzed into storage buffer (20 mM NaP_i, 100 mM NaCl, 1 mM EDTA, 20% glycerol; pH 7.5) and stored in working aliquots at −80 °C. Protein activity was verified with a glycosylase assay.

5.2.4 Time-Resolved Spectroscopy

Time-resolved spectroscopic experiments were performed at the Beckman Institute Laser Resource Center. Time-resolved emission and TA measurements were conducted using instrumentation that has been described.[33] Briefly, the third harmonic (355 nm) of a 10 Hz, Q-switched Nd:YAG laser (Spectra-Physics Quanta-Ray PRO-Series) was used as an excitation source (pump pulse duration ≈8 ns). For the measurement of transient absorbance spectra, a white light flashlamp of ∼15 ns duration was employed as the probe lamp, and two photodiode arrays (Ocean Optics S1024DW Deep Well Spectrometer) detected the measurement and reference beams. For the measurement of transient kinetics, the probe light was provided by a pulsed 75 W arc lamp (PTI model A 1010) and detected with a photomultiplier tube (Hamamatsu R928) following wavelength selection by a double monochromator (Instruments SA DH-10). For both spectral and kinetic measurements, the pump and probe beams were collinear, and scattered laser light was rejected from the detectors using suitable filters. The samples were held in 1-cm-path-length quartz cuvettes (Starna) equipped with stir bars and irradiated at 355 nm with 500–1000 laser pulses at 5 mJ $pulse^{-1}$. Samples were monitored for degradation by UV/visible absorbance and exchanged for fresh sample when necessary. Samples were prepared with a maximum absorbance of 0.8 in order to achieve high signal-to-noise ratios in TA experiments. TA measurements were made with and without excitation, and were corrected for background light, scattering, and fluorescence. Transient spectra were smoothed using a boxcar algorithm to reduce the effect of instrumental noise. In some cases, additional correction was needed in the form of scaled

blank subtraction.

Kinetic traces were fit to exponential equations of the form

$$I(t) = a_0 + \sum_n a_n \exp(-t/\tau_n),$$

where $I(t)$ is the signal intensity as a function of time, a_0 is the intensity at long time, a_n is a pre-exponential factor that represents the relative contribution from the nth component to the trace, and τ_n is the lifetime of the nth component. Up to two exponential terms were used in the model function to obtain acceptable fits. Kinetic traces were smoothed logarithmically prior to fitting in order to decrease the weight of long time data on the fit.

5.3 Results & Discussion

5.3.1 Oxidation Strategies

Two strategies for the formation of oxidative damage are shown in Scheme 5.1. Direct photooxidation is the most straightforward way to inject charge into DNA. Generally, photoexcitation of an intercalated metal complex results in the formation of a strong excited state oxidant. Strong electronic coupling between the intercalating ligand and the base stack facilitate efficient charge injection, generating the reduced metal complex and a cation radical within the base stack. DNA-mediated CT to a low potential site such as guanine results in charge localization at the site. Subsequent reaction with water or dioxygen traps the radical, forming a permanent product. The yield of the charge trapped product can be decreased if BET from the target cation to the reduced metal complex is competitive with trapping. This oxidation strategy has been used in numerous experiments to explore the factors affecting the yield of DNA-mediated oxidation. Such factors include distance,[25] oxidation target,[34] DNA structure,[35–38] DNA sequence,[39] and protein binding.[5,6,11,40] This method has also been used to study the repair of thymine dimers,[41,42] to oxidize DNA *in vivo*,[12–15] to oxidize DNA-bound proteins *in vitro*,[18,24] and to compare hole transfer with electron transfer (ET).[43–45]

The flash-quench technique was originally established for the study of intramolecular

ET through proteins. Although mechanistically more complex than direct photooxidation, this method allows for observation of CT rates over an extremely wide range. The mechanism of the oxidative flash-quench method is as follows. Excitation of an intercalated metal complex oxidant is followed by excited state quenching, usually through bimolecular ET with a diffusing quencher such as $[Ru(NH_3)_6]^{3+}$, methylviologen, or $[Co(NH_3)_5Cl]^{2+}$. The resulting ground state species is a strong, long-lived oxidant that can proceed to oxidize the redox target. Again, formation of the target radical is followed by trapping to form a permanent product. The flash-quench method is not limited to oxidative systems; a long-lived Ir ground state reductant has also been prepared using 5-bromouridine as the quencher.[44,45] Like direct photooxidation, the flash-quench technique has been used in a number of experimental systems for guanine oxidation,[25,27,34,46–48] methylindole oxidation,[49–51] peptide and protein oxidation,[10,16,17,24,28,29] and DNA-peptide crosslinking.[52]

These two methods of oxidation appear quite similar. They both involve photoexcitation of the charge donor, and they both result in the formation of permanent oxidative damage at low potential charge acceptors. However, differences in these two mechanisms may make one method more suitable than the other for a particular experiment. For example, charge injection in direct photooxidation occurs rapidly, allowing for the observation of very fast processes. On the other hand, since CT must occur within the lifetime of the excited state, processes with very slow rates, such as tunneling through high potential media or CT over long distances, cannot be observed. Additionally, BET in these systems may be quite facile since the conditions that are conducive to efficient forward CT, such as strong electronic coupling between the donor/acceptor pair and the bridge, also permit efficient BET. In the flash-quench reaction, CT processes with very slow rates can be observed, but diffusion of the quencher limits the study of fast processes. BET in flash-quench systems also behaves differently. Since the donor returns to its initial oxidation state upon charge injection, direct charge recombination is unlikely. The product yield may still be diminished, however, through ET from the reduced quencher. By using a sacrificial quencher such as $[Co(NH_3)_5Cl]^{2+}$, even these recombination pathways can be abolished, although additional challenges may be introduced. Therefore, for systems in which very fast processes must be

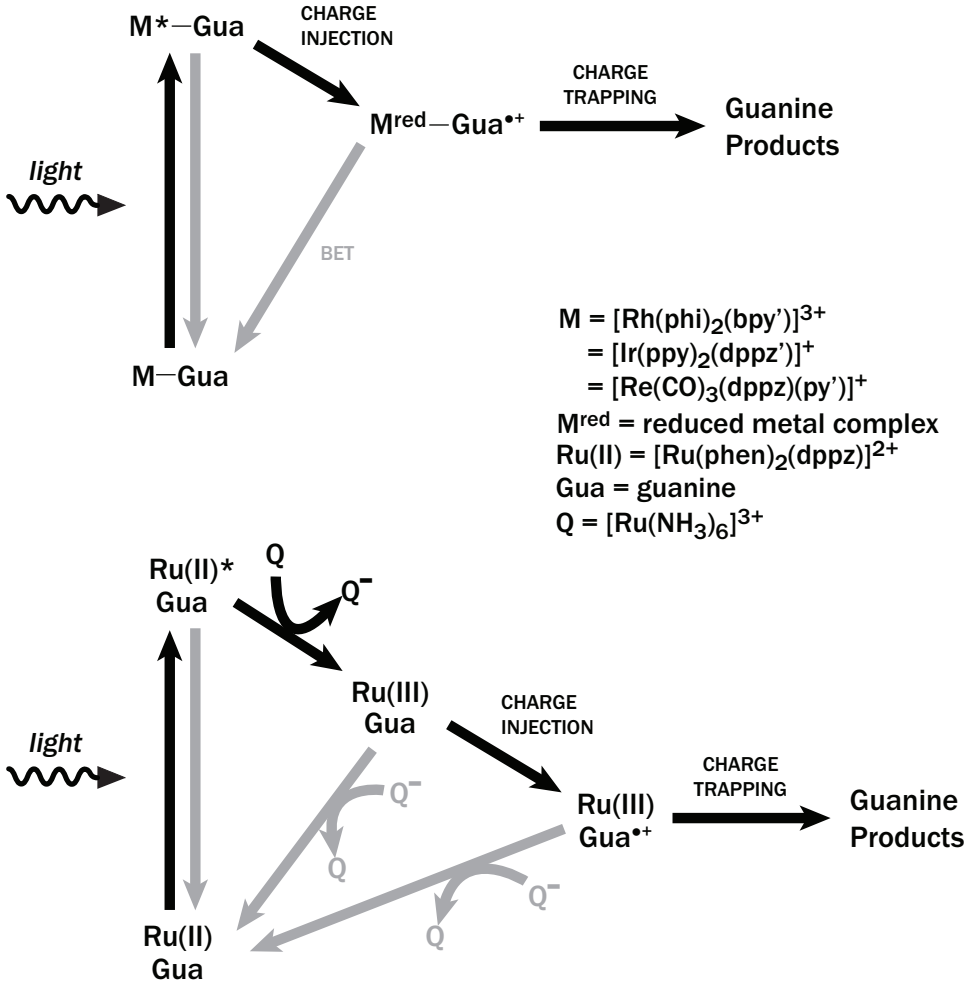

Scheme 5.1: Comparing direct photooxidation and the flash-quench technique. Top, direct photooxidation: excitation of an intercalated metal complex (M) results in formation of the metal complex excited state (M*). CT through the DNA base stack causes oxidation of guanine, forming the guanine cation radical ($G^{\bullet+}$). A bound protein can be oxidized by the relatively long-lived guanine radical. BET may occur to neutralize the radical, or reaction with water or oxygen can form permanent oxidized guanine products. Bottom, the flash-quench technique: the excitation of $[Ru(phen)_2(dppz)]^{2+}$, Ru(II), results in the formation of the excited species Ru(II)*. Oxidative quenching by a diffusing quencher, Q, forms the ground state oxidation Ru(III). Ru(III) proceeds to oxidize guanine. Protein oxidation may result. Here, BET involves reduction by the reduced quencher.

observed, direct photooxidation should be used, but when high product yields are desired, the flash-quench technique is the better option.

5.3.2 p53

The protein p53 is a transcriptional regulator that mediates the cellular response to a number of stress signals, including DNA damage, hypoxia, and ribonucleotide depletion.[53,54] Depending on the type and severity of stress, the p53 response may induce apoptosis, senescence, cell cycle arrest, DNA repair, or differentiation. Because of the central role that p53 plays in many cellular pathways, its stability is necessary for cell survival. Single point mutations in the DNA binding core domain are extremely disruptive to protein function. Such mutations are found in over 50% of human cancers. For this reason, a full understanding of the biochemical reactivity of p53 is imperative. Experimental evidence has already shown that p53 can be oxidized via DNA-mediated CT.[18] Knowledge of the specific pathway by which this reaction occurs may help us understand how oxidative stress affects the function of p53.

Experimental Details

The 393-amino acid p53 is made up of several domains, including some regions that are natively unfolded.[55] For example, the transactivation domain in the N-terminal region interacts with a number of regulatory proteins. The DNA-binding core domain (residues 94–292) binds specifically as a homotetrameric complex to double-stranded DNA at two "half-site" motifs, each with the sequence 5′-Pu-Pu-Pu-C-(A,T)-(T,A)-G-Py-Py-Py-3′ (Pu = A, G; Py = C, T) separated by up to 13 base pairs.[56] The binding affinity of the p53 complex depends on the DNA sequence. The tetramerization domain is found in the C-terminal region (residues 325–356). Both the N-termus and C-terminus domains are largely unfolded except in the presence of certain regulatory proteins. The DNA binding domain and the tetrameric domain, on the other hand, have well defined conformations. While the whole protein has defied crystallization, crystal structures of the DNA binding domain and the tetrameric domain have been solved. Even these domains are relatively unstable, with

melting temperatures only slightly above 37 °C.

Because of the low melting temperature and the high degree of disorder in the p53 termini, the expression and study of p53 and destabilizing mutants can be extremely challenging. For this reason, it is often necessary to use mutationally stabilized or truncated versions of the protein in biophysical experiments. In most of the experiments described below, a superstable quadruple mutant, *T*-p53C (4×), was used.[57] This version of p53 contains the mutations M133L, V203A, N239Y, and N268D, and is stabilized versus the wild-type protein by 2.6 kcal mol^{-1}. Since the design of this mutant was based on natural variations of p53 in many different species, protein function has been retained. Intriguingly, asparagine 239 in the wild-type protein is in contact with the DNA backbone. It is possible that substitution of this residue for tyrosine in the 4× mutant establishes a CT path into the core of the protein, as was observed for *Pseudomonas aeruginosa* azurin.[58] For this reason, the 3× mutant lacking this mutation was also studied.

Time-resolved spectroscopic experiments were conducted to observe the oxidation of DNA-bound p53 by DNA-mediated CT. The experimental design is shown in Figure 5.2. These studies were based on the experiments of Wagenknecht et al., in which the flash-quench technique was used to generate the tyrosine radical in the DNA-bound Lys-Tyr-Lys tripeptide.[16] In those experiments, the photoexcitation of covalently tethered $[Ru(phen)(bpy')(dppz)]^{3+}$ (bpy′ = 4-methyl-4′-(butyric acid)-2,2′-bipyridine) resulted in the formation of a strong transient absorbance signal at 405 nm. The growth rate of this signal, ∼30 μs, matched the decay rate of guanine cation radical ($G^{\bullet+}$), observed at 510 nm, indicating an intermediating role for the latter species. The decay rate of the tyrosine radical was ∼100 μs. Both the rate of formation and the rate of decay of the tyrosine radical were observed to depend on the DNA sequence. Here, formation of the tyrosine radical is also expected upon Ru excitation due to the close proximity of tyrosine 239 to DNA in the 4× mutant. In addition, the DNA sequence included the consensus sequence 5′–AAATCAGCACTA<u>CAACATGTTGGGACATGTTC</u>–3′ as a putative p53 binding site (promotor region underlined). The oxidation targets in these experiments are adjacent cysteine pairs within the DNA binding domain of p53: cysteines 275 and 277, and cys-

teines 135 and 141.[18] Upon oxidation, these cysteine pairs may form disulfite bonds. The oxidation potential of cysteine is ∼0.42 V vs. NHE[59], so it should be easily oxidized using the flash-quench method ($E°[Ru^{3+}/Ru^{2+}]$ = 1.6 V vs. NHE; $E°[G^{\bullet+}/G]$ = 1.29 V vs. NHE).[60,61]

Oxidation of Lys-Tyr-Lys

Before examining the DNA-mediated oxidation of p53, it was prudent to repeat the experiments of Wagenknecht et al.[16] regarding the oxidation of the tripeptide Lys-Tyr-Lys. In this way, we could ensure that the current instrumentation would be sufficiently sensitive for experiments involving the protein. Samples were prepared with 750 μM (base pairs) herring testes DNA (42% GC content), 40 μM $[Ru(phen)_2(dppz)]^{2+}$, 600 μM $[Ru(NH_3)_6]^{3+}$ quencher, and 0 or 600 μM Lys-Tyr-Lys in phosphate buffer (10 mM NaP_i, 50 mM NaCl; pH 7.5).

The transient spectrum measured 50 μs after 480 nm excitation is shown in Figure 5.3. In the absence of tripeptide, the transient signal of $[Ru(phen)_2(dppz)]^{3+}$ is observed. The bleach centered at 440 nm is due to depletion of the Ru(II) ground state; the transient band that appears at higher wavelengths is typical of the 3+ species. In the presence of tripeptide, the spectrum changes dramatically. An intense positive band appears at 405 nm accompanied by a minor band near 460 nm. No evidence remains for the Ru(II/III) bleach, and the intensity of the low energy transient is very low, suggesting that at these high concentrations, oxidation of the tripeptide is nearly quantitative. This spectrum is almost identical to the one measured by Wagenknecht et al., so it is assigned to the tyrosine cation radical.

While the tyrosine cation radical spectrum can be consistently produced at high intensity using the experimental conditions listed above, it was also necessary to measure this control at the same concentrations and in the same buffer as the p53 experiment. This was a challenging task. In order to maintain stability, the protein must be dissolved in a complex buffer containing many components. In particular, the higher ionic strength and viscosity are expected to diminish the efficiency of charge injection, since a higher ion

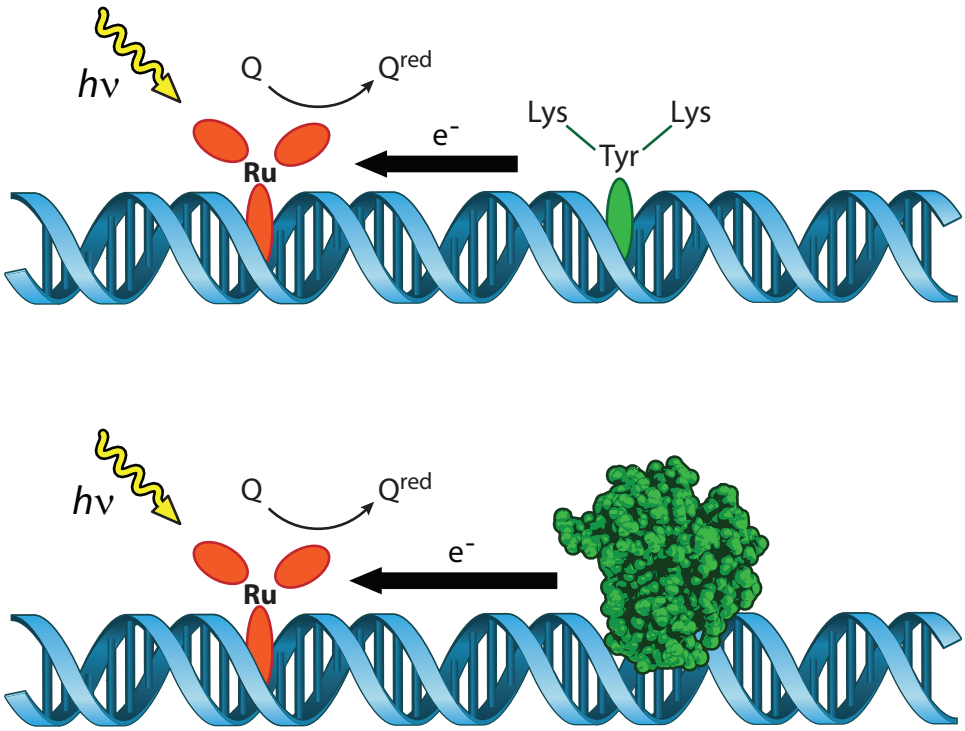

Figure 5.2: The p53 transient absorption experiment. Excitation of $[Ru(phen)_2(dppz)]^{2+}$ at 470 nm and quenching by $[Ru(NH_3)_6]^{3+}$ (Q) results in formation of $[Ru(phen)_2(dppz)]^{3+}$. This species can oxidize guanine to form the guanine cation radical, $G^{\bullet+}$. Top: hole transfer from $G^{\bullet+}$ to Lys-Tyr-Lys results in the formation of the tyrosine cation radical. Bottom: hole transfer from $G^{\bullet+}$ to p53 results in the formation of a disulfide bond in the protein.

content will decrease the electrostatic attraction between the Ru(II) oxidant and DNA, and higher viscosity will retard quencher diffusion. Additionally, since p53 solutions are not stable at concentrations higher than approximately 50 μM, low concentrations of tripeptide must be used.

For these reasons, transient absorption spectra were also measured for solutions containing 20 μM consensus sequence DNA (32-mer), 20 μM $[Ru(phen)_2(dppz)]^{2+}$, 600 μM $[Ru(NH_3)_6]^{3+}$ quencher, and 0 or 50 μM Lys-Tyr-Lys in p53 buffer (20 mM Tris, 100 mM NaCl, 0.2 mM EDTA, 0.1% bovine serum albumin, 0.1% MP-40 detergent, 10% glycerol; pH 8.0). These measurements are shown in Figure 5.4(left). In the absence of tripeptide, the Ru(III) bleach is clearly observed, even at times as long at 75 μs after excitation. With the addition of tripeptide, the change in the spectral profile is modest. At 30 and 50 μs, the bleach and transient due to Ru(III) formation are clearly visible, indicating that much of the oxidant remains unreacted. The main difference is the appearance of a narrow transient band near 405 nm. Despite the noise, this band is observed at all three time points. Based on the transient spectrum observed at a lower salt concentration and a higher tripeptide concentration, this narrow band can be assigned to the tyrosine cation radical as well.

Oxidation of p53

The flash-quench experiment was also conducted with p53. Transient spectra are shown in Figure 5.4 (right) for samples including 20 μM $[Ru(phen)_2(dppz)]^{2+}$, 20 μM consensus sequence DNA, 600 μM $[Ru(NH_3)_6]^{3+}$ quencher, and 0 or 50 μM p53 in protein buffer following 470 nm excitation. At each time point, the addition of protein results in a decrease in the intensity of the Ru(III) bleach, suggesting that p53 acts as an additional hole sink. In addition, a low intensity transient band appears near 410 nm, which is especially apparent at short times. The position and breadth of this band suggest that it is due to the same process as the positive band in the Lys-Tyr-Lys controls, namely, absorption of the tyrosine cation radical. Its disappearance at long times may indicate further reaction, as is expected for an aromatic residue that lies along the CT pathway to an even stronger low potential trap[58,62].

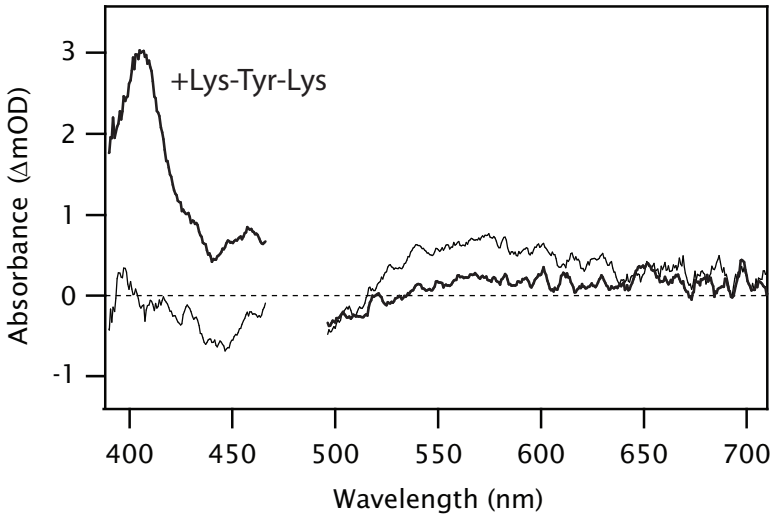

Figure 5.3: Transient absorption spectra without (thin) and with (thick) Lys-Tyr-Lys, as done by Wagenknecht, et al.[16] Samples contained 750 μM (base pairs) herring testes DNA (42% GC content), 40 μM $[Ru(phen)_2(dppz)]^{2+}$, 600 μM $[Ru(NH_3)_6]^{3+}$ quencher, and 0 or 600 μM Lys-Tyr-Lys in phosphate buffer (10 mM NaP_i, 50 mM NaCl; pH 7.5). Spectra were measured 50 μs after 480 nm laser excitation. Data between 470 nm and 490 nm were removed due to scatter from the excitation beam.

The spectra shown in Figure 5.4 were the best obtained for this system. Although the experiment was attempted several times and under different sets of conditions, it was not possible to improve the signal. Experiments involving the 3× mutant, which were conducted to determine whether the tyrosine radical observed corresponds to the residue introduced by mutagenesis, were inconsistent. As indicated above, the sample conditions that are necessary to maintain protein stability are not conducive to spectroscopy. While the influences of additional sample components such as EDTA and detergents on interactions between macromolecules and metal complexes are unknown, the effects of unstable proteins are usually worse; precipitated protein scatters pump and probe light, decreasing the signal-to-noise ratio of transient absorption data dramatically. Another challenge is proving that oxidation occurs by DNA-mediated CT. Stability of p53 also requires the presence of DNA, so it is impossible to perform a control experiment in which DNA is absent. Despite these challenges, the results presented above are promising. Based on these data, it appears that the oxidation of p53 can be observed by transient absorption spectroscopy.

5.3.3 SoxR

SoxR is a bacterial redox-active transcriptional regulator that contains a [2Fe-2S] cluster.[63] Oxidation of the cluster activates the protein, but it does not affect protein folding, DNA binding, or promoter affinity.[23,64] Following oxidation, the DNA-bound protein is thought to undergo a conformational change, unwinding the promoter for SoxS, a transcription factor that controls the cellular response to oxidative stress. Experiments on DNA-modified gold electrodes have shown that the redox potential of DNA-bound SoxR is 400 mV higher than that of SoxR in solution.[23] In addition, SoxR can be activated by DNA-mediated oxidation *in vitro* and *in vivo* using either a direct photooxidant or the flash-quench technique. In these experiments, indirect evidence for SoxR activation by DNA-mediated oxidation entailed a diminution in guanine oxidation or increased levels of *soxS* transcript upon addition of protein. Observation of oxidized SoxR by time-resolved spectroscopy would provide complementary direct evidence for this process.

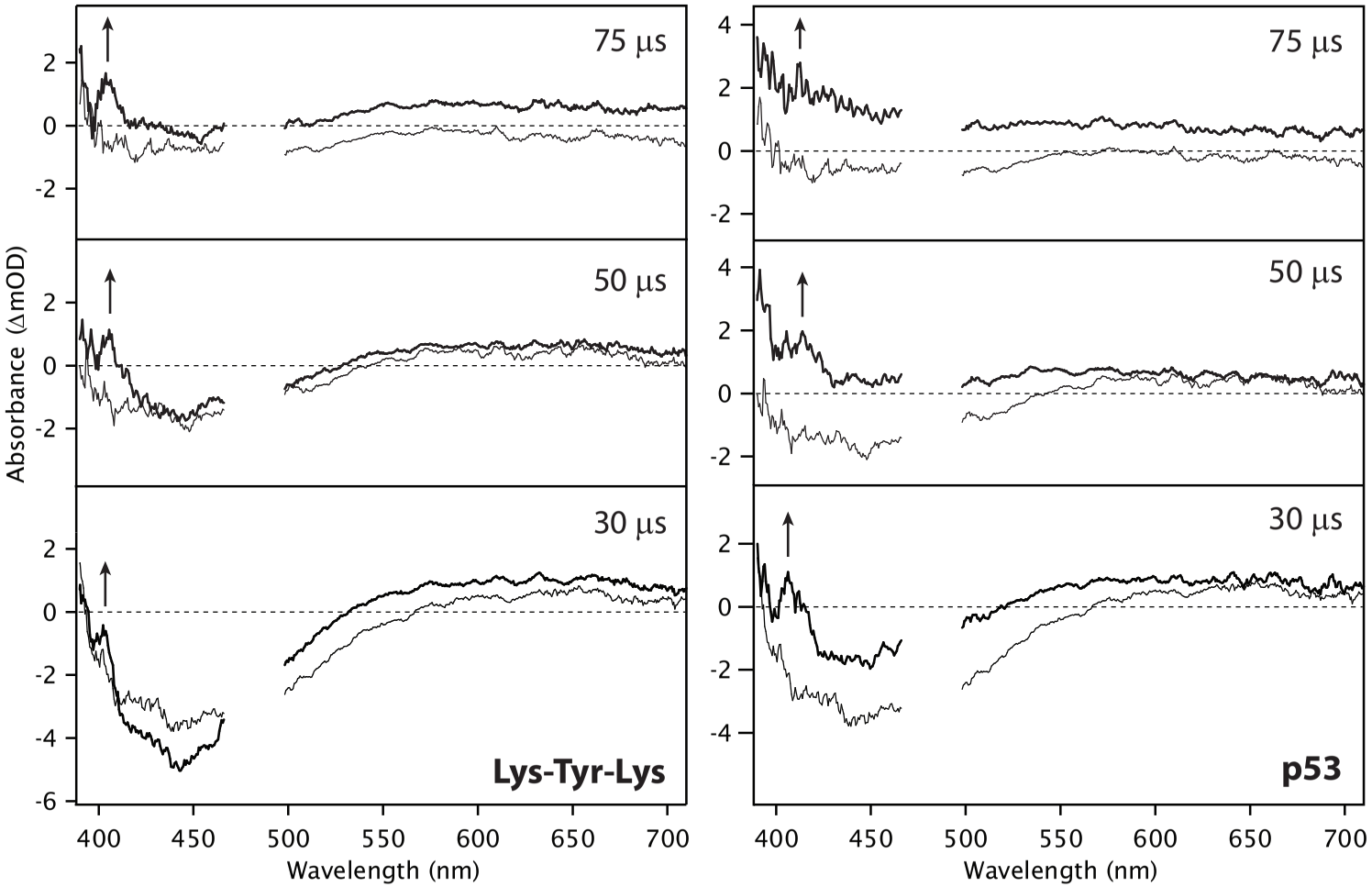

Figure 5.4: Transient absorption spectra in the absence (thin) and presence (thick) of Lys-Tyr-Lys (left) or p53 (right). Samples contained 20 μM consensus sequence DNA (32-mer), 20 μM $[Ru(phen)_2(dppz)]^{2+}$, 600 μM $[Ru(NH_3)_6]^{3+}$ quencher, and 0 or 50 μM Lys-Tyr-Lys or p53 in protein buffer (20 mM Tris, 100 mM NaCl, 0.2 mM EDTA, 0.1% bovine serum albumin, 0.1% MP-40 detergent, 10% glycerol; pH 8.0). Spectra were measured 30, 50, or 75 μs after 470 nm laser excitation, as indicated. Arrows show the direction of change with the addition of protein.

Experimental Details

The flash-quench method was used in SoxR oxidation experiments. This method has been used previously to show that the addition of SoxR to samples including $[Ru(phen)_2(dppz)]^{2+}$, the sacrificial quencher $[Co(NH_3)_5Cl]^{2+}$, and DNA decreases the yield of guanine oxidation.[24] Our experiments required the use of $[Ru(NH_3)_6]^{3+}$ as the quencher, since the reductive decomposition observed for the Co complex would prevent our ability to use repetitive photocycles. The DNA sequence we used is shown in Figure 5.5. This sequence encodes the *soxS* promotor, to which SoxR is known to bind specifically.[65] The remainder of the DNA strand provides ample room for the Ru oxidant to bind.

As with p53, the preparation of samples suitable for spectroscopic measurement proved challenging. At low protein concentrations, the protein is stable, but no signal can be observed. At high protein concentrations and following irradiation, precipitates tend to form. By systematically varying the buffer conditions, it was possible to find a buffer system that maintains protein stability at relatively high concentrations. This buffer included 50 mM sodium phosphate (pH 8) and 150 mM NaCl. At such high ionic strength, it is necessary to use 1 M $[Ru(NH_3)_6]^{3+}$ to efficiently form the Ru(III) oxidant. Another challenge involves the requirement that SoxR remain in the reduced state. Since the presence of molecular oxygen in solution would lead to the oxidation of SoxR, precluding our ability to oxidize it using redox chemistry, the molecular oxygen scavenger dithionite must be included in solution. Samples must also be prepared anaerobically and sealed to prevent the introduction of oxygen.

Dithionite Decreases Ru(II)* Luminescence

The presence of dithionite has a strong effect on the kinetics of the system, even in the absence of SoxR. Without dithionite, a bleach is observed at 418 nm due to depletion of the Ru(II) ground state. This bleach exhibits a biexponential recovery with lifetimes of 61 ns (74%) and 1.1 μs (26%) due to relaxation from the excited state and reaction of Ru(III), respectively. When 100 μM dithionite is added, the intensity of the long-lived component increases and the recovery lifetimes change to 45 ns (55%) and 4.5 μs (45%). When excess

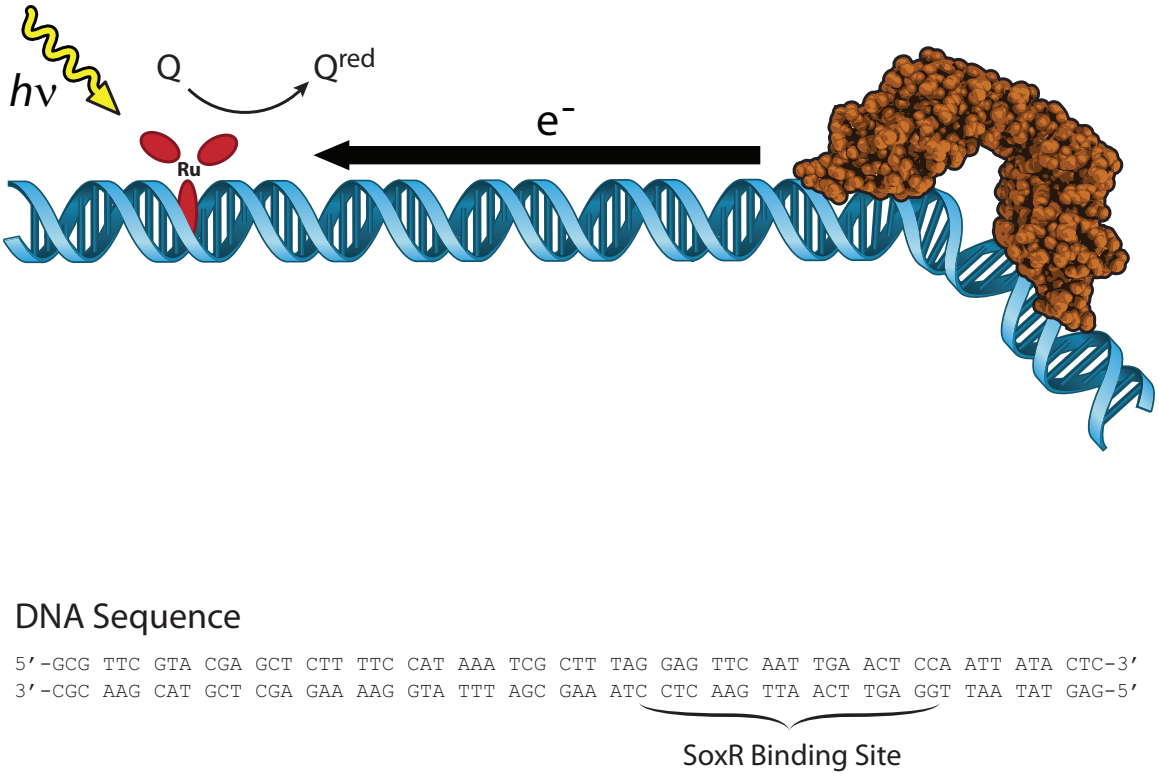

Figure 5.5: The SoxR transient absorption experiment. Top: Photoexcitation of $[Ru(phen)_2(dppz)]^{2+}$ at 470 nm results in the formation of the ground state oxidant $[Ru(phen)_2(dppz)]^{3+}$ following oxidative quenching by $[Ru(NH_3)_6]^{3+}$ (Q). This Ru(III) species oxidizes guanine by DNA-mediated CT. Hole transfer from $G^{\bullet+}$ to SoxR results in oxidation of the [2Fe-2S] cluster. Bottom: the DNA sequence used in SoxR oxidation experiments. The SoxR binding site is indicated.

dithionite is added, the intensity of the bleach decreases dramatically, and the fast recovery component is no longer observed. Similarly, in the absence of dithionite, Ru(II)* emission at 610 nm decays with a rate of 52 ns. When dithionite is added, the intensity of emission decreases, although the emission lifetime remains approximately the same.

The TA and emission traces are shown in Figure 5.6. Of particular interest, the Stern-Volmer plot shows that the dependence of luminescence yield on dithionite concentration is linear. Since the lifetime of the emissive species does not change with increasing dithionite, it appears that Ru(II)* luminescence is statically quenched by dithionite. Considering the low redox potential of dithionite (approximately -500 mV vs. NHE),[66] it should easily be able to reduce the excited state of $[Ru(phen)_2(dppz)]^{2+}$ ($E^\circ[Ru^{2+*}/Ru^+] = 1.2$ V vs. NHE).[67] A static mechanism for this quenching is also reasonable since the electrostatic attraction between the Ru oxidant (2+) and dithionite (2−) should be quite strong.

If static quenching by dithionite occurs, then an additional reaction pathway from Ru(II)* is possible. A revised reaction scheme is shown in Scheme 5.2. Notably, in the dithionite quenching experiments, the $[Ru(NH_3)_6]^{3+}$ quencher was also present. In such systems, excitation to form Ru(II)* can be followed by either oxidative quenching by $[Ru(NH_3)_6]^{3+}$ or reductive quenching by dithionite. Dithionite could also presumably donate an electron to Ru(III), preventing the oxidation of guanine, or it could donate an electron to $G^{\bullet+}$, preventing the formation of permanent guanine damage as well as hole injection into SoxR.

Preliminary Evidence for SoxR Oxidation

Comparison between oxidized SoxR and SoxR treated with dithionite under anaerobic conditions shows that oxidized SoxR absorbs more strongly than reduced SoxR between 380 nm and 580 nm.[68] Therefore, in transient absorption studies, we would expect to see an increase in the absorbance of the sample following photoexcitation and oxidation via the flash-quench technique.

Our best evidence for the DNA-mediated oxidation of SoxR was obtained using samples in which dithionite had been removed by dialysis in an anaerobic environment.

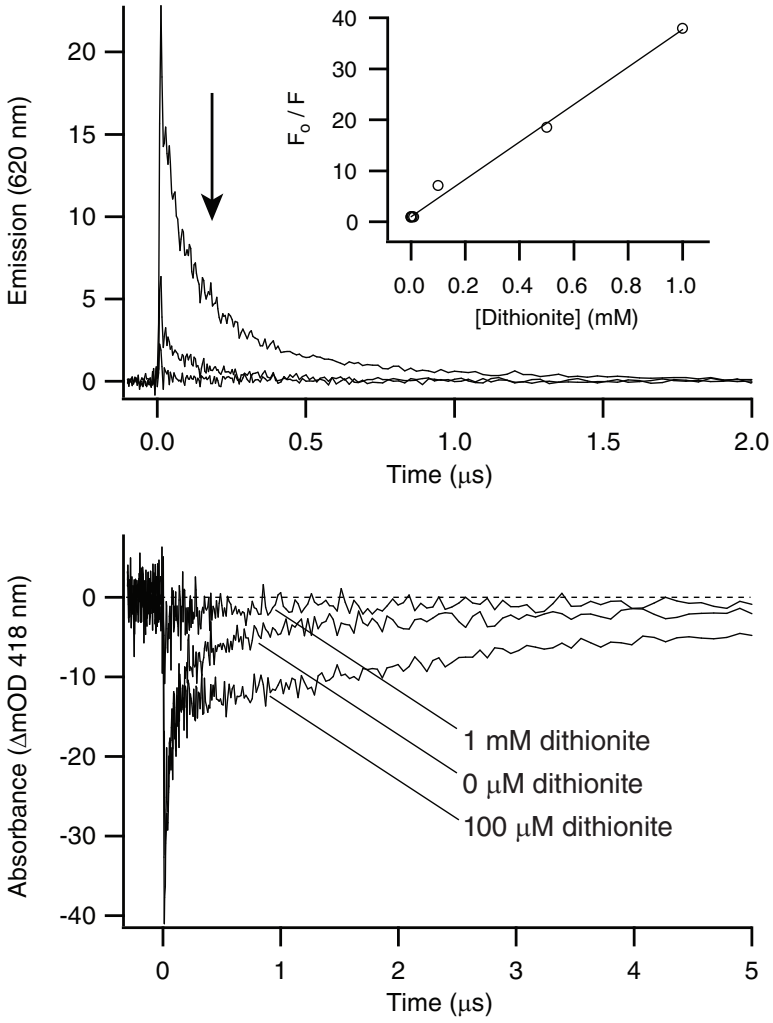

Figure 5.6: Transient absorption bleach recoveries at 418 nm and emission decay at 620 nm of 5 μM DNA duplex, 10 μM $[Ru(phen)_2(dppz)]^{2+}$, 200 μM $[Ru(NH_3)_6]^{3+}$, and 0, 100, or 1000 μM dithionite following 470 nm excitation. Inset: Stern-Volmer plot for the addition of dithionite ($K = 3.67 \times 10^4$ M^{-1}).

The protein was kept cold during dialysis in order to prevent cluster degradation. TA traces were measured at 418 nm for a sample consisting of 5 μM DNA duplex, 10 μM $[Ru(phen)_2(dppz)]^{2+}$, 200 μM $[Ru(NH_3)_6]^{3+}$, and 5 μM SoxR before and after introduction of ambient oxygen (Figure 5.7). In both traces, a large negative signal is seen at short times that recovers with a lifetime of 6.4 μs. This bleach signal is due to the formation of Ru(III). In the reduced sample, a very weak, positive transient grows in with a lifetime of 20 μs and persists for the duration of the measurement. After the introduction of ambient oxygen, this transient is no longer observed.

Although the intensity of the long-lifetime transient in the reduced sample is low, its appearance is consistent with the formation of oxidized SoxR as a result of DNA-mediated CT. While CT through DNA is expected to be very fast (10–100 ps),[69] CT through proteins will be much slower. The dependence of ET rate on distance has been determined in a wide variety of media.[70] Based on the crystal structure of oxidized SoxR bound to DNA,[71] the closest distance between the [2Fe-2S] cluster and the DNA base stack is 26 Å. From observations of ET through proteins, the time needed to transfer an electron over 26 Å should be approximately 1 ms. CT through SoxR is 50× faster than this. At present, it is unclear whether the unexpectedly high CT rate is due to the presence of aromatic residues along the CT pathway, which have been shown to mediate ET in azurin.[58] It is also possible that the distance between the cluster and the DNA is shorter when the protein is in the reduced form (no crystal structure of reduced SoxR is available).

5.3.4 Endonuclease III

The BER glycosylase/lyase EndoIII is a redox-active protein involved with detecting and removing oxidized pyrimidines. All BER enzymes can be classified as either monofunctional DNA glycosylases, which remove damaged bases through insertion of an activated water molecule at the glycosidic bond, or glycosylase/lyases, which cleave the glycosidic bond via nucleophilic attack before degrading the associated sugar by Schiff base/conjugate elimination, leaving an apurinic/apyrimidinic (AP) site.[72] Some BER enzymes, such as the *E. coli* glycosylase/lyases MutY and EndoIII, contain $[4Fe\text{-}4S]^{2+}$ clusters ligated by the sequence

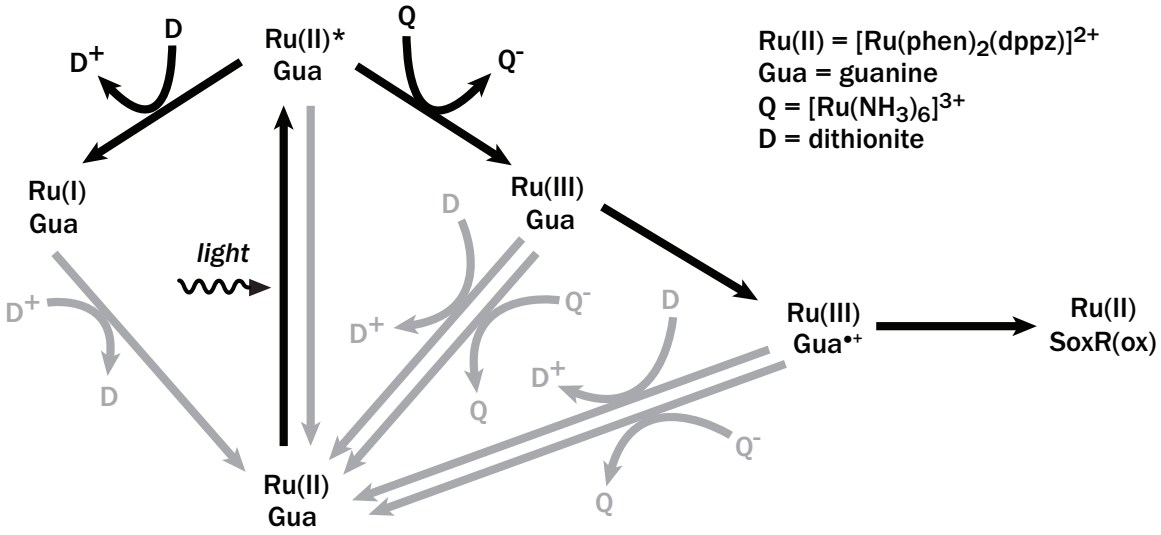

Scheme 5.2: Flash-quench reduction and oxidation of Ru(II)*. Following photoexcitation, Ru(II) can be oxidized by $[Ru(NH_3)_6]^{3+}$ or reduced by dithionite. Dithionite can also reduce Ru(III) and $G^{\bullet+}$, preventing the oxidation of SoxR.

Cys-X_6-Cys-X_2-Cys-X_5-Cys.[73] This sequence is unique to cluster-bearing BER enzymes; the clusters of other proteins that contain iron-sulfur clusters, such as high-potential iron proteins (HiPIPs) and ferredoxins (Fds), possess different cluster ligation sequences.[74]

Although the general action of all BER enzymes is the same, the mechanisms by which they efficiently discover and distinguish between various oxidative lesions are poorly understood. Early mechanistic models suggested that the human glycosylase OGG1 recognizes its target lesion, 7,8-dihydro-8-oxo-2′-deoxyguanosine (8-oxo-dG), through specific hydrogen bonding interactions between the enzyme active site and 8-oxo-dG. However, this is only part of the picture; complexation of OGG1 with undamaged guanine results in only one fewer hydrogen bond than complexation with 8-oxo-dG. Such a subtle thermodynamic difference can hardly form the basis for accurate interrogation.[75] The mechanisms of recognition for more indiscriminate BER enzymes like EndoIII must be even more complex. The list of known substrates for EndoIII includes thymine glycol, cytosine glycol, urea, *N*-substituted urea, 5-hydroxy-5-methylhydantoin, and 5,6-dihydrothymine. Although these are all saturated, opened, or contracted pyrimidine rings, the broad spectrum of shapes and reactivity they present suggests that only careful study of the structure and dynamics of BER enzymes will lead to a full understanding of the mechanisms of lesion recognition.[76]

Experimental Details

The focus of experiments involving EndoIII has been to measure the rate of CT to the protein cluster. Previously, the transient spectrum of an oxidized MutY/maltose binding protein fusion was observed using the flash-quench technique.[29] The transient spectrum of oxidized EndoIII is expected to exhibit a similar increase in absorbance near 410 nm, due to the greater molar extinction of the $[4Fe\text{-}4S]^{3+}$ cluster ($\sim$20 000 M^{-1} cm^{-1})[77] than the $[4Fe\text{-}4S]^{2+}$ cluster (17 000 M^{-1} cm^{-1}).[19] In some experiments, the flash-quench technique was used in an effort to generate a high yield of oxidized protein. In other experiments, direct photooxidation was used so that the observable rates would not be limited by diffusion of the quencher (Figure 5.8). In these latter experiments, the oxidants $[Rh(phi)_2(bpy')]^{3+}$, $[Ir(ppy)_2(dppz')]^{+}$, and $[Re(CO)_3(dppz)(py')]^{+}$ were used. Because these complexes bind

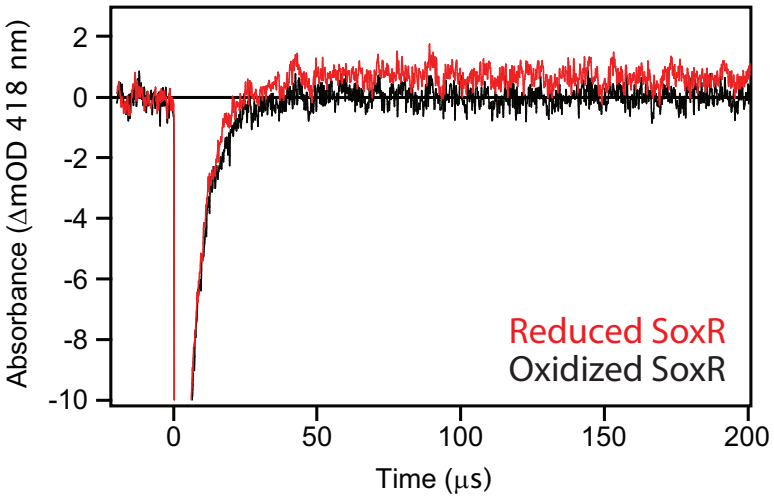

Figure 5.7: Transient absorption measured at 418 nm for samples of 5 μM DNA duplex, 10 μM $[Ru(phen)_2(dppz)]^{2+}$, 200 μM $[Ru(NH_3)_6]^{3+}$, and 5 μM SoxR. Before introduction of oxygen (red), a weak absorption is observed at long time. After introduction of oxygen (black), this component is no longer observed.

to DNA through different ligands and show different oxidation efficiencies,[78] we expected that one of them would be a better redox partner with EndoIII than the other two. All three complexes can be covalently linked to DNA through carboxyalkyl linkers, ensuring a 1:1 ratio of complex to DNA.

Experiments Using the Flash-Quench Technique

Early experiments with EndoIII involved an analogous system to that used by Yavin et al. for the oxidation of MutY. One equivalent of EndoIII was included in solution with 20 μM $[Ru(phen)_2(dppz)]^{2+}$, 600 μM $[Ru(NH_3)_6]^{3+}$, and excess poly(dG-dC). Excitation at 470 nm led to oxidation of guanine by the flash-quench technique. The $G^{\bullet+}$ species formed should be sufficiently oxidizing to oxidize the $[4Fe\text{-}4S]^{2+}$ cluster of the protein. The results of the experiment are shown in Figure 5.9. In the absence of quencher and EndoIII, a short lived bleach appears with recovery lifetimes of 41 ns (62%) and 320 ns (38%). This bleach is due to formation of the Ru(II)* excited state. With the addition of quencher, the bleach recovery lifetime shortens to 34 ns, and a transient appears that decays with a lifetime of 21 μs. Based on similar observations in a nearly identical system, this transient can be assigned to the neutral guanine radical, $G^{\bullet}$.[27] When EndoIII is added, interestingly, the lifetime of the short-lived component is similar to that observed without protein, but the guanine radical no longer appears. Instead, a negative signal with a large amplitude is observed. The recovery lifetime of this component is 6.1 μs.

According to our reaction model, a new transient is expected when EndoIII is added. However, based on comparisons between the absorption spectra of the 2+ and 3+ states of other [4Fe-4S] proteins such as Fds and HiPIPs, the transient formed upon oxidation of EndoIII should give a positive signal, not a negative one. The identity of the species that generates this large negative signal is therefore difficult to determine. In control samples lacking an oxidant, no signal was observed. The only transient species that are expected to cause a decrease in the absorbance at 410 nm are the degraded $[4Fe\text{-}4S]^{+}$ cluster, Ru(II)* and Ru(III). If the cluster is being degraded, a permanent decrease in absorption should be observed; here, the signal recovers to the baseline over time. It is very unlikely that

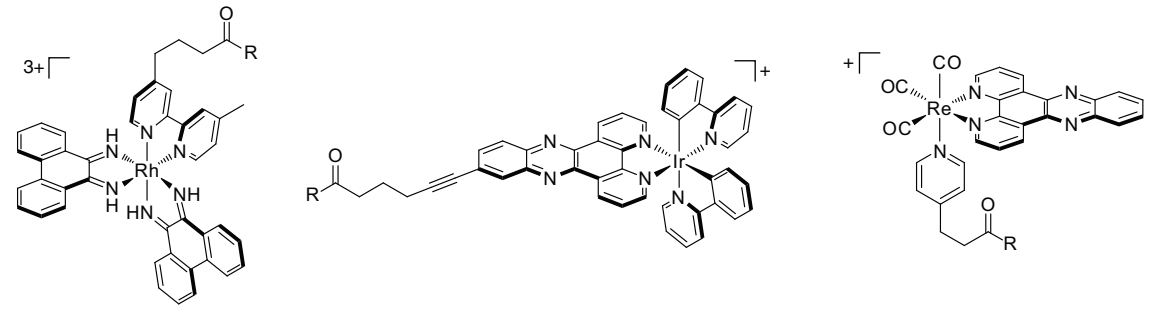

$[Rh(phi)_2(bpy')]^{3+}$ $[Ir(ppy)_2(dppz')]^{+}$ $[Re(CO)_3(dppz)(py')]^{+}$

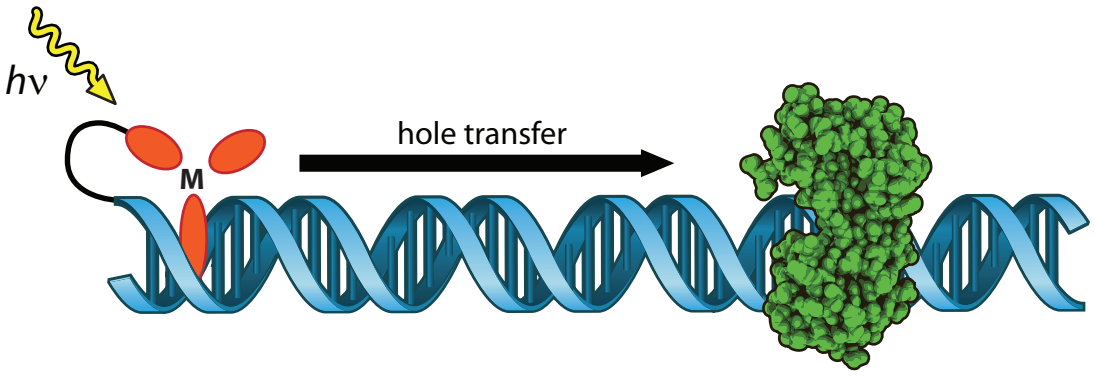

Figure 5.8: The EndoIII transient absorption experiment. Top: structures of the intercalating photooxidants $[Rh(phi)_2(bpy')]^{3+}$, $[Ir(ppy)_2(dppz')]^{+}$, and $[Re(CO)_3(dppz)(py')]^{+}$ and metal complex-DNA conjugates. Bottom: excitation of the covalent photooxidant results in charge injection, forming the guanine cation radical, $G^{\bullet+}$. Hole transfer to EndoIII results in oxidation of the $[4Fe\text{-}4S]^{2+}$ cluster to form $[4Fe\text{-}4S]^{3+}$.

the addition of EndoIII results in an increase in the excited state lifetime of Ru(II) by over two orders of magnitude. However, the other alternative, that addition of protein results in a longer-lived Ru(III) species is also difficult to reconcile considering the high guanine content still present and the facile oxidation of guanine observed in the absence of protein. Another interpretation involves formation of the reduced cluster. The one-electron reduced $[4Fe\text{-}4S]^{+}$ cluster is expected to absorb 10–20% less at 410 nm than the $[4Fe\text{-}4S]^{2+}$ cluster.[19] If the signal is due to reduced EndoIII, the identity of the reductant is unclear. Solution studies indicate that the reduction potential of EndoIII in solution is < -600 mV vs. NHE,[79] and electrochemistry experiments on graphite surfaces suggest that it is closer to -300 mV.[9] The reduction potential of EndoIII bound to DNA could not be determined electrochemically, suggesting that it is outside the operating range of the electrochemical instrument ($E^{\circ} < -300$ mV). In any case, the reduced quencher, $[Ru(NH_3)_6]^{2+}$ is not sufficiently strong to reduce the protein ($E^{\circ}[Ru^{3+}/Ru^{2+}] = 50$ mV vs. NHE).[80] The oxidation potential of $[Ru(phen)_2(dppz)]^{2+*}$ is -0.72 V vs. NHE,[81] indicating that excited Ru may be strong enough to reduce EndoIII. Such a pathway, however, would have to compete with oxidative quenching. This seems unlikely considering the much higher concentration and much more facile diffusion of $[Ru(NH_3)_6]^{3+}$ than of EndoIII.

Additional control experiments will be necessary before the behavior of this flash-quench system can be fully understood. For example, the ability of EndoIII to quench the Ru(II)* excited state could be tested by observing the dependence of Ru(II)* luminescence lifetime and yield on EndoIII concentration. Measurement of transient spectra at various delay times after laser excitation may also provide information about the particular species present in solution throughout the reaction.

Direct Photooxidation Experiments

In order to remove complications introduced by the diffusing quencher on the EndoIII oxidation pathway, several systems were studied involving direct photooxidants rather than the flash-quench technique. Figure 5.10 shows transient spectra of 15 μM Ir-DNA, Rh-DNA, and Re-DNA conjugates in the absence and presence of 15 μM EndoIII at 60 ns following

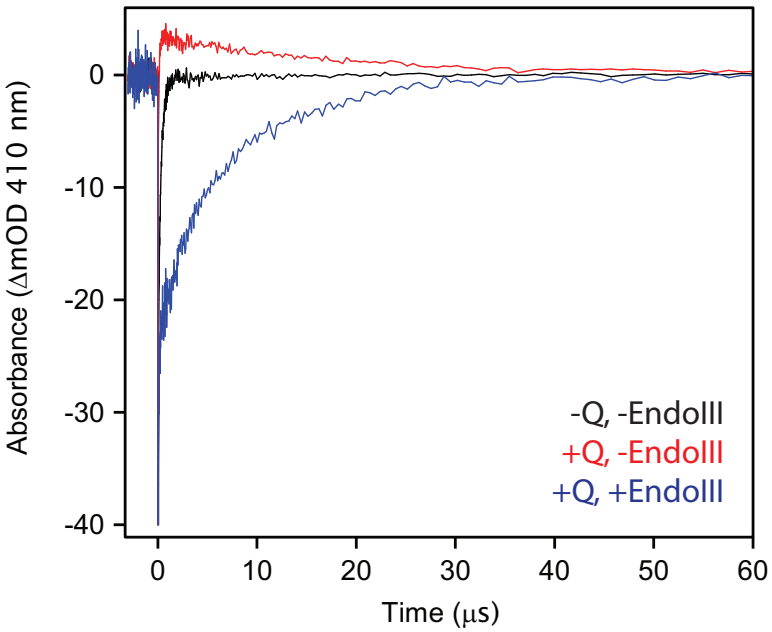

Figure 5.9: Transient absorption of 20 μM $[Ru(phen)_2(dppz)]^{2+}$ in the presence of 1 mM (base pairs) poly(dG-dC), 600 μM $[Ru(NH_3)_6]^{2+}$ quencher, and 20 μM EndoIII in buffer (10 mM NaP_i, 50 mM NaCl; pH 7.5). In the absence of quencher and EndoIII (black), no long-lived products are formed. In the presence of quencher (red), a long-lived positive transient is observed. With both quencher and EndoIII (blue) a long-lived negative signal appears.

355 nm photoexcitation. Interestingly, the three systems behave quite differently. In the Ir system, the introduction of EndoIII results in a decrease in absorption in the bleach region (between 390 nm and 425 nm) and an increase in the absorption at higher wavelengths. Thus, it appears that no new absorbing species are formed, but that the intensity of the Ir transient increases. In the Rh system, the opposite is true. No new absorbing species are observed, but the intensity of the Rh signal decreases with the addition of protein. In the Re system, no change is observed upon the introduction of EndoIII.

Based on comparisons between the reduced state spectra of the metal complexes determined by spectroelectrochemistry and the transient absorption spectra of the metal complex-DNA conjugates obtained by transient absorption spectroscopy, it appears that the transient signals seen in the absence of EndoIII are due to the formation of the reduced metal complexes, or to mixtures of excited and reduced states.[78] This interpretation is consistent with the excited state redox properties of the complexes; each of them should be sufficiently strong excited state oxidants to form $G^{\bullet+}$, resulting in reduction of the complexes themselves. Comparing these results with spectra obtained in the absence and presence of EndoIII, then, suggests that the addition of protein increases the concentration of the reduced Ir species and decreases the concentration of the reduced Rh species, while the Re conjugate is unaffected. The increase in the concentration of reduced Ir upon the addition of EndoIII is consistent with our reaction model, since the addition of protein provides an additional low potential hole trap and decreases the propensity for BET. The decrease in the concentration of reduced Rh with the addition of EndoIII, however, is difficult to explain. It does not appear that EndoIII interacts with the excited state of Rh, since the lifetime of the signal is $\sim$150 nm with and without protein. Inner filtering by the protein can be ruled out, since a similar effect would be observed in the Ir sample as well. The lack of change in the Re sample can be explained by inefficient hole injection, since other studies suggest that a large population of Re* persists after excitation, even in the presence of DNA containing guanine.[78,82]

Interestingly, titrations with EndoIII show that the intensity of the negative TA signal near 400 nm in Ir-DNA samples depends directly on the concentration of protein in

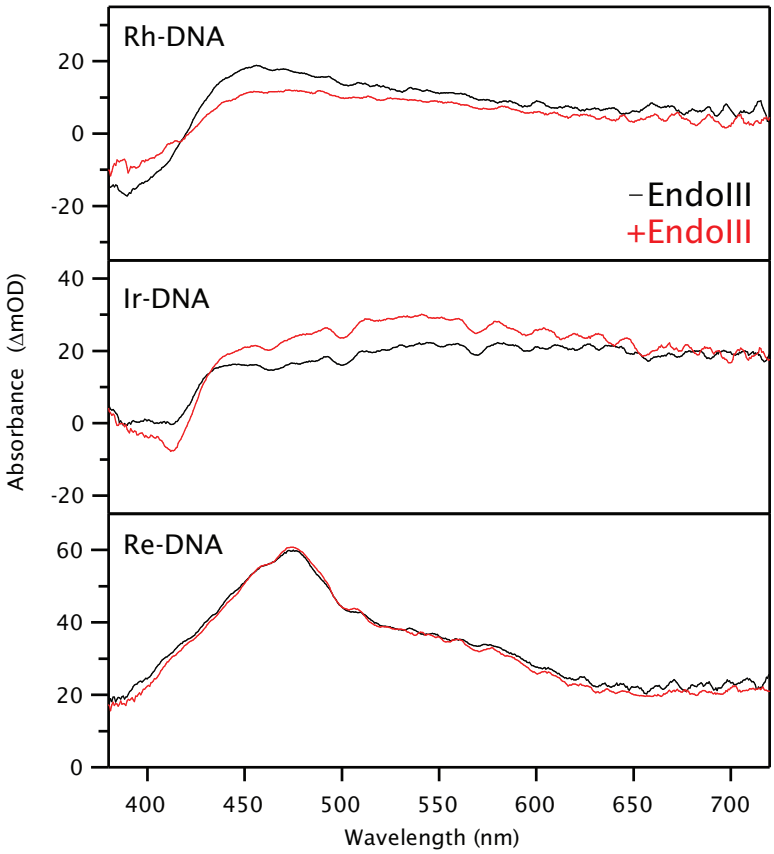

Figure 5.10: Transient absorption spectra of metal complex-DNA conjugates with and without EndoIII. The metal complexes $[Rh(phi)_2(bpy')]^{3+}$, $[Ir(ppy)_2(dppz')]^{+}$, and $[Re(CO)_3(dppz)(py')]^{+}$ were covalently tethered to the 5′-ends of DNA strands with the sequence 5′-ACAITATACCGACTGACTGACT-3′. The transient absorption spectra of the associated DNA duplexes (20 μM) were recorded 60 ns after 355 nm photoexcitation in the absence (black) and presence (red) of 20 μM EndoIII.

solution (Figure 5.11). No change in lifetime is observed, however. Similarly, the intensity of the positive transient near 450 nm increases increasing EndoIII concentration, and the lifetime of the transient decreases from 240 ns with 0 equivalents of EndoIII to 190 ns with 4 equivalents.

The changes observed in the TA spectra and kinetics traces of metal complex-DNA conjugates upon the addition of EndoIII indicate that some physical or chemical change is occuring. We expect that oxidation of the protein cluster should occur; however, no direct evidence has been observed for such a process. Instead, data suggest that changes in the lifetimes and intensities of the observed transients are due to changes in the efficiency of metal complex reduction or BET. These results, therefore, may comprise secondary evidence for DNA-mediated EndoIII oxidation. Evidence for photochemistry can also be observed in steady-state spectrophotometric measurements made before and after photolysis. In the absence of protein, little change is observed in the spectra. In the presence of protein, large differences are typically observed, including a decrease in the absorption of the $[4Fe\text{-}4S]^{2+}$ cluster and increased absorbance at higher wavelengths. Such differences are consistent with degradative oxidation of the cluster.

5.4 Concluding Remarks

Experiments in a variety of systems show that DNA-mediated CT is possible in a biological context. The efficiency of CT can be modulated by protein binding, and evidence is accumulating for the specific utilization of DNA-mediated oxidation in cellular processes such as damage sequestration, lesion detection, and transcriptional activation. Transient absorption experiments involving several redox-active DNA-binding proteins have provided initial direct evidence for similar processes *in vitro*. Oxidation of p53 by the flash-quench technique leads to the formation of a small transient band that bears the signatures of the tyrosine radical cation. Oxidation of SoxR by the flash-quench technique after removal of dithionite has similarly provided tantalizing evidence for the oxidation of the protein by DNA-mediated CT. Finally, experiments with EndoIII involving DNA-conjugated intercalating metal complex photooxidants show that the presence of the protein perturbs the

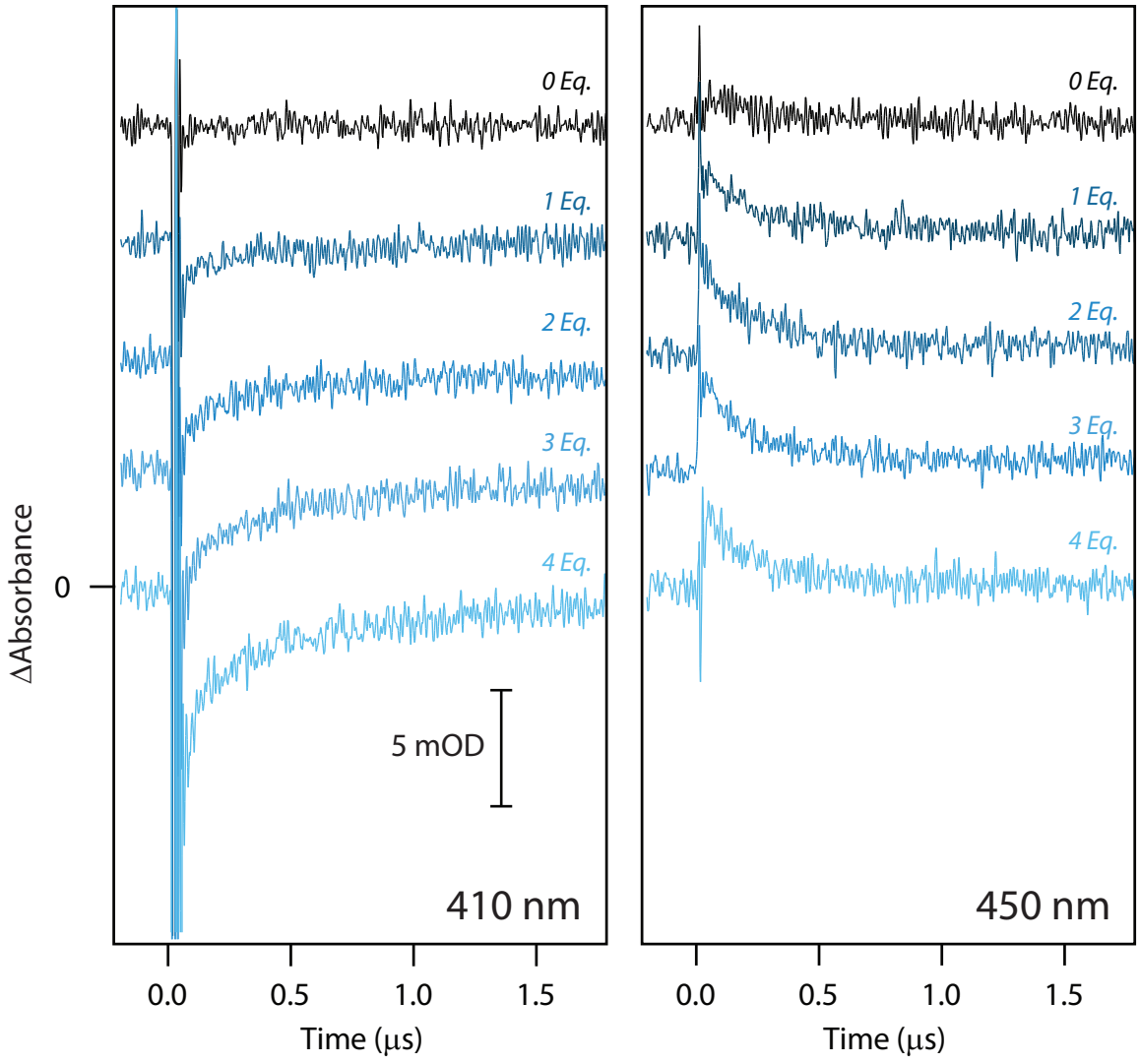

Figure 5.11: Transient absorption spectra of 5 μM Ir-DNA with increasing amounts of EndoIII (0, 1, 2, 3, or 4 equivalents, as indicated). Kinetics were measured at 410 nm (left) and 450 nm (right). Samples were excited at 355 nm. Traces are vertically offset for clarity.

system, although further experiments are needed to fully understand the processes that are occuring. In all of the systems described here, expanded exploration of the experimental parameters is expected to increase the quality of the data, leading to more consistent explanations for the chemistry that is occuring and a greater understanding of the role that redox-active proteins may play in DNA-mediated CT. This work therefore provides a solid basis for future experiments.

References

[1] Genereux, J. C., and Barton, J. K. "Mechanisms for DNA charge transport." *Chem. Rev.* **110**, 1642–1662 (2010).

[2] Kelley, S. O., Boon, E. M., Barton, J. K., Jackson, N. M., and Hill, M. G. "Single-base mismatch detection based on charge transduction through DNA." *Nucl. Acids Res.* **27**, 4830–4837 (1999).

[3] Boon, E. M., Ceres, D. M., Drummond, T. G., Hill, M. G., and Barton, J. K. "Mutation detection by electrocatalysis at DNA-modified electrodes." *Nat. Biotech.* **18**, 1096–1100 (2000).

[4] Boal, A. K., and Barton, J. K. "Electrochemical detection of lesions in DNA." *Bioconj. Chem.* **16**, 312–321 (2005).

[5] Rajski, S. R., Kumar, S., Roberts, R. J., and Barton, J. K. "Protein-Modulated DNA Electron Transfer." *J. Am. Chem. Soc.* **121**, 5615–5616 (1999).

[6] Rajski, S. R., and Barton, J. K. "How different DNA-binding proteins affect long-range oxidative damage to DNA." *Biochemistry* **40**, 5556–5564 (2001).

[7] Boon, E. M., Salas, J. E., and Barton, J. K. "An electrical probe of protein-DNA interactions on DNA-modified surfaces." *Nat. Biotech.* **20**, 282–286 (2002).

[8] Gorodetsky, A. A., Hammond, W. J., Hill, M. G., Slowinski, K., and Barton, J. K. "Scanning electrochemical microscopy of DNA monolayers modified with Nile Blue." *Langmuir* **24**, 14282–14288 (2008).

[9] Gorodetsky, A. A., Ebrahim, A., and Barton, J. K. "Electrical detection of TATA binding protein at DNA-modified microelectrodes." *J. Am. Chem. Soc.* **130**, 2924–2925 (2008).

[10] Wagenknecht, H.-A., Rajski, S. R., Pascaly, M., Stemp, E. D. A., and Barton, J. K. "Direct observation of radical intermediates in protein-dependent DNA charge transport." *J. Am. Chem. Soc.* **123**, 4400–4407 (2001).

[11] Núñez, M. E., Noyes, K. T., and Barton, J. K. "Oxidative charge transport through DNA in nucleosome core particles." *Chem. Biol.* **9**, 403–415 (2002).

[12] Núñez, M. E., Holmquist, G. P., and Barton, J. K. "Evidence for DNA Charge Transport in the Nucleus." *Biochemistry* **40**, 12465–12471 (2001).

[13] Merino, E. J., and Barton, J. K. "Oxidation by DNA charge transport damages conserved sequence block II, a regulatory element in mitochondrial DNA." *Biochemistry* **46**, 2805–2811 (2007).

[14] Merino, E. J., and Barton, J. K. "DNA oxidation by charge transport in mitochondria." *Biochemistry* **47**, 1511–1517 (2008).

[15] Merino, E. J., Davis, M. L., and Barton, J. K. "Common mitochondrial DNA mutations generated through DNA-mediated charge transport." *Biochemistry* **48**, 660–666 (2009).

[16] Wagenknecht, H.-A., Stemp, E. D. A., and Barton, J. K. "DNA-Bound peptide radicals generated through DNA-mediated electron transport." *Biochemistry* **39**, 5483–5491 (2000).

[17] Wagenknecht, H.-A., Stemp, E. D. A., and Barton, J. K. "Evidence of Electron Transfer from Peptides to DNA: Oxidation of DNA-Bound Tryptophan Using the Flash-Quench Technique." *J. Am. Chem. Soc.* **122**, 1–7 (2000).

[18] Augustyn, K. E., Merino, E. J., and Barton, J. K. "A role for DNA-mediated charge transport in regulating p53: Oxidation of the DNA-bound protein from a distance." *Proc. Natl. Acad. Sci. USA* **104**, 18907–18912 (2007).

[19] Cunningham, R. P., Asahara, H., Bank, J. F., Scholes, C. P., Salerno, J. C., Surerus, K., Munck, E., McCracken, J., Peisach, J., and Emptage, M. H. "Endonuclease III is an iron-sulfur protein." *Biochemistry* **28**, 4450–4455 (1989).

[20] Gorodetsky, A. A., Boal, A. K., and Barton, J. K. "Direct electrochemistry of endonuclease III in the presence and absence of DNA." *J. Am. Chem. Soc.* **128**, 12082–12083 (2006).

[21] Boal, A. K., Yavin, E., Lukianova, O. A., O'Shea, V. L., David, S. S., and Barton, J. K. "DNA-bound redox activity of DNA repair glycosylases containing [4Fe-4S] clusters." *Biochemistry* **44**, 8397–8407 (2005).

[22] Boon, E. M., Livingston, A. L., Chmiel, N. H., David, S. S., and Barton, J. K. "DNA-mediated charge transport for DNA repair." *Proc. Natl. Acad. Sci. USA* **100**, 12543–12547 (2003).

[23] Gorodetsky, A. A., Dietrich, L. E. P., Lee, P. E., Demple, B., Newman, D. K., and Barton, J. K. "DNA binding shifts the redox potential of the transcription factor SoxR." *Proc. Natl. Acad. Sci. USA* **105**, 3684–3689 (2008).

[24] Lee, P. E., Demple, B., and Barton, J. K. "DNA-mediated redox signaling for transcriptional activation of SoxR." *Proc. Natl. Acad. Sci. USA* **106**, 13164–13168 (2009).

[25] Núñez, M. E., Hall, D. B., and Barton, J. K. "Long-range oxidative damage to DNA: effects of distance and sequence." *Chem. Biol.* **6**, 85–97 (1999).

[26] Boal, A. K., Genereux, J. C., Sontz, P. A., Gralnick, J. A., Newman, D. K., and Barton, J. K. "Redox signaling between DNA repair proteins for efficient lesion detection." *Proc. Natl. Acad. Sci. USA* **106**, 15237–15242 (2009).

[27] Stemp, E. D. A., Arkin, M. R., and Barton, J. K. "Oxidation of Guanine in DNA by $Ru(phen)_2(dppz)^{3+}$ Using the Flash-Quench Technique." *J. Am. Chem. Soc.* **119**, 2921–2925 (1997).

[28] Stemp, E. D. A., and Barton, J. K. "The Flash-Quench Technique in Protein-DNA Electron Transfer: Reduction of the Guanine radical by Ferrocytochrome *c*." *Inorg. Chem.* **39**, 3868–3874 (2000).

[29] Yavin, E., Boal, A. K., Stemp, E. D. A., Boon, E. M., Livingston, A. L., O'Shea, V. L., David, S. S., and Barton, J. K. "Protein-DNA charge transport: redox activation of a DNA repair protein by guanine radical." *Proc. Natl. Acad. Sci. USA* **102**, 3546–3551 (2005).

[30] Shao, F., Elias, B., Lu, W., and Barton, J. K. "Synthesis and characterization of iridium(III) cyclometalated complexes with oligonucleotides: insights into redox reactions with DNA." *Inorg. Chem.* **46**, 10187–10199 (2007).

[31] Sitlani, A., Long, E. C., Pyle, A. M., and Barton, J. K. "DNA Photocleavage by Phenanthrenequinone Diimine Complexes of Rhodium(III): Shape-Selective Recognition and Reaction." *J. Am. Chem. Soc.* **114**, 2303–2312 (1992).

[32] Boal, A. K. "DNA-Mediated Charge Transport in DNA Repair." Ph.D. thesis, California Institute of Technology, 2008.

[33] Dempsey, J. L., Winkler, J. R., and Gray, H. B. "Kinetics of electron transfer reactions of H_2-evolving cobalt diglyoxime catalysts." *J. Am. Chem. Soc.* **132**, 1060–1065 (2010).

[34] Shao, F., Augustyn, K. E., and Barton, J. K. "Sequence dependence of charge transport through DNA domains." *J. Am. Chem. Soc.* **127**, 17445–17452 (2005).

[35] Hall, D. B., and Barton, J. K. "Sensitivity of DNA-Mediated Electron Transfer to the Intervening π-Stack: A Probe for the Integrity of the DNA Base Stack." *J. Am. Chem. Soc.* **119**, 5045–5046 (1997).

[36] Odom, D. T., Dill, E. A., and Barton, J. K. "Robust charge transport in DNA double crossover assemblies." *Chem. Biol.* **7**, 475–481 (2000).

[37] Odom, D. T., Dill, E. a., and Barton, J. K. "Charge transport through DNA four-way junctions." *Nucl. Acids Res.* **29**, 2026–2033 (2001).

[38] Delaney, S., and Barton, J. K. "Charge transport in DNA duplex/quadruplex conjugates." *Biochemistry* **42**, 14159–14165 (2003).

[39] Williams, T. T., Odom, D. T., and Barton, J. K. "Variations in DNA Charge Transport with Nucleotide Composition and Sequence." *J. Am. Chem. Soc.* **122**, 9048–9049 (2000).

[40] Boon, E. M., Pope, M. A., Williams, S. D., David, S. S., and Barton, J. K. "DNA-Mediated Charge Transport as a Probe of MutY/DNA Interaction." *Biochemistry* **41**, 8464–8470 (2002).

[41] Dandliker, P. J., Holmlin, R. E., and Barton, J. K. "Oxidative Thymine Dimer Repair in the DNA Helix." *Science* **275**, 1465–1468 (1997).

[42] Dandliker, P. J., Núñez, M. E., and Barton, J. K. "Oxidative charge transfer To repair thymine dimers and damage guanine bases in DNA assemblies containing tethered metallointercalators." *Biochemistry* **37**, 6491–6502 (1998).

[43] Shao, F., and Barton, J. K. "Long-range electron and hole transport through DNA with tethered cyclometalated iridium(III) complexes." *J. Am. Chem. Soc.* **129**, 14733–14738 (2007).

[44] Elias, B., Shao, F., and Barton, J. K. "Charge migration along the DNA duplex: hole versus electron transport." *J. Am. Chem. Soc.* **130**, 1152–1153 (2008).

[45] Elias, B., Genereux, J. C., and Barton, J. K. "Ping-pong electron transfer through DNA." *Angew. Chem. Int. Ed.* **47**, 9067–9070 (2008).

[46] Arkin, M. R., Stemp, E. D. A., Coates Pulver, S., and Barton, J. K. "Long-range oxidation of guanine by Ru(III) in duplex DNA." *Chem. Biol.* **4**, 389–400 (1997).

[47] Schiemann, O., Turro, N. J., and Barton, J. K. "EPR Detection of Guanine Radicals in a DNA Duplex under Biological Conditions: Selective Base Oxidation by $Ru(phen)_2dppz^{3+}$ Using the Flash-Quench Technique." *J. Phys. Chem. B* **104**, 7214–7220 (2000).

[48] Bhattacharya, P. K., and Barton, J. K. "Influence of intervening mismatches on long-range guanine oxidation in DNA duplexes." *J. Am. Chem. Soc.* **123**, 8649–8656 (2001).

[49] Delaney, S., Yoo, J., Stemp, E. D. A., and Barton, J. K. "Charge equilibration between two distinct sites in double helical DNA." *Proc. Natl. Acad. Sci. USA* **101**, 10511–10516 (2004).

[50] Yoo, J., Delaney, S., Stemp, E. D. A., and Barton, J. K. "Rapid radical formation by DNA charge transport through sequences lacking intervening guanines." *J. Am. Chem. Soc.* **125**, 6640–6641 (2003).

[51] Pascaly, M., Yoo, J., and Barton, J. K. "DNA mediated charge transport: characterization of a DNA radical localized at an artificial nucleic acid base." *J. Am. Chem. Soc.* **124**, 9083–9092 (2002).

[52] Copeland, K. D., Lueras, A. M. K., Stemp, E. D. A., and Barton, J. K. "DNA cross-linking with metallointercalator-peptide conjugates." *Biochemistry* **41**, 12785–12797 (2002).

[53] Vousden, K. H., and Lu, X. "Live or let die: the cell's response to p53." *Nat. Rev. Cancer* **2**, 594–604 (2002).

[54] Ang, H. C., Joerger, A. C., Mayer, S., and Fersht, A. R. "Effects of common cancer mutations on stability and DNA binding of full-length p53 compared with isolated core domains." *J. Biol. Chem.* **281**, 21934–21941 (2006).

[55] Joerger, A. C., and Fersht, A. R. "Structure-function-rescue: the diverse nature of common p53 cancer mutants." *Oncogene* **26**, 2226–2242 (2007).

[56] El-Deiry, W. S., Kern, S. E., Pietenpol, J. A., Kinzler, K. W., and Vogelstein, B. "Definition of a consensus binding site for p53." *Nat. Genet.* **1**, 45–49 (1992).

[57] Nikolova, P. V., Henckel, J., Lane, D. P., and Fersht, A. R. "Semirational design of active tumor suppressor p53 DNA binding domain with enhanced stability." *Proc. Natl. Acad. Sci. USA* **95**, 14675–14680 (1998).

[58] Shih, C., Museth, A. K., Abrahamsson, M., Blanco-Rodríguez, A. M., Di Bilio, A. J., Sudhamsu, J., Crane, B. R., Ronayne, K. L., Towrie, M., Vlček, A., Richards, J. H., Winkler, J. R., and Gray, H. B. "Tryptophan-accelerated electron flow through proteins." *Science* **320**, 1760–1762 (2008).

[59] Williams, J. W., and Drissen, E. M. "Oxidation-Reduction Potentials of Certain Sulfhydryl Compounds." *J. Biol. Chem.* **87**, 441–451 (1930).

[60] Murphy, C. J., Arkin, M. R., Ghatlia, N. D., Bossmann, S. H., Turro, N. J., and Barton, J. K. "Fast photoinduced electron transfer through DNA intercalation." *Proc. Natl. Acad. Sci. USA* **91**, 5315–5319 (1994).

[61] Steenken, S., and Jovanovic, S. V. "How Easily Oxidizable Is DNA? One-Electron Reduction Potentials of Adenosine and Guanosine Radicals in Aqueous Solution." *J. Am. Chem. Soc.* **119**, 617–618 (1997).

[62] Romano, C. A., Sontz, P. A., and Barton, J. K. "Mutants of the Base Excision Repair Glycosylase, Endonuclease III: DNA Charge Transport as a First Step in Lesion Detection." *Biochemistry* **50**, 6133–6145 (2011).

[63] Hidalgo, E., and Demple, B. "An iron-sulfur center essential for transcriptional activation by the redox-sensing SoxR protein." *EMBO J.* **13**, 138–146 (1994).

[64] Ding, H., Hidalgo, E., and Demple, B. "The redox state of the [2Fe-2S] clusters in SoxR protein regulates its activity as a transcription factor." *J. Biol. Chem.* **271**, 33173–33175 (1996).

[65] Hidalgo, E., Leautaud, V., and Demple, B. "The redox-regulated SoxR protein acts from a single DNA site as a repressor and an allosteric activator." *EMBO J.* **17**, 2629–2636 (1998).

[66] Mayhew, S. G. "The Redox Potential of Dithionite and SO_2^- from Equilibrium Reactions with Flavodoxins , Methyl Viologen and Hydrogen plus Hydrogenase." *Eur. J. Biochem.* **85**, 535–547 (1978).

[67] Moucheron, C., Kirsch-De Mesmaeker, A., and Choua, S. "Photophysics of $Ru(phen)_2(PHEHAT)^{2+}$: A Novel 'Light Switch' for DNA and Photo-oxidant for Mononucleotides." *Inorg. Chem.* **36**, 584–592 (1997).

[68] Hidalgo, E., Bollinger, J. M., Bradley, T. M., Walsh, C. T., and Demple, B. "Binuclear [2Fe-2S] clusters in the Escherichia coli SoxR protein and role of the metal centers in transcription." *J. Biol. Chem.* **270**, 20908–20914 (1995).

[69] Wan, C., Fiebig, T., Kelley, S. O., Treadway, C. R., Barton, J. K., and Zewail, A. H. "Femtosecond dynamics of DNA-mediated electron transfer." *Proc. Natl. Acad. Sci. USA* **96**, 6014–6019 (1999).

[70] Tezcan, F. A., Crane, B. R., Winkler, J. R., and Gray, H. B. "Electron tunneling in protein crystals." *Proc. Natl. Acad. Sci. USA* **98**, 5002–5006 (2001).

[71] Watanabe, S., Kita, A., Kobayashi, K., and Miki, K. "Crystal structure of the [2Fe-2S] oxidative-stress sensor SoxR bound to DNA." *Proc. Natl. Acad. Sci. USA* **105**, 4121–4126 (2008).

[72] Verdine, G. L., and Bruner, S. D. "How do DNA repair proteins locate damaged bases in the genome?" *Chem. Biol.* **4**, 329–334 (1997).

[73] Thayer, M. M., Ahern, H., Xing, D., Cunningham, R. P., and Tainer, J. A. "Novel DNA binding motifs in the DNA repair enzyme endonuclease III crystal structure." *EMBO J.* **14**, 4108–4120 (1995).

[74] Kuo, C.-F., Mcree, D. E., Fisher, C. L., O'Handley, S. F., Cunningham, R. P., and Tainer, J. A. "Atomic Structure of the DNA Repair [4Fe-4S] Enzyme Endonuclease III." *Science* **258**, 434–440 (1992).

[75] van Loon, B., Markkanen, E., and Hübscher, U. "Oxygen as a friend and enemy: How to combat the mutational potential of 8-oxo-guanine." *DNA repair* **9**, 604–616 (2010).

[76] Aspinwall, R., Rothwell, D. G., Roldan-Arjona, T., Anselmino, C., Ward, C. J., Cheadle, J. P., Sampson, J. R., Lindahl, T., Harris, P. C., and Hickson, I. D. "Cloning and characterization of a functional human homolog of Escherichia coli endonuclease III." *Proc. Natl. Acad. Sci. USA* **94**, 109–114 (1997).

[77] Lippard, S. J., and Berg, J. M. *Principles of Bioinorganic Chemistry*; University Science Books: Mill Valley, California, 1994.

[78] Olmon, E. D., Hill, M. G., and Barton, J. K. "Using Metal Complex Reduced States to Monitor the Oxidation of DNA." *Inorg. Chem.* **Submitted**, (2011).

[79] Fu, W., O'Handley, S., Cunningham, R. P., and Johnson, M. K. "The Role of the Iron-Sulfur Cluster in *Escherichia coli* Endonuclease III: A Resonance Raman Study." *J. Biol. Chem.* **267**, 16135–16137 (1992).

[80] Stemp, E. D. A., Holmlin, R. E., and Barton, J. K. "Electron transfer between metal complexes bound to DNA: variations in sequence, donor, and metal binding mode." *Inorg. Chim. Acta* **297**, 88–97 (2000).

[81] Delaney, S. "Oxidative DNA Damage by Long-Range Charge Transport." Ph.D. thesis, 2004.

[82] Olmon, E. D., Sontz, P. A., Blanco-Rodríguez, A. M., Towrie, M., Clark, I. P., Vlček, A., and Barton, J. K. "Charge Photoinjection in Intercalated and Covalently Bound $[Re(CO)_3(dppz)(py)]^+$-DNA Constructs Monitored by Time-Resolved Visible and Infrared Spectroscopy." *J. Am. Chem. Soc.* **133**, 13718–13730 (2011).

Chapter 6

Summary and Perspectives

A large body of past experiments has provided a strong foundation for the work presented here. Beginning with the first demonstration of DNA-mediated charge transport (CT) between metallointercalators in 1993,[1] strong evidence began to accumulate that the π stack of the DNA helix can serve as a medium for the conduction of charge. Through the development of new chemical systems and ingenious experimental devices, and the systematic modification of experimental parameters, the factors that affect the efficiency of DNA-mediated CT have come into focus.[2] It is now known that mismatches, lesions, and bulges intervening between the CT donor and the acceptor decrease the efficiency of the reaction. In addition, proteins that bend the DNA duplex disrupt CT, while proteins that fill gaps in the base stack with aromatic residues restore it. The efficiency of charge injection into DNA depends strongly on the driving force of the reaction and on the extent of electronic coupling between the CT trigger and the DNA base stack. Conversely, these factors also govern the efficiency of back electron transfer (BET), which decreases the yield of permanent products formed by DNA-mediated CT. We now undertand the factors affecting the efficiency of DNA-mediated CT at such a level that we can engineer chemical systems in which CT is intentionally facilitated or hindered.

We know considerably less about the factors affecting the rate of DNA-mediated CT. From the first fluorescence quenching experiments, in which an instrument with a response time of 10 ns was incapable of resolving the quenching event, it was apparent that this process is rapid. Ultrafast transient absorption experiments have shown that CT can occur over a distance of several base pairs at rates of $\sim 10^{11}$ s^{-1}. In studies involving ethidium as an electron acceptor, no dependence of the rate on distance was observed, but the distances that could be studied were limited by poor coupling of ethidium to the base stack.[3] In a related study, the absorbance of the excited charge donor, 2-aminopurine (Ap), was monitored over time in several DNA assemblies. With increasing distance between Ap and the charge acceptor, the lifetime of *Ap increased dramatically. The strong distance dependence observed in this system does not agree with the shallow distance dependence observed in the ethidium system or in guanine oxidation experiments.[4] Such discrepancies highlight our lack of knowledge regarding the kinetics of DNA-mediated CT. This is therefore an area

rich with possibilities for future research.

We have developed a rhenium-based vibrationally-active metallointercalor for use as a photooxidant in time-resolved studies of DNA-mediated CT. The photophysical characteristics and redox potential of $[Re(CO)_3(dppz)(py'\text{-}OR)]^+$ are similar to those of other Re photooxidants. Electrochemical and biochemical experiments show that the Re complex is a sufficiently strong oxidant from the excited state to oxidize guanine. Results from time-resolved infrared (TRIR) experiments agree. In the presence of DNA that does not contain guanine, a vibrational band due to the metal-to-ligand charge transfer (MLCT) excited state is observed. In solution with DNA that contains only guanine and cytosine, several observations suggest that quenching of the MLCT state occurs at an ultrafast time scale. These include the disappearance of the MLCT band, a relative decrease in the intensity of the other transient bands formed, and lower emission intensity. The formation of a transient band in this sample near 1700 cm^{-1} is also consistent with the formation of the guanine radical. These results show that excitation of these Re photooxidants can trigger long-range oxidation and that fast vibrational spectroscopy is a viable method by which to probe DNA-mediated CT.

The physical and photochemical characteristics of $[Re(CO)_3(dppz)(py'\text{-}OR)]^+$ are similar to those of other metal complex photooxidants. DNA binding leads to hypochromicity of the metal complex absorption and raises the melting temperature of DNA, indicating that the complex binds by intercalation. In guanine oxidation experiments, the photooxidation efficiency of the Re complex was between that of $[Rh(phi)_2(bpy')]^{3+}$ and that of $[Ir(ppy)_2(dppz')]^+$. When these complexes are bound to DNA, excitation of the metal complexes results in formation of their reduced states. This is consistent with the ability of the complexes to oxidize guanine. The lifetime of each reduced species, which corresponds to the rate of BET, is correlated to the yield of guanine damage, suggesting that BET is a major limiting factor in the formation of damage. These results verify our knowledge about the factors that affect the efficiency of DNA-mediated CT: the stronger binding strength and higher driving force for oxidation by the Rh complex result in a high yield of guanine damage, and the shorter excited state lifetime and more facile BET observed in the Ir

system result in a low yield of guanine damage.

Time-resolved spectroscopic experiments conducted in the presence of redox-active proteins are promising. Evidence has been observed for the DNA-mediated oxidation of p53 using the flash-quench technique. Similarly, a weak signal observed at long time by TA spectroscopy upon the addition of SoxR to solution is consistent with oxidation of this protein. The results of experiments on EndoIII are not as straightforward, although it is clear that the addition of protein does affect the system. These preliminary results support biological models for the use of these proteins in DNA-mediated lesion detection and transcriptional activation. In future expeirments, refinement of the experimental parameters and more sensitive instrumentation may enable measurements of the rates of DNA-mediated protein oxidation.

Much is yet to be learned about the factors affecting the kinetics of DNA-mediated CT. In light of the successful use of TRIR spectroscopy to study the oxidation of guanine, time-revolved vibrational spectroscopy will be an invaluable tool for understanding how DNA-mediated CT systems evolve over time. Similarly, the preliminary evidence for the DNA-mediated oxidation of p53, SoxR, and EndoIII will provide a solid foundation for further spectroscopic experiments involving redox-active proteins. Just as our work builds on that of others who have come before us, the experimental results presented here will provide a basis for future explorations of DNA-mediated CT.

References

[1] Murphy, C. J., Arkin, M. R., Jenkins, Y., Ghatlia, N. D., Bossmann, S. H., Turro, N. J., and Barton, J. K. "Long-range photoinduced electron transfer through a DNA helix." *Science* **262**, 1025–1029 (1993).

[2] Genereux, J. C., and Barton, J. K. "Mechanisms for DNA charge transport." *Chem. Rev.* **110**, 1642–1662 (2010).

[3] Wan, C., Fiebig, T., Kelley, S. O., Treadway, C. R., Barton, J. K., and Zewail, A. H. "Femtosecond dynamics of DNA-mediated electron transfer." *Proc. Natl. Acad. Sci. USA* **96**, 6014–6019 (1999).

[4] Núñez, M. E., Hall, D. B., and Barton, J. K. "Long-range oxidative damage to DNA: effects of distance and sequence." *Chem. Biol.* **6**, 85–97 (1999).